2013-04-29

Identification of Novel Mechanisms for Myogenic Control of Cerebral Arterial Diameter

Zhong, Xi

UNIVERSITY OF CALGARY

Identification of Novel Mechanisms for Myogenic Control of Cerebral Arterial Diameter

by

Xi Zhong

A THESIS

SUBMITTED TO THE FACULTY OF GRADUATE STUDIES

IN PARTIAL FULFILMENT OF THE REQUIREMENTS FOR THE

DEGREE OF DOCTOR OF PHILOSOPHY

DEPARTMENT OF CARDIOVASCULAR & RESPIRATORY SCIENCES

CALGARY, ALBERTA

APRIL, 2013

Abstract

Myogenic control of cerebral arterial diameter plays a fundamental role in the maintenance of normal vascular resistance and blood flow in the brain. Myogenic control of cerebral artery diameter is achieved by inherent pressure-dependent mechanisms of Ca^{2+}-CaM-MLCK activation, ROK-mediated Ca^{2+} sensitization and cytoskeleton reorganization. The findings presented in this thesis identify novel elements in these molecular mechanisms, including: (1) $K_v9.3$ subunits that co-assemble with $K_v2.1$ subunits to form ScTx1-sensitive channels that regulate E_m, (2) $K_v7.4$-containing channels that also regulate E_m, and (3) a cytoskeleton protein, VASP, that is involved in a dynamic process of actin polymerization in response to pressure elevation. Both $K_v2.1/9.3$ channels and $K_v7.4$-containing channels of cerebral myocytes were shown to contribute to native K_v currents in myogenic control of cerebral arterial diameter. Regulation of VASP phosphorylation in the process of cytoskeleton reorganization was shown to participate in the pressure-dependent myogenic response and NO-mediated vasodilation of cerebral arteries. In summary, these findings provide novel understanding of the basic molecular mechanisms that contribute to the precise control of vascular smooth muscle contractility, and provide potentially important insights for identification of dysfunctional mechanisms leading to abnormal arterial regulation in pathological conditions, as well as the development of therapeutic strategies to treat arterial dysfunction.

Acknowledgements

I would like to thank my supervisor, Dr. William Cole for his constant guidance, encouragement and support. I would also like to thank Dr. Michael Walsh, Dr. Wayne Chen, Dr. Justin MacDonald, Dr. Donald Welsh and Dr. Iain Greenwood (St. George's University of London) for their advice and support. I would like to acknowledge the contribution of Dr. Maksym Harhun (St. George's University of London) and Dr. Susumu Ohya (Nagoya City University), who performed the experiments and analysis of Kv7 protein and message expression described in Figure 4.2, Dr. Hai-lei Zhu who assisted in collecting large numbers of tissue samples and performed some western blot experiments for the VASP project presented in Chapter 5, Emma Walsh who provided plasmids for the Kv2 and Kv7 projects presented in Chapter 3 and 4, respectively, helped with cell cultures, RT-PCR, real-time PCR, and the pressure myograph experiments for the Kv2 project, Khaled Abdel-Rahman who helped with the Kv2.1/9.2 patch clamp experiment described in Table 2.1, and Chiu-Hsiang Liao who helped with the Kv1.2/1.5 PLA experiment described in Figure 3.15. Thanks to all members of the Cole laboratory for their valuable input. Thanks to my parents and husband for always being there for me.

To my grandpa, Zhaoyue Zhong

Table of Contents

List of Tables

List of Figures

List of Symbols, Abbreviations and Nomenclature

Symbol	Definition
$[Ca^{2+}]_i$	Intracellular Ca^{2+} concentration
4-AP	4-aminopyridine
AMPK	AMP-activated protein kinase
Bay K8644	1,4-Dihydro-2,6-dimethyl-5-nitro-4-(2-[trifluoromethyl]phenyl)pyridine-3-carboxylic acid methyl ester
BK_{Ca}	Large conductance Ca^{2+}-activated K^+ channel
BSA	Bovine serum albumin
CaM	Calmodulin
CAPS	3-[Cyclohexylamino]-1-propanesulfonic acid
COF	Cofilin
COX	Cyclooxygenase
DMEM	Dulbecco's Modified Eagle's medium
EDHF	Endothelium-derived hyperpolarizing factor
E_m	Membrane potential
eNOS	Endothelial nitric oxide synthase
F-actin	Filamentous actin
FAK	Focal adhesion kinase
G-actin	Globular actin
GFP	Green fluorescent protein
GK	Goto-Kakizaki
H_2O_2	Hydrogen peroxide
H_2S	Hydrogen sulfide
HEK 293	Human embryonic kidney cell
HRP	Horseradish peroxidase
HSP	Heat shock protein
IK_{Ca}	Intermediate conductance Ca^{2+}-activated K^+ channel
IP3	Inositol 1,4,5-trisphosphate
IRAG	IP_3 receptor-associated PKG-I substrate
K_{DR}	Delayed rectifier K^+ channel
K_{ir}	Inwardly rectifying K^+ channel
K_{TO}	Transient outward K^+ channel
K_v	Voltage-gated K^+ channel
LC_{20}	20 kDa myosin regulatory light chain
LimK	Lim kinase
Linopirdine	3,3-bis(4-pyridinylmethyl)-1-phenylindolin-2-one
L-NAME	$L\text{-}N^G$-nitroarginine methyl ester
MiRPs	MinK-related peptides
MLCK	Myosin light chain kinase
MLCP	Myosin light chain phosphatase

MYPT1	Myosin phosphatase targeting subunit 1
NCX	Sodium-calcium exchanger
NO	Nitric oxide
NSCCs	Non-selective cation channels
N-WASp	Neuronal Wiskott-Aldrich syndrome protein
ODQ	1H-[1,2,4]oxadiazolo[4,3-a]quinoxalin-1-one
PAX	Paxillin
PBS	Phosphate-buffered saline
PCR	Polymerase chain reaction
PdBu	Phorbol 12,13-dibutyrate
PGI_2	Prostacyclin
PIPES	1,4-piperazinediethanesulfonic acid
PKA	Protein kinase A
PKC	Protein kinase C
PKG	Protein kinase G
QPCR	Quantitative reverse transcription PCR
RCAs	Rat cerebral arteries
ROK	RhoA-associated kinase
RyR	Ryanodine receptor
S-1	(*S*)-*N*-[1-(3-morpholin-4-yl-phenyl)-ethyl]-3-phenyl-acrylamide
SAH	Subarachnoid hemorrhage
ScTx1	Stromatoxin
SDS	Sodium dodecyl sulfate
sGC	Soluble guanylyl cyclase
SK_{Ca}	Small conductance Ca^{2+}-activated K^+ channel
SMDS	Smooth muscle dissection solution
SR	Sarcoplasmic reticulum
TASK	Two-pore domain acid-sensitive K^+ channel
TBS	Tris-buffered saline
U46619	9,11-Dideoxy-11α,9α-epoxymethanoprostaglandin $F_{2\alpha}$
VASP	Vasodilator-stimulated phosphoprotein
VGCCs	Voltage-gated Ca^{2+} channels
VSM	Vascular smooth muscle
VSMCs	Vascular smooth muscle cells
XE991	10,10-bis(4-pyridinylmethyl)-9(10H)-anthracenone

Chapter One: General introduction to the molecular basis of myogenic regulation of cerebral arterial diameter

1.1 Cerebral arteries

The brain, known as the "command center", is the most complex organ in the body. Normal function of the brain requires an adequate supply of oxygen and nutrients, as well as the removal of carbon dioxide and metabolic by-products, via the cerebral circulation. The right and left carotid and vertebral arteries are the four major vessels responsible for conducting blood from the heart to the brain. At the base of the brain, the carotid and vertebral arteries, and their associated branches (cerebral arteries, as well as anterior and posterior communicating arteries) connect to form a circle of arteries, known as the Circle of Willis (Padget, 1944; Alpers *et al.,* 1959) (Figure 1.1). Because the arteries form a circle, blockage of any one of the main arteries of the circle does not interrupt flow delivery as the alternative arteries of the circle can maintain flow around the site to support brain activity.

The cerebral arteries that arise from the Circle of Willis consist of three major pairs of vessels: anterior cerebral arteries, middle cerebral arteries and posterior cerebral arteries. These arteries are linked via anterior and posterior communicating arteries. The cerebral arteries are pial arteries on the surface of the brain that extend over all regions of the organ. Penetrating arterioles branch off the pial arteries to supply blood to deeper structures within the brain.

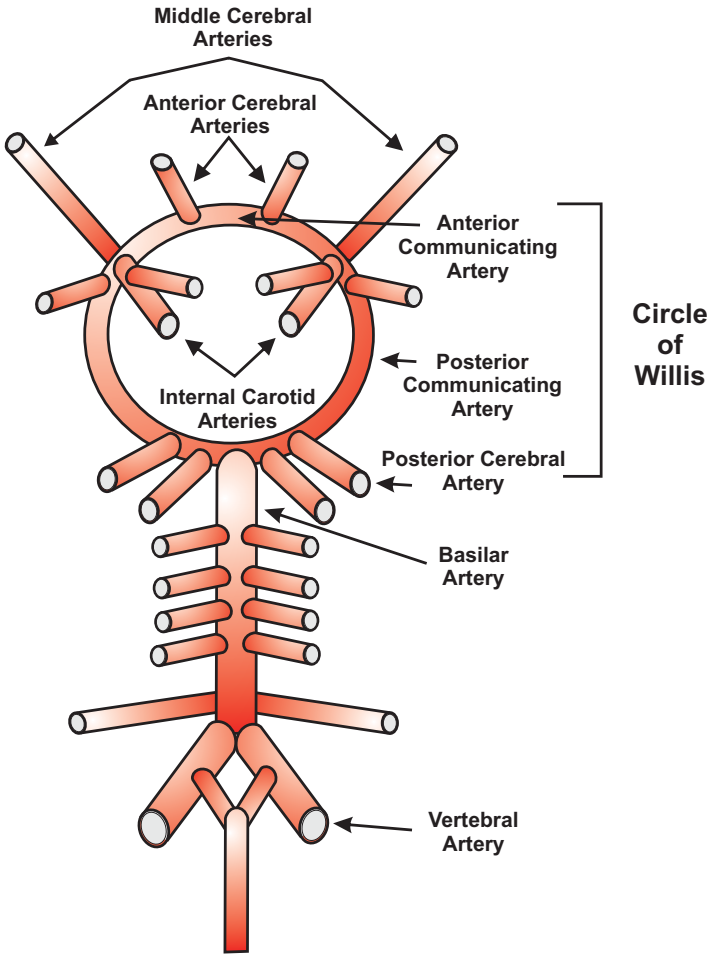

Figure 1.1: The Circle of Willis and cerebral arteries.

The circle of Willis is an anastomotic system of arteries that lies at the base of the brain. The anterior circulation of the Circle of Willis is formed when the internal carotid artery branches into the left and right middle and anterior cerebral arteries. The posterior circulation of the Circle of Willis is formed when the basilar artery branches into the left and right posterior cerebral arteries. The circle is closed by the left and right anterior and posterior communicating arteries.

1.2 Structure of cerebral arteries

The vascular wall of cerebral arteries is composed of three major layers: the tunica adventitia, tunica media and tunica intima (Figure 1.2). The cerebral adventitial layer makes up a smaller proportion of the vessel wall compared to non-cerebral arteries. This layer contains connective tissues including elastin, collagen, fibroblast cells, mast cells and macrophages, which provide anchorage to the surrounding tissue, as well as structural support and protection of the vessel. This layer also contains perivascular nerves that release neurotransmitters that affect vessel diameter (Mulvany & Aalkjaer, 1990).

The tunica media is the major component of the cerebral vascular wall. It is composed of multiple layers of smooth muscle cells. The spindle-shaped smooth muscle cells are arranged circumferentially and packed closely together along the length of the vessel (Figure 1.3). The volume of the media occupied by smooth muscle cells depends on the size of the vessel. For example, an early scanning electron-microscopic study of dog cerebral arteries reported that arteries of >100 μm had four to ten layers of smooth muscle cells, whereas arterioles of ~30-100 μm in diameter had only two to three layers of smooth muscle cells (Shiraishi *et al.,* 1986).

The tunica intima contains a single sheet of endothelial cells. It is separated from the vessel lumen by a basal lamina. Cerebral endothelial cells form specialized, cell-to-cell, tight junctions that contribute to the blood-brain barrier, which permits only a selective trans-endothelial movement of molecules (Ge *et al.,* 2005). Cerebral endothelial cells also send finger-like processes across the internal elastic lamina to make contact

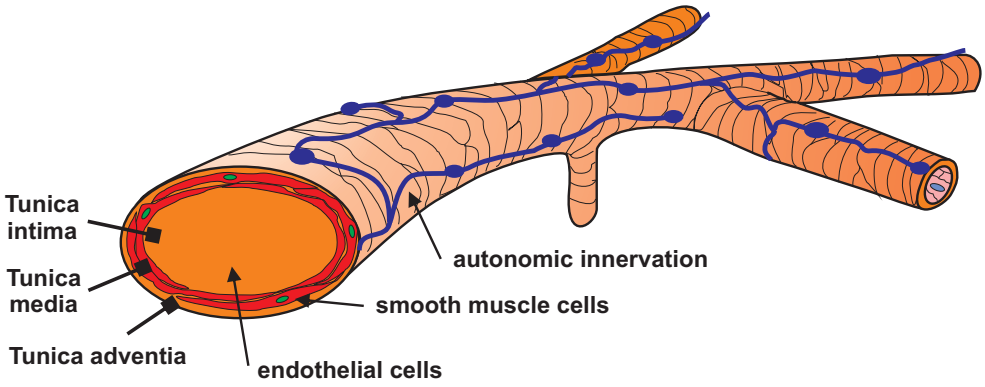

Figure 1.2: Structure of the cerebral artery.

The vascular wall of cerebral arteries is composed of three major layers: the tunica adventitia, tunica media and tunica intima. The tunic intima is composed of a single layer of endothelial cells. The tunic media is composed of multiple layers (2-5) of smooth muscle cells depending on vessel size. The tunic adventitia mainly contains collagen and fibroblast cells. It also contains perivascular nerves that release neurotransmitters to affect smooth muscle cells and endothelial cells within the vessel.

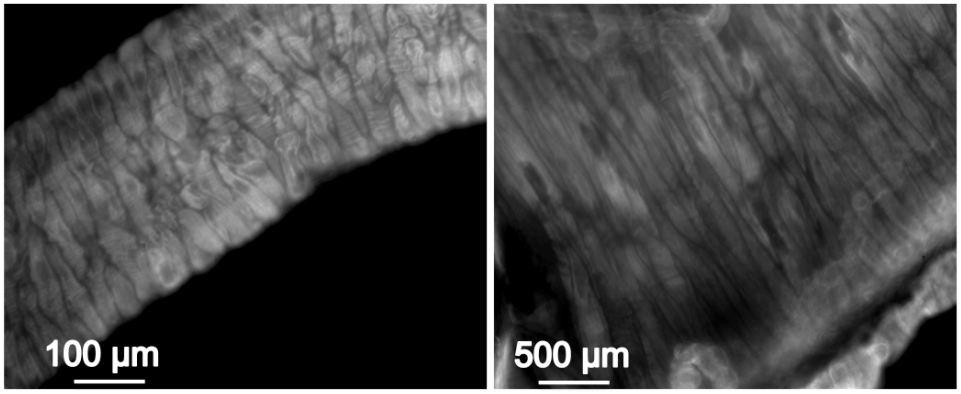

Figure1.3: Vascular smooth muscle cells of rat cerebral arteries.

The endothelium-denuded rat cerebral artery was fixed with 4% paraformaldehyde and permeabilized with 0.1% Triton X-100 before phalloidin staining of F-actin in the smooth muscle cells. Note: the spindle-shaped smooth muscle cells are arranged circumferentially and packed closely together along the length of the vessel.

with medial smooth muscle cells (Andresen *et al.*, 1990). One of the significant features of endothelial cells is their ability to sense shear stress owing to blood flow across the luminal surface of the vascular wall. Signaling of this information to surrounding smooth muscle cells plays a crucial role in regulating cerebral blood flow to the brain under dynamic physiological conditions.

1.3 Cerebral hemodynamics

The cerebral artery can be modeled from a physical perspective as blood flow in a tube. Assuming that blood flow is steady and uniform through a non-distensible, long and straight tube, Ohm's law indicates blood flow (F) is proportional to the pressure drop (ΔP) divided by the vascular resistance to flow (R), $F = \Delta P/R$. In the brain, ΔP represents cerebral perfusion pressure (CPP), which is the difference between the mean pressure in the arteries *versus* in the veins. Venous pressure is normally low (2–5 mmHg), whereas mean arterial pressure is directly related to cardiac output, a function of heart rate and stroke volume. Blood flow is also described by Poiseuielle's law, which states that flow is related to ΔP, blood viscosity (η), the length of the vessel (L), and the fourth power of vessel radius: $F = (\pi \times \Delta P \times r^4)/8\eta L$ (Sumpio, 1993; Cipolla, 2009).

Of all the factors that affect blood flow, vessel radius is the most important. When the blood vessels dilate to twice the normal diameter, the blood flow increases sixteen-fold, whereas when they constrict to one-half of their normal size, flow reduced sixteen-fold. Since a small change in diameter has a huge impact on blood flow, control of arterial diameter plays a crucial role in maintaining appropriate blood supply to the brain under dynamic physiologic conditions (Brekke *et al.*, 2002).

The blood vessel wall is constantly stretched due to transmural pressure, which is the difference between the blood pressure inside the vessel (intraluminal) and the pressure in the surrounding tissue. Wall tension (T) represents the tension within the vessel wall, that can be estimated by Laplace's Law, $T = (P \times R) / M$, where P is the transmural pressure (the pressure difference across the wall), R is the radius of the vessel, and M is the thickness of the wall (Burton, 1951). Since wall tension is directly proportional to the vessel radius, the wall tension of relatively large vessels is significantly higher compared to that of small vessels at the same transmural pressure.

Vascular resistance is defined as the resistance to flow that must be overcome by the cardiac pump (Hilton & Spyer, 1980). The resistance provided by the peripheral circulation is known as the systemic vascular resistance, or the total peripheral resistance. The resistance provided by the vasculature of the lungs is known as the pulmonary vascular resistance. Since vascular resistance is inversely related to the fourth power of vessel radius, it is largely dependent on vessel size. In the peripheral circulation, the vessels that contribute to peripheral resistance are, in general, small arterioles of <100 μm in diameter, as well as small arteries of ~100 to 400 μm in diameter (Harper *et al.*, 1984). The importance of relatively large resistance arteries *versus* small arterioles to total vascular resistance is particularly evident in the brain, where they contribute to more than one-half of vascular resistance (Faraci & Heistad, 1990).

1.4 The myogenic response in control of cerebral arterial diameter

1.4.1 The intrinsic nature of the myogenic response

The myogenic response was discovered more than one hundred years ago by Sir William Bayliss, who observed large increases in the volume of the dog hindlimb

following the release of brief aortic occlusions (Bayliss, 1902). The myogenic response refers to the ability of vessels to constrict in response to pressure elevation and dilate to pressure reduction. As illustrated in Figure 1.4A, after pressure elevation, an initial passive dilation is followed by two phases (transient phase and sustained phase) of constriction, and upon pressure reduction, the vessel transiently collapses, and then dilates. The myogenic response is not present in large conduit vessels, but it is prevalent in resistance arteries and arterioles, as well as some veins and lymphatic vessels (Berczi *et al.,* 1992; Zawieja, 1996).

The myogenic behaviour of resistance arteries can be traced to vascular smooth muscle cells (VSMCs). The myogenic response has been widely studied using isolated, pressurized vessels via a technique widely referred to as pressure myography. This approach allows vessels to be studied *in vitro* at known levels of intraluminal pressure, and in conditions devoid of the extrinsic metabolic, neural or endothelial influences (Folkow, 1949; Davis & Hill, 1999). Figure 1.4B shows a typical pressure myograph recording of the change in rat cerebral arterial diameter in response to a series of intraluminal pressure steps from 10 mmHg to 100 mmHg in increments of 20 mmHg. Note that pressure evokes vessel constriction at >40-60 mmHg. In the absence of extracellular Ca^{2+}, only passive dilation is observed in response to pressure elevation. The difference in diameter in the presence of extracellular Ca^{2+} compared to the passive dilation represents the extent of active myogenic constriction as a result of pressure-dependent activation of myogenic mechanisms inherent to VSMCs.

The physiological operating range of pressures for the myogenic response varies in different vascular beds. For example, cerebral arteries normally exhibit myogenic

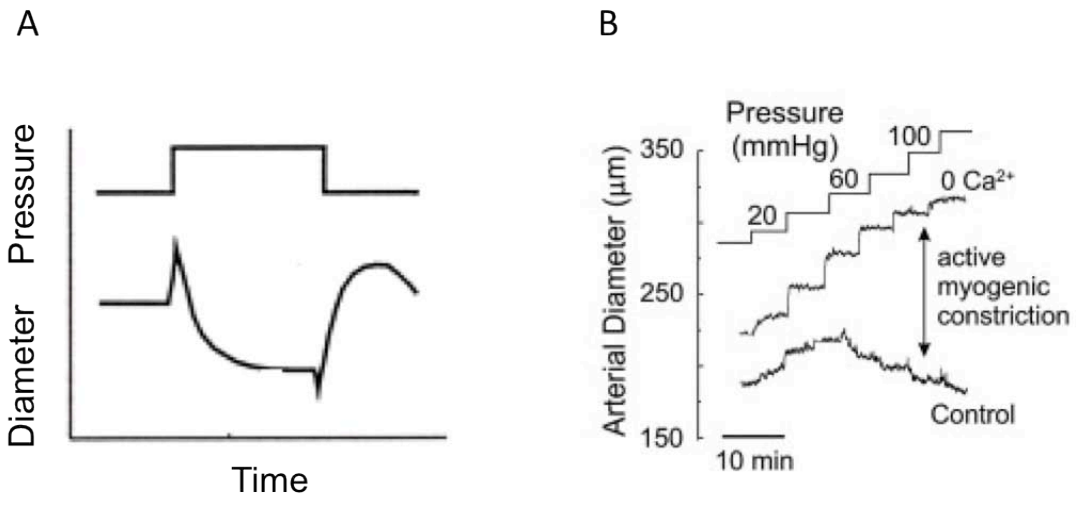

Figure 1.4: The myogenic response of small resistance arteries.

(A) Diagramatic representation of a typical myogenic response of a small resistance artery to a step increase in intraluminal pressure. Intraluminal pressure elevation leads to a spontaneous vasoconstriction after an initial passive dilation, whereas pressure reduction results in a spontaneous vasodilation after a transient constriction. (B) Representative traces of rat middle cerebral arterial diameter in response to step increases in intraluminal pressure between 10 to 20 and 120 mmHg in 20 mmHg increments, in 2.5 mM external Ca^{2+} (Control) followed by zero external Ca^{2+} (0 Ca^{2+})-containing Krebs' solution. The difference in diameter ± external Ca^{2+} represents the active myogenic constriction. Note the myogenic constriction is enhanced concomitant to pressure elevation (at >~40 mmHg).

constriction between ~60 and 140 mmHg (Knot & Nelson, 1998; Osol *et al.,* 2002), whereas penetrating arterioles are active even at low pressures of ~20 mmHg, and renal afferent arterioles are active even at a very high pressure of ~200 mmHg (Loutzenhiser *et al.*, 2006).

The extent of myogenic constriction also varies among vascular beds and species. For example, small mesenteric arteries exhibit a weak myogenic response, whereas similar sized cerebral or skeletal muscle arterioles develop a strong myogenic response, and rat cerebral arteries (RCAs) have a larger myogenic response compared to mouse cerebral arteries (Schubert & Mulvany, 1999). The molecular basis of these differences is not known.

1.4.2 The physiological importance of the myogenic response

The myogenic response is crucial for autoregulation of blood flow to the brain (Johnson, 1986). Blood flow autoregulation allows the brain to maintain relatively constant blood flow despite changes in perfusion pressure within the physiological range. Normal cerebral blood flow is maintained at approximately 55 mL per 100 g of brain tissue per minute when cerebral perfusion pressure is in the range of ~50-140 mmHg, values of pressure that are consistent with the operating pressure range for the myogenic response of pressurized cerebral arteries (Figure 1.5) (Cipolla, 2009). Beyond this range, autoregulation is lost, which can cause a nearly two-fold to three-fold change in cerebral blood flow. Significant brain injury always occurs when the autoregulation of blood flow is impaired. For instance, an acute elevation in intravascular pressure above the autoregulatory limit can induce forced dilation of cerebral arteries, which may lead to

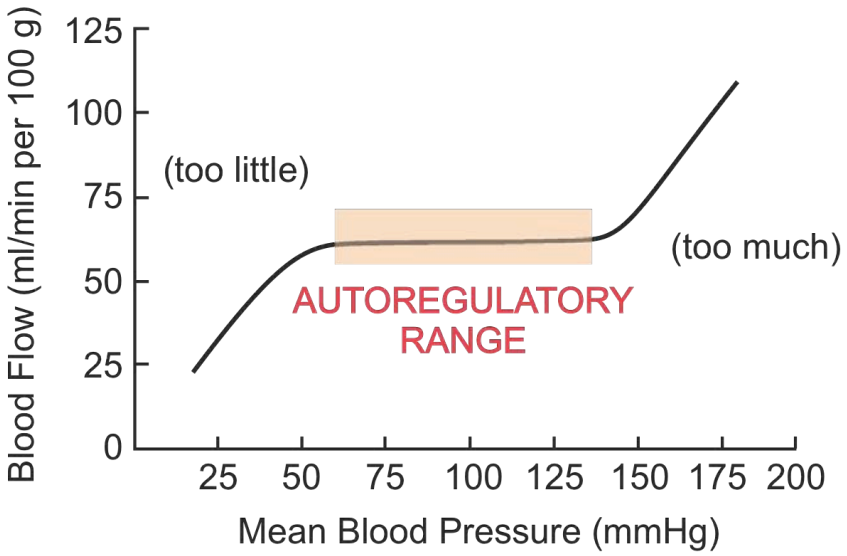

Figure 1.5: Relationship between blood flow and perfusion pressure.

The myogenic response permits constant blood flow over a wide range of pressure between ~50 and ~140 mmHg in rat cerebral arteries. Outside the autoregulatory pressure range, there is either too little or too much blood flow owing to the loss of the myogenic regulation of cerebral arterial diameter.

autoregulatory breakthrough, blood-brain barrier disruption and edema formation (Euser & Cipolla, 2007).

An abnormal myogenic response is a hallmark of a variety of diseases. Enhanced myogenic constriction at low pressure is observed, for example, in hypertension, cerebral vasospasm, hemorrhagic stroke, and chronic heart failure. Conversely, attenuated myogenic constriction is associated with endotoxic shock, cerebral hyperaemia, cerebral microhemorrhage and Alzheimer's disease (Gschwend *et al.,* 2003; Izzard *et al.,* 2003; Sonoyama *et al.,* 2007; Ren *et al.,* 2010; Ryan *et al.,* 2011; Giles *et al.,* 2012).

The presence of an inappropriate myogenic response is associated with significant reduction in neurological function (Olsen *et al.,* 1981; Davis & Hill, 1999; Osol *et al.,* 2002; Khavandi *et al.,* 2009; Hill & Davis, 2012): (1) it impairs the fundamental mechanism of blood flow autoregulation in the brain, (2) it disrupts the establishment of a regional blood flow reserve, which allows local flow to match metabolic demand by permitting reactive vasodilation from a partially constricted state, (3) it fails to provide a critical shield that protects brain capillaries and the blood-brain barrier from damage by elevated pressure, and (4) it may lead to abnormal vascular remodeling within the vessel wall associated with hypertrophy and/or hyperplasia. For instance, in hypertension, impaired myogenic dilation at low perfusion pressure disrupts blood flow reserve and increases the risk of ischemia (Cipolla *et al.,* 2001; Coulson *et al.,* 2002; Heagerty *et al.,* 2010). In type-2 diabetes, the loss of the myogenic response results in uncontrolled, elevated levels of blood flow that may be accompanied by blood-brain barrier disruption, small vessel rupture, increased intracranial pressure and edema (Sonoyama *et al.,* 2007; Khavandi *et al.,* 2009).

1.4.3 Modulation of the intrinsic myogenic response via extrinsic factors

Although the myogenic response is inherent to VSMCs, it can be modulated by various extrinsic factors that permit local control of vascular tone and blood flow to match dynamic physiological demands. This extrinsic modulation is accomplished via numerous metabolic, neural or endothelial factors, that evoke vasoconstriction or vasodilation that are superimposed on a basal level of myogenic tone development. Therefore, although extrinsic factors do not directly participate in the myogenic regulation of arterial diameter, they are capable of modulating arterial diameter in response to various stimuli (Figure 1.6).

In the cerebral circulation, the major extrinsic factors that contribute to the regulation of arterial diameter include: (1) neurotransmitters released by sympathetic nerve fibres (e.g. serotonin), (2) circulating factors (e.g. angiotensin II), (3) metabolic products (e.g. oxygen, carbon dioxide) and (4) endothelial-derived vasoactive factors (Davis & Hill, 1999; Schubert & Mulvany, 1999; Andresen *et al.,* 2006).

Among the extrinsic factors, endothelial factors are the most abundant, and chemically, as well as functionally diverse. They include constrictors (e.g. endothelin-1, thromboxane A2) and dilators (e.g. nitric oxide (NO), prostacyclin (PGI_2), endothelium-derived hyperpolarizing factor (EDHF)) (Feliciano *et al.,* 1993; Andresen *et al.,* 2006). NO-mediated vessel vasodilation will be discussed in Chapter 5. PGI_2 is the most extensively studied cyclooxygenase (COX) metabolite in cerebral endothelium. Following its synthesis via the COX pathway, PGI_2 diffuses to the smooth muscle, where it activates adenylyl cyclase through G-protein-coupled receptors, leading to an increase in cyclic AMP content and protein kinase A activity (Bogatcheva *et al.,* 2005).

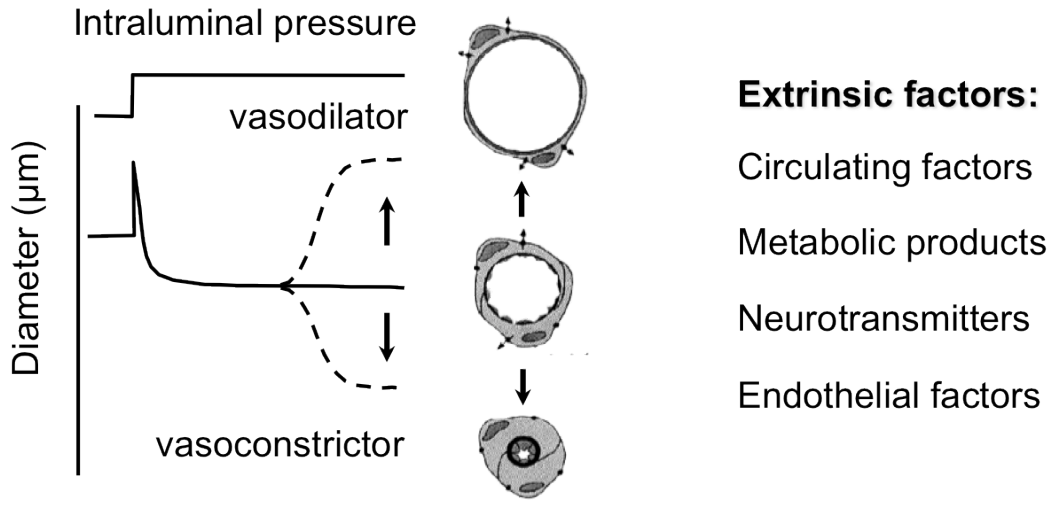

Figure 1.6: Intrinsic myogenic mechanisms are modulated by extrinsic factors.
Control of cerebral arterial diameter is dependent on myogenic mechanisms inherent to smooth muscle cells that are subjected to modification by a variety of extrinsic factors, including: circulating factors, metabolic products, neurotransmitters and endothelial factors. These extrinsic factors can evoke vasoconstriction or vasodilation in the presence of a basal level of myogenic tone, permitting local control of vascular tone and blood flow to match physiological demands.

Abnormal synthesis of PGI_2 in the cerebral circulation was found to be associated with many pathological conditions, such as hypertension (Giles *et al.,* 2012).

EDHF-mediated vessel dilation is described as a phenomenon independent of NO and COX metabolite-mediated dilation. EDHF arises from endothelial cells and induces hyperpolarization of smooth muscle. The concept of EDHF came from early experiments showing that some dilators can cause endothelial membrane potential (E_m) hyperpolarization, followed by smooth muscle E_m hyperpolarization. Later studies indicate that this event is a result of electrical coupling endothelial hyperpolarization due to intermediate and small conductance Ca^{2+}-activated K^+ (IK_{Ca} and SK_{Ca}) channels, and electrical coupling with smooth muscle cells via myoendothelial gap junctions. In addition to a direct spread of E_m hyperpolarization, K^+ released from endothelial SK_{Ca} and IK_{Ca} channels was suggested to cause smooth muscle hyperpolarization by activating smooth muscle inwardly rectifying K^+ (K_{ir}) channels and/or Na^+/K^+ ATPase activity (Edwards *et al.,* 1998; Golding *et al.,* 2002). Recent evidence suggests that some small diffusible molecules, such as hydrogen peroxide (H_2O_2) and hydrogen sulfide (H_2S) may also contribute to EDHF-mediated vessel dilation (Zhao & Wang, 2002; Shimokawa & Hiroaki, 2010; Ohashi *et al.,* 2012).

1.5 Contemporary view of the molecular basis of the myogenic response

Considering that myogenic regulation of arterial diameter plays an indispensable role in determining blood flow, it is of great importance to understand the molecular basis of the myogenic response, as this knowledge will provide crucial insights concerning the nature of the defects associated with the myogenic response in disease.

1.5.1 Traditional Ca^{2+}-dependent mechanism

Considerable progress has been made in determining the molecular mechanisms of the myogenic response, but a complete picture is yet to emerge. The traditional working model (Knot & Nelson, 1998; Davis & Hill, 1999) holds that myogenic constriction is a result of the following cellular events: first, pressure elevation induces E_m depolarization due to the activation of non-selective cation channels (NSCCs) and possibly stretch-activated chloride or Ca^{2+} channels (Doughty & Langton, 2001; Brayden *et al.,* 2008; Sharif-Naeini *et al.,* 2008). Integrins and G protein-coupled receptors (GPCR) have been postulated to serve as the myogenic mechanosensors, but the identity of the mechanosensor that reacts to pressure-induced changes in wall stress remains controversial (Martinez-Lemus *et al.,* 2005; Mederos y Schnitzler *et al.,* 2008). Second, E_m depolarization induces the activation of voltage-gated Ca^{2+} channels (VGCCs), followed by an increase in intracellular Ca^{2+} ($[Ca^{2+}]_i$). L-type Ca^{2+} channels are thought to make a major contribution to this Ca^{2+} entry, yet a role of T-type Ca^{2+} channels has also been documented (VanBavel *et al.,* 2002; Abd El-Rahman *et al.,* 2013). Third, free Ca^{2+} binds to calmodulin (CaM) forming the Ca^{2+}-CaM complex that activates myosin light chain kinase (MLCK). Fourth, MLCK phosphorylates the 20 kDa myosin regulatory light chain (LC_{20}) leading to actomyosin ATPase activation, cross-bridge cycling and smooth muscle contraction.

1.5.1.1 E_m and $[Ca^{2+}]_i$ in the myogenic response

The importance of E_m depolarization and $[Ca^{2+}]_i$ elevation in mediating myogenic constriction is well characterized by many studies using pressure myography. For example, an increase in intraluminal pressure from 10 to 60 mmHg in pressurized RCAs

was associated with E_m depolarization from ~-65 to -40 mV and an increase in $[Ca^{2+}]_i$ from ~100 to 200 nM (Osol *et al.,* 2002). High concentrations of external K^+ also evoked E_m depolarization leading to vessel constriction, whereas inhibition of VGCCs or removal of extracellular Ca^{2+} resulted in vessel dilation (Knot & Nelson, 1998).

Although Ca^{2+} influx through VGCCs is believed to be the primary determinant of the level of $[Ca^{2+}]_i$, other sources of Ca^{2+} are also present (Davis & Hill, 1999; Hill *et al.,* 2001); NSCCs and reverse mode activity of the sodium-calcium exchanger (NCX) have been suggested to contribute to Ca^{2+} entry (Potocnik & Hill, 2001; Brayden *et al.,* 2008; Raina *et al.,* 2008). $[Ca^{2+}]_i$ is also affected by Ca^{2+} release from intracellular sarcoplasmic reticulum (SR) stores via inositol 1,4,5-trisphosphate (IP3) receptors and ryanodine (RyR) receptors (Hill *et al.,* 2001; Thorneloe & Nelson, 2005). In addition, pressure elevation was reported to induce SR-dependent Ca^{2+} sparks (a localized transient release of Ca^{2+}) and Ca^{2+} waves (a propagating slower temporal release of Ca^{2+}) (Nelson *et al.,* 1995; Jaggar, 2001; Mufti *et al.,* 2010). The role of Ca^{2+} sparks will be discussed in Chapter Three (3.1.2); in brief, it exerts a negative control of $[Ca^{2+}]_i$ via activation of large conductance Ca^{2+}-activated K^+ (BK_{Ca}) channels and an associated hyperpolarization (Nelson *et al.,* 1995). The role of Ca^{2+} waves in the myogenic response remains controversial. Jaggar (2001) concluded that Ca^{2+} waves do not contribute significantly to global $[Ca^{2+}]_i$ and, therefore, were not important to the development of the myogenic response. This view was based on a consideration of wave frequency, duration and the number of myocytes exhibiting waves. In contrast, Mufti *et al.* (2011) showed that suppression of Ca^{2+} waves was associated with a reduction in the phosphorylation of

LC_{20} and myogenic constriction, suggesting a role for Ca^{2+} waves in the myogenic response.

1.5.1.2 Ion channels in control of E_m

E_m is a result of a separation of positive and negative-charged ions across the cell membrane. E_m depolarization results from a flow of cations into, or anions out of the cell that induces a reduction of charge separation, and a less negative membrane potential. In contrast, E_m hyperpolarization results from a flow of anions into, or cations out of the cell that induces an increase of charge separation, and a more negative membrane potential.

In VSMCs, E_m is tightly controlled by a number of ion channels present in the smooth muscle plasma membrane (Thorneloe & Nelson, 2005) (Figure 1.7). Activation of chloride channels, NSCCs and VGCCs evokes E_m depolarization, whereas activation of K^+ channels leads to an efflux of K^+ and promotes E_m hyperpolarization. Expression of a broad complement of K^+ channels has been detected in VSMCs. To date, five major types of K^+ channel have been described: voltage-gated K^+ (K_v), BK_{Ca}, ATP-sensitive K^+ (K_{ATP}), K_{ir} channels and the recently identified two-pore domain acid-sensitive K^+ (TASK) channels (Nelson & Quayle, 1995; Standen & Quayle, 1998; Cole *et al.,* 2005; Ko *et al.,* 2008).

The role of K_v and BK_{Ca} channels in control of myogenic depolarization will be described in detail in Chapter 3.1.2. K_{ATP}, K_{ir} and TASK channels are not able to directly participate in control of the myogenic depolarization because their activity is E_m independent. On the other hand, they do contribute to background K^+ conductance that affects resting E_m and, therefore, basal VSM tone (Quayle *et al.,* 1997; Gurney *et al.,* 2002; Gurney *et al.,* 2003; Olschewski *et al.,* 2006; Ko *et al.,* 2008).

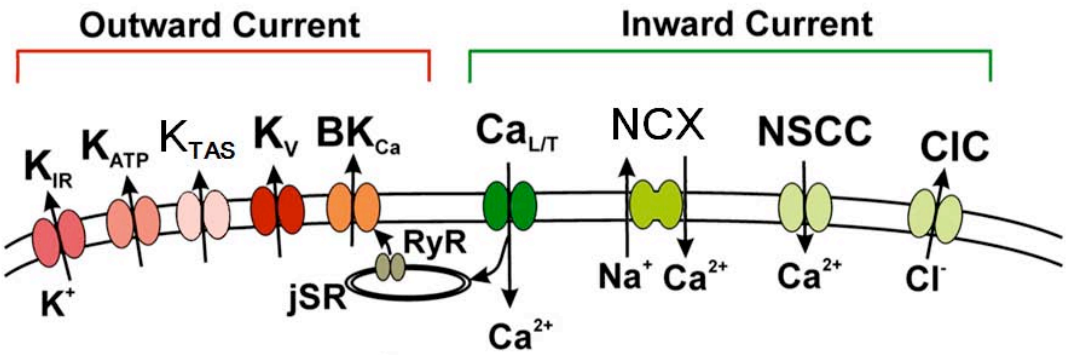

Figure 1.7: Ion channels in control of vascular smooth muscle E_m and Ca^{2+} influx.
The E_m of vascular smooth muscle cells is tightly controlled by a number of ion channels present in the plasma membrane. Activation of chloride channels (CIC), non-selective cation channels (NSCC), or L/T-type voltage-gated Ca^{2+} channels ($Ca_{L/T}$) evokes E_m depolarization, whereas E_m hyperpolarization is mediated by activation of different types of K^+ channels, including: voltage-gated K^+ (K_v), large-conductance Ca^{2+} -activated K^+ (BK_{Ca}), ATP-sensitive K^+ (K_{ATP}), inwardly rectifying K^+ (K_{ir}) and two-pore domain acid-sensitive K^+ (TASK) channels. Ca^{2+} influx is proposed to be carried by $Ca_{L/T}$, NSCC and possibly reverse mode activity of the Na^+-Ca^{2+} exchanger (NCX). Ca^{2+} entry from $Ca_{L/T}$ following E_m depolarization is the most significant pathway responsible for the increase in $[Ca^{2+}]_i$ during vascular smooth muscle contraction.

1.5.1.3 MLCK in the myogenic response

Cross-bridge cycling plays an important role in force generation during the myogenic response, and is primarily determined by thick filament (myosin) regulation. Smooth muscle myosin is composed of two heavy chains with actin binding domains and ATP pockets, two 17 kDa essential light chains and two 20 kDa regulatory light chains (Figure 1.8). LC_{20} monophosphorylation at amino acid residue serine-19 (Ser19) or diphosphorylation at Ser19 and threonine-18 leads to an increase in myosin MgATPase activity and the activation of cross-bridge cycling (Cole & Welsh, 2011).

LC_{20} phosphorylation is determined by the balance between MLCK and myosin light chain phosphatase (MLCP) activities (Figure 1.8). The traditional view of the myogenic mechanism holds that the change of LC_{20} phosphorylation associated with myogenic constriction is exclusively accomplished by MLCK. Pressure elevation induces an increase in $[Ca^{2+}]_i$ promoting Ca^{2+} binding to form $(Ca^{2+})_4$-CaM that activates MLCK and phosphorylates LC_{20} (Knot & Nelson, 1998; Davis & Hill, 1999; Schubert & Mulvany, 1999). Direct analysis of skeletal muscle arterioles and cerebral arteries demonstrated that the rise in phospho-LC_{20} content was coincident with the rise in $[Ca^{2+}]_i$ in response to pressure elevation. Also, the MLCK inhibitor, ML-7, was able to suppress the increased phospho-LC_{20} content as well as the myogenic constriction. Treatment with VGCC blockers or zero Ca^{2+} external solution induced full dilation of pressurized vessels (Zou *et al.,* 1995; Knot & Nelson, 1998; Zou *et al.,* 2000; Johnson *et al.,* 2009b; El-Yazbi *et al.,* 2010; Moreno-Dominguez *et al.,* 2013; Abd El-Rahman *et al.,* 2013).

However, a number of observations imply that the level of LC_{20} phosphorylation is not exclusively dependent on MLCK activity. For instance, in RCAs and skeletal

A

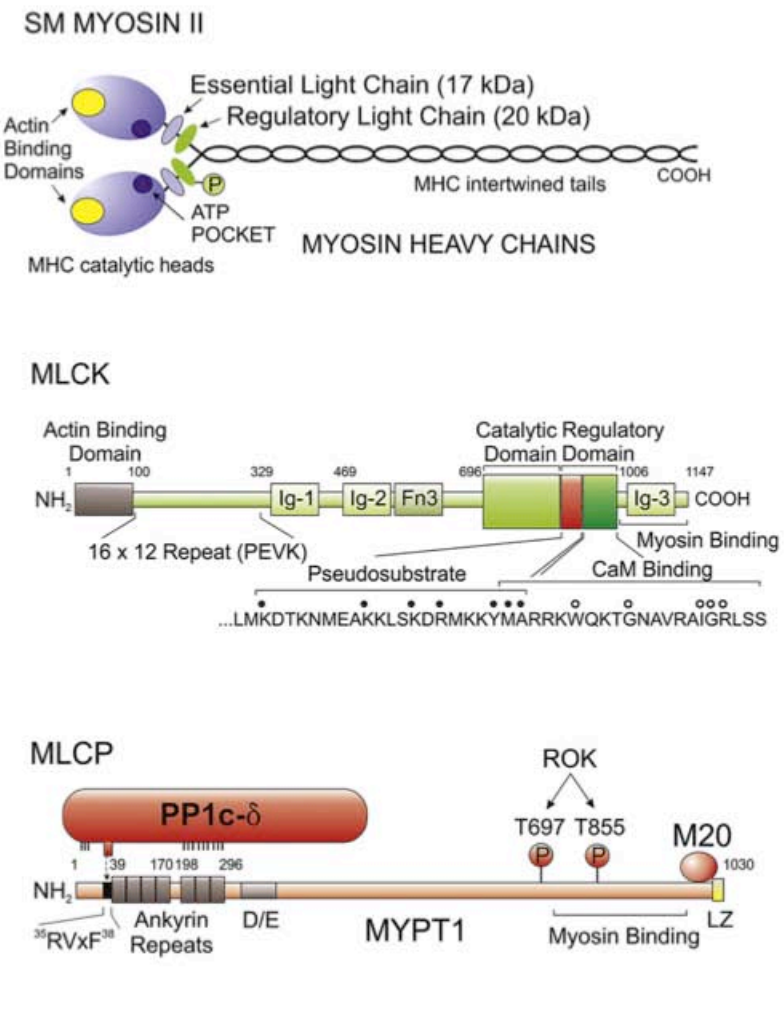
SM MYOSIN II
Essential Light Chain (17 kDa)
Regulatory Light Chain (20 kDa)
Actin Binding Domains
MHC intertwined tails
COOH
P
ATP POCKET
MYOSIN HEAVY CHAINS
MHC catalytic heads
MLCK
Actin Binding Domain
Catalytic Regulatory Domain Domain
1
100
329
469
696
1006
1147
NH2
Ig-1
Ig-2
Fn3
Ig-3
COOH
16 x 12 Repeat (PEVK)
Pseudosubstrate
CaM Binding
Myosin Binding
...LMKDTKNMEAKKLSKDRMKKYMARRKWQKTGNAVRAIGRLSS
MLCP
ROK
PP1c-δ
T697 T855
M20
1030
1
39
170198
296
NH2
35RVxF38
Ankyrin Repeats
D/E
MYPT1
Myosin Binding
LZ

B

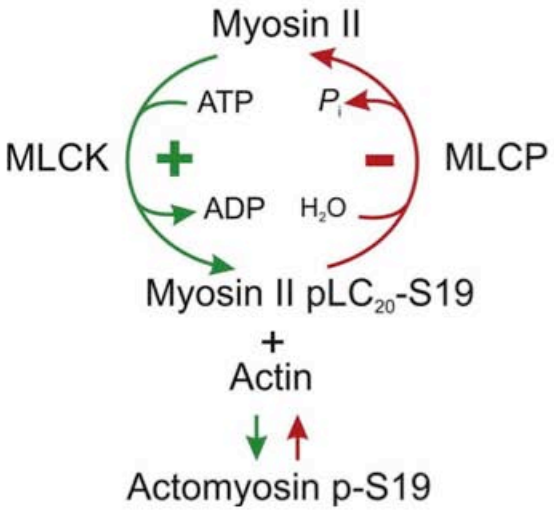
Myosin II
ATP
Pi
MLCK
+
−
MLCP
ADP
H2O
Myosin II pLC20-S19
+
Actin
Actomyosin p-S19

Figure 1.8: Smooth muscle myosin II, myosin light chain kinase and myosin light chain phosphatase.

(A) Diagramatic representations of smooth muscle myosin II, myosin light chain kinase (MLCK) and myosin light chain phosphatase (MLCP). Smooth muscle myosin II is composed of two heavy chains (MHC) with actin binding domains and ATP pockets, two 17 kDa essential light chains and two 20 kDa regulatory light chains (LC_{20}). MLCK is composed of an N-terminal actin binding domain, a C-terminal catalytic domain, a pseudosubstrate autoinhibitory domain and a (Ca^{2+})-CaM binding regulatory domain. MLCP is composed of a catalytic subunit (PP1cδ), a myosin phosphatase targeting subunit (MYPT1) and a small subunit, M_{20} of unknown function. Threonine-697 (T697) and threonine-855 (T855) (rat numbering) are two major sites on MYPT1 that exhibit ROK-mediated phosphorylation. (B) The level of LC_{20} phosphorylation is determined by the balance between MLCK and MLCP activities. Phosphorylation of LC_{20} at serine-19 (S19) permits myosin ATPase activation, leading to cross-bridge cycling and, therefore, force generation. (Figure is modified from Cole & Welsh 2010; Arch Biochem Biophys 510: 160-173.)

muscle arterioles, although significant depolarization (~25 mV) occurred between 0 and 60 mmHg, there was relatively little further depolarization (~5-10 mV) between 60 and 120 mmHg, and myogenic tone development increased substantially as evidenced by the maintenance or further reduction of arterial diameter. Similarly, there was a dissociation of tone development and arterial wall $[Ca^{2+}]_i$, since $[Ca^{2+}]_i$ did not change substantially above ~60 mmHg (Knot & Nelson, 1998; Davis & Hill, 1999; Hill *et al.*, 2001; Osol *et al.*, 2002; Kotecha & Hill, 2005).

1.5.2 The Ca^{2+} sensitization-dependent mechanism

1.5.2.1 Myosin light chain phosphatase

There is abundant evidence that in addition to Ca^{2+}-CaM-MLCK control of LC_{20} phosphorylation, other mechanisms are also involved (Somlyo & Somlyo, 2003; Ihara & MacDonald, 2007; Walsh, 2011). One mechanism, referred to as Ca^{2+} sensitization, involves the inhibition of MLCP via the activation of RhoA/Rho-associated kinase (ROK) or protein kinase C (PKC) signaling, leading to an increase in LC_{20} phosphorylation and force generation in the absence of a further change in $[Ca^{2+}]_i$.

MLCP is a type I protein serine/threonine phosphatase. The native enzyme is a trimer composed of a ~38 kDa catalytic subunit (PP1cδ), a 110~130 kDa myosin phosphatase targeting subunit 1 (MYPT1) and a ~20 kDa subunit with unknown function (Figure 1.8) (Somlyo & Somlyo, 2003; Cole & Welsh, 2011). MYPT1 is a major regulator of MLCP activity, with phosphorylation of several sites known to exert a strong inhibitory effect on MLCP activity. In agonist-induced smooth muscle contraction, activation of $G_{12/13}$-coupled receptors evokes Ca^{2+} sensitization via activation of the small GTPase, RhoA (Somlyo & Somlyo, 2000), which subsequently activates ROK resulting

in MYPT1 phosphorylation and inhibition of MLCP activity (Sward *et al.,* 2003; Somlyo & Somlyo, 2004). Threonine-697 (Thr697) and threonine-855 (Thr855) in the rat sequence (Thr695 and Thr850 in the human sequence) are two major sites on MYPT1 that exhibit ROK-mediated phosphorylation (Feng *et al.,* 1999; Muranyi *et al.,* 2005). Furthermore, previous studies indicate the cross-talk between ROK and cyclic nucleotide-dependent kinase signaling pathways in the regulation of the MLCP activity. Serine-696 (Ser696) and Serine-854 (Ser854) on MYPT1 may be phosphorylated in response to protein kinase A (PKA) or protein kinase G (PKG) stimulation, leading to an inhibitory effect on ROK-mediated MYPT1 phosphorylation on Thr-697 and Thr-855 (Grassie *et al.,* 2012). In addition, activation of Gq-coupled receptors induces Ca^{2+} sensitization via PKC activation (Somlyo & Somlyo, 2003; Eto, 2009). PKC phosphorylates a 17-kDa PKC-potentiated protein phosphatase 1 inhibitor protein (CPI-17) at threonine 38, with the phosphorylated CPI-17 a potent inhibitor of MLCP that directly suppresses PP1c-δ activity (Eto *et al.,* 1995; Eto, 2009). In addition, ROK-mediated CPI-17 phosphorylation has been reported in the context of agonist-induced smooth muscle contraction (Pang *et al.,* 2005; Sakai *et al.,* 2005; Eto, 2009).

1.5.2.2 Ca^{2+} sensitization in the myogenic response

The Ca^{2+} sensitization mechanism was first identified in the context of agonist-induced smooth muscle contraction (Somlyo & Somlyo, 2004; Hirano, 2007). Later on, considerable evidence was provided to indicate that ROK-mediated Ca^{2+} sensitization might also contribute to the myogenic response. For instance, inhibition of ROK signaling via ROK inhibitor or overexpression of dominant negative RhoA or ROK suppressed myogenic constriction in the absence of significant change in $[Ca^{2+}]_i$, or under

conditions wherein E_m was held constant owing to exposure to high concentrations of external K^+, or when $[Ca^{2+}]_i$ was constant due to α-toxin permeabilization (VanBavel *et al.,* 2001; Lagaud *et al.,* 2002; Bolz *et al.,* 2003; Gokina *et al.,* 2005; Jarajapu & Knot, 2005; Schubert *et al.,* 2008). Furthermore, activation of ROK-mediated Ca^{2+} sensitization was directly confirmed by the recent development of a biochemical approach that permits direct quantification of phosphoprotein content (e.g. phospho-LC_{20}, phospho-MYPT1) in a single segment of pressurized artery. Specifically, in RCAs and skeletal muscle arterioles, myogenic constriction was found to be associated with a coincident increase in LC_{20} phosphorylation at Ser19 and MYPT1 phosphorylation at Thr855 (yet not at Thr696). Inhibition of ROK with H1152 significantly inhibited myogenic constriction and suppressed the increased phosphorylation of MYPT1 and LC_{20} associated with pressure elevation (Johnson *et al.,* 2009b; Moreno-Dominguez *et al.,* 2013).

In addition, a recent study indicates that ROK-mediated Ca^{2+} sensitization is involved in the integration of extrinsic vasoconstrictor stimuli with the myogenic response. In RCAs, vasoconstriction induced by serotonin at 10 mmHg was not associated with a change in MYPT1 phosphorylation. However, a combination of serotonin treatment with an increase in intraluminal pressure to 60 mmHg elicited an increase in MYPT1 phosphorylation, indicating the activation of ROK-mediated Ca^{2+} sensitization (El-Yazbi *et al.,* 2010).

It is important to note that although CPI-17 phosphorylation contributes to Ca^{2+} sensitization in mediating agonist-induced VSM contraction (e.g. phorbol 12,13-dibutyrate (PdBu)-induced contraction) (Eto *et al.,* 1995; Sakai *et al.,* 2005; Wang *et al.,* 2009; El-Yazbi *et al.,* 2010; Wang *et al.,* 2012), direct biochemical analysis did not detect

a change in CPI-17 phosphorylation in the myogenic response in RCAs or rat skeletal muscle arterioles (Johnson *et al.,* 2009b; Moreno-Dominguez *et al.,* 2013). Also, a change in CPI-17 phosphorylation was not detected in serotonin-induced vasoconstriction of RCAs in the presence or absence of myogenic constriction (El-Yazbi *et al.,* 2010). These observations suggest that CPI-17 phosphorylation-mediated Ca^{2+} sensitization is not involved in the myogenic response.

1.5.3 The Cytoskeleton reorganization-dependent mechanism

1.5.3.1 Dynamic cytoskeleton reorganization

The term actin cytoskeleton refers to the collection of actins and actin-associated proteins within cells. Actins are connected to each other at cytosolic dense bodies and anchored to the plasma membrane at focal adhesions in smooth muscle cells. Focal adhesions are large complexes of proteins located at the plasma membrane that include, for example, actin, integrin, actin-binding proteins and signaling proteins. The interconnection of these elements permits force transmission between the contractile filaments and plasma membrane/extracellular matrix (Zhang & Gunst, 2008). It has long been assumed that in comparison to the dynamic cytoskeletal structure of migrating or proliferating cells, contractile smooth muscle cells possess a largely static actin cytoskeleton. However, emerging evidence suggests that the actin cytoskeleton undergoes a dynamic remodelling during smooth muscle contraction/relaxation, and may actually contribute to smooth muscle force generation (Kim *et al.,* 2008a; Zhang & Gunst, 2008; Walsh & Cole, 2012) (Figure 1.9).

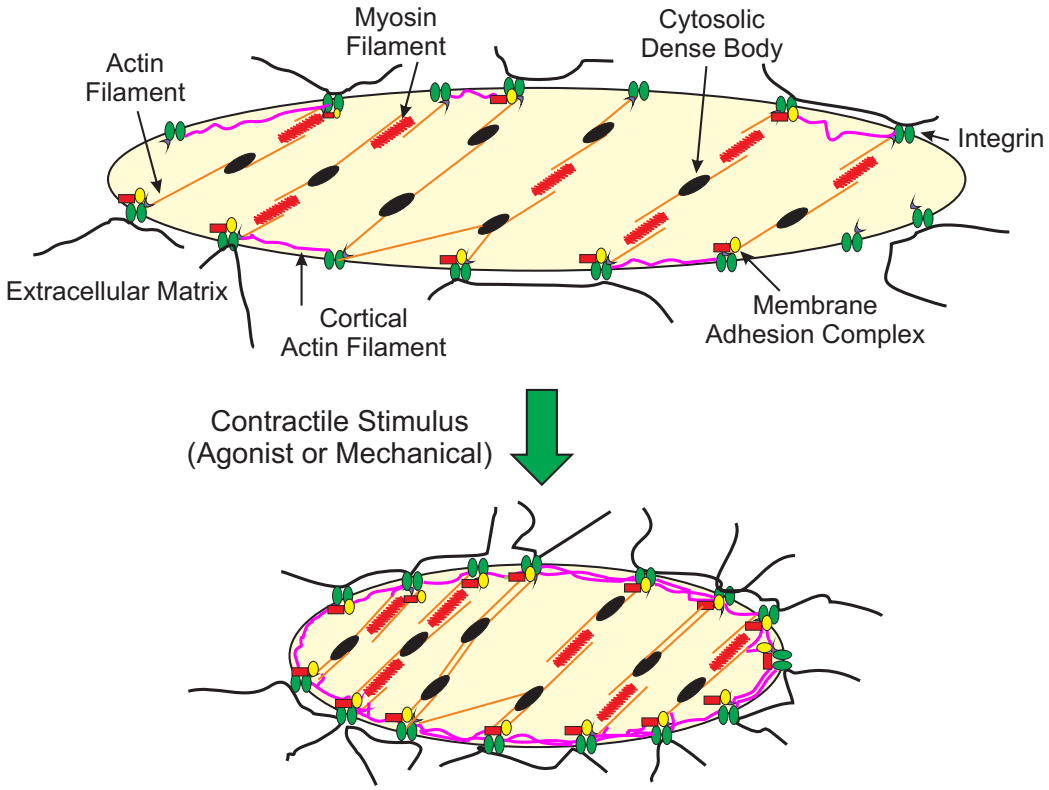

Figure 1.9: Diagrammatic representation of cytoskeleton reorganization in association with smooth muscle contraction.

Activation of smooth muscle cells by contractile stimuli promotes *de novo* actin polymerization, which increases F-actin content from an available cytosolic pool of G-actin under the cell membrane and around cytosolic dense bodies. The increased cortical actin network (colored in magenta) and additional contacts to cytosolic dense bodies strengthen the actin cytoskeleton, and enhance force transmission from the contractile apparatus to the cell membrane and extracellular matrix. (Figure is modified from Gunst & Zhang 2008; Am J Physiol Cell Physiol 295:C576-C587.)

It is now proposed that smooth muscle actin includes 'contractile actin' that interacts with myosin and contributes to cross-bridge cycling, and 'cytoskeletal actin' that is not involved in cross-bridge cycling (Kim *et al.,* 2008a; Zhang & Gunst, 2008; Walsh & Cole, 2012). Contractile actin is mainly stabilized in the form of filamentous actin (F-actin), whereas the cytoskeletal actin exists as either F-actin or globular actin (G-actin). The transformations from G-actin to F-actin, and F-actin to G-actin, are referred to as actin polymerization and depolymerization, respectively. The model of dynamic cytoskeleton reorganization holds that a reversible actin polymerization and depolymerization occurs within the cytoskeletal actin pool during smooth muscle contraction and relaxation. It is believed that activation of smooth muscle cells by contractile stimuli promotes *de novo* actin polymerization, which increases F-actin content from an available cytosolic pool of G-actin under the cell membrane and around cytosolic dense bodies. The increased cortical network and additional contacts to cytosolic dense bodies strengthen the actin cytoskeleton, and enhance force transmission from the contractile apparatus to the cell membrane and extracellular matrix.

It is also proposed that enhanced force transmission is associated with dynamic assembly of cytoskeletal proteins within focal adhesions prior to actin polymerization (Zhang & Gunst, 2008). The recruitment of various cytoskeletal protein such as β-integrin, focal adhesion kinase (FAK), paxillin (PAX), vinculin, α-actinin, neuronal Wiskott-Aldrich syndrome protein (N-WASp) and vasodilator-stimulated phosphoprotein (VASP) to the focal adhesion sites of airway and vascular smooth muscle cells has been documented in response to contractile stimuli (Opazo Saez *et al.,* 2004; Zhang *et al.,* 2005; Zhang & Gunst, 2006; Kim *et al.,* 2008b; Kim *et al.,* 2010a). The recruitment of

these structural and signaling proteins to the cell membrane may serve to catalyze actin polymerization and strengthen the network of newly formed actin filaments for enhanced force transmission (Figure 1.10). However, the mechanism by which proteins are recruited to adhesion sites in response to various stimuli and whether dynamic protein recruitment is indispensible for mediating actin polymerization remains unclear.

1.5.3.2 Cytoskeleton reorganization in smooth muscle contraction

Actin polymerization-dependent cytoskeleton reorganization can be monitored by measuring the amount of G-actin and/or F-actin by several methods, including DNase I inhibition assay, fluorescence imaging, electron microscopy and differential centrifugation (Mehta & Gunst, 1999; Barany *et al.,* 2001; Cipolla *et al.,* 2002; Herrera *et al.,* 2004; Flavahan *et al.,* 2005; Kim *et al.,* 2010a ; Zhang *et al.,* 2010). A large body of evidence suggests that smooth muscle contraction in many conditions is associated with a decrease in G-actin content and/or an increase in F-actin, implying the presence of cytoskeleton reorganization during contraction (Mehta & Gunst, 1999; Tang & Tan, 2003; Tang & Gunst, 2004; Zhang *et al.,* 2005; Kim *et al.,* 2008a; Zhang & Gunst, 2008; Walsh & Cole, 2012). For example, in vascular and airway smooth muscle, F-actin was increased from ~70%-80% at rest to ~80%-90% in response to contractile stimuli, leading to the suggestion that a small proportion of cytosolic actin (~10-15%) undergoes polymerization concomitant with smooth muscle contraction (Tang & Tan, 2003; Zhang *et al.,* 2005; Kim *et al.,* 2008b; Zhang *et al.,* 2010).

The importance of actin polymerization in smooth muscle contraction is indicated by several studies employing pharmacological inhibitors of actin polymerization, such as

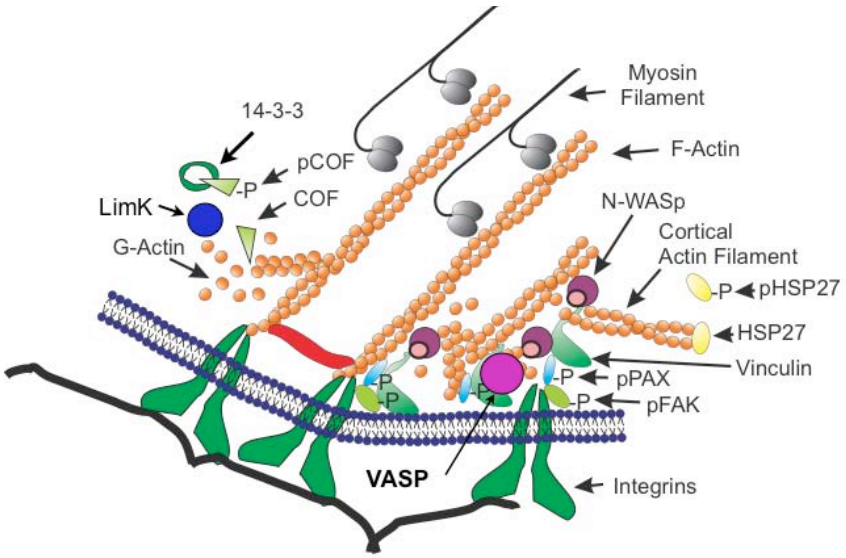

Figure 1.10: Diagrammatic representation of focal adhesion complexes in association with smooth muscle contraction.

Focal adhesions are large complexes of proteins located at the plasma membrane that includes, for example, actin, integrin, actin-binding proteins and signaling proteins. The recruitment of various cytoskeletal proteins to the focal adhesion may serve to catalyze actin polymerization and strengthen the network of newly formed actin filaments for enhanced force transmission. Several studies indicate that the signaling pathways responsible for the *de novo* actin polymerization in association with agonist-induced smooth muscle contraction may involve the N-WASP, LimK-cofilin, HSP27 or VASP-mediated pathways. However, the signaling pathways responsible for the *de novo* actin polymerization in association with the myogenic response remain unclear. LimK, Lim kinase; (p)COF, (phospho)cofilin; HSP, heat shock protein; FAK, focal adhesion kinase; (p)PAX, (phospho)paxillin; N-WASp, neuronal Wiskott-Aldrich syndrome protein; VASP, vasodilator-stimulated phosphoprotein. (Figure is modified from Gunst & Zhang 2008; Am J Physiol Cell Physiol 295:C576-C587.)

cytochalasins and latrunculins. Cytochalasins cap the barbed end of F-actins and blockactin polymerization, whereas latrunculins sequester G-actin and suppress actin polymerization. Both drugs were found to significantly attenuate contraction in airway, gastrointestinal and vascular smooth muscle (Mauss *et al.,* 1989; Obara & Yabu, 1994; Wright & Hurn, 1994; Saito *et al.,* 1996; Cipolla *et al.,* 2002; Dowell *et al.,* 2005; Flavahan *et al.,* 2005). Also, an indirect inhibition of the specific signal (e.g. mediated by a small GTPase Cdc42, N-WASp or VASP) that is proposed to affect actin polymerization via expression of siRNA or dominant negative constructs was found to impair agonist-induced smooth muscle contraction (Tang & Tan, 2003; Zhang *et al.,* 2005; Kim *et al.,* 2010a).

It is significant that the inhibition of actin polymerization leads to impaired contraction with little or no detectable change in LC_{20} phosphorylation and, presumably, cross-bridge cycling. For example, the treatment of rat aorta with cytochalasin D substantially inhibited the contraction induced by norepinephrine or high concentrations of external K^+, but it did not affect the level of intracellular Ca^{2+}, phosphorylated LC_{20} or myosin ATPase activity (Saito *et al.,* 1996). Similarly, expression of N-WASp dominant-negative peptides that inhibit actin polymerization, markedly attenuated force development in airway smooth muscle with a lack of change in LC_{20} phosphorylation (Zhang *et al.,* 2005). Other studies in various types of smooth muscle have reported similar observations (Walsh & Cole, 2013). These findings suggest that cytoskeleton reorganization itself does not affect the extent of LC_{20} phosphorylation that is determined by MLCK and MCLP activities.

1.5.3.3 Cytoskeleton reorganization in the myogenic response

As discussed above, the myogenic response of cerebral arteries is associated with MLCK activation, as well as MLCP inhibition, leading to an increase in LC_{20} phosphorylation. However, several observations indicate that myogenic regulation of arterial diameter in RCAs cannot be fully explained by the LC_{20} phosphorylation-dependent mechanism. For example, inhibition of PKC with GF109203X abolished the myogenic response of RCAs without a change in phosphorylation of LC_{20}, CPI-17, or MYPT1 (Johnson *et al.,* 2009b); serotonin-induced constriction of pressurized RCAs was accompanied by a much smaller increase in LC_{20} phosphorylation at 60 mmHg than at 10 mmHg, whereas the percentage of serotonin-induced vasoconstriction at 60 mmHg was considerably greater compared to that at 10 mmHg (El-Yazbi *et al.,* 2010). Also, recent studies have shown that under three different experimental conditions, including an increase in intraluminal pressure from 80 to 120 mmHg, the application of serotonin at 80 mmHg, and pressurization to 80 mmHg in the presence of serotonin, myogenic constriction was enhanced without a further detectable increase in LC_{20} phosphorylation (El-Yazbi *et al.,* 2010; Cole lab, unpublished observations). These findings suggest that the myogenic response may involve a third mechanism that is independent of changes in the level of LC_{20} phosphorylation.

Treatment of vessels with cytochalasins or latrunculins that inhibit actin polymerization completely suppressed myogenic constriction of resistance arteries (Cipolla *et al.,* 2002; Gokina & Osol, 2002; Flavahan *et al.,* 2005; Moreno-Dominguez *et al.,* 2013). The effect of latrunculins on the myogenic response was not likely due to disruption of the contractile actin filaments since the drug had little effect on the diameter

of pressurised RCAs at low intraluminal pressure (Luykenaar *et al.,* 2009; Moreno-Dominguez *et al.,* 2013). Furthermore, a decrease in G-actin and/or an increase in F-actin content were shown to be concomitant with the myogenic constriction responding to pressure elevation; inhibition of the change in G-actin and/or F-actin impaired the myogenic response (Cipolla *et al.,* 2002; Flavahan *et al.,* 2005; Moreno-Dominguez *et al.,* 2013; Cole lab, unpublished observations). These findings indicate that the myogenic response may involve dynamic actin polymerization, and therefore, cytoskeleton reorganization.

1.6 Summary: Identification of the molecular mechanisms underlying myogenic regulation of cerebral arterial diameter

Precise control of cerebral arterial diameter is key to the autoregulation of blood flow in the brain, the establishment of a regional blood flow reserve and the protection of the blood-brain barrier from damage caused by excessive pressure elevation. Control of arterial diameter is achieved by the myogenic response inherent to VSM cells. In addition, the intrinsic myogenic response is subject to modulation via numerous extrinsic vasoconstrictor and vasodilatory substances (Davis & Hill 1999). Ca^{2+}-dependent, Ca^{2+} sensitization-dependent, and cytoskeleton reorganization-dependent mechanisms have all been shown to contribute to myogenic regulation of cerebral arterial diameter in the brain (Cole & Welsh, 2011; Walsh & Cole, 2013) (Figure 1.11), yet there are many deficits remaining in our knowledge of the details of these mechanisms.

First, the Ca^{2+}-CaM-MLCK mechanism is mediated by an increase in E_m depolarization and $[Ca^{2+}]_i$, leading to activation of MLCK (Cole & Welsh, 2011). Native delayed rectifier K^+ (K_{DR}) currents have a huge impact on the extent of change in E_m, and

it has been shown that K_v1-containing channels contribute to K_{DR} currents and the negative feedback control of myogenic depolarization (Plane *et al.,* 2005; Chen *et al.,* 2006). However, 4-aminopyridine (4-AP) sensitive K_v1 currents are not the only component of K_{DR} currents in smooth muscle. 4-AP-resistant K_{DR} currents have also been recorded in myocytes isolated from cerebral arteries and other vessel types (Amberg & Santana, 2006, Moreno-Dominguez *et al.,* 2009, Yeung *et al.,* 2007, 2008, Jepps *et al.,* 2009). Therefore, knowledge of the full complement of K_V channels that contribute to KDR currents and the control of arterial diameter is of great importance. In addition, although K_V1-containing channels have been shown to be formed by multiple Kv1 subunits (Thorneloe et al., 2001; Ottschytsch et al., 2002; Plane et al., 2005; Chen et al., 2006), the molecular basis of other types of Kv channels in VSMCs remains unclear.

Second, the modulation of the myogenic response through various extrinsic factors is important in the control of vascular tone and blood flow to match dynamic physiological demands (Davis & Hill 1999). A number of studies have indicated that extrinsic factor-mediated regulation can be achieved by affecting the Ca^{2+}-dependent and/or Ca^{2+} sensitization-dependent mechanisms underlying the myogenic response (e.g. by influencing K_v channel gating or MYPT1 phosphorylation) (Harder, 1988; Lombard *et al.,* 1990; Meininger & Faber, 1991; Anschutz & Schubert, 2005; El-Yazbi *et al.,* 2010). However, whether extrinsic factors may also affect cytoskeleton reorganization in the context of the myogenic response remains undefined.

Third, emerging evidence has supported the concept that Ca^{2+} sensitization and cytoskeleton reorganization–dependent mechanisms contribute to myogenic regulation of cerebral arterial diameter. Biochemical measurement of MYPT1 phosphorylation, as well

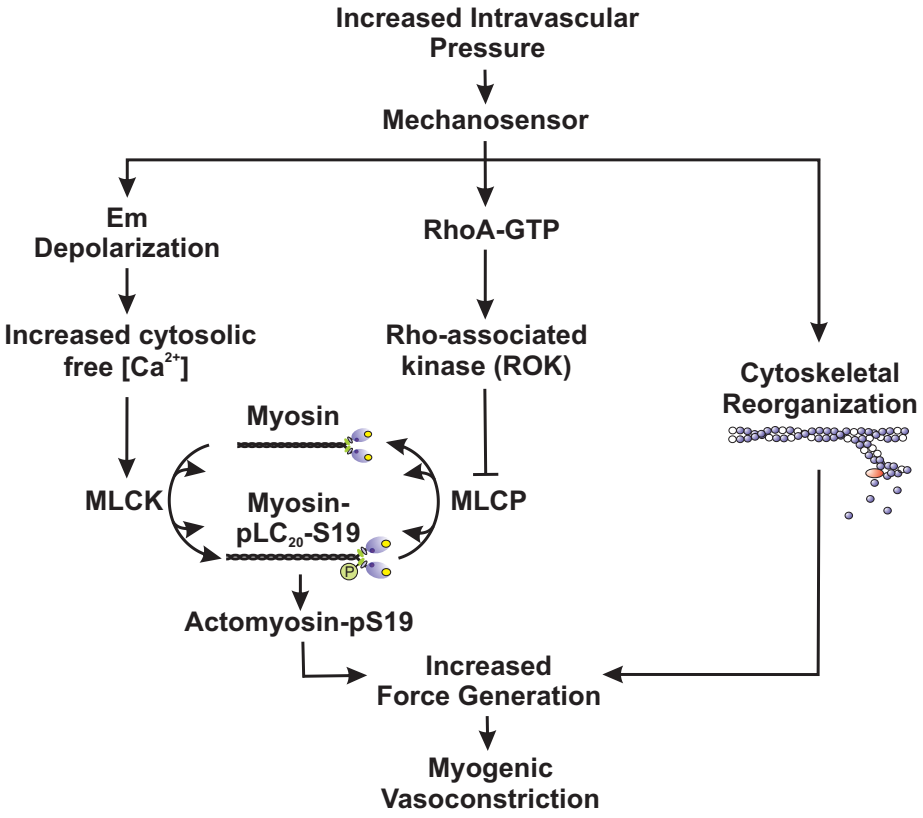

Figure 1.11: Contemporary view of the molecular basis of the myogenic response. Three mechanisms have been identified to contribute to the myogenic response: (1) Ca^{2+}-dependent mechanism involving graded depolarization of membrane potential (E_m) that increases the level of intracellular Ca^{2+} ($[Ca^{2+}]_i$), resulting in the activation of myosin light chain kinase (MLCK). (2) ROK-mediated Ca^{2+}-sensitization mechanism involving activation of RhoA and Rho-associated kinase (ROK) that decreases myosin light chain phosphatase (MLCP) activity. The activation of MLCK and inhibition of MLCP leads to an increase in the level of LC_{20} phosphorylation, which provokes cross-bridge cycling and force generation. (3) Cytoskeleton reorganization-dependent mechanism involves dynamic reorganization of the actin cytoskeleton to enhance force transmission from the contractile apparatus to the cell membrane and extracellular matrix.

as G-actin and/or F-actin content permits direct quantification of the signaling. Given the little change in E_m and $[Ca^{2+}]_i$ *versus* the significant change in MYPT1 phosphorylation and G (F)-actin content over the physiological operating range of the myogenic response, (~60-120 mmHg), Ca^{2+} sensitization and cytoskeleton reorganization-dependent mechanisms would therefore appear to exert a more significant influence on arterial diameter compared to the traditional Ca^{2+}-CaM-MLCK mechanism for myogenic regulation (Cole & Welsh, 2011; Walsh & Cole, 2013). It has been shown that the Ca^{2+} sensitization-dependent mechanism involves RhoA-mediated ROK activation in response to pressure elevation (Cole & Welsh, 2011). However, the signaling pathways contributing to cytoskeleton reorganization have not yet been clarified.

Therefore, the objectives presented in this thesis aim to expand our current understanding of the molecular mechanisms that are involved in myogenic regulation of cerebral arterial diameter through examination of the contribution of K_v2 and K_v7-containing channels to cerebral myogenic regulation, and through the identification of novel signaling pathways involved in the regulation of cytoskeleton reorganization in the cerebral myogenic response, as well as endothelium-dependent, NO-mediated vasodilation in the presence of a basal level of myogenic tone.

1.7 Major objectives

The major objectives of the work in this thesis were three-fold:

(1) To investigate the role of stromatoxin (ScTx1)-sensitive, K_v2 currents in myogenic regulation of cerebral arterial diameter, and to determine the molecular basis of native K_v2-containing channels in RCA myocytes (Chapter 3).

(2) To identify the contribution of K_v7 currents to native K_{DR} currents in RCA myocytes, and whether pharmacological manipulation of K_v7 channel gating affects myogenic regulation of rat cerebral arterial diameter (Chapter 4).

(3) To determine the major mechanism(s) underlying NO-mediated vasodilation in pressurized RCAs, and to identify whether this involves the activation of novel signaling pathway(s) that regulate cytoskeleton reorganization in the myogenic response of rat cerebral arteries (Chapter 5).

1.8 Significance

The findings of the experiments presented in this thesis provide novel evidence for understanding molecular mechanisms for the control of cerebral arterial diameter. It also provides important additional knowledge for understanding dysfunctional regulation of cerebral arterial diameter that is associated with cardiovascular disease, and may stimulate the development of novel strategies to reverse cerebral arterial dysfunction.

Chapter Two: Methods

2.1 Cell culture and transfection

Human embryonic kidney (HEK 293) cells were maintained on 10 cm plastic culture dishes in high glucose Dulbecco's Modified Eagle's medium (DMEM) supplemented with 10% fetal bovine serum and 5% ampicillin/streptomycin at 37 °C in 5% CO_2 as previously described (Johnson *et al.*, 2009a). Transfections were performed using FuGENE 6 Transfection Reagent (Roche) as per the vendor's instructions. cDNAs encoding green fluorescent protein (GFP) and K_v subunits were subcloned into pcDNA3.1.

For patch clamp recordings, HEK 293 cells were allowed to grow to ~70% confluence on 10 cm plastic culture dishes before transfection. Cells were re-plated onto 35 mm plastic culture dishes one day after transfection. Patch clamp recordings were made 36-48 h afterwards. For proximity ligation assay, cells were fixed at ~60% confluence on 35 mm plastic culture dishes. For biochemical experiments, cells were harvested at ~90% confluence on 10 cm plastic culture dishes after transfection.

For experiments described in Chapter 3 in the study of K_v2.1/9.3, cells were transfected with: (1) 4 μg GFP, (2) 4 μg GFP & 2 μg K_v2.1, (3) 4 μg GFP & 6 μg K_v9.3, (4) 4 μg GFP & 4 μg K_v1.2, (5) 4 μg GFP & 4 μg K_v1.5, (6) 4 μg GFP, 4 μg K_v1.2 & 4 μg K_v1.5, (7) 4 μg GFP, 2 μg K_v2.1 & 6 μg K_v9.3, (8) 4 μg GFP, 2 μg K_v2.1, 6 μg K_v9.3 & 4 μg K_v1.5, (9) 4 μg GFP, 6 μg K_v9.3 & 4 μg K_v1.5, (10) 4 μg GFP, 4 μg K_v2.1 & 4 μg K_v1.5, (11) 4 μg GFP, 4 μg K_v1.2 & 4 μg K_v2.1.

For experiments described in Chapter 4 in the study of K_v7, cells were transfected with: (1) 4 μg GFP, (2) 4 μg GFP & 4 μg $K_v7.4$, (3) 4 μg GFP, 4 μg $K_v1.2$ & 4 μg $K_v1.5$, (4) 4 μg GFP, 2 μg $K_v2.1$ & 6 μg $K_v9.3$.

2.2 Preparation of cell lysates from HEK 293 cells and immunoprecipitation

HEK 293 cells were harvested in ice-cold extraction buffer containing: Tris 20 mM (pH 7.5), NaCl 138 mM, KCl 3 mM, EDTA 2 mM, EGTA 1 mM, DTT 1 mM, benzamidine 1 mM, aprotinin 5 μg/ml, leupeptin 5 μg/ml, pepstatin A 5 μg/ml, and Triton X-100 1% (v/v). The collection of cell lysates was centrifuged at 13,000 g. The supernatant was stored at −80°C for a maximum of 3 months.

Immunoprecipitation experiments employed in Chapter 3.3.6 were done as previously described (Thorneloe *et al.,* 2001), and all procedures were performed at 4°C. Lysates from HEK cells or rat cerebral arties were pre-cleared for 1 h with 25 μL of Protein A Sepharose (Pharmacia) and incubated overnight at 4 °C with $K_v2.1$ antibody (1: 200) (Alomone). Antibody-bound $K_v2.1$ channel complexes were captured by the addition of 50 μL of Protein A Sepharose and incubated for 2 h to facilitate binding. Protein A Sepharose was spun down at 500 g for 3 min, washed twice with extraction buffer and once with Triton X-100 free extraction buffer. Protein complexes were then eluted from beads by adding SDS-PAGE sample buffer. A three-step western blot was performed to detect $K_v2.1$ and $K_v9.3$ protein. The protocol was carried out as described in 2.10.1, $K_v2.1$ antibody (1:500, Alomone) and $K_v9.3$ antibody (1:300, Santa Cruz) was employed.

2.3 RT-PCR and Real-time PCR

RT-PCR and real-time PCR experiments described in Chapter 3.3.3 were carried out as previously described (Plane *et al.,* 2005). Total RNA was extracted from rat brain, endothelium-denuded, intact RCAs or isolated RCA myocytes using an RNeasy Mini kit with DNase treatment (Qiagen). K_v2.1, K_v2.2, K_v5.1, K_v6.1-K_v6.3, and K_v9.1-K_v9.3 primer pairs were designed in-house or purchased from Qiagen (Mississauga). Rat brain mRNA was used as a positive control to confirm the viability of all primer pairs employed. The sequences of subunit-specific primers (5'-3') designed in house were:

K_v2.1 (89 bp):

Forward CGAGGGTCAGCTGCTCTACAG,

Reverse GTTCTAGCTCCAGTGCTGAACTTG;

K_v2.2 (91 bp):

Forward TTGATAACACCTGCTGC,

Reverse GATGGCCAGGATCTTTG;

K_v6.3 (119 bp):

Forward TGTCTATGGTGGTGCTGTG,

Reverse AGCTTCAATTATCCCGGA;

β-actin (98 bp):

Forward TATGAGGGTTACGCGCTCCC,

Reverse ACGCTCGGTCAGGATCTTCA.

Each primer set used: (1) had an efficiency of > 90% that did not differ by > 5% at an annealing temperature of ~58°C, (2) produced a single peak with no evidence of additional amplicons or dimer formation during melt curve analysis and (3) yielded

amplicons of an expected size. Real-time PCR was performed with SYBR-Green reaction kit with a start at 95 °C for 15 min, followed by 40 cycles of 94 °C for 15 s, 58 °C for 30 s and 72 °C for 30 s. Threshold cycle was determined using a Bio-Rad iCycler and vendor-supplied software; transcript abundance was calculated by the $2^{-\Delta\Delta Ct}$ method using β-actin as a reference for normalization (Livak & Schmittgen, 2001). Negative control wells were applied by adding water as a blank control, or using primers for the neuronal K+ channel, Erg-3 and endothelial factor, endothelin-1, as markers of contamination of the myocyte mRNA samples by neuronal and endothelial message, respectively (Plane et al. 2005).

2.4 Animals

Male Sprague-Dawley rats (250-275 g; Charles River) were maintained and terminated by halothane inhalation and exsanguination according to the standards of the Canadian Council on Animal Care and a protocol reviewed by the Animal Care Committee of the Faculty of Medicine, University of Calgary**.**

2.5 Rat cerebral arterial myocyte isolation

Rat brains were carefully removed and placed in an ice-cold smooth muscle dissection solution (SMDS) containing (in mM): NaCl 60, Na-glutamate 80, KCl 5, $MgCl_2$ 2, glucose 10, and HEPES 10 (pH 7.4). Rat middle and posterior cerebral arteries were removed from the brain and dissected free of the surrounding tissue. Single myocytes were enzymatically isolated using a method modified from Plane *et al.* (2005). Arteries were equilibrated in SMDS containing bovine serum albumin (BSA; 1 mg/ml) at 37 °C for 10 min, exposed to the same solution supplemented with papain (0.5 mg/ml) and DTT (1.5 mg/ml) at 37 °C for 8-10 min, washed in ice-cold SMDS, then incubated in

SMDS containing: 100 μM Ca^{2+}, BSA (1 mg/ml) and collagenase (0.7 mg/ml type F and 0.4 mg/ml type H) at 37 °C for 8-10 min and again washed in ice-cold SMDS. Isolated myocytes were liberated from the digested vessels by gentle trituration using a wide-bore glass pipette and kept in ice-cold SMDS containing 1 mg/ml BSA until use (within 12 h).

2.6 Whole-cell patch clamp electrophysiology

Whole-cell currents were recorded using an Axopatch 200A amplifier (Axon Instruments) as previously described (Chen *et al.*, 2006; Johnson *et al.*, 2009a). Recordings were filtered at 1 kHz before 5 kHz digitization with a 122 A/D converter (Axon Instruments). Voltage protocols were applied and data were analyzed using pClamp version 6.0 software (Axon Instruments). The bath solution contained (in mM): NaCl 120, $NaHCO_3$ 3, KCl 4.2, KH_2PO_4 1.2, $MgCl_2$ 2, $CaCl_2$ 0.1, glucose 10, and HEPES 10 (pH 7.4). The patch pipette solution contained (in mM): potassium gluconate 110, KCl 30, $MgCl_2$ 0.5, HEPES 5, EGTA 10, Na_2ATP 5, and GTP 1 (pH 7.2). The junction potential was determined to be 15 mV for the recording conditions employed and this value was used to correct all voltage protocols.

Cell capacitance was determined by integration of the capacity transient recorded for a step from −75 to −70 mV. Whole-cell currents were recorded by applying voltage-steps of 325 ms duration between −95 and +25 or +45 mV in increments of 10 mV from a holding potential of −75 mV. Peak tail current amplitudes of native and recombinant channel currents were determined during 625 ms repolarizing steps to −45 and −55 mV, respectively. Current density (pA/pF) *versus* voltage relations were determined from the end-pulse current amplitude normalized to cell capacitance and plotted as a function of the step voltage. Current recordings for the analysis of the time constants of tail current

decay were assessed at −45 mV following steps to +25 mV and were fitted by a two-exponential function.

2.7 Proximity ligation assay

For the PLA experiments described in Chapter 3.3.6, freshly dissociated RCA myocytes or transfected HEK 293 cells were studied using the Duolink™ *in situ* PLA detection kit 563 (Olink) as per the vendor's instructions (Figure 2.1). For experiments on isolated myocytes, 35 mm glass coverslips were pre-soaked in ethanol overnight, and flame dried before use. Cleaned coverslips were placed in a chamber of a four-well dish, and myocytes in ice-cold SMDS solution were added dropwise directly onto each coverslip. Cells were left to adhere to coverslips for 60 min at room temperature (RT). Cells were fixed in phosphate-buffered saline (PBS) containing paraformaldehyde (3% for HEK 293 cells and 4% for myocytes) for 15 min, permeabilized in PBS containing 0.1% Triton X-100 for 15 min and quenched in PBS containing 100 mM glycine for 5 min. Cells were then washed with PBS, blocked for 30 min at 37 °C in Duolink™ blocking solution, and incubated overnight at 4 °C with a pair of primary antibodies in Duolink™ antibody diluent solution; i.e. rabbit anti-K_v2.1 (1: 500, Alomone) and goat anti-K_v9.3 (1: 300, Santa Cruz) or mouse anti-K_v1.2 (1:500, Neuromab) and rabbit anti-K_v1.5 (1:500, Alomone). Control experiments employed only one primary antibody or cells transfected with cDNAs encoding only one type of K_v subunit. Cells were labeled with Duolink™ PLA PLUS and MINUS probes for 2 h at 37°C. Anti-goat PLUS and anti-rabbit MINUS were employed to detect K_v2.1 and K_v9.3 co-assembly, whereas anti-mouse PLUS and anti-rabbit MINUS were used for K_v1.2 and K_v1.5. The secondary antibodies of PLA PLUS and MINUS probes were attached to synthetic oligonucleotides

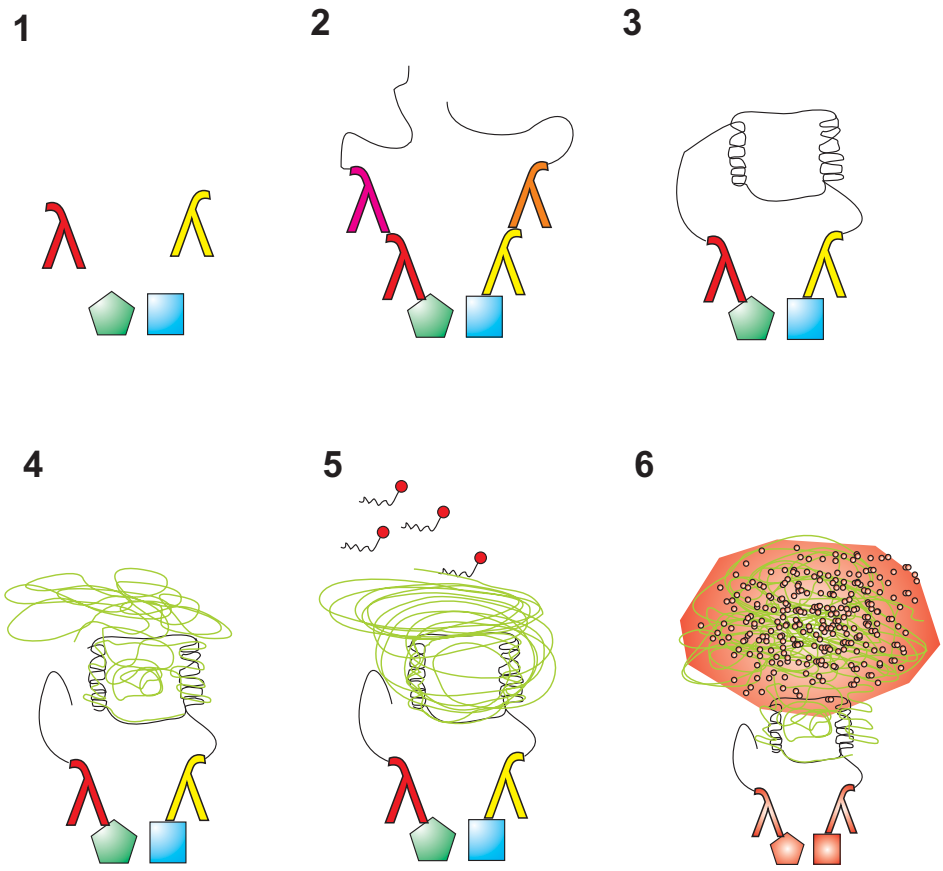

Figure 2.1: Proximity Ligation Assay (PLA) principle.

Duolink® *in situ* PLA assay required six steps: (1) following fixation, permeabilization and blocking, samples were incubated with a pair of primary antibodies that bind to the proteins to be detected; (2) secondary antibodies conjugated to oligonucleotides (PLA probe MINUS and PLA probe PLUS) were added to bind specifically to the primary antibodies; (3) the hybridization solution, consisting of two oligonucleotides (illustrated as red bands), was added to permit the oligonucleotides to hybridize with the two PLA probes if they were in close proximity (<30-40 nm); (4) the ligation solution was added together with ligase, joining the two hybridized oligonucleotides in a closed circle; (5) the

amplification solution, consisting of nucleotides, was added together with polymerase to start a rolling-circle amplification reaction using the ligated circle as a template; this generates a concatemeric product extending from the oligonucleotide arm of the PLA probe; (6) the detection solution, consisting of fluorescently labelled oligonucleotides, was added and the labelled oligonucleotides hybridized to the RCA product. The signal was then detected by fluorescence microscopy as distinct fluorescent puncta. (Figure is modified from www.olink.com.)

that hybridize when in close proximity (i.e. <40 nm separation). The hybridized oligonucleotides were then ligated prior to rolling circle amplification. The concatemeric amplification products extending from the oligonucleotide arm of the PLA probes were then detected using red fluorescent fluorophore-tagged, complementary oligonucleotide sequences and a Zeiss ApoTome epifluorescence microscope (Carl Zeiss) using 0.3-0.5 μm optical sections.

2.8 Cerebral arterial pressure myography

Rat brains were carefully removed and placed in ice-cold Krebs' solution containing (in mM): NaCl 120, $NaHCO_3$ 25, KCl 4.8, NaH_2PO_4 1.2, $MgSO_4$ 1.2, glucose 11, $CaCl_2$ 1.8 (pH 7.4 when aerated with 95% air / 5% CO_2). Rat middle and posterior cerebral arteries were dissected from the brain and free of the surrounding tissue and cut into ~1-2 mm segments.

Vessels were mounted in an arteriograph chamber attached to a pressure myograph (Living Systems) for measurement of outer diameter with an automated edge detection system (IonOptix) (Figure 2.2). Endothelial cells were denuded by briefly passing a stream of air through the vessel lumen as previously described (Johnson *et al.*, 2009b). Endothelium of RCAs was denuded for all experiments except for ACh ± ODQ experiments presented in Chapter 5.

Vessels were warmed at 37 ^{o}C for 10-15 min in Krebs' solution, pressurized to 80 mmHg and allowed to develop active myogenic tone over 20-30 min. All vessels (except those employed for experiments of 120 mmHg before and after the initial development of myogenic tone; described in Chapter 5.3.11) were subjected to at least one 5 min pressure step from 10 to 80 mmHg to ensure the development of a stable myogenic constriction.

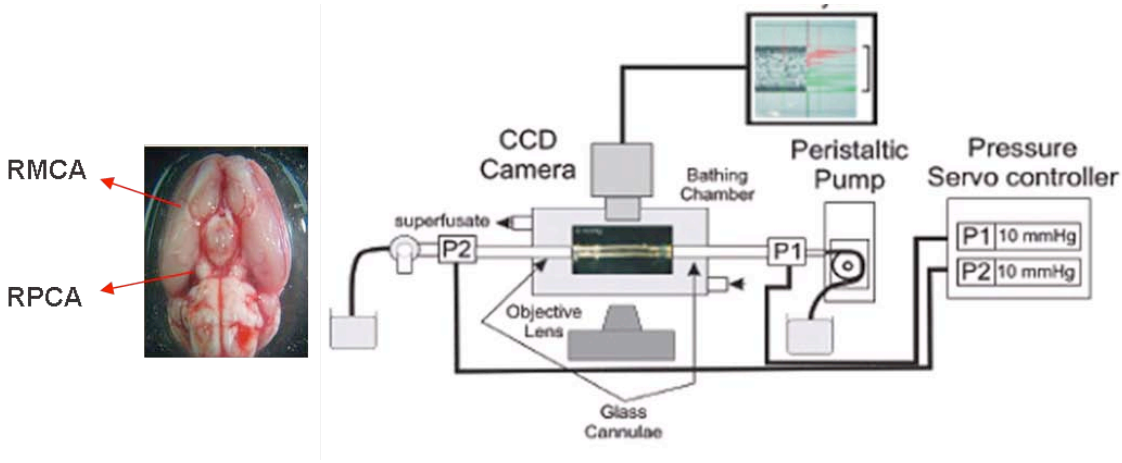

Figure 2.2: Schematic representation of pressure myography.

A segment of rat middle cerebral artery (RMCA) or posterior cerebral artery (RPCA) was mounted between two glass cannulae within a bathing chamber filled with Krebs' solution at 37 °C. Intraluminal pressure was detected by proximal (P1) and distal (P2) pressure transducers and controlled by an adjustable pressure servo controller connected to a peristaltic pump. The pressurized vessel was visualized via an inverted microscope and a CCD camera coupled to a computer. Image captures and outer arterial diameter recordings were achieved by IonOptix software.

Vessels that did not exhibit active myogenic constriction or exhibited leaks were discarded. Vessels were kept at 10 mmHg for ~10 min, then subjected to specific pressure protocols as described in the individual experimental protocols.

2.9 Vessel flash-freezing and protein extraction

At the completion of the protocol in each pressure myograph experiment, vessel segments were maintained at a constant intraluminal pressure, and quickly submerged in wet ice-cold acetone containing 10% trichloroacetic acid (TCA) and 10 mM dithiothreitol (DTT). Vessel segments were then carefully removed from the cannula, left in ice-cold TCA/DTT/acetone for ~15 min, and then washed once in ice-cold acetone containing 10 mM DTT for ~15 min. The two cannulated ends of each vessel segment were removed since they were not pressurized properly. The middle, pressurized part of each vessel segment was lyophilized overnight (freeze dry system, LABCONCO) and stored at –80 °C prior to protein extraction.

For protein extraction, each vessel segment was added to ~30-80 µl (according to the size of the segment) 1x sample buffer containing 4% sodium dodecyl sulfate (SDS), 100 mM, freshly made DTT, 10% glycerol, 0.01% bromophenol blue, 60 mM Tris-HCl (pH 6.8). Samples were then heated at 95 °C for 10 min and rotated overnight at 4 °C and stored at –80 °C prior to gel electrophoresis.

2.10 Western blotting

2.10.1 Measurement of LC_{20} phosphorylation

The protocol for measurement of phosphorylated LC_{20} content was carried out as previously described with minor modifications (Takeya *et al.*, 2008; Johnson *et al.*, 2009b; El-Yazbi *et al.*, 2010; Walsh *et al.*, 2011). Unphosphorylated and

monophosphorylated LC_{20} were separated by Phos-tag SDS-PAGE with incorporated Mn^{2+}-Phos-tag. The phos-tag ligand is able to interact with phosphoryl groups of phosphorylated proteins, which retards the movement of phosphorylated proteins through the gel leading to a separation of phosphorylated and unphosphorylated proteins.

The 4.5% stacking gel was composed of 4.5% acrylamide, 0.12% *N,N'* methylenebisacrylamide, 0.1% SDS, 125 mM Tris-HCl pH 6.8, 0.1% ammonium persulfate and 0.17% TEMED. The 10% resolving gel was composed of 10% acrylamide, 0.32% *N,N'*-methylenebisacrylamide, 0.1% SDS, 375 mM Tris-HCl pH 8.8, 0.05% ammonium persulfate, 0.07% TEMED (together with 50 μM Phos-tag acrylamide (NARD Institute Ltd., Japan) and 100 μM $MnCl_2$ specifically for a phos-tag gel). Electrophoresis was carried out in 1.5 mm thick mini gels at 30 mA for ~1.5 h in a Mini Protean Cell (Bio-Rad) with the running buffer containing: 0.1% SDS, 25 mM Tris and 192 mM glycine. After electrophoresis, gels were soaked in 3-[cyclohexylamino]-1-propanesulfonic acid (CAPS, 10 mM, pH 11) transfer buffer (containing 15% methanol, 2 mM EDTA) for 15 min, and then equilibrated in CAPS transfer buffer without EDTA for 15 min at 4°C.

Proteins were then transferred to PVDF membranes (0.2 μm pore size, BioRad) at 100 V for 80 min at 4°C. Membranes were washed in PBS for 5 min, and LC_{20} was cross-linked and fixed on membranes by soaking the membranes in PBS containing 0.25% glutaraldehyde at RT for 45 min. Membranes were then washed in Tris-buffered saline solution (TBS; 137 mM NaCl, 3 mM KCl, 20 mM Tris-HCl pH 7.5) prior to 0.2% ECL blocking solution (GE Healthcare) in 0.1% TBST (TBS plus 0.1%(v/v) Tween-20) at RT for 2 h. To enhance detection sensitivity, a three-step protocol was carried out as

follows: all forms of LC_{20} (unphosphorylated, monophosphorylated and diphosphorylated) proteins were detected using the rabbit polyclonal LC_{20} antibody (Santa Cruz; 1:1000) in 0.1% TBST incubated overnight at 4°C. Membranes were washed in 0.05% TBST, incubated with biotin-conjugated goat anti-rabbit IgG (Chemicon; 1:40,000) in 0.1% TBST for 1 h at RT, washed in 0.05% TBST, and incubated with horseradish peroxidase (HRP)-conjugated streptavidin (1:20,000; Pierce) in 0.1% TBST at RT for 30 min. Membranes were then washed in 0.05% TBST, followed by signal detection using SuperSignal West Femto reagent (Pierce) or Amersham ECL advanced reagent (GE Healthcare). The emitted light was detected and quantified with a chemiluminescence imaging analyzer (LAS3000mini, Fujifilm). Obtained images were analyzed with Multi Gauge v3.0 software (Fujifilm).

2.10.2 Measurement of MYPT1 phosphorylation at Thr855

Electrophoresis was carried out as described in 2.10.1. Gels were cut at the 70 kDa molecular weight marker. High molecular mass proteins were transferred to nitrocellulose membranes (0.2 μm pore size, BioRad) at 100 V at 4 °C for 2 h in transfer buffer containing: 25 mM Tris-HCl, 192 mM glycine, 1% SDS and 20% methanol. Low molecular mass proteins were transferred to 0.2 μm nitrocellulose membranes at 100 V at 4 °C for 90 min in transfer buffer containing: 25 mM Tris-HCl, 192 mM glycine and 20% methanol. Membranes were then rinsed in PBS and fixed in PBS containing 0.25% glutaraldehyde for 15 min, washed in 0.1% TBST and blocked with 5% non-fat dried milk in 0.1% TBST for 2 h. A three-step protocol was carried out as described in 2.10.1 for measurement of phospho-MYPT1-Thr855 content, except membranes containing high molecular mass proteins were incubated with the rabbit polyclonal, Thr855

phospho-specific MYPT1 antibody (1:1000; Upstate) at 4 °C overnight. A two-step protocol was carried out for measurement of actin content. Membranes containing low molecular mass proteins were incubated with the rabbit polyclonal, pan-actin antibody (1:1000; Cytoskeleton) at 4 °C overnight, washed in 0.05% TBST, and incubated with the HRP-conjugated anti-rabbit IgG (1:10,000; Rockford) in 0.1% TBST containing 1% milk at RT for 2 h. Membranes were then washed with 0.05% TBST following by detection as described in 2.10.1.

2.10.3 Measurement of VASP phosphorylation

Electrophoresis was carried out as described in 2.10.1. Proteins were transferred to 0.2 μm PVDF membranes at 100 V at 4 °C for 90 min in transfer buffer containing: 25 mM Tris-HCl, 192 mM glycine and 20% methanol. Membranes were then rinsed in PBS and fixed in PBS containing 0.5% glutaraldehyde for 15 min, washed in 0.1% TBST, and blocked with 5% non-fat dried milk in 0.1% TBST for 2h. Phosphorylation of VASP at Ser157 leads to an apparent shift in molecular mass from 46 to 50 kDa in standard 10% SDS-PAGE (see 5.1.13 for details). A three-step protocol was carried out as described in 2.10.1 to measure phospho-VASP-Ser157 and unphospho-VASP-Ser157 content using a pan-VASP antibody, except that the membranes were incubated with the rabbit polyclonal, pan-VASP antibody (1:800; Cytoskeleton) in 0.1% TBST containing 5% BAS at 4 °C overnight. For measurement of phospho-VASP-Ser157 or phospho-VASP-Ser239 content using phospho-specific antibodies, the protocol was the same as above except membranes were incubated with the rabbit polyclonal Ser157 or Ser239 phospho-specific VASP antibody (1:800, Cytoskeleton) at 4 °C overnight. After successful

measurement of VASP, membranes were washed in TBST (0.05%), followed by a two-step protocol for measurement of actin content as described in 2.10.2.

The molecular masses of VASP and actin are 46/50 kDa and 42 kDa, respectively. This raised a concern that the signals of VASP and actin detected on the same membranes may not have sufficient separation to permit precise quantification. Given that actin signals were of considerably higher intensity than VASP signals (i.e. actin bands required less than 5 s exposure, whereas VASP bands required ~150-250 s), we concluded that signals of actin and VASP could be successfully quantified without cross interference.

2.11 G-actin assay

G-actin content was quantified as previously described (Corteling *et al.,* 2007; Luykenaar *et al.,* 2009; Walsh *et al.,* 2011; Moreno-Dominguez *et al.,* 2013). At the completion of the protocol in each pressure myograph experiment, vessel segments were quickly transferred to 37 °C F-actin-stabilization buffer (Cytoskeleton) while intraluminal pressure was maintained at a constant level. F-actin-stabilization buffer (containing: 50 mM 1,4-piperazinediethanesulfonic acid (PIPES) (pH 6.9), 50 mM KCl, 5 mM $MgCl_2$, 5 mM EGTA, 5% (v/v) glycerol, 0.1% Nonidet P40, 0.1% Triton X-100, 0.1% Tween 20, 0.1% 2-mercaptoethanol and 0.001% antifoam) was employed to stabilize F- and G-actin content. Vessel segments were removed from the cannula, and the unpressurized ends were cut off. The middle, pressurized part of each vessel segment was homogenized in 100 µl F-actin-stabilization buffer at RT using a pellet pestle motor (Kontes). The homogenate was then transferred to 7 x 20 mm centrifuge tubes (Beckman Coulter), and centrifuged at 100,000 g at RT for 1 h using an Optima Max-TL ultracentrifuge

(Beckman Coulter). This allowed the separation of G-actin (and SM22) and F-actin into the supernatant and pellet, respectively. Next, 30 µl supernatant containing G-actin and SM22 was carefully removed and mixed with 30 µl 2x sample buffer. Samples were then heated at 95 °C for 10 min and stored at –20 °C prior to gel electrophoresis. To assess SM22 contamination in the pellet control experiments described in Chapter 5.3.6, the pellet of each vessel segment was recovered and resuspended in 100 µl 1x sample buffer, heated at 95 °C for 10 min, rotated overnight at 4 °C and stored at –20 °C prior to gel electrophoresis.

Electrophoresis was carried out as described in 2.10.1. Proteins were transferred to 0.2 µm nitrocellulose membranes at 100 V at 4 °C for 90 min in transfer buffer containing 25 mM Tris-HCl, 192 mM glycine and 20% methanol. Membranes were rinsed in PBS, fixed in PBS containing 0.25% glutaraldehyde for 15 min, washed in 0.05% TBST and blocked with 5% non-fat dried milk in 0.1% TBST for 2 h. The membranes were then cut at the 35 kDa molecular mass marker.

For measurement of G-actin content, membranes containing high molecular mass proteins were incubated with the rabbit polyclonal, actin antibody (1:1000; Cytoskeleton) in 0.1% TBST containing 1% milk at 4 °C overnight, washed in 0.05% TBST, and then incubated with the HRP-conjugated anti-rabbit IgG (1:10,000; Rockford) in 0.1% TBST containing 1% milk at RT for 2 h. For measurement of SM22 content, membranes containing low molecular mass proteins were incubated with the goat polyclonal, SM22α antibody (1:2000; Novus) in 0.1% TBST containing 1% milk at 4 °C overnight, washed in 0.05% TBST, and incubated with the HRP-conjugated anti-goat IgG (1:5000;

Millipore) in 0.1% TBST containing 1% milk at RT for 2 h. Membranes were then washed with 0.05% TBST following by detection as described in 2.10.1.

2.12 Materials

K_v7.4 and K_v9.3 cDNAs were purchased from Thermo Scientific Open Biosystem (AL, USA). All chemicals were purchased from Sigma (Oakville, ON, Canada) unless indicated. XE991 (10,10-bis(4-pyridinylmethyl)-9(10H)-anthracenone) was obtained from Tocris (MO, USA), retigabine (ethyl N-[2-amino-4-[(4-fluorophenyl)methylamino]phenyl]carbamate) was a gift from Dr. M Schwake (Germany). S-1 ((S)-N-[1-(3-morpholin-4-yl-phenyl)-ethyl]-3-phenyl-acrylamide) was synthesized and supplied by NeuroSearch A/S (Denmark). Proximity ligation assays (PLA) used the Duolink™ *in situ* PLA kit (Olink, Uppsala, Sweden). Phos-tagTM acrylamide was obtained from NARD Institute Ltd. (Japan). Rabbit LC_{20} and goat K_v9.3 antibodies were purchased from Santa Cruz Biotechnology (Santa Cruz, CA, USA), MYPT1 phospho specific at Thr855 antibody was from Upstate (Charlottesville, VA, USA), actin antibody, VASP pan antibody and VASP phospho specific antibody at Ser157 or Ser239 were from Cytoskeleton (Denver, CO, USA), SM22α antibody was from Novus (Oakville, ON, Canada), ScTx1, K_v1.5 and K_v2.1 antibodies were from Alomone (Jerusalem, Israel), K_v1.2 antibody was from UC Davis/NIH Neuromab (Davis, CA, USA), HRP-conjugated goat anti-rabbit secondary antibody and HRP-conjugated streptavidin were from Pierce Biotechnology (Rockford, CT, USA), biotin-conjugated goat anti-rabbit IgG was from Chemicon (Temecula, CA, USA). HRP-conjugated anti-goat IgG secondary antibody was from Millipore (Billerica, MA, USA)

2.13 Statistical analysis

All values are presented as means ± SEM, with n values indicative of the number of cells or vessels studied under each treatment. Statistical difference was determined using Student's t-test, as well as between-subjects one-way ANOVA or within-subjects repeated measures ANOVA, followed by Bonferoni's *post hoc* test for the comparison of all groups. P value of < 0.05 was considered to be statistically significant.

Chapter Three: Contribution of stromatoxin-sensitive, heteromultimeric $K_v2.1/K_v9.3$ channels to myogenic regulation of cerebral arterial diameter

3.1 Introduction

3.1.1 Voltage-dependent potassium (K_v) channels

3.1.1.1 Classification and structure of K_v channels

K_v channels are one of the most diverse groups of ion channel subunits. More than 20 types of K_v channel subunits have been identified in mammalian tissues (Gutman *et al.,* 2003; Yan *et al.,* 2004). The superfamily of K_v channel subunits can be divided into 9 sub-families, $K_v1.x$ to $K_v9.x$, based on their primary amino acid sequences (Figure 3.1). Members of K_v1-4 and K_v7 sub-families are referred as pore-forming subunits that are able to form functional K_v channels. Members of K_v5, K_v6, K_v8 and K_v9 sub-families are referred as silent subunits. This is based on the inability of Kv5, K_v6, K_v8 or K_v9 subunits to form functional channels when expressed as homomultimers, but they are able to assemble with $K_v2.1$ or $K_v2.2$ subunits to produce heteromultimeric K_v2-containing channels with properties distinct from homomultimeric K_v2 channels (Drewe *et al.,* 1992; Hugnot *et al.,* 1996; Patel *et al.,* 1997; Salinas *et al.,* 1997b; Zhu *et al.,* 1999; Ottschytsch *et al.,* 2002).

K_v channels are tetrameric structures that contain four pore-forming α subunits (Figure 3.2) (Long *et al.,* 2005; Tombola *et al.,* 2006). Each α-subunit is composed of 6 transmembrane-spanning segments (S1–S6) (Trauner, 2005). The primary voltage sensor, S4, contains positively charged, basic residues that respond to a change in E_m, which triggers a conformational change leading to channel opening or closing (Bezanilla *et al.,* 2000). The S5, S6 segments and the P-loop located between them, form a central

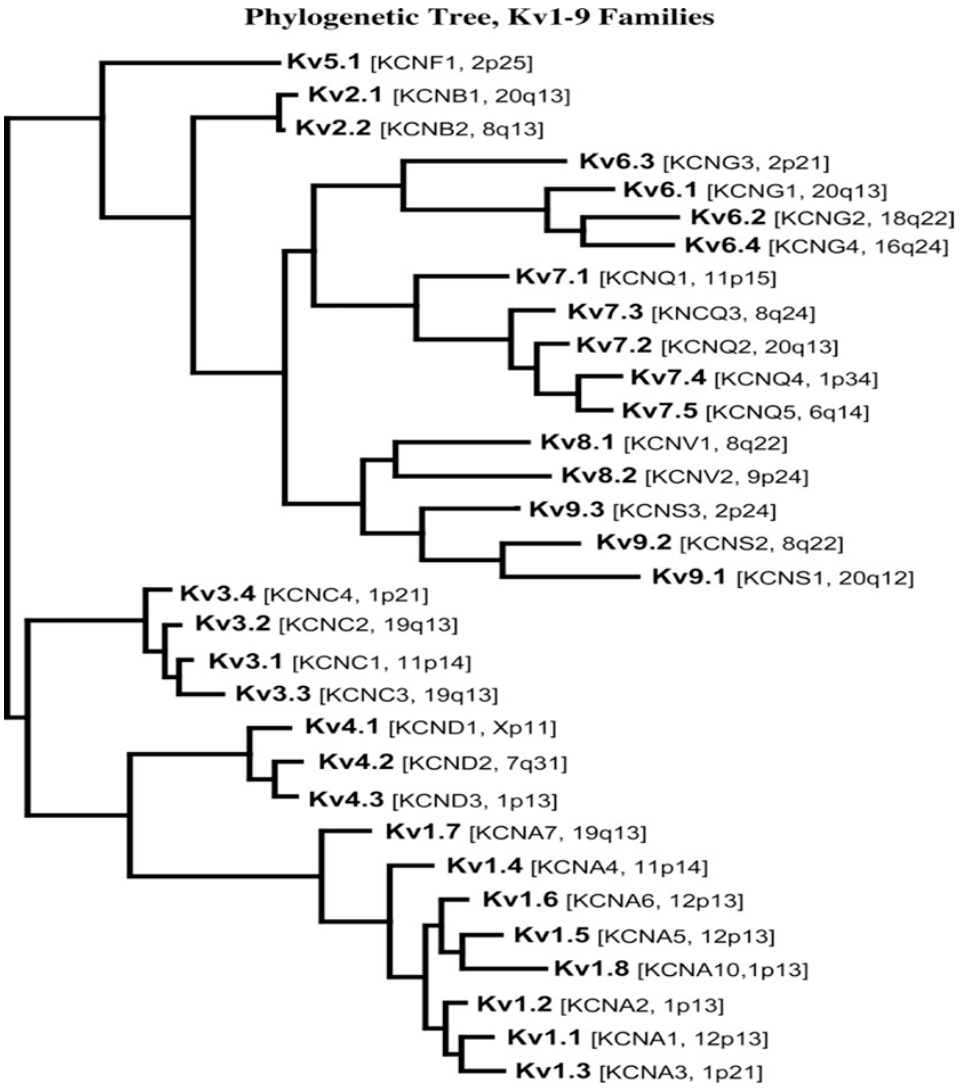

Figure 3.1: Phylogenetic tree of K_v 1-9 sub-families

The superfamily of K_v channel subunits can be divided into 9 sub-families, K_v1.x to K_v9.x, based on their primary amino acid sequences. Members of K_v1-4 and K_v7 sub-families are referred as pore-forming subunits that can form functional K_v channels, whereas members of K_v5, K_v6, K_v8 and Kv9 sub-families are referred as silent subunits that cannot form functional channels when expressed as homomultimers. (Figure is modified from Gutman *et al.*, 2003; Pharmacol Rev 55: 583-586.)

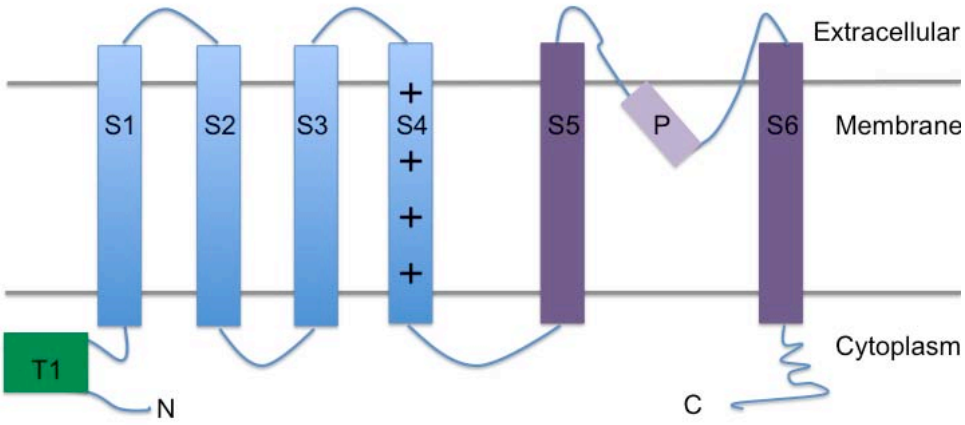

Figure 3.2 Topology of K_v α-subunits.

Each K_v α-subunit consists of six-transmembrane domains (S1-S6). The primary voltage sensor, S4, contains positively charged, basic residues that respond to a change in E_m, and triggers a conformational change leading to channel opening or closing. The P-loop located between the S5 and S6 segments contains a highly conserved glycine-tyrosine-glycine (G-Y-G) motif that forms the K^+ selectivity filter. The cytoplasmic, N-terminal tertramerization domain (T1) is believed to play a role in subunit tetramerization and subunit specific assembly.

selective pore region of the channel. The P-loop contains a highly conserved glycine-tyrosine-glycine (G-Y-G) motif, which allows the channel to be selectively permeable to K^+ ions (Heginbotham *et al.,* 1994). K_v channels also contain a cytoplasmic tetramerization domain (T1) within the N-terminal region. This T1 domain is believed to play a role in subunit tetramerization and subunit specific assembly (Shen & Pfaffinger, 1995; Kreush *et al.,* 1998; Bixby *et al.,* 1999; Gulbis *et al.,* 2000).

3.1.1.2 Vascular smooth muscle K_v currents

Two phenotypes of K_v currents have been identified in VSM tissues, including the transient outward, K_{TO} currents (also known as A-type currents) and the delayed rectifier K_{DR} currents. K_{TO} currents have a limited distribution in VSM tissues, and are generally present in phasic vessels, such as portal vein, as well as in cardiac and gastrointestinal tissues (Beech & Barnes, 1989; Imaizumi *et al.,* 1993; Amberg *et al.,* 2002; Niwa & Nerbonne, 2010). K_{TO} currents display rapid voltage-dependent activation and inactivation. Full activation occurs within ~20-50 ms followed by complete inactivation within 100 ms on E_m depolarization to voltages positive to ~−50 mV (Beech & Barnes, 1989; Beech & Bolton, 1989a). Given that E_m in most VSM is generally positive to −50 mV, K_{TO} currents appear not to play an important role in controlling VSM E_m owing to their narrow window currents and rapid kinetics (Thorneloe & Nelson, 2005).

In contrast to K_{TO} currents, K_{DR} currents have been documented in almost all types of VSM tissues. Voltage-dependent K_{DR} currents exhibit sustained current with a relatively slow inactivation (Thorneloe & Nelson, 2005). They are believed to be crucial for controlling the level of VSM E_m , and show activity given that they present at voltages

consistent with the E_m of VSMCs (Beech & Bolton, 1989a; Knot & Nelson, 1995; Nelson & Quayle, 1995; Aiello, *et al.*,1998; Cole *et al.*, 2005).

VSM K_{DR} currents were found to consist of 4-AP-sensitive and 4-AP-resistant components with distinct properties (Okabe *et al.*, 1987; Beech & Bolton, 1989b; Thornbury *et al.*, 1992). K_v1 and K_v2-containing channels were identified to contribute to 4-AP-sensitive and 4-AP-resistant components of K_{DR} currents, respectively (Cole *et al.*, 2005; Thorneloe & Nelson, 2003, 2005). However, recent studies suggest that K_v7-containing channels may also contribute to the 4-AP-resistant component (Yeung & Greenwood, 2005; Yeung *et al.*, 2007). In addition, a number of studies indicate a difference in the biophysical properties and density of K_{DR} currents in myocytes isolated from, for example, cerebral, mesenteric and coronary arteries (Nelson & Quayle, 1995; Cole *et al.*, 2005; Thorneloe & Nelson 2005). These findings support the view that multiple types of K_v channels with varied combinations of K_v pore-forming, as well as modulatory subunits may be expressed by VSM in a vessel-specific manner.

3.1.2 K_v channels in myogenic control of E_m depolarization

3.1.2.1 Regulation of myogenic depolarization

Following E_m depolarization, the activation of L-type Ca^{2+} channels is capable of leading to an increase in Ca^{2+} influx. However, no Ca^{2+}-dependent action potentials are observed under certain circumstances. If actin potentials are present, then the vessel would exhibit phasic tone elevation, as is apparent in the portal vein (Mironneau & Gargouil, 1979; Shimamura & Sunano, 1990). Small resistance arteries exhibit steady-state changes in E_m and graded alterations in $[Ca^{2+}]_i$ in response to intraluminal pressure elevation between 10 and 140 mmHg (Nelson *et al.*,1995; Osol *et al.*, 2002). This is

attributed to a precise negative feedback regulation of myogenic depolarization, which is mediated by BK_{Ca} and K_{DR} channels that provide opposing hyperpolarizing K^+ currents to offset the Ca^{2+} currents and permit steady-state, low amplitude changes E_m and $[Ca^{2+}]_i$ (Brayden & Nelson, 1992; Nelson *et al.,* 1995; Albarwani *et al.,* 2003; Chen *et al.,* 2006).

3.1.2.2 BK_{Ca} and K_v1-containing channels

BK_{Ca} channels are composed of $K_{Ca}1.1$ pore-forming α-subunits and β1 modulatory subunits (Brenner *et al.,* 2000; Cox & Aldrich, 2000; Wei *et al.,* 2005). Activation of BK_{Ca} channels is found to be enhanced by Ca^{2+} release from SR Ca^{2+} stores (i.e. Ca^{2+} sparks). A number of findings demonstrate that BK_{Ca} channels act as a Ca^{2+}-dependent brake that limits Ca^{2+} influx and myogenic depolarization (Figure 3.3). For example, selective inhibition of BK_{Ca} channels, targeted deletion of BK_{Ca} β1-subunit, or a reduction in β1 subunit expression in hypertensive rats were all associated with the development of an enhanced myogenic response (Brayden & Nelson, 1992; Nelson *et al.,* 1995; Brenner *et al.,* 2000; Amberg & Santana, 2003).

Heteromultimeric Kv1 channels are widely expressed in VSM tissues, the composition of which may vary in a vessel-specific manner. RCAs express the channel containing at a minimum, $K_v1.2$ and $K_v1.5$ pore-forming subunits (Albarwani *et al.,* 2003; Chen *et al.,* 2006), whereas in other types of vessels (e.g. rabbit portal vein and mesenteric arteries), the channel also contains accessory $K_v\beta$ subunits ($K_v\beta$1-2) (Thorneloe *et al.,* 2001; Plane *et al.,* 2005). K_v1-containing channels are believed to act as a voltage-dependent brake that opposes myogenic depolarization (Figure 3.3). For example, selective pharmacological suppression of K_v1-containing channels with 4-AP (≤300 μM) or correolide (1-10 μM) enhanced E_m depolarization and the myogenic

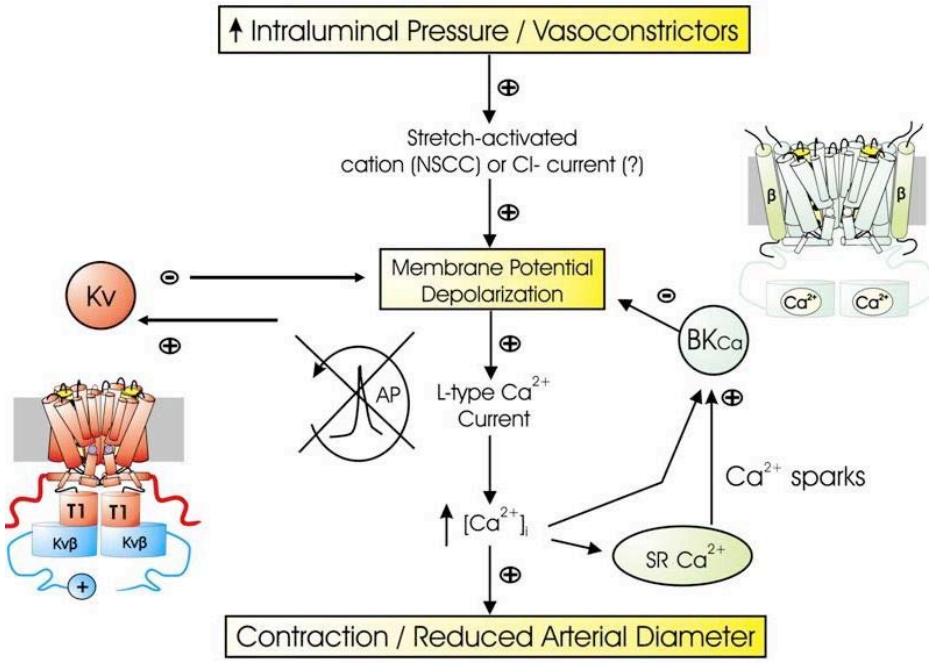

Figure 3.3: Model for the role of K_v1 and BK_{Ca} channels in the negative feedback control of myogenic depolarization.

Pressure elevation-evoked E_m depolarization subsequently induces Ca^{2+} entry from voltage-dependent Ca^{2+} channels, an increase in intracellular $[Ca^{2+}]_i$, activation of MLCK, phosphorylation of LC_{20}, cross bridge cycling, and, therefore, vasoconstriction. Large-conductance Ca^{2+}-activated K^+ (BK_{Ca}) and voltage-gated K_v1 channels contribute to the negative feedback control of E_m depolarization so as to prevent regenerative Ca^{2+} influx and action potentials. BK_{Ca} channels are activated by Ca^{2+} sparks owing to SR Ca^{2+} release, and act as a Ca^{2+}-dependent brake to maintain a steady-state increase in E_m and $[Ca^{2+}]_i$. K_v1 channels are activated by E_m depolarization and act as a voltage-dependent brake to oppose further E_m depolarization.

response of small resistance arteries (e.g. cerebral arteries, small mesenteric arteries) (Knot & Nelson, 1995; Albarwani *et al.*, 2003; Plane *et al.*, 2005). Over-expression of a dominant-negative $K_v1.5$ or wild-type $K_v1.5$ subunits was found to enhance or suppress the cerebral myogenic response, respectively (Chen *et al.*, 2006).

3.1.2.3 K_v2-containing channels

It is important to note that K_v1-containing channels are not the only type of K_v channels that contribute to K_{DR} currents and control of E_m depolarization in VSM. K_v2 message and/or protein expression has been detected in various VSM tissues, for example, cerebral arteries (Amberg & Santana, 2006), pulmonary arteries (Patel *et al.*, 1997; Coppock & Tamkum, 2001; Platoshyn *et al.*, 2001; Smirnov *et al.*, 2002), mesenteric arteries (Moreno-Dominguez *et al.*, 2009), aorta (Belevych *et al.*, 2002), coronary arteries (Thorne *et al.*, 2002) and placental vasculature (Wareing *et al.*, 2006). Moreover, inhibition of K_v2-containing channels appears to be associated with a change in the myogenic response. For instance, Amberg & Santana (2006) showed that ScTx1 suppression of K_v2 currents enhanced constriction in RCAs at an intraluminal pressure of 80 mmHg. Also, abnormal regulation of arterial diameter in hypertension and in a canine model of subarachnoid hemorrhagic stroke was shown to be accompanied by a reduction in whole-cell K_v2 current and/or subunit expression (Yuan *et al.*, 1998; Wang *et al.*, 2005; Amberg & Santana, 2006; Jahromi *et al.*, 2008a,b; Moreno-Dominguez *et al.*, 2009). These findings suggest a potential role of K_v2-containing channels in myogenic control of E_m depolarization and arterial diameter, however, their specific contribution remains unclear.

3.1.2.4 Silent subunits in association with K_v2 subunits

K_v2 subunits can co-assemble with K_v5, K_v6, K_v8 or K_v9 silent subunits to form heteromultimeric channels with a subunit stoichiometry of 3:1 (Kerschensteiner *et al.,* 2005; Coetzee *et al.,* 2006). The presence of silent subunits affects the biophysical properties of the channel complex. Specifically, the kinetics of activation and deactivation, voltage-dependence of activation and inactivation, and/or current amplitude are altered (Patel *et al.,* 1997; Salinas *et al.,* 1997a,b; Kerschensteiner & Stocker, 1999; Shepard & Rae, 1999; Ottschytsch *et al.,* 2002; Kerschensteiner *et al.,* 2003, 2005). These alterations have the potential to affect the contribution of the channels to the control of E_m.

Transcripts encoding members of the K_v5, K_v6 and K_v9 sub-families were found to be expressed in pulmonary, placental arteries (Patel *et al.,* 1997; Platoshyn *et al.,* 2001; Davies & Kozlowski, 2001; Wareing *et al.,* 2006), and urinary bladder ($K_v5.1$ and $K_v6.1$-6.3, Thorneloe & Nelson, 2003; $K_v9.3$, Chen *et al.,* 2010). The possibility that K_v2 channels of RCA myocytes might be heteromultimers containing silent subunits was considered by Amberg & Santana (2006), yet the molecular composition of the channels was not determined.

Whether silent subunits associate with K_v2 subunits to form K_v2-containing channels in cerebral myocytes and how the channels contribute to control of E_m and arterial diameter is an important question that must be addressed to understand cerebral myogenic regulation. In addition, the knowledge may provide insights concerning the presence of multiple types of K_v channels in resistance arterial myocytes, and the

pathophysiological significance of reduced K_v2 currents in association with arterial dysfunction.

3.2 Hypothesis and objectives of the study

Here, we tested the specific **hypothesis** that ScTx1-sensitive, K_v2-containing channels that contribute to control of cerebral arterial diameter are heteromultimeric channels owing to the co-assembly of $K_v2.1$ or $K_v2.2$ with silent subunit(s). The four primary objectives of this study were as follows:

(1) To determine the expression of mRNA transcripts encoding $K_v2.1$, $K_v2.2$ and silent subunits in RCA myocytes.

(2) To evaluate the contribution of ScTx1-sensitive, K_v2-containing channels to control of RCA diameter over the entire intraluminal pressure range from 10 to 100 mmHg.

(3) To conduct a comparison of the biophysical properties of ScTx1-sensitive, K_v2-containing channels and recombinant $K_v2.1$, as well as $K_v2.1/K_v9.3$ channels.

(4) To detect the co-localization of $K_v2.1$ and $K_v9.3$ proteins at the plasma membrane of RCA myocytes.

3.3 Results

3.3.1 Control pressure myograph experiments

As shown in Figure 3.4A & B, after development and stabilization of the myogenic response (see Chapter 2.8 for the protocol in detail), RCAs were pressurized to 120 mmHg for ~45 min, the approximate time required to complete all drug treatment experiments described. No change in arterial diameter was observed over this period. The same results were obtained in experiments when RCAs were pressurized to

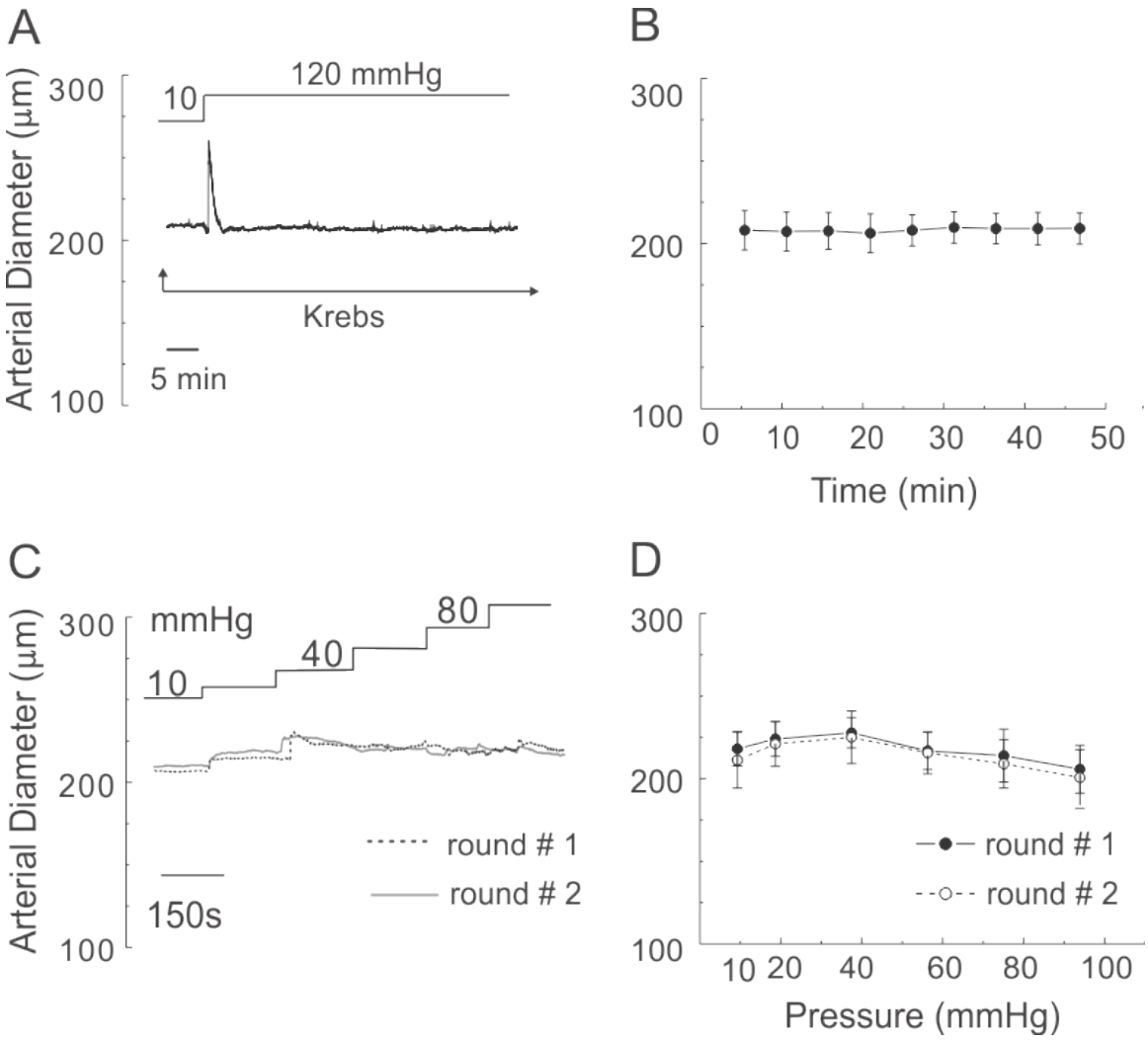

Figure 3.4: Time control experiments for diameter analysis of the myogenic response in pressurized RCAs.

(A, B) Representative recording of arterial diameter and mean values ± SEM of RCAs (n=3) held for ~45 min following a pressure step from 10 to 120 mmHg in control Krebs' solution (containing 2.5 mM Ca^{2+}). (C, D) Representative recording of arterial diameter and mean values ± SEM of RCAs (n=5) subjected to two rounds of step-wise elevation in intraluminal pressure from 10 to 100 mmHg in increments of 20 mmHg in control Krebs' solution.

80 mmHg or 10 mmHg for ~45 min (n=3, each). These observations indicate that any changes in arterial diameter of pressurized RCAs in response to drug treatments were not due to a loss of the myogenic response with time *in vitro*.

As shown in Figure 3.4C & D, after development and stabilization of the myogenic response, RCAs were subjected to two sequential rounds of step-wise elevation in intraluminal pressure from 10 to 100 mmHg in increments of 20 mmHg in control Krebs' solution. The changes in arterial diameter measured during the two rounds of pressure changes were identical.

3.3.2 Effect of ScTx1 on the cerebral myogenic response

Figure 3.5A & B shows the concentration-dependent vasoconstriction evoked by 5-30 nM ScTx1 in RCAs pressurized to 80 mmHg. A near peak constriction was obtained at 80 mmHg with 30 nM ScTx1, as previously described (Amberg & Santana, 2006). ScTx1 evoked a stable, sustained vasoconstriction that was of similar magnitude during repeated applications of the toxin and unaffected by endothelial removal or when the toxin was repeatedly applied (data not shown). Figure 3.5C & D shows representative recordings and mean ± SEM values of RCA diameter for intraluminal pressure between 10 and 100 mmHg in control Krebs' solution, during exposure to 30 nM ScTx1, and then Ca^{2+}-free Krebs' solution. RCA diameter was either maintained or decreased with increasing intraluminal pressure in control Krebs' solution at >~40 mmHg. ScTx1 treatment caused a significant decrease in arterial diameter and an increase in active myogenic constriction (i.e. the difference between the passive diameter recorded in Ca^{2+}-free Krebs' solution and in control or ScTx1-containing Krebs' solution) at all pressures tested, including the range of 10 to 40 mmHg (Figure 3.5C-E). Figure 3.5F shows a

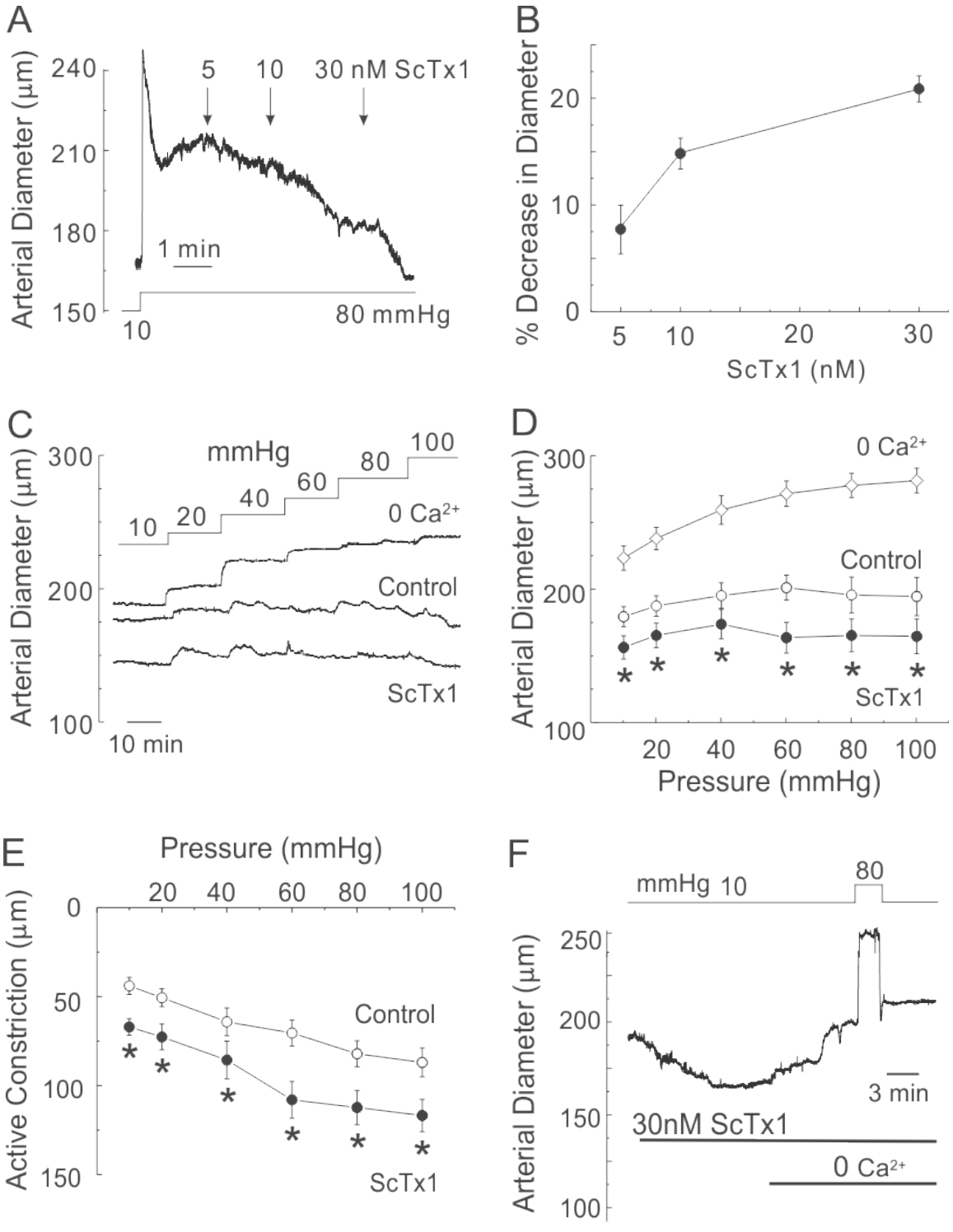
A
Arterial Diameter (μm)
240
210
180
150
5
10
30 nM ScTx1
1 min
10
80 mmHg
B
% Decrease in Diameter
20
10
0
5
10
20
30
ScTx1 (nM)
C
Arterial Diameter (μm)
300
200
100
mmHg
10
20
40
60
80
100
0 Ca2+
Control
ScTx1
10 min
D
Arterial Diameter (μm)
300
200
100
0 Ca2+
Control
ScTx1
*
20
40
60
80
100
Pressure (mmHg)
E
Pressure (mmHg)
20
40
60
80
100
Active Constriction (μm)
0
50
100
150
Control
ScTx1
*
F
mmHg 10
80
Arterial Diameter (μm)
250
200
150
100
3 min
30nM ScTx1
0 Ca2+

Figure 3.5: Effect of ScTx1 on the cerebral myogenic response.

(A) Representative recording of arterial diameter at 80 mmHg showing a concentration-dependent constriction of RCA treated with 5-30 nM ScTx1. (B) Mean values ± SEM (n = 4) for the % decrease in RCA diameter in the presence of ScTx1 at 80 mmHg. (C & D) Representative recordings and mean values ± SEM (n = 7) of RCA diameter between 10 and 100 mmHg under control conditions, and following 30 nM ScTx1 prior to exposure to 0 Ca^{2+} Krebs' solution to determine passive diameter at each pressure. (E) Mean values ± SEM (n = 7) for active constriction under control conditions and the treatment with ScTx1 (value for active constriction is the difference between control or ScTx1 diameter and passive diameter). (F) Representative recording of vasoconstriction evoked by ScTx1 at 10 mmHg. *Significantly different ($P < 0.05$) from value in the control condition at each pressure.

representative example of the constriction evoked by 30 nM ScTx1 at 10 mmHg that was 27 ± 4.5 μm in 17 RCAs.

Given that E_m between 10 and 40 mmHg was reported to be <−50 mV in RCAs (Knot & Nelson, 1998), the nature of the channel(s) responsible for the influx of Ca^{2+} warranted examination. Figure 3.6A-D shows representative recordings and mean ± SEM values for RCA diameter at 10 mmHg in the presence of ScTx1 followed by treatment with diltiazem (10 μM), nifedipine (1 μM), mibefradil (1 μM) or SKF96365 (10-30 μM), prior to exposure to Ca^{2+}-free Krebs' solution. Inhibition of VGCCs via diltiazem, nifedipine or mibefradil reversed the ScTx1-induced constriction at 10 mmHg, whereas inhibition of NSCCs via SKF96365 had no effect, although it was able to suppress the myogenic response evoked by a subsequent pressure step from 10 to 80 mmHg. These observations indicate that inhibition of VGCCs, but not NSCCs, is responsible for the influx of Ca^{2+} associated with ScTx1-evoked vasoconstriction at 10 mmHg.

3.3.3 Expression of K_v2.1 and K_v9.3 subunits in rat cerebral artery (RCA) myocytes

The voltage range reported for the activation of homomultimeric K_v2.1 channels expressed in Xenopus oocytes or mammalian cells is positive to −40 mV (Patel *et al.*, 1997; Salinas *et al.*, 1997a,b; Kerschensteiner & Stocker, 1999; Shepard & Rae, 1999; Ottschytsch *et al.*, 2002; Kerschensteiner *et al.*, 2003, 2005). Considering the ability of ScTx1 to evoke constriction of RCAs between 10 and 40 mmHg at which E_m is <–50 mV (Knot & Nelson, 1998), it appeared that the K_v2-containing channels must contain silent subunit(s) to account for the ScTx1 sensitivity at low pressure. Therefore, the expression of transcripts encoding members of the K_v5, K_v6 and K_v9 subfamilies previously demonstrated to be expressed in SMCs were examined. As shown in figure 3.7B, mRNA

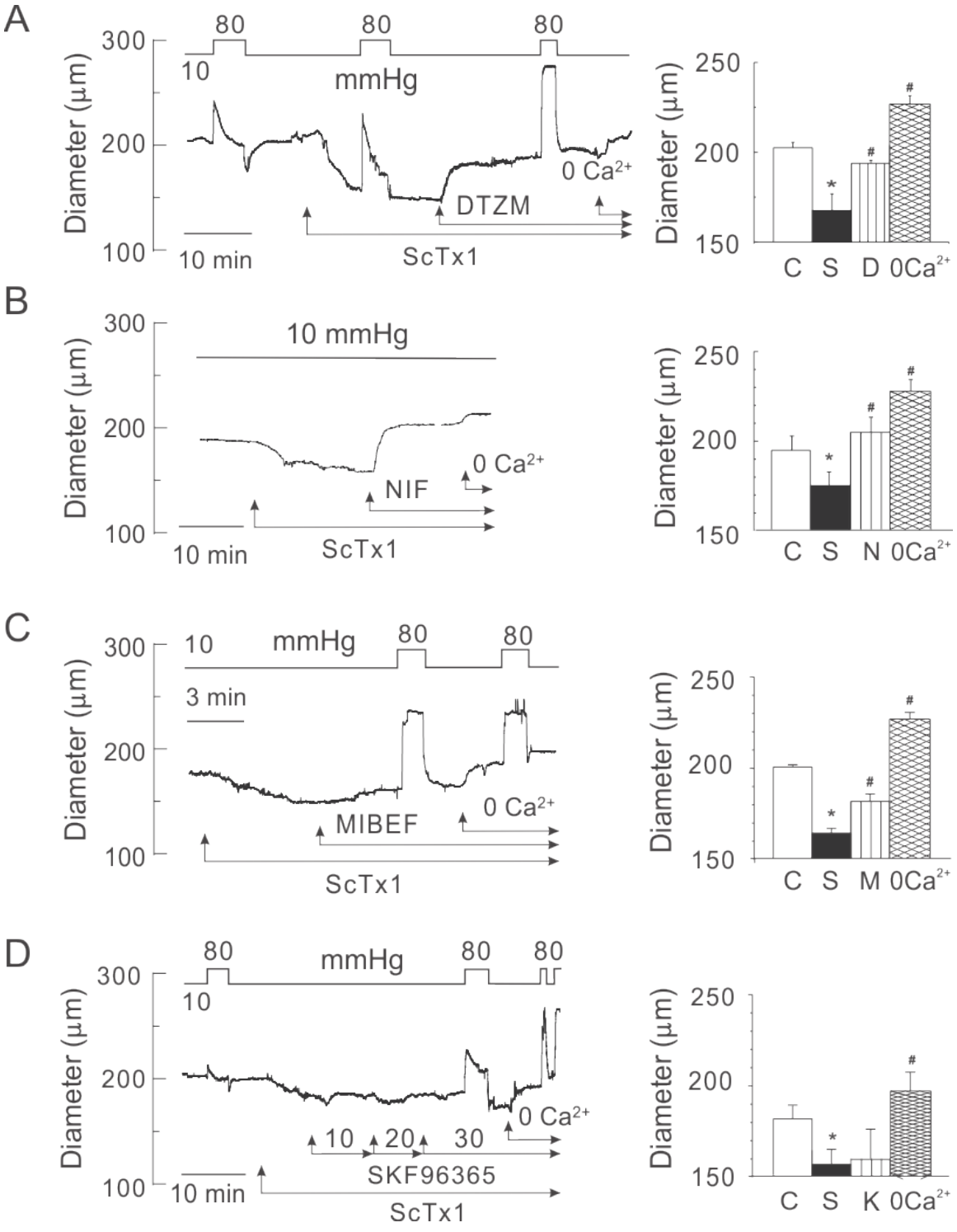
A
80
80
80
10
mmHg
300
200
100
Diameter (μm)
0 Ca2+
DTZM
10 min
ScTx1
250
200
150
Diameter (μm)
C S D 0Ca2+
B
10 mmHg
0 Ca2+
NIF
10 min
ScTx1
C S N 0Ca2+
C
10
mmHg
80
80
3 min
MIBEF
0 Ca2+
ScTx1
C S M 0Ca2+
D
80
mmHg
80
80
10
0 Ca2+
10
20
30
SKF96365
10 min
ScTx1
C S K 0Ca2+

Figure 3.6: Inhibition of VGCCs but not NSCCs reverses ScTx1-evoked vasoconstriction.

(A) Representative recording and mean values ± SEM (n = 4) of RCA diameter at 10 mmHg under control conditions and following sequential treatment with ScTx1 (30 nM), diltiazem (10 μM) and 0 Ca^{2+} Krebs' solution. Brief steps to 80 mmHg show that the extent of the myogenic response was enhanced by ScTx1 and inhibited by diltiazem. (B) Representative recording and mean values ± SEM (n = 6) of RCA diameter at 10 mmHg under control conditions and following sequential treatment with ScTx1 (30 nM), nifedipine (1 μM) and 0 Ca^{2+} Krebs' solution. (C) Representative recording and mean values ± SEM (n = 4) of RCA diameter at 10 mmHg under control conditions and following sequential treatment with ScTx1 (30 nM), mibefradil (1 μM) and zero Ca^{2+} solution. Brief steps to 80 mmHg show that the myogenic response was inhibited by mibefradil to level observed in 0 Ca^{2+} Krebs' solution. (D) Representative recording and mean values ± SEM (n = 4) of RCA diameter at 10 mmHg under control conditions and following sequential treatment with ScTx1 (30 nM), 10, 20, and 30 μM SKF96365 and 0 Ca^{2+} Krebs' solution. SKF96365 did not affect ScTx1-evoked constriction, and brief steps to 80 mmHg indicated that the extent of the myogenic response was reduced by SKF96365 confirming that effective block of NSCCs was achieved. * and $^{\#}$ are significantly different ($P < 0.05$) from value in control solution and ScTx1, respectively.

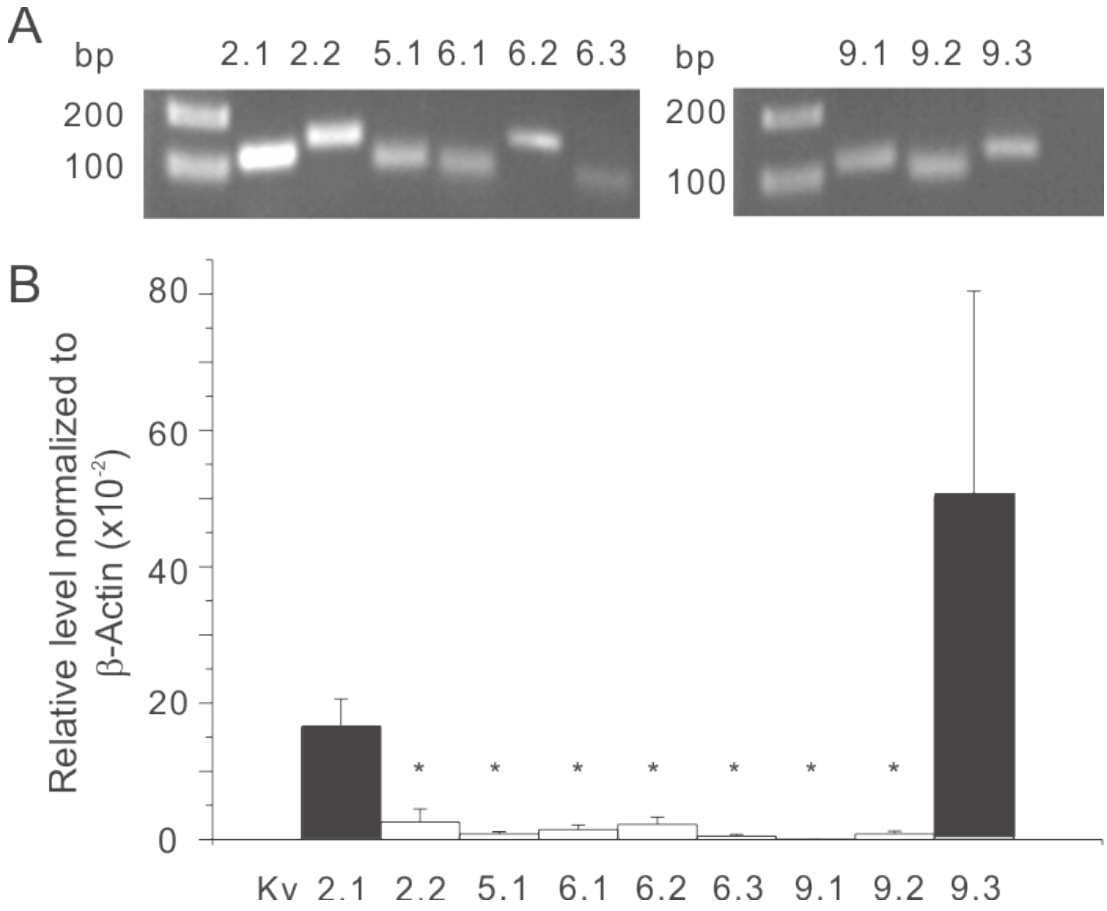

Figure 3.7: K_v2.1 and K_v9.3 are predominant transcripts expressed by RCA myocytes.

(A) Representative gels indicating generation of amplicons of appropriate sizes using QPCR primer pairs for K_v2.1, K_v2.2, K_v5.1, K_v6.1-K_v6.3, K_v9.1-9.3 and mRNA extracted from rat brain. Similar results were obtained from 7 additional experiments. (B) Mean values ± SEM (n = 4) for level of K_v2.1, K_v2.2, K_v5.1, K_v6.1-K_v6.3, K_v9.1-9.3 transcript expression relative to β-actin determined by real-time PCR and mRNA derived from RCA myocytes from different rats. Relative transcript levels were determined using the $2^{\Delta\Delta Ct}$ method. * Significantly different ($P < 0.05$) from value for K_v2.1.

transcripts for K_v2.1 and K_v9.3 were expressed at a substantially high level, whereas transcripts for K_v2.2, K_v5.1, K_v6.1-6.3, K_v9.1 and K_v9.2 were expressed only at very low or undetectable levels. Figure 3.7A shows the result of RT-PCR using QPCR primer pairs and mRNA derived from rat brain. Each of the QPCR primer pairs generated amplicons of appropriate size.

3.3.4 Properties of ScTx1-sensitive K_v2 current of RCA myocytes

Based on the abundance of K_v2.1 and K_v9.3 message expression in RCAs, we employed standard whole-cell voltage clamp recording methods to determine the functional identity of the native ScTx1-sensitive current of freshly isolated myocytes with currents owing to heterologous expression of K_v2.1 or K_v2.1/K_v9.3 channels in HEK 293 cells at both 22 °C and 35 °C.

Figure 3.8 shows that 100 nM ScTx1 caused a ~90% inhibition of K_v2.1/K_v9.3 current in HEK cells, as previously described (Escoubas *et al.,* 2002). Figure 3.9A & B shows 100 nM ScTx1 significantly suppressed whole-cell K_v currents of RCA myocytes. ScTx1-sensitive currents were determined by digital subtraction of the residual current in the presence of ScTx1 from control currents. The ScTx1-sensitive component accounted for ~60% of total K_v currents recorded at +25 mV (Figure 3.9C). Figure 3.9D shows that increasing the temperature of the bathing solution from 22 °C to 35 °C caused a marked increase in amplitude, as well as the kinetics of activation and deactivation. The level of steady-state activation of native current as a function of voltage was determined at 22 °C and 35 °C by normalization of tail current amplitude at –45 mV following steps to between –95 and +45 mV (Figure 3.9E). Increasing temperature from 22 °C to 35 °C caused an

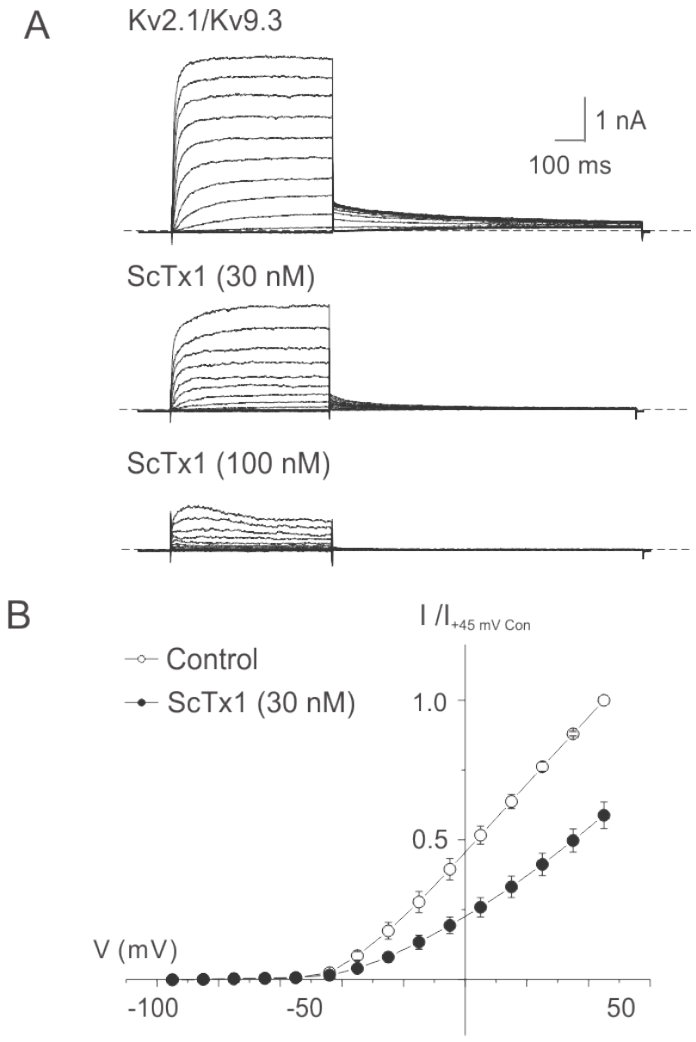

Figure 3.8: Suppression of $K_v2.1/K_v9.3$ current by ScTx1 in HEK 293 cells.

(A) Representative family of $K_v2.1/K_v9.3$ currents in the absence ($K_v2.1/K_v9.3$) and presence of 30 or 100 nM ScTx1. Voltage steps of 325 ms duration between −95 and +45 mV in increments of 10 mV prior to repolarization to − 55 mV were applied from a holding potential of −75 mV. (B) Mean values ± SEM (n = 6) of normalized current (to control value at +45 mV) *versus* voltage in the absence (Control) and presence of 30 nM ScTx1.

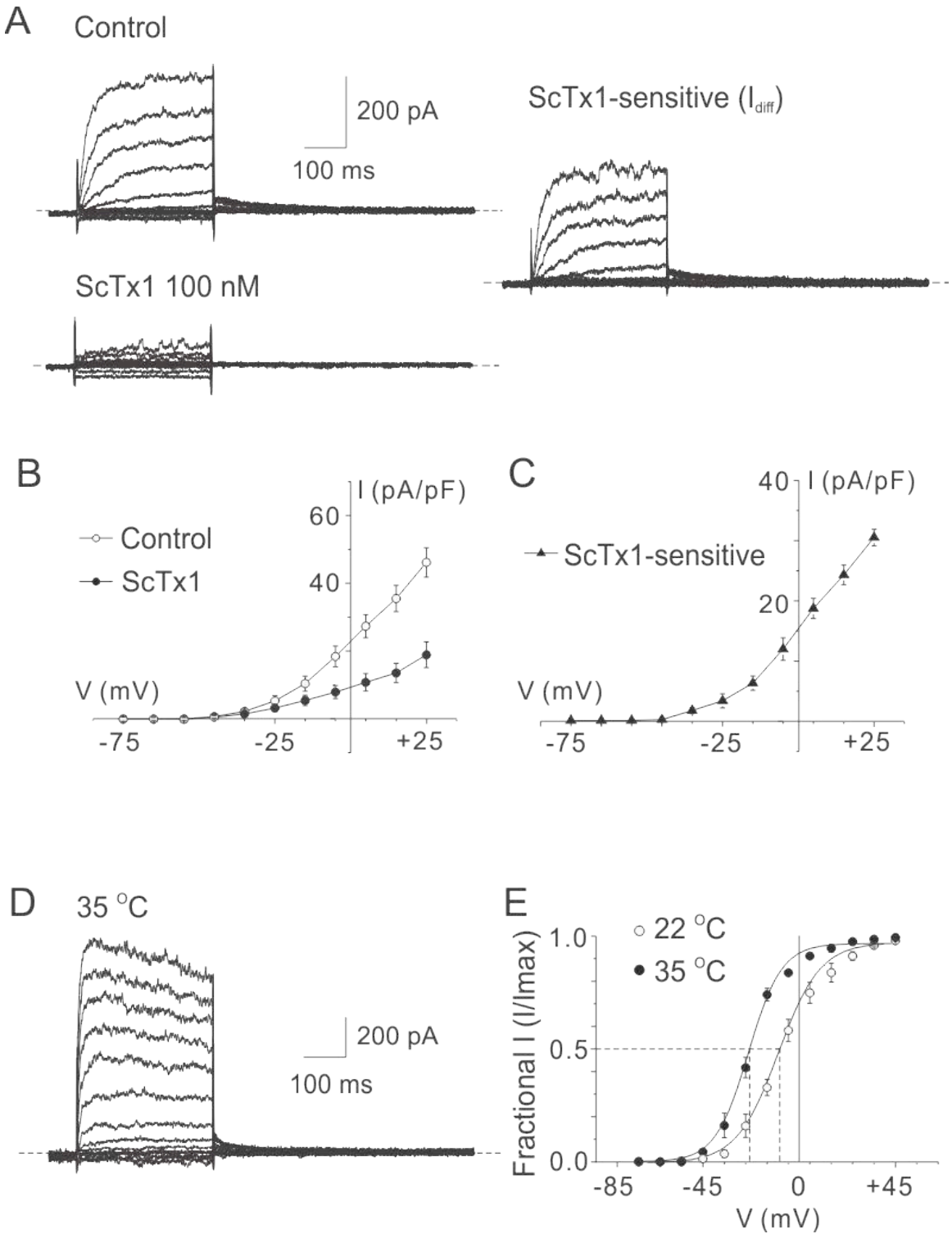
A
Control
200 pA
100 ms
ScTx1-sensitive (I_{diff})
ScTx1 100 nM
B
I (pA/pF)
60
40
Control
ScTx1
V (mV)
-75
-25
+25
C
40
I (pA/pF)
ScTx1-sensitive
20
V (mV)
-75
-25
+25
D
35 °C
200 pA
100 ms
E
22 °C
35 °C
Fractional I (I/Imax)
1.0
0.5
0.0
-85
-45
0
+45
V (mV)

Figure 3.9: ScTx1-sensitive K_v2 current in RCA myocytes.

(A) Representative recordings of whole-cell K_v currents of an RCA myocyte in the absence (Control) and presence of 100 nM ScTx1 (left) and the ScTx1-sensitive current (right) determined by digital subtraction of residual current in the presence of ScTx1 from Control current at 22ºC. Voltage steps of 325 ms duration between −95 and +45 mV in increments of 10 mV prior to repolarization to −45 mV were applied from a holding potential of −75 mV. Similar recordings were obtained from 7 additional myocytes from cell isolations of RCAs of 3 rats. (B & C) Mean values ± SEM (n = 6) for whole-cell and ScTx1-sensitive I-V relations. (D) Representative recordings of ScTx1-sensitive K_v current of RCA myocytes at 35ºC. (E) Mean values ± SEM for normalized tail current amplitude *versus* command step voltage for native current at 22 and 35ºC (n = 6 and 3, respectively) that exhibited complete suppression of tail current following treatment with ScTx1. Solid lines represent best fits to the data points using a standard Boltzmann function.

Table 3.1: Biophysical properties of native, $K_v2.1$ and $K_v2.1/K_v9.3$ currents.

	Native K_v	$K_v2.1/K_v9.3$	$K_v2.1$	$K_v2.1/K_v9.2$
$V_{0.5}$ act (22 °C)	−8.5± 1.9 mV (n = 6)	−12.8 ± 4.6 mV (n = 8)	−4.8 ± 1.1 mV* (n = 6)	−13.3 ± 1.3 mV (n = 6)
$V_{0.5}$ act (35 °C)	−25.2 ± 3 mV (n = 3)	−28.4 ± 1.3 mV (n = 5)	−14.6 ± 3 mV* (n = 4)	n.a.
Deact τ_{fast} (+25 mV & 22 °C)	82 ± 22 ms (n = 6)	66 ± 11 ms (n = 8)	16 ± 1 ms* (n = 6)	14 ± 0.5 ms* (n = 6)
Deact τ_{slow} (+25 mV & 22 °C)	442 ± 60 ms (n = 6)	298 ± 60 ms (n = 8)	69 ± 18 ms* (n = 6)	53 ± 3 ms* (n = 6)

$V_{0.5}$ act, value of voltage for half-maximal activation; Deact τ_{fast}, deactivation time constant. ***** Significantly different from value for native current. All values are based on n cells obtained from three or more rats or cell transfections.

increase in current in the range of −55 to −25 mV and a significant leftward shift in the activation curve from ~−9 mV to −25 mV (Table 3.1).

3.3.5 Comparison of recombinant and native ScTx1-sensitive currents

Whole-cell currents owing to homomultimeric $K_v2.1$ and heteromultimeric $K_v2.1$ and $K_v9.3$ were recorded under identical conditions as native RCA myocyte current. Figure 3.10A & B shows representative families (at 22 and 35 °C) and mean current density *versus* voltage relations for $K_v2.1$ and $K_v2.1/K_v9.3$ currents (at 22 °C), respectively. Note that the amplitude of $K_v2.1/K_v9.3$ current within the physiological range of E_m was significantly greater than that of $K_v2.1$ at both temperatures. This is evident in Figure 3.10C, which shows that at 35 °C, the current due to $K_v2.1/K_v9.3$, but not $K_v2.1$ was activated during steps from −75 to −55 and −45 mV. Also, the decay of the tail current on repolarization to −55 mV was slower for $K_v2.1/K_v9.3$ compared to $K_v2.1$ at both temperatures (Figure 3.10A), which is apparent in the expanded representative recordings at 22 °C shown in Figure 3.10D.

Figure 3.11 shows expanded tail currents for ScTx1-sensitive current of RCA myocytes, recombinant $K_v2.1$, $K_v2.1/K_v9.2$ and $K_v2.1/K_v9.3$ channels of HEK 239 cells, recorded at −45 mV following steps to +25 mV (Figure 3.11A), as well as superimposed recordings of each normalized to peak amplitude of native tail current (Figure 3.11B). Note that each recording was best fitted by a bi-exponential function (continuous lines). The decay of the native and $K_v2.1/K_v9.3$ tail currents were identical and slower than that of $K_v2.1$. The similarity in rate of deactivation of the native and $K_v2.1/K_v9.3$ currents *versus* $K_v2.1$ was also apparent from the values determined for the fast and slow time

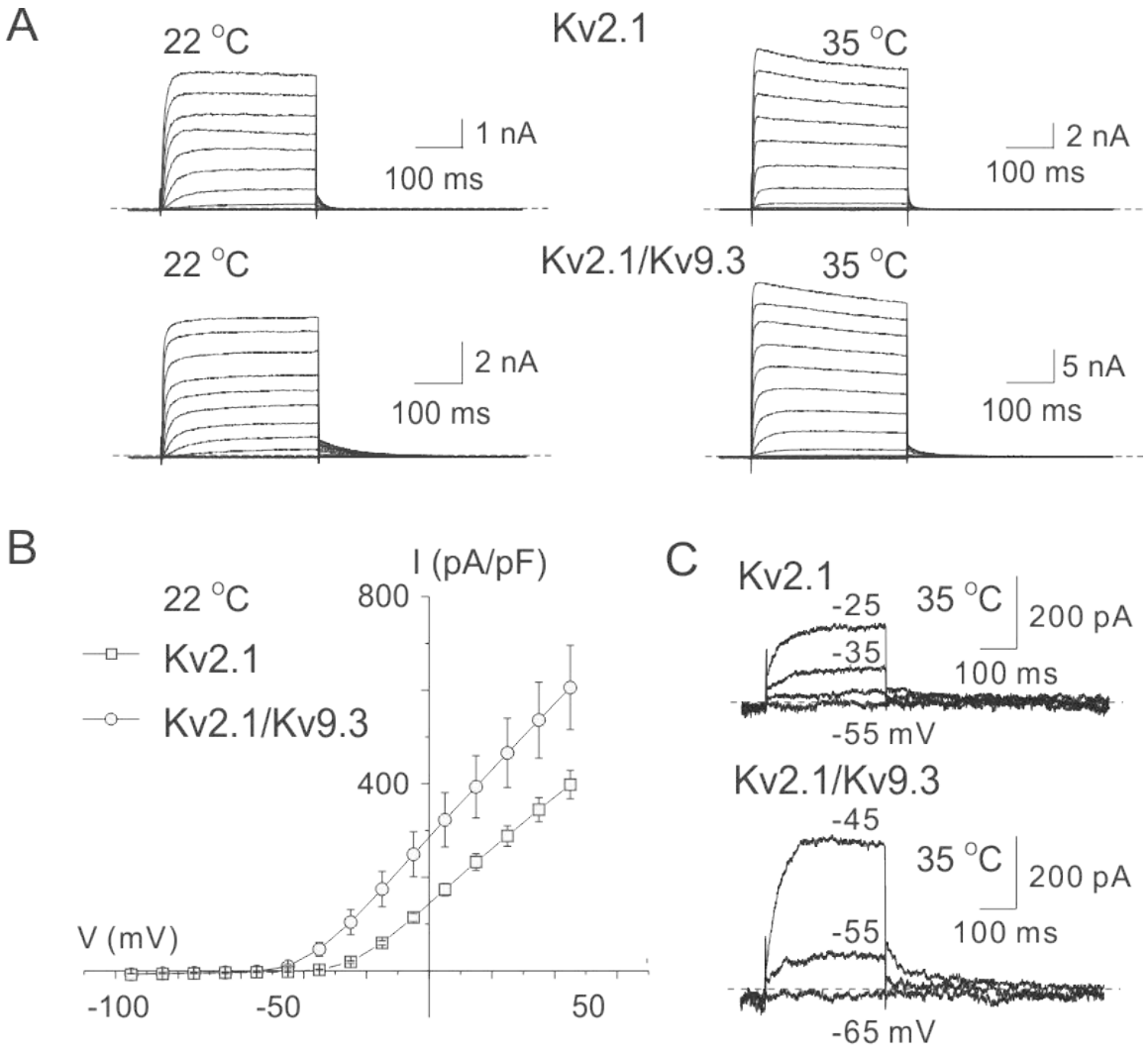
A
22 °C
Kv2.1
35 °C
1 nA
100 ms
2 nA
100 ms
22 °C
Kv2.1/Kv9.3
35 °C
2 nA
100 ms
5 nA
100 ms
B
I (pA/pF)
22 °C
Kv2.1
Kv2.1/Kv9.3
800
400
V (mV)
-100
-50
50
C
Kv2.1
-25
35 °C
200 pA
-35
100 ms
-55 mV
Kv2.1/Kv9.3
-45
35 °C
200 pA
-55
100 ms
-65 mV
D
Kv2.1
22 °C
200 pA
25 ms
Kv2.1/Kv9.3
22 °C
400 pA
25 ms

Figure 3.10: $K_v2.1$ and $K_v2.1/K_v9.3$ currents in HEK 293 cells.

(A) Representative families of whole-cell currents due to expression of $K_v2.1$ (upper) and $K_v2.1/K_v9.3$ (lower) channels in HEK 293 cells recorded at 22 and 35ºC (left and right, respectively). Voltage steps of 325 ms duration between -95 and +45 mV in increments of 10 mV prior to repolarization to −55 mV were applied from a holding potential of −75 mV. (B) Mean values ± SEM (n = 6 and 8, respectively) for current density (pA/pF) *versus* voltage relation for $K_v2.1$ and $K_v2.1/K_v9.3$ channels in HEK 293 cells at 22ºC. (C) Representative $K_v2.1$ and $K_v2.1/K_v9.3$ currents recorded in response to command steps to between −55 and −25 mV and between −65 and −45 mV, respectively. Note the activation of current due to heteromultimeric, but not homomultimeric channels at −55 mV. (D) Representative families of expanded $K_v2.1$ and $K_v2.1/K_v9.3$ tail currents recorded at −50 mV at 22ºC illustrating the significantly slower deactivation kinetics of the heteromultimeric channels.

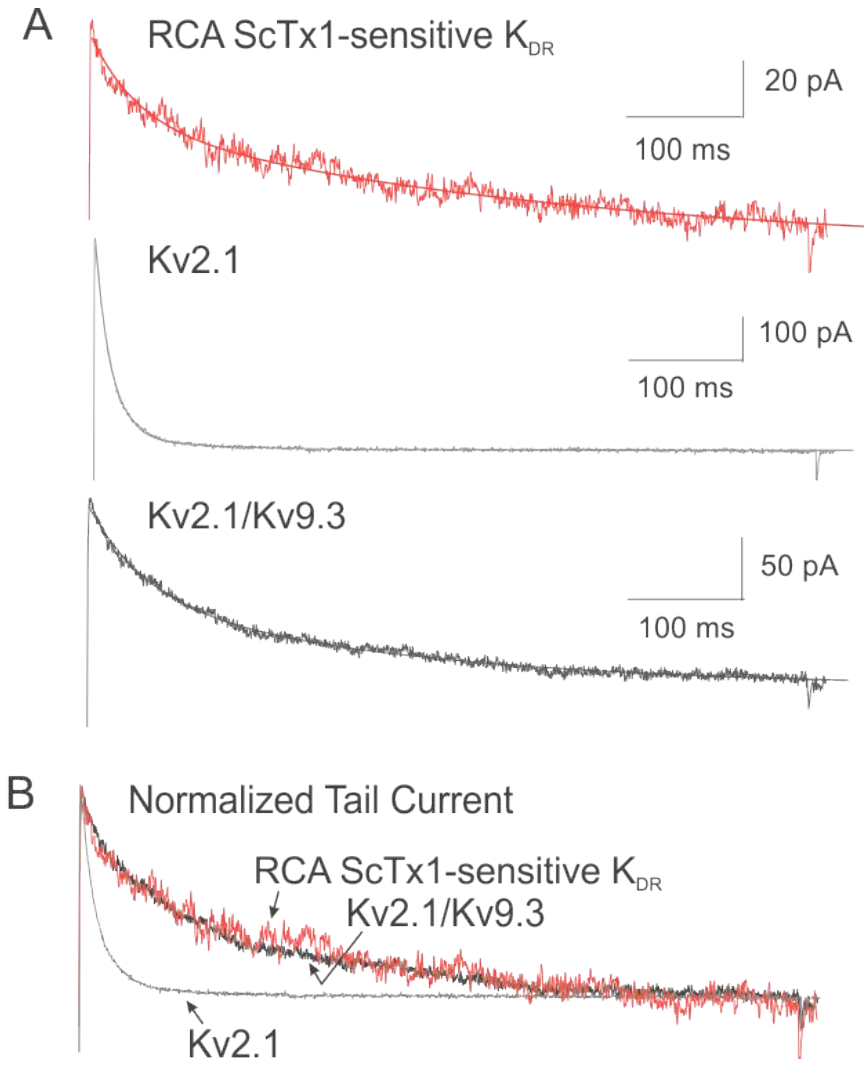

Figure 3.11: Decay of native ScTx1-sensitive K_v2 current mimics that of $K_v2.1/K_v9.3$, but not $K_v2.1$ channels.

(A) Expanded representative recordings of tail currents of native RCA ScTx1-sensitive K_v, $K_v2.1$ and $K_v2.1/K_v9.3$ channels at −45 mV following steps to +25 mV at 22ºC. Solid lines through each recording represent the best fit using a two-exponential function. (B) Superimposed tail current recordings from panel A with currents for $K_v2.1$ and $K_v2.1/K_v9.3$ normalized to value of peak tail current of native channels.

constants of the decay, as shown in Table 3.1. We also evaluated $K_v2.1/9.2$ recombinant currents. The fast and slow time constants of deactivation of $K_v2.1/9.2$ currents were significantly different from $K_v2.1/9.3$ currents and native currents (Table 3.1). This is consistent with a previous report for $K_v2.1/K_v9.2$ and $K_v2.1/K_v9.1$ channels expressed in Xenopus oocytes, both of which exhibited fast decay of tail currents (Salinas *et al.,* 1997b).

A further comparison between the native and recombinant currents was made through determination of the voltage dependence of activation of $K_v2.1$ and $K_v2.1/K_v9.3$ currents at 22 and 35 °C. Figure 3.12A shows that steady-state activation of $K_v2.1/9.3$ occurred over a more negative voltage range compared to $K_v2.1$ at 22 °C. Figure 3.12B & C shows that increasing the temperature to 35 °C caused a negative shift in the voltage dependence of activation of $K_v2.1$ and $K_v2.1/K_v9.3$ current. When compared to the activation of native ScTx1-sensitive current at the same temperatures (indicated by the dashed lines; data were obtained from Figure 3.9E), the activation curves for $K_v2.1/K_v9.3$ at 22 and 35 °C, but not those for $K_v2.1$ homomultimeric channels, closely mimicked the activation of the native current. Mean values for half-maximal activation of the native and recombinant currents of cells/myocytes are indicated in Table 3.1.

3.3.6 PLA detection of the co-localization of $K_v2.1$ and $K_v9.3$ proteins in RCA myocytes

We attempted to detect the co-assembly of $K_v2.1$ and $K_v9.3$ subunits using a co-immunoprecipitation approach that was previously used for $K_v1.2/K_v1.5$ channels of rabbit portal vein and RCAs (Thorneloe *et al.,* 2001; Albarwani *et al.,* 2003). $K_v2.1$ proteins were detected in anti-$K_v2.1$ immunoprecipitates of RCAs and HEK 293 cells transfected with $K_v2.1/K_v9.3$, but the commercially available $K_v9.3$ antibodies were not

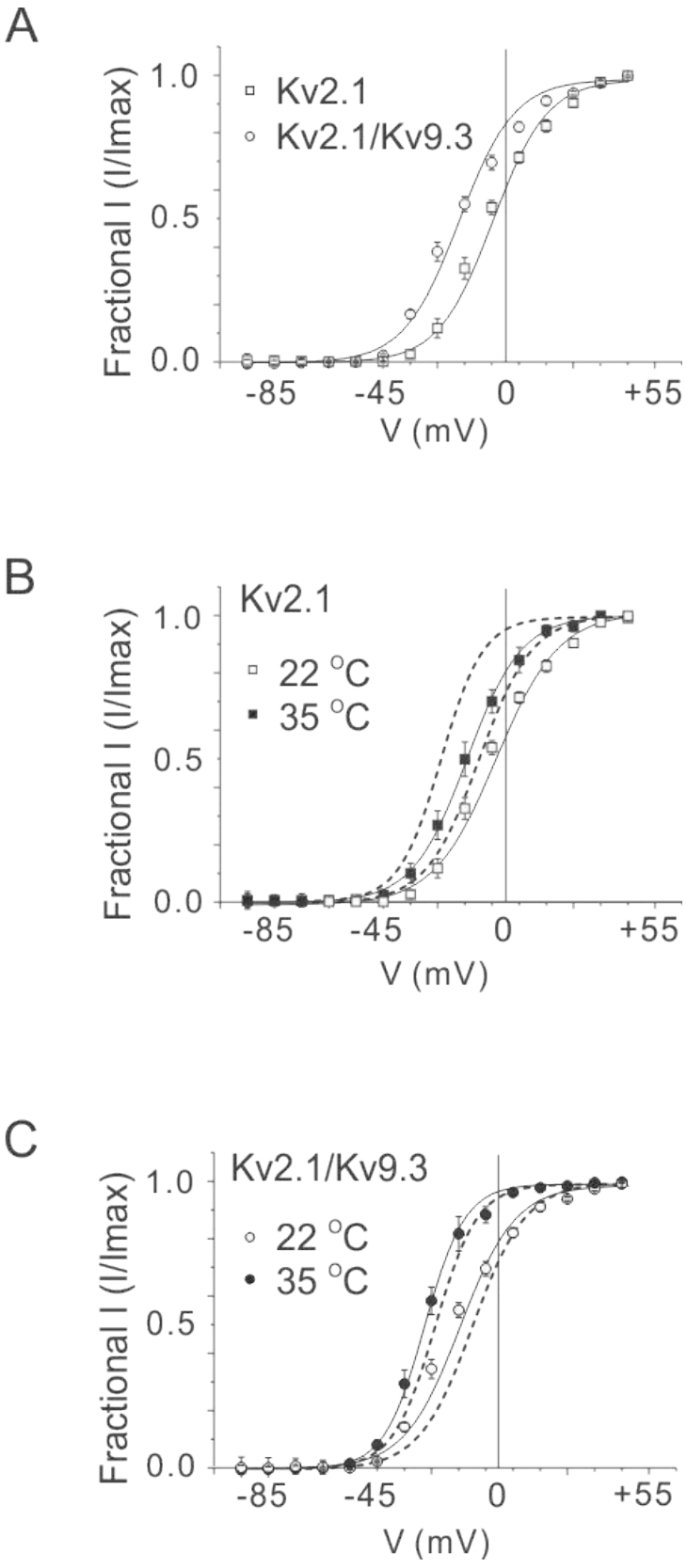
A
Fractional I (I/Imax)
1.0
0.5
0.0
Kv2.1
Kv2.1/Kv9.3
-85
-45
0
+55
V (mV)
B
Fractional I (I/Imax)
1.0
0.5
0.0
Kv2.1
22 °C
35 °C
-85
-45
0
+55
V (mV)
C
Fractional I (I/Imax)
1.0
0.5
0.0
Kv2.1/Kv9.3
22 °C
35 °C
-85
-45
0
+55
V (mV)

Figure 3.12: Voltage-dependence of activation of $K_v2.1/K_v9.3$, but not $K_v2.1$ channels mimics that of native K_v2 current.

(A) Mean values ± SEM for normalized tail current amplitude *versus* command step voltage for $K_v2.1$ and $K_v2.1/K_v9.3$ currents at 22ºC (n = 6 and 8, respectively). Note the negative shift in voltage-dependence of $K_v2.1/K_v9.3$. (B) Mean values ± SEM for normalized tail current amplitude *versus* command step voltage for $K_v2.1$ current at 22 and 35 ºC (n = 6 and 3, respectively). (C) Mean values ± SEM for normalized tail current amplitude *versus* command step voltage for $K_v2.1/K_v9.3$ current at 22 and 35ºC (n = 8 and 5, respectively). Dashed lines indicate the relation for activation of native current from Figure 3.9E for comparison; note the similarity in voltage-dependence of native and recombinant channel current activation at both recording temperatures.

of sufficient quality to detect the presence of $K_v9.3$ proteins in anti-$K_v2.1$ immunoprecipitates, even when a high sensitivity, three-step western blotting technique was used (Figure 3.13). For this reason, a novel PLA technique was employed to investigate the proximity of $K_v2.1$ and $K_v9.3$ channel within plasma membrane of RCAs.

To validate the PLA method, we first determined whether the technique could detect the presence of $K_v1.2/K_v1.5$ and $K_v2.1/K_v9.3$ channels expressed in HEK 293 cells. Figure 3.14 shows representative images of Hoechst 33342-stained cells transfected with cDNAs encoding GFP and $K_v1.2/K_v1.5$ (Figure 3.14A) or $K_v2.1/K_v9.3$ (Figure 3.14C), and treated with $K_v1.2$ and $K_v1.5$ or $K_v2.1$ and $K_v9.3$ primary antibodies, respectively, as well as appropriately matched PLA PLUS and MINUS probes. PLA signals were consistently detected at the plasma membrane of green fluorescent, GFP-positive cells, but not in untransfected GFP-negative cells (100–200 cells for each). In contrast, PLA signals were not detected in 100-200 GFP-positive cells from three transfections using cDNAs for only one subunit of each pair; Figure 3.14B & D shows cells expressing only $K_v1.5$, probed for $K_v1.2/K_v1.5$ and $K_v2.1$, probed for $K_v2.1/K_v9.3$, respectively.

PLA was then employed to detect the presence of $K_v1.2/K_v1.5$ or $K_v2.1/K_v9.3$ at the plasma membrane of freshly isolated RCA myocytes. Figure 3.15A shows differential interference contrast (DIC) and fluorescence micrographs of a representative myocyte probed for $K_v1.2$ and $K_v1.5$ co-localization. PLA signals were detected at the cell periphery of this myocyte and an additional 60 myocytes from three cell isolations using RCAs of different rats. No PLA signals were detected when the $K_v1.5$ primary antibody was omitted while applying identical PLA PLUS and MINUS secondary antibodies

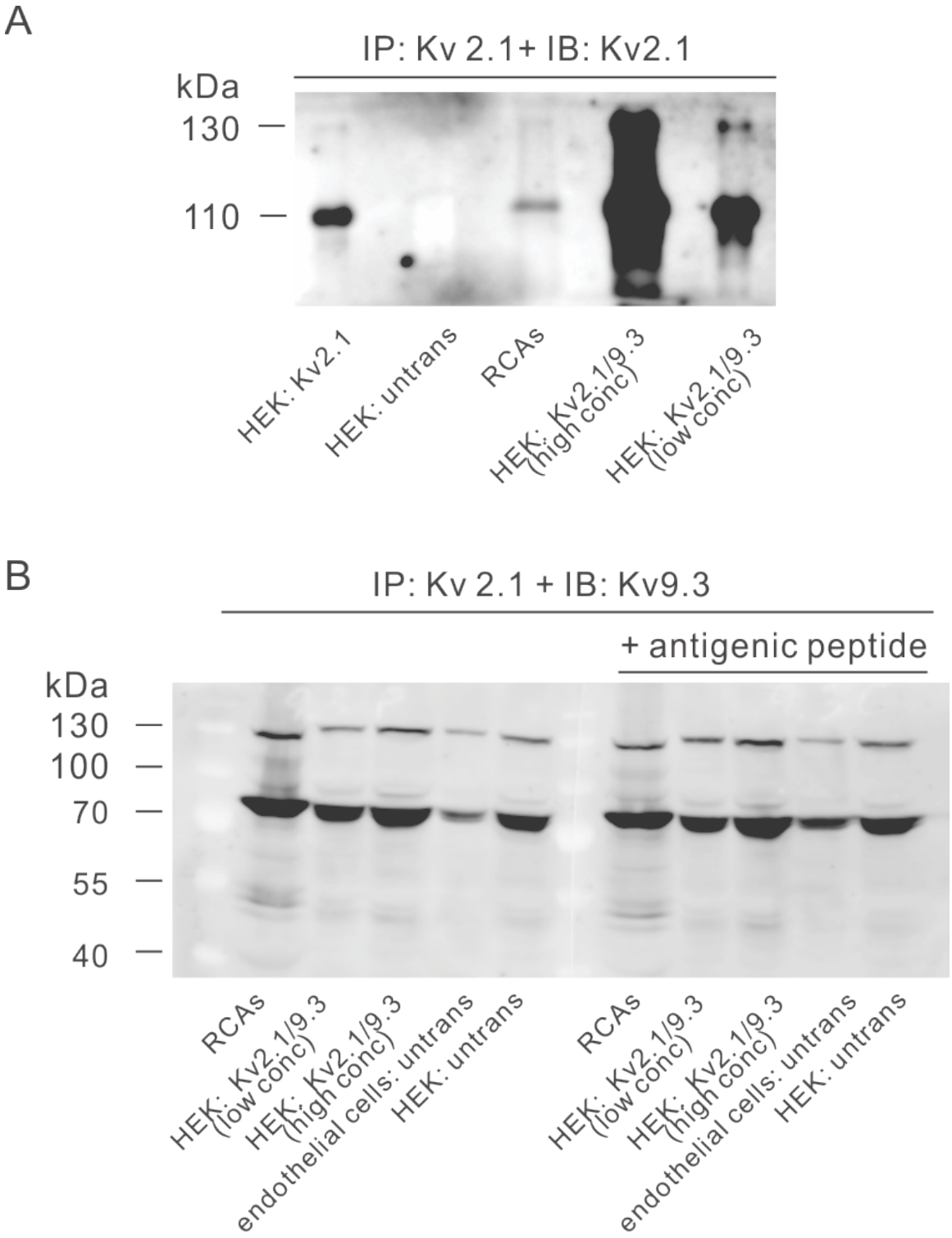
A
IP: Kv 2.1+ IB: Kv2.1
kDa
130
110
HEK: Kv2.1
HEK: untrans
RCAs
HEK: Kv2.1/9.3 (high conc)
HEK: Kv2.1/9.3 (low conc)
B
IP: Kv 2.1 + IB: Kv9.3
+ antigenic peptide
kDa
130
100
70
55
40
RCAs
HEK: Kv2.1/9.3 (low conc)
HEK: Kv2.1/9.3 (high conc)
endothelial cells: untrans
HEK: untrans
RCAs
HEK: Kv2.1/9.3 (low conc)
HEK: Kv2.1/9.3 (high conc)
endothelial cells: untrans
HEK: untrans

Figure 3.13: Identification of K_v2.1 and K_v9.3 proteins in RCAs.

(A) K_v2.1 protein (~110 kDa) was identified by immunoprecipitation with anti-K_v2.1 followed by immunoblotting with anti-K_v2.1 using protein samples derived from pooled RCAs, as well as HEK 293 cells transfected with cDNAs encoding K_v2.1 alone, or K_v2.1 and K_v9.3. Cell lysates from untransfected HEK 293 cells were employed as a negative control. (B) K_v9.3 protein was detected by immunoprecipitation with anti-K_v2.1 followed by immunoblotting with anti-K_v9.3 (Santa Cruz) using protein samples derived from pooled RCAs, as well as HEK 293 cells transfected with cDNAs encoding K_v2.1 and K_v9.3. Untransfected HEK 293 cells and cultured endothelial cells were employed as negative controls. However, a convincing Kv9.3 band was not identified near the expected molecular mass for K_v9.3 protein (~55 kDa).

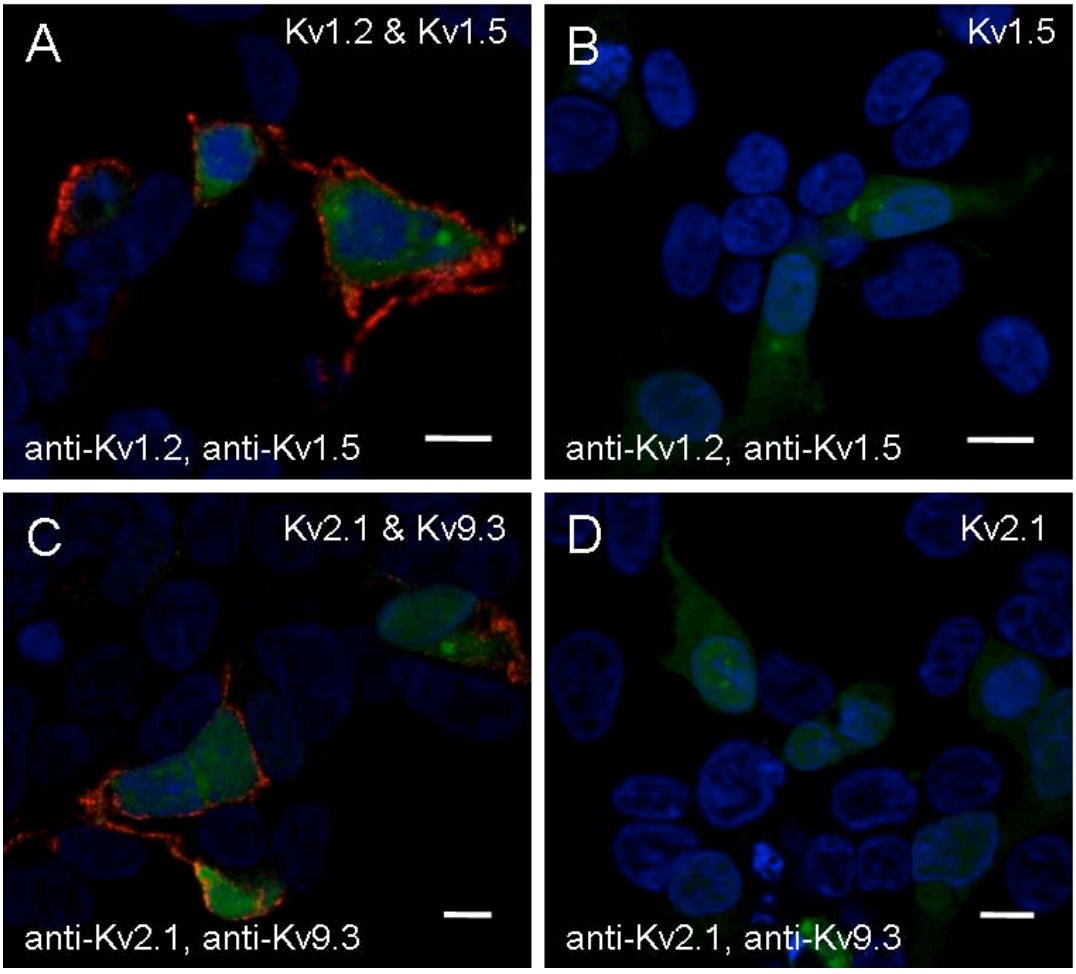

Figure 3.14: PLA detection of plasma membrane expression of recombinant K_v channel protein in HEK 293 cells.

(A) PLA reaction product indicated by red fluorescent dots was detected at the periphery of GFP-positive HEK 293 cells transfected with cDNAs encoding GFP, K_v1.2 and K_v1.5, but not in non-transfected GFP-negative cells probed with K_v1.2 and K_v1.5 primary antibodies. Here and in subsequent panels, the nuclei of GFP-positive and negative-cells are indicated by the blue Hoechst 33342 stain, the K_v channel cDNAs and primary antibodies used are indicated in the upper right and lower left corners, respectively. The scale bars are 10 μm in length and each image is an optical section of 0.3-0.5 μm

thickness at a mid-cell depth. (B) Lack of PLA reaction product at the periphery of GFP-positive cells transfected with K_v1.5 only (i.e. no K_v1.2) and probed with K_v1.2 and K_v1.5 primary antibodies. (C) PLA signals were detected at the periphery of GFP-positive cells transfected with K_v2.1 and K_v9.3, but not in GFP-negative cells probed with K_v2.1 and K_v9.3 primary antibodies. (D) Lack of PLA signals at the periphery of GFP-positive cells transfected with Kv2.1 only (i.e. no K_v9.3) and probed with K_v2.1 and K_v9.3 primary antibodies.

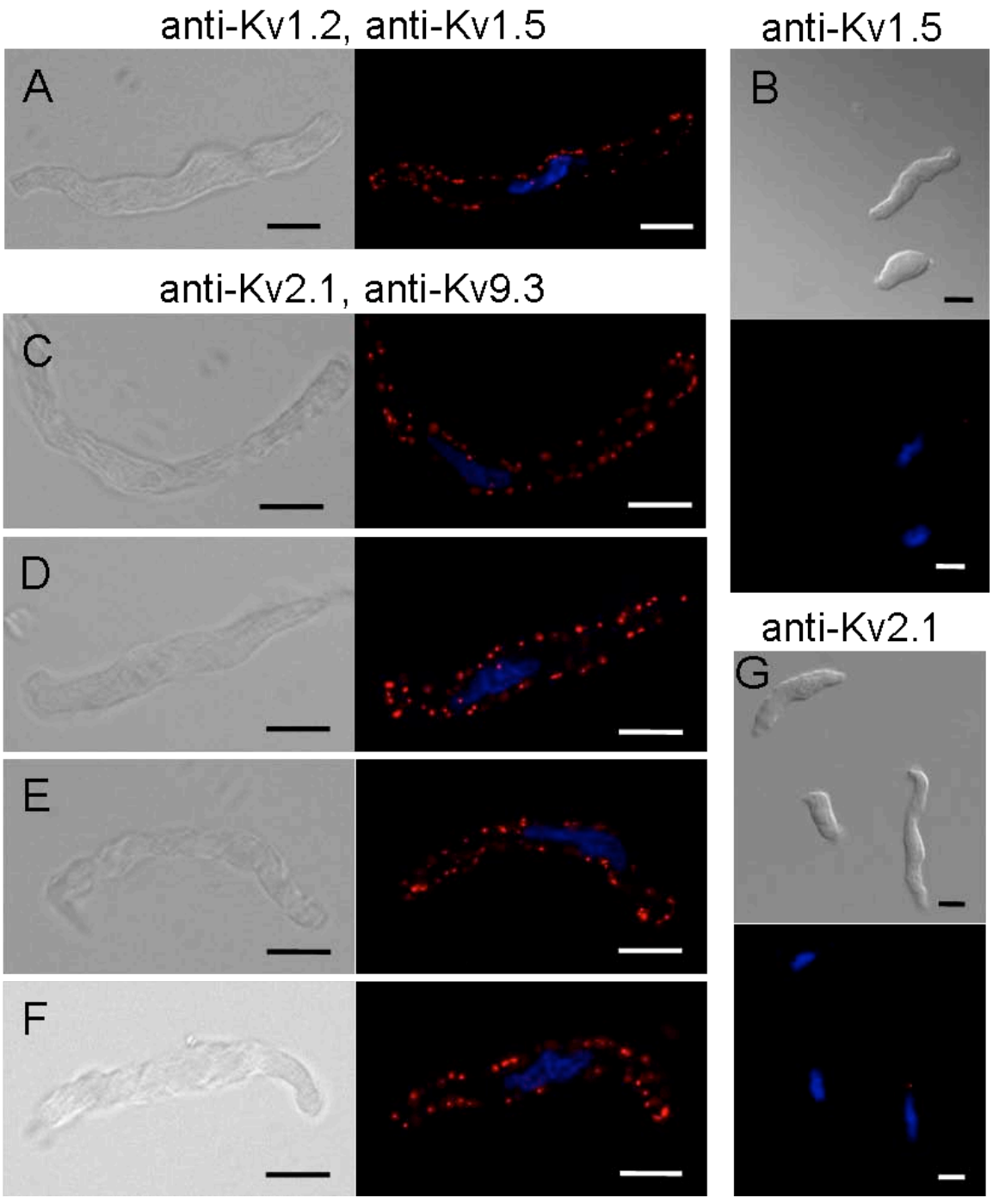
anti-Kv1.2, anti-Kv1.5
A
anti-Kv1.5
B
anti-Kv2.1, anti-Kv9.3
C
D
E
F
anti-Kv2.1
G

Figure 3.15: PLA detection of plasma membrane expression of K_v channel protein in RCA myocytes.

(A) DIC (left) and fluorescence (right) micrographs of an RCA myocyte probed for co-localization of $K_v1.2$ and $K_v1.5$ with PLA signals at the cell periphery when probed with $K_v1.2$ and $K_v1.5$ primary antibodies. Here and in subsequent panels, the nuclei of GFP-positive and -negative cells are indicated by the blue Hoechst 33342 stain; the primary antibodies used are indicated above the panels. The scale bars are 10 μm in length and each image is an optical section of 0.3-0.5 μm thickness at mid-cell depth. (B) Lack of PLA signals in two myocytes probed for $K_v1.2$ and $K_v1.5$ co-localization when $K_v1.2$ primary antibody was omitted. (C-F) Four representative RCA myocytes exhibiting PLA signals when probed with $K_v2.1$ and $K_v9.3$ primary antibodies. (G) Lack of PLA signals in three myocytes probed for $K_v2.1$ and $K_v9.3$ co-localization when $K_v9.3$ primary antibody was omitted.

(Figure 3.15B). Figure 3.15C-F shows representative myocytes from four cell isolations that were probed for $K_v2.1$ and $K_v9.3$ co-localization. An identical detection of PLA signals was obtained for 80 additional myocytes, but no reaction product was detected when $K_v9.3$ primary antibody was omitted (Figure 3.15G). These observations are consistent with previous data exhibiting co-assembly of $K_v1.2/K_v1.5$ and show, for the first time, co-localization of $K_v9.3$ and $K_v2.1$ at the plasma membrane of RCA myocytes.

The presence of localized 'hot spots' of PLA signal detection at the plasma membrane of RCA myocytes suggested the possibility of K_v channel targeting to microdomains. It is well-known that K_v1 subunits do not co-assemble with K_v2 or K_v9 (Coetzee *et al.,* 2006); however, the separation of adjacent channels may be reduced by over-expression in a heterologous cell type, or due to targeting to microdomains, such as the reported targeting of K_v channels to lipid rafts (Martens *et al.,* 2001; Xia *et al.,* 2004). If the K_v channels of RCAs are targeted to microdomains and at a higher local density, the channel-to-channel separation may fall within the range of <40 nm required for hybridization of the PLA probes. In this case, PLA signals would be detected in the absence of co-assembly within a single channel complex. We examined the possibility that K_v1 and $K_v2/K_v9.3$ channels target to similar microdomains in RCA myocytes and whether the expression of $K_v9.3$ at the plasma membrane could be detected with anti-$K_v1.5$ in addition to anti-$K_v2.1$. We first studied HEK 293 cells transfected with cDNAs encoding GFP and (1) $K_v1.2$ and $K_v2.1$, (2) $K_v1.5$ and $K_v9.3$, (3) $K_v1.5$, $K_v9.3$ and $K_v2.1$ and (4) $K_v1.5$ and $K_v2.1$. Figure 3.16A shows that PLA signals were detected in cells expressing $K_v1.2$ and $K_v2.1$ using $K_v1.2$ and $K_v2.1$ antibodies, indicating that the commercial PLA probes can detect the co-localization of subunits in adjacent K_v1 and

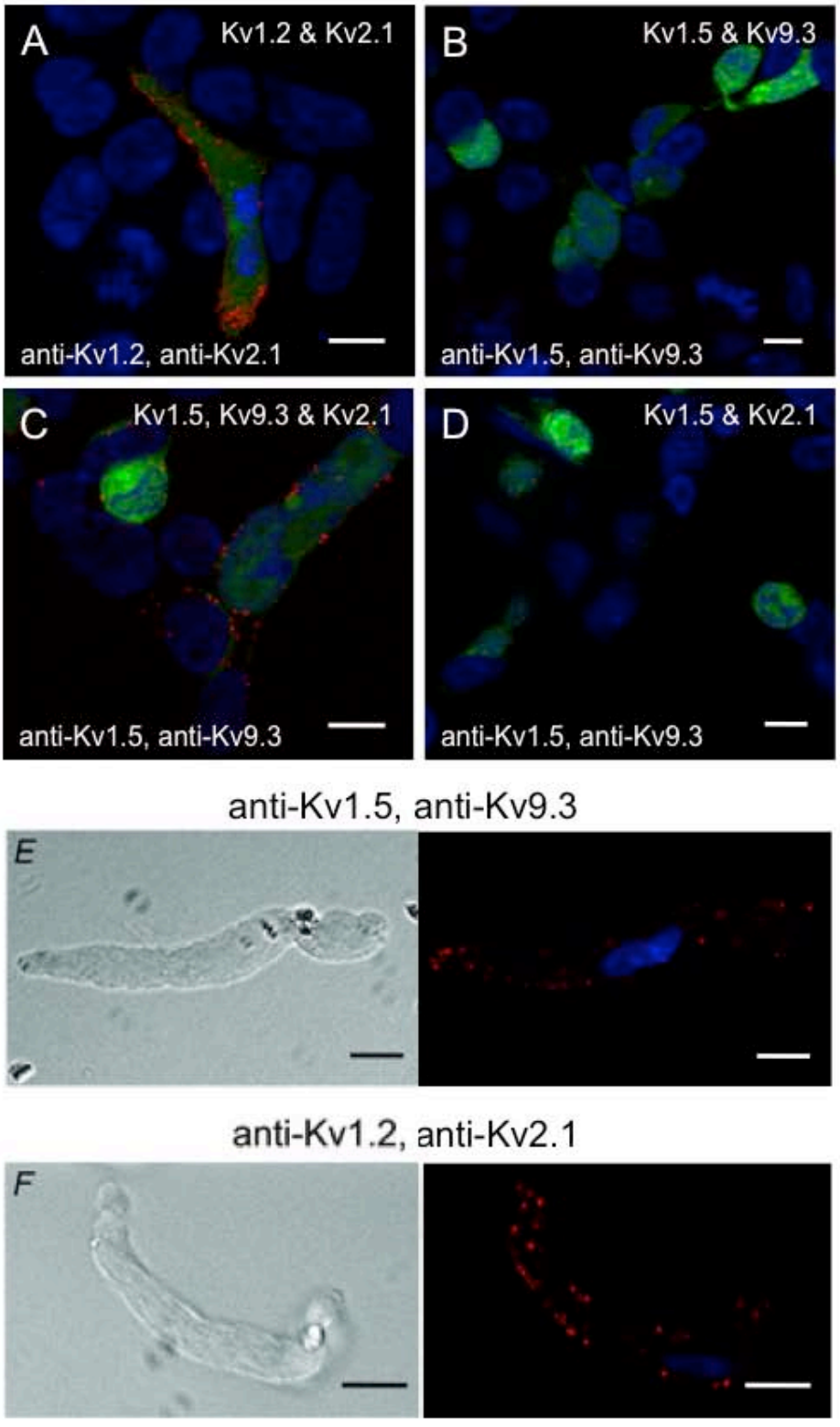
A
Kv1.2 & Kv2.1
anti-Kv1.2, anti-Kv2.1
B
Kv1.5 & Kv9.3
anti-Kv1.5, anti-Kv9.3
C
Kv1.5, Kv9.3 & Kv2.1
anti-Kv1.5, anti-Kv9.3
D
Kv1.5 & Kv2.1
anti-Kv1.5, anti-Kv9.3
anti-Kv1.5, anti-Kv9.3
E
anti-Kv1.2, anti-Kv2.1
F

Figure 3.16: PLA detection of K_v subunit protein in adjacent channel complexes in HEK 293 cells and RCA myocytes

(A) PLA signals were detected at the periphery of GFP-positive cells transfected with K_v1.2 and K_v2.1, but not in GFP-negative cells probed with K_v1.2 and K_v2.1 primary antibodies. Here and in subsequent panels B-D, the nuclei of GFP-positive and -negative cells are indicated by the blue Hoechst 33342 stain; the primary antibodies used are indicated above the panels. (B) PLA signals were not detected at the periphery of GFP-positive cells transfected with K_v1.5 and K_v9.3 and probed with K_v1.5 and K_v9.3 primary antibodies. (C) PLA signals were detected at the periphery of GFP-positive cells transfected with K_v1.5, K_v9.3 and K_v2.1, but not in GFP-negative cells probed with K_v1.5 and K_v9.3 primary antibodies. (D) PLA signals were not detected at the periphery of GFP-positive cells transfected with K_v1.5 and K_v2.1 and probed with K_v1.5 and K_v9.3 primary antibodies. (E) Representative RCA myocyte exhibiting PLA signals at the periphery when probed with K_v1.5 and K_v9.3 primary antibodies. (F) Representative RCA myocyte exhibiting PLA signals at the periphery when probed with K_v1.2 and K_v2.1 primary antibodies. The scale bars of all panels are 10 μm in length and each image is an optical section of 0.3-0.5 μm thickness at mid-cell depth.

K_v2 channels. In contrast, PLA signals were not detected with anti-$K_v1.5$ and anti-$K_v9.3$ using cells expressing $K_v1.5$ and $K_v9.3$ alone, a result that is consistent with previous studies showing the lack of membrane expression of homomultimeric $K_v9.3$ channels (Figure 3.16B). However, product was detected in cells with co-incident expression of $K_v2.1$ with $K_v1.5$ and $K_v9.3$ indicating the rescue of $K_v9.3$ trafficking in the presence of $K_v2.1$ (Figure 3.16C). That the positive PLA reaction in Figure 3.16C required the presence of $K_v9.3$ at the plasma membrane was confirmed by the absence of product in cells expressing homomultimeric $K_v1.5$ and $K_v2.1$ channels and probed with the same pair of $K_v1.5$ and $K_v9.3$ antibodies (Figure 3.16D). Finally, Figure 3.16E & F shows that PLA signals were detected in RCA myocytes probed with $K_v1.5$ and $K_v9.3$ or $K_v1.2$ and $K_v2.1$ primary antibodies (similar data were obtained for >40 myocytes from three cell isolations in each case). This suggests that $K_v1.2/K_v1.5$ and $K_v2.1/K_v9.3$ channels may be trafficked to similar regions of the plasma membrane of RCA myocytes resulting in a channel–channel separation of <40 nm.

3.4 Discussion

3.4.1 Summary of findings

This is the first study to identify the presence of heteromultimeric $K_v2.1/K_v9.3$ channels in RCA myocytes and provide evidence of a distinct functional contribution to control of cerebral resistance arterial diameter. Here we show that: (1) transcripts encoding $K_v2.1$ and $K_v9.3$ are the predominant mRNAs encoding K_v2 and silent subunits expressed in RCA myocytes, (2) co-localized $K_v2.1$ and $K_v9.3$ proteins are present at the plasma membrane of RCA myocytes, (3) ScTx1-sensitive native K_v and $K_v2.1/K_v9.3$ channels exhibit functional identity based on deactivation kinetics and voltage

dependence of activation that are distinct from those of homomultimeric $K_v2.1$ channels, and (4) $K_v2.1/K_v9.3$ currents were detected at all voltages ≥−55 mV at 35 °C and ScTx1 induced constriction of RCAs over the entire range of intraluminal pressure from 10 to 100 mmHg. Taken together, the findings indicate that heteromultimeric $K_v2.1/K_v9.3$ channels are expressed by RCA myocytes and contribute to myogenic control of E_m and arterial diameter over a wider range of intraluminal pressure than that previously reported for K_v1 and BK_{Ca} channels (Brayden & Nelson, 1992; Nelson *et al.*, 1995; Knot & Nelson, 1995; Chen *et al.*, 2006; Yang *et al.*, 2009).

3.4.2 Evidence for the presence of heteromultimeric $K_v2.1/9.3$ channels in RCA myocytes

Previous studies indicated that ScTx1-sensitive, K_v2-containing channels contribute to RCA K_{DR} currents (Amberg & Santana, 2006), yet the molecular identity of the subunits was not determined. Our findings suggest that the predominant K_v2-containing channel type expressed by RCA myocytes is a heteromultimeric channel containing $K_v2.1$ and $K_v9.3$. Homomultimeric $K_v2.1$ channels may be present in RCAs, but at a level of expression that does not have a significant influence on the functional properties of the native ScTx1-sensitive K_v current. This conclusion is based on the following observations:

First, as shown in Figure 3.7, expression of message encoding $K_v2.2$ and the silent subunits, $K_v5.1$, $K_v6.1$-6.3, and $K_v9.1$–9.2 was very low or undetectable in RCAs and more than 10-fold less than the level of $K_v2.1$ and $K_v9.3$ transcripts. $K_v5.1$ expression was previously reported for RCAs (Amberg & Santana, 2006), and we also detected

K_v5.1 transcripts by RT-PCR. However, the level of expression was very low compared to K_v9.3 when assessed by quantitative real-time PCR.

Second, we employed PLA to detect co-localization of K_v2.1 and K_v9.3 proteins at the plasma membrane of RCA myocytes. The commercially available Duolink™ PLA PLUS and MINUS probes employed in this study consist of synthetic oligonucleotides attached to species-specific secondary antibodies that interact with primary antibodies bound to proteins of interest. If the proteins are separated by <40 nm, the oligonucleotides will hybridize and following ligation are capable of generating a unique concatameric oligonucleotide product extending from one oligonucleotide by rolling circle amplification (Fredriksson *et al.* 2002). The amplification products are then detected with complementary oligonucleotides conjugated to a fluorophore as individual fluorescent puncta at sites of protein co-localization. The necessity for dual recognition of the co-localized proteins in the PLA method has the advantage of minimizing detection errors in immunocytochemical analysis owing to possible non-specific binding of the primary antibodies employed. It is also not limited by the lack of precision in assessing co-localization that is associated with any comparison of the extent of overlap of two fluorescent signals. To validate the PLA method, we employed antibody pairs against K_v1.2 and K_v1.5 or K_v2.1 and K_v9.3, and detected PLA signals in HEK 293 cells expressing K_v1.2 & K_v1.5 or K_v2.1 & K_v9.3 heteromultimeric, but not homomultimeric K_v1.5, K_v1.2, K_v2.1 or K_v9.3 channels. Moreover, we detected co-localization of K_v1.2 and K_v1.5 proteins in RCA myocytes, consistent with the findings of Albarwani *et al.* (2003) showing co-assembly of K_v1.2 and K_v1.5 by co-immunoprecipitation from protein extracts of RCAs.

Third, the native ScTx1-sensitive K_v2 currents of RCA myocytes are delayed rectifier K^+ currents that exhibit functional identity with currents owing to heteromultimeric $K_v2.1/K_v9.3$, but not homomultimeric $K_v2.1$ channels expressed in HEK 293 cells. ScTx1 is known to suppress K_v currents due to K_v4 channels, as well as homomultimeric and heteromultimeric K_v2 channels (Escoubas *et al.,* 2002). We do not attribute the effect of ScTx1 to an inhibition of K_v4 channels based on the absence of a rapid, transient component of outward K_v currents (known as K_{TO} currents) (here and previous studies: e.g. Albarwani *et al.,* 2003; Amberg & Santana, 2006; Luykenaar *et al.,* 2009). On the other hand, the fast and slow time constants for decay of tail current amplitude were similar for native ScTx1-sensitive and $K_v2.1/K_v9.3$ channels, and significantly greater than the values for $K_v2.1$ channels under identical conditions. In addition, the voltage dependence of native current activation, as indicated by the $V_{0.5}$ values for half-maximal activation at 22 and 35°C, was similar to that of $K_v2.1/K_v9.3$, but not $K_v2.1$ channels. The similarities in rate of tail current decay and voltage dependence of activation are consistent with the view that the native ScTx1-sensitive current of RCA myocytes is due to the expression of heteromultimeric $K_v2.1/K_v9.3$, but not homomultimeric $K_v2.1$ channels. Moreover, these characteristics also exclude any contribution of heteromultimeric channels containing $K_v2.1$ with $K_v9.1$ or $K_v9.2$ subunits. Salinas *et al.,* (1997b) showed that there was little/no difference in rate of deactivation of $K_v2.1/K_v9.1$ and $K_v2.1/9.2$ compared to $K_v2.1$ channels expressed in Xenopus oocytes and confirmed here for $K_v2.1/K_v9.2$ expressed in HEK 293 cells. It is also unlikely that K_v5 or K_v6 subunits are involved, as the voltage dependence of activation of $K_v2.1/K_v5.1$ channels is positive to that of $K_v2.1$ channels (Kramer *et al.,* 1998). K_v6 subunits did not

cause a large shift in activation or slowing of deactivation as $K_v9.3$ did, and $K_v6.3$ was found to reduce $K_v2.1$ current amplitude (Post *et al.,* 1996; Zhu *et al.,* 1999; Sano *et al.,* 2002; Thorneloe & Nelson, 2003; Bocksteins *et al.,* 2009; Moreno-Dominguez *et al.,* 2009).

Fourth, the vasoconstriction induced by ScTx1 between 10 and 40 mmHg is consistent with a role for $K_v2.1/K_v9.3$, but not $K_v2.1$ channels in control of RCA diameter. We do not attribute the actions of ScTx1 to the inhibition of channels in the endothelium, as endothelial damage did not affect the response to ScTx1. Also, it is unlikely that an ScTx1-induced release of vasoactive neurotransmitter(s) was involved, as sustained constrictions of identical amplitude were observed during repeated applications of the toxin. A decline in response would be expected if ScTx1 caused neurotransmitter-mediated constriction. Rather, we attribute the vasoconstriction evoked by ScTx1 at <40 mmHg to the inhibition of $K_v2.1/K_v9.3$ channels leading to depolarization and Ca^{2+} influx via VGCCs (T-type and/or L-type VGCCs; Kuo *et al.,* 2010). This view is based on: (1) the demonstrated activity of $K_v2.1/K_v9.3$ channels at voltages consistent with the level of E_m between 10 and 40 mmHg (Knot & Nelson, 1995, 1998), and (2) the reversal of the ScTx1-induced constriction by diltiazem, nifedipine or mebifradil, but not SKF96365 (Figure 3.6). Although we did not determine the effect of ScTx1 on membrane potential of RCAs between 10 and 40 mmHg, previous studies of rat and rabbit cerebral arteries indicated that E_m in this range of pressure is ≤ -50 mV (Knot & Nelson, 1995, 1998). This range of E_m is negative to the activation voltage for homomultimeric K_v2 channels, but within the range associated with steady-state activity of $K_v2.1/K_v9.3$ channels. As shown here, and in previous studies (e.g. Patel *et al.,* 1997), $K_v2.1/K_v9.3$ activate over a more

negative range of voltage than $K_v2.1$ channels. Substantial $K_v2.1/K_v9.3$, but not $K_v2.1$, current activation was detected at −55 mV at a near physiological temperature of 35 °C. Also, the membrane potential of COS cells co-expressing $K_v2.1$ and $K_v9.3$ was −50.6 ± 0.9 *versus* −30.7 ± 1.3 mV when transfected with $K_v2.1$ alone (Patel *et al.,* 1997). For this reason, inhibition of $K_v2.1/K_v9.3$, but not $K_v2.1$, channels can account for ScTx1-evoked constriction of RCAs at 10-40 mmHg.

3.4.3 PLA detection of protein co-localization

The novel PLA technique permits detection of protein-protein interactions, when the two proteins are in close proximity (<~30-40 nm) (Fredriksson *et al.* 2002). It is important to recognize that the commercially available Duolink reagents do not exclusively detect subunits co-assembled within single channel complexes (Coetzee *et al.* 2006). Rather, the Duolink PLUS and MINUS oligonucleotides were of sufficient length to detect proteins within adjacent channel complexes. Specifically, in this study, $K_v1.5$ co-localization with $K_v9.3$, and $K_v1.2$ with $K_v2.1$, were detected at the cell membrane of HEK 293 cells and RCA myocytes although the inability of these pairs to co-assemble is well-known (Figure 3.16C & E-F). Nevertheless, this caveat is not a limitation in the present study, as $K_v9.3$ is not expressed at the plasma membrane unless assembled in a heteromultimeric complex with K_v2 subunits (Salinas *et al.,* 1997a,b; Shepard & Rae, 1999; Ottschytsch *et al.,* 2002). This is also evident here by the lack of PLA signal in cells expressing $K_v1.5$ and $K_v9.3$ in the absence of $K_v2.1$ expression (Figure 3.16B). The PLA signals detected at the plasma membrane of RCA myocytes using $K_v9.3$ & $K_v2.1$ or $K_v9.3$ & $K_v1.5$ antibody pairs thus indicate the presence of $K_v9.3$ trafficking to the plasma membrane owing to the expression of heteromultimeric $K_v2.1/K_v9.3$ channels.

3.4.4 Role of heteromultimeric K_v2.1/9.3 channels in myogenic control of E_m

Here, we show that inhibition of K_v2.1/9.3 channels with ScTx1 has a constricting effect on cerebral arterial diameter over the entire pressure range between 10 and 100 mmHg. The contribution of K_v2.1/9.3 channels to E_m and arterial diameter is different from those voltage-independent K^+ channels such as K_{ATP} or K_{ir} channels, which only affect the resting E_m and basal VSM tone independent of transmural pressures. Since ScTx1-sensitive, K_v2.1/9.3 channels exhibited voltage-dependent activation in RCA myocytes (Figure 3.9), we attribute K_v2.1/9.3 channels to myogenic control of E_m and arterial diameter. The reason that ScTx1 induced vasoconstriction between 10 and 40 mmHg is probably because K_v2.1/9.3 channels activate at a very negative E_m, as described in 3.3.2. The reason that ScTx1 did not induce a significantly larger effect in altering arterial diameter at high pressures compared to at low pressures is probably due to the compensatory effects of other K^+ channels, such as K_v1 and BK_{Ca} channels, which only activate when the intraluminal pressure is above 50 mmHg. Therefore, the contribution of K_v2.1/9.3 channels to myogenic control of E_m may be important in maintaining the low level of E_m when transmural pressure is relatively low, and the negative feedback control of myogenic depolarization when E_m is hyperpolarized below the activation range of K_v1 and BK_{Ca} channels (e.g. via vasodilators that increase voltage-independent K_{ATP} or K_{ir} currents) (Nelson & Quayle, 1995).

Note: The data presented in this chapter were previously published in Zhong et al. (2010a) J Physiol 588: 4519-4537.

Chapter Four: Contribution of K_v7-containing channels to myogenic regulation of cerebral arterial diameter

4.1 Introduction

As indicated in Chapter 3.1, the important role played by K_{DR} currents in myogenic control of E_m and arterial diameter provides justification for a comprehensive determination of the K_v channel subunits as it may indicate novel drug targets. The K_v7 subunits encoded by KCNQ genes form homomultimeric and/or heteromultimeric K_v7-containing channels that exhibit voltage-dependent activation and minimal inactivation at relatively negative E_m (Jentsch, 2000; Robbins, 2001; Greenwood & Ohya, 2009). The K_v7 family consists of 5 members, $K_v7.1$ to $K_v7.5$. $K_v7.1$ subunits were first identified in cardiac myocytes, in which they are thought to contribute to repolarization of the cardiac action potential. $K_v7.2$-7.5 subunits were originally recognized in neurons, in which they are thought to contribute to neurotransmitter-evoked action potential firing. The expression of K_v7 message and protein has recently been identified in several VSM tissues, such as portal vein, aorta, pulmonary, as well as carotid, femoral and mesenteric arteries (Ohya *et al.,* 2003; Yeung & Greenwood, 2005; Brueggemann *et al.,* 2007; Yeung *et al.,* 2007, Mackie *et al.,* 2008; Joshi *et al.,* 2009). Various K_v7 modulating drugs, including the inhibitors, XE991 and linopirdine, as well as the activators, S-1, retigabine and flupirtine (Lamas *et al.,* 1997; Zaczek *et al.,* 1998; Wang *et al.,* 2000; Dupuis *et al.,* 2002; Greenwood & Ohya, 2009) (Figure 4.1), have been employed to obtain evidence for the contribution of K_v7 channels to membrane currents and/or the regulation of contractility in these tissues. For example, XE991 or linopirdine were

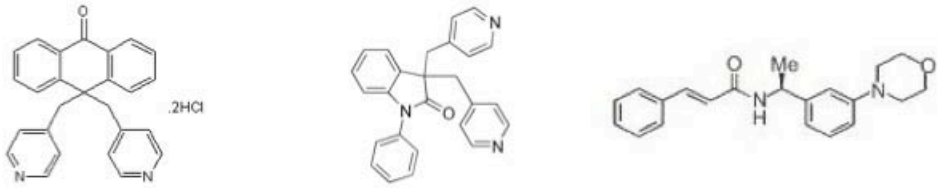

XE 991 Linopirdine S-1

Figure 4.1: Chemical structures of XE 991, linopirdine and S-1.

XE991: 10,10-bis(4-pyridinylmethyl)-9(10H)-anthracenone

Linopirdine: 3,3-bis(4-pyridinylmethyl)-1-phenylindolin-2-one

S-1: (*S*)-*N*-[1-(3-morpholin-4-yl-phenyl)-ethyl]-3-phenyl-acrylamide

shown to suppress membrane K_{DR} currents and/or induce contraction of murine portal vein, rat and murine pulmonary arterial rings, and large mesenteric arteries, whereas flupirtine or retigabine were found to stimulate membrane K_{DR} currents and/or relax pre-contracted aorta, pulmonary arterial rings and large mesenteric arteries (Yeung & Greenwood, 2005; Joshi *et al.,* 2006; Brueggemann *et al.,* 2007; Mackie *et al.,* 2008; Yeung *et al.,* 2007, 2008; Joshi *et al.,* 2009). Additionally, the cyclo-oxygenase inhibitors, meclofenamic acid and celecoxib, were shown to activate K_v7 channels and relax pre-contracted VSM tissues (Yeung *et al.,* 2007; Brueggemann *et al.,* 2009).

Although the potential role of K_v7-containing channels in affecting VSM contractility has been addressed in several types of vessels, no study has examined the contribution of K_v7-containing channels to myogenic control of E_m depolarization and arterial diameter in cerebral arteries. Considering the essential contribution of the cerebral myogenic response to blood flow autoregulation in the brain, this lack of information limits our understanding of the molecular basis of cerebral myogenic regulation, and may prevent the development of novel strategies to reverse cerebral arterial dysfunction. Given that K_v7 channels are the only type of K_v channels for which selective activators are available, it is of potential therapeutic importance to determine whether pharmacological manipulation of K_v7 channel gating can alter RCA diameter in conditions with an abnormal myogenic response.

4.2 Hypothesis and objectives of the study

Here, we tested the specific **hypothesis** that K_v7-containing channels contribute to whole-cell K_v currents of cerebral myocytes and myogenic regulation of cerebral arterial diameter. The four primary objectives of this study were as follows:

(1) To identify the expression of KCNQ genes in RCA myocytes.

(2) To determine the contribution of K_v7-containing channels to whole-cell K_v currents of RCA myocytes.

(3) To assess the ability of K_v7 channel blockers and activators to enhance and suppress the cerebral myogenic response, respectively.

(4) To evaluate whether pharmacological manipulation of K_v7 currents with K_v7 channel activator, S-1, is able to reverse abnormal vasoconstriction.

4.3 Results

4.3.1 KCNQ gene expression in RCA myocytes

Figure 4.2A & B shows QPCR detection of KCNQ (KCNQ1-5) and KCNE (KCNE1-5) transcript expression relative to β-actin in mRNAs extracted from RCAs. $K_v7.1$, $K_v7.4$ and $K_v7.5$ subunits were found to be highly expressed. Figure 4.1C shows immunofluorescence specific to $K_v7.1$, $K_v7.4$ and $K_v7.5$ was localized to the plasma membrane of RCA myocytes and not present in control experiments when primary antibodies were omitted. Figure 4.2D shows mean fluorescence data for $K_v7.1$, $K_v7.4$ and $K_v7.5$ in RCA myocytes. Overall, these observations suggest that RCA myocytes have a KCNQ expression profile of KCNQ4 > KCNQ5 and KCNQ1, and products of their expression show appropriate trafficking to the plasma membrane. Note, experiments and analysis for this figure were all performed by Dr. Maksym I. Harhun of St George's University of London, and Dr. Susumu Ohya of Nagoya City University.

4.3.2 Identification of the presence of K_v7 current in RCA myocytes

RCA myocytes were previously shown to express K_v1 (Albarwani *et al.* 2003; Chen *et al.* 2006) and K_v2-containing (Amberg & Santana, 2006; Zhong *et al.* 2010b)

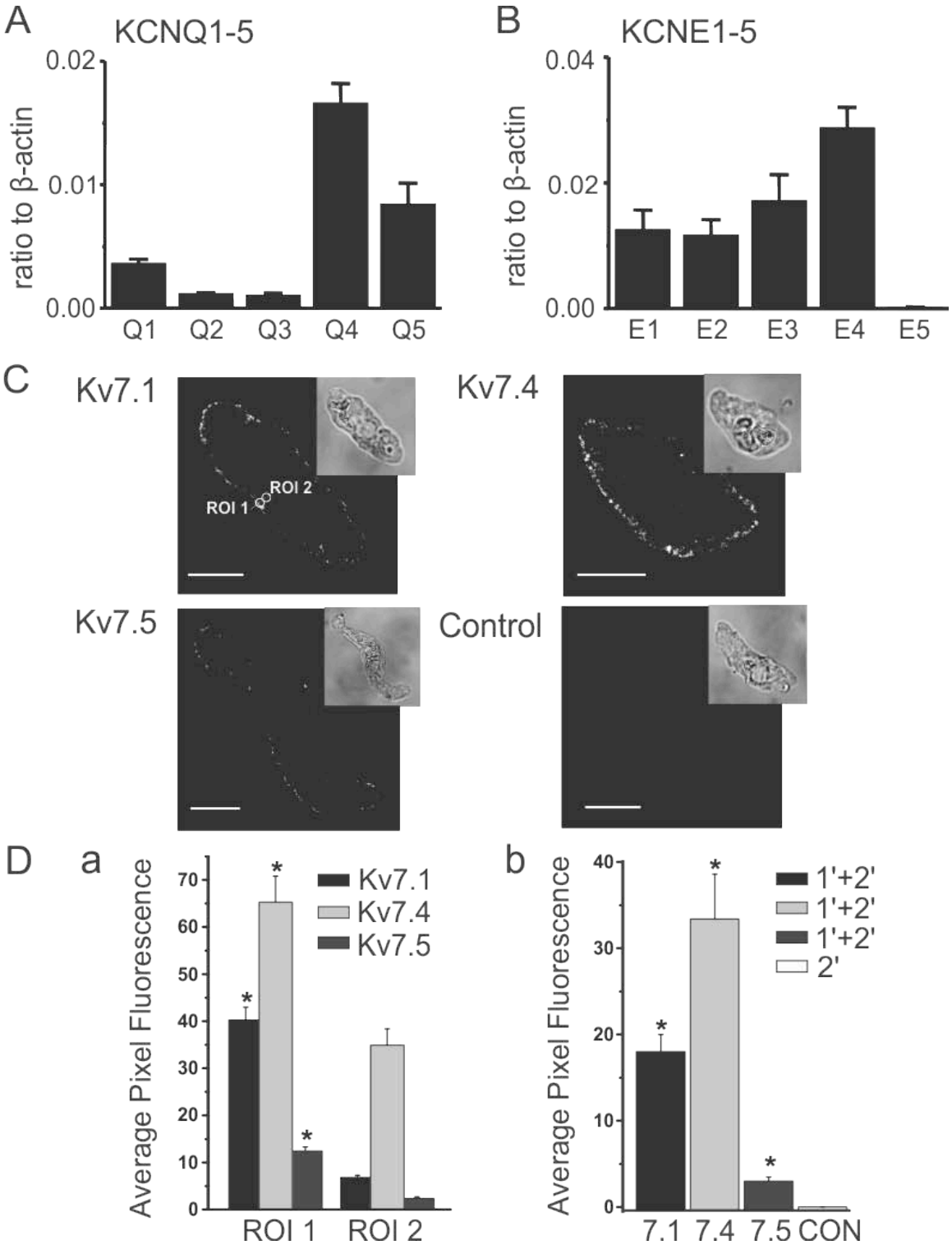
A
KCNQ1-5
ratio to β-actin
0.02
0.01
0.00
Q1
Q2
Q3
Q4
Q5
B
KCNE1-5
ratio to β-actin
0.04
0.02
0.00
E1
E2
E3
E4
E5
C
Kv7.1
ROI 1
ROI 2
Kv7.4
Kv7.5
Control
D
a
Average Pixel Fluorescence
Kv7.1
Kv7.4
Kv7.5
ROI 1
ROI 2
b
Average Pixel Fluorescence
1'+2'
1'+2'
1'+2'
2'
7.1
7.4
7.5
CON

Figure 4.2: Expression of KCNQ genes in RCA myocytes.

(A & B) Real-time PCR detection of KCNQ (KCNQ1-5) and KCNE (KCNE1-5) subunit transcript expression relative to β-actin in mRNA extracted from RCA myocytes. All expression data are expressed as mean ± SEM (n = 4 for each). (C) Immunostaining of freshly isolated myocytes using anti-K_v7.1, -K_v7.4, or -K_v7.5, and a control experiment in which primary antibody was omitted. The transmitted light image for each cell is shown in upper right inset images. Circles indicate regions of interest; ROI 1 and ROI 2, which were used to analyze the localization of fluorescence. The calibration bar represents 10 μm. (D-a) Summarized data for localization of K_v7.1, K_v7.4 and K_v7.5 immunofluorescence in RCA myocytes. There was significantly more fluorescence in the region of plasma membrane (ROI 1) than in deep cytoplasm (ROI 2) (n = 10 myocytes for each antibody). (D-b) summarized data for average pixel fluorescence in a whole-cell confocal plane compared to control myocyte that demonstrated a lack of immunofluorescence in the absence of primary antibody (n = 10; 1' primary antibody; 2' secondary antibody). * Significantly different ($P < 0.05$) from value for the control. Note: experiments and analysis for this figure were performed by Dr. Maksym I. Harhun of St George's University of London, and Dr. Susumu Ohya of Nagoya City University.

channels that exhibit sensitivity to 4-AP (100-300 μM) or correolide (1-10 μM), and tetraethylammonium ion (TEA^+; 2-10 mM) or ScTx1 (10-300 nM), respectively. Based on these data, we sequentially exposed freshly isolated RCA myocytes to 4-AP (100 μM) and TEA^+ (4 mM) prior to treatment with XE991, a blocker of all K_v7 channels with an IC_{50} of ~1 μM. Figure 4.3A-C shows representative families of K_v currents, currents recorded at +25 mV, as well as mean normalized (to peak current in control conditions at +45 mV) current-voltage (I-V) relations for RCA myocytes exposed to control conditions and following sequential treatment with 4-AP, 4-AP & TEA^+, and 4-AP, TEA^+ & XE991. Treatment with 4-AP and TEA^+ caused a progressive inhibition of K_v currents, and 10 μM XE991 inhibited the 4-AP and TEA^+ resistant component of ~20% total current amplitude, indicating the presence of K_v1, K_v2 and K_v7 currents in RCA myocytes. However, Figure 4.3D & E shows that XE991 alone caused a significant suppression of whole-cell K_v currents; this extent of block is not consistent with a selective inhibition of K_v7 channels, as the amplitude of residual currents was considerably less than that expected for the sum of the 4-AP-sensitive K_v1 and TEA^+-sensitive K_v2 currents.

To determine whether XE991 was selective for K_v7 channels at the concentration of 10 μM used in many studies of VSMCs, this drug was applied to HEK 293 cells expressing heterotetrameric $K_v1.2/K_v1.5$ and $K_v2.1/K_v9.3$ channels, that we and others have identified in RCA myocytes (Albarwani *et al.* 2003; Chen *et al.* 2006; Zhong *et al.* 2010b). HEK 293 cells expressing homotetrameric $K_v7.4$ were assessed as a positive control. As shown in Figure 4.4, XE991 caused a marked inhibition of $K_v7.4$ currents as expected; however, it also significantly reduced the amplitude of $K_v1.2/K_v1.5$ and

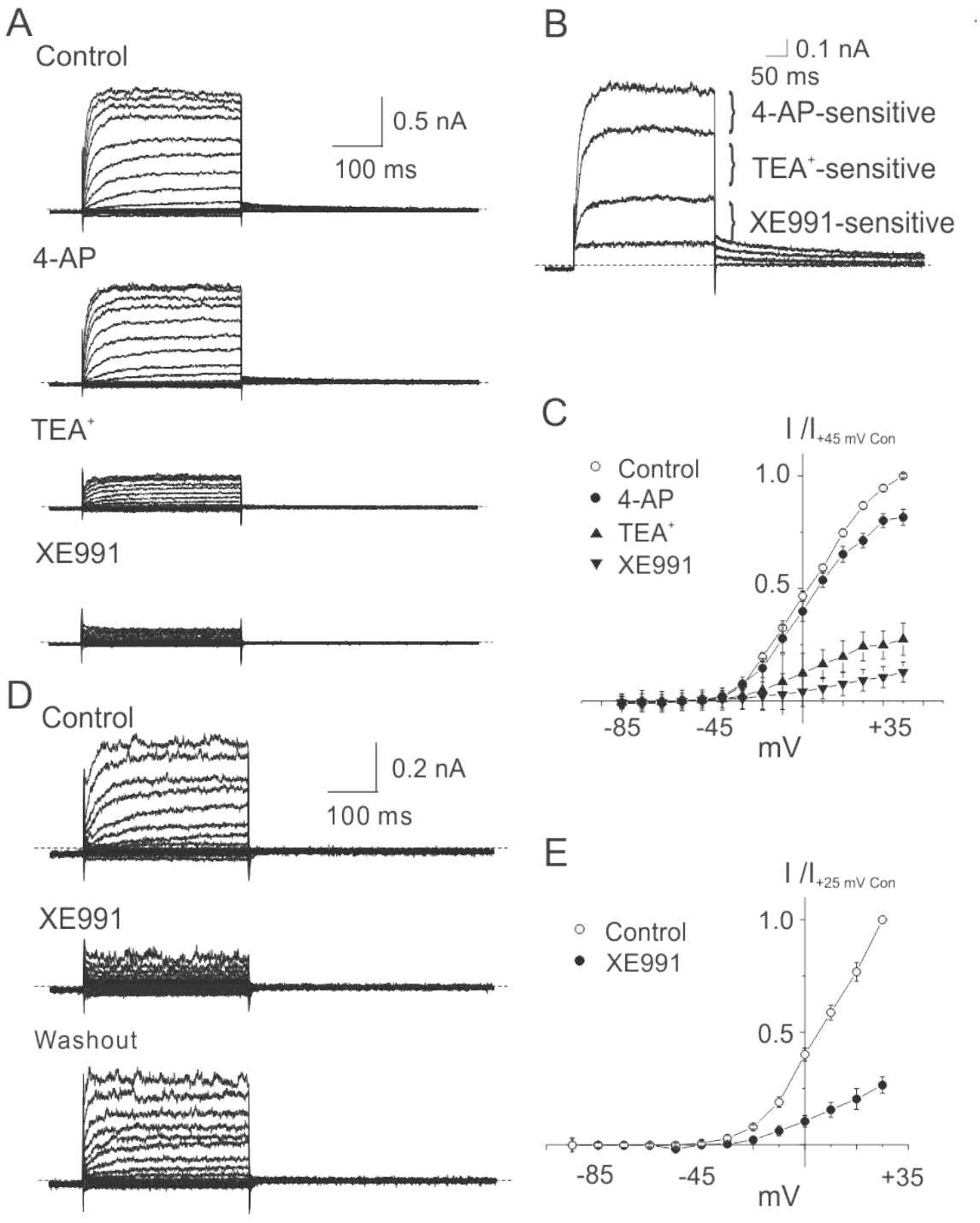

Figure 4.3: Suppression of K_v currents by XE991 in RCA myocytes.

(A) Representative families of K_v currents of a RCA myocyte evoked by 300 ms steps to between −95 and +45 mV prior to repolarization to −55 mV (a similar protocol was used

for all recordings unless indicated otherwise) in the absence (Control) and presence of 100 μM 4-AP, 4-AP & 4 mM TEA^+, and 4-AP & TEA^+ & 10 μM XE991. (B) Representative traces from panel A for voltage steps to +25 mV showing the 4-AP-, TEA^+- and XE991-sensitive components of whole-cell K_v currents. (C) Mean ± SEM normalized (to peak current at +45 mV in control condition) I-V relations for K_v currents of RCA myocytes (n = 3) sequentially treated with 4-AP, TEA^+ and XE991 as in panel A. (D) Representative families of K_v currents of a RCA myocyte in the absence and presence of 10 μM XE991 followed by drug washout. Voltage protocol was the same as in panel A except for from -95 to +25 mV only. (E) Mean ± SEM normalized (to peak current at +25 mV in control condition) I-V relations for K_v currents of RCA myocytes (n = 5) in the absence (Control) and presence of 10 μM XE991. Note XE991 caused a significant suppression of whole-cell K_v currents of RCA myocytes.

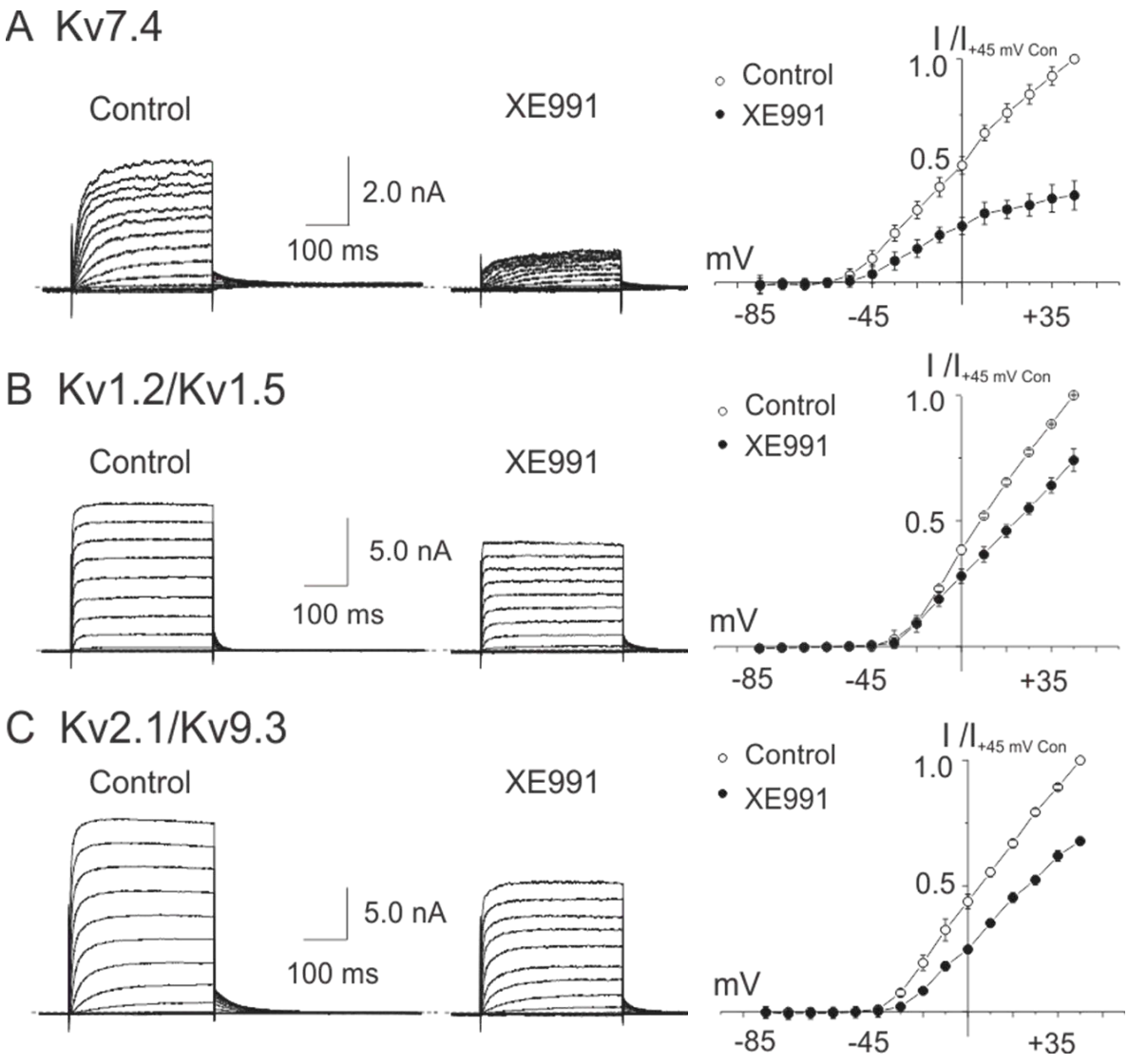

Figure 4.4: Suppression of recombinant homomultimeric K_v7.4 current and heteromultimeric K_v1.2/K_v1.5 and K_v2.1/K_v9.3 currents by XE991 in HEK 293 cells.
(A) Representative families and mean ± SEM (n = 3) I-V relations for whole-cell K_v7.4 current of HEK 293 cells in the absence (Control) and presence of 10 μM XE991. (B) Representative families and mean ± SEM (n = 3) normalized (to peak current at +45 mV in control condition) I-V relations for whole-cell K_v1.2/K_v1.5 current of HEK 293 cells in the absence (Control) and presence of 10 μM XE991 (note voltage steps were to between

−95 and +25 mV only). (C) Representative families and mean ± SEM (n = 3) normalized (to peak current at +45 mV in control condition) I-V relations for whole-cell $K_v2.1/K_v9.3$ current of HEK 293 cells in the absence (Control) and presence of 10 μM XE991. Note the suppression of $K_v1.2/K_v1.5$ and $K_v2.1/K_v9.3$ currents by XE991 at 10 μM.

$K_v2.1/K_v9.3$ currents. The block of $K_v1.2/K_v1.5$ channels was voltage-dependent, and evident only at voltages positive to −15 mV. In contrast, the suppression of $K_v2.1/K_v9.3$ channels by XE991 was apparent at all potentials positive to −45 mV. These data indicate that XE991 at 10 μM has non-selective effects on other heteromultimeric K_v channels expressed by RCA myocytes.

Owing to the identified non-selective actions of XE991, we employed two additional compounds, linopirdine and S-1, known to inhibit and activate K_v7 channels, respectively. Effects of linopirdine and S-1 were first studied using recombinant channels to identify appropriate concentrations that affected $K_v7.4$, but not $K_v1.2/K_v1.5$ or $K_v2.1/K_v9.3$ channels. Figures 4.5A & 4.6A show that linopirdine at 1 μM and S-1 at 3 μM significantly inhibited and increased recombinant $K_v7.4$ current amplitude, respectively, whereas they did not affect $K_v1.2/K_v1.5$ or $K_v2.1/K_v9.3$ channels (Figures 4.5B & C and 4.6B & C). A higher concentration of linopirdine of 10 μM caused 12.5 ± 3.5% reduction of $K_v2.1/K_v9.3$ currents at +25 mV (n = 3). Application of a higher concentration of S-1 at 20 μM did not cause an increase in either $K_v1.2/K_v1.5$ or $K_v2.1/K_v9.3$ currents, although $K_v7.4$ current amplitude was further augmented (n = 3). Based on these observations, linopirdine was used at 1 μM and S-1 at 3 or 20 μM in subsequent experiments.

Figures 4.7 & 4.8 show the effects of linopirdine (1 μM) and S-1 (3 μM) on native K_v currents in RCA myocytes, respectively. The amplitude of K_v currents was reduced in the presence of linopirdine compared to control conditions (Figure 4.7A), with the extent of block ~20% at +5 mV (representative traces in Figure 4.7B and mean normalized amplitude data in Figure 4.7D). The linopirdine-sensitive component of

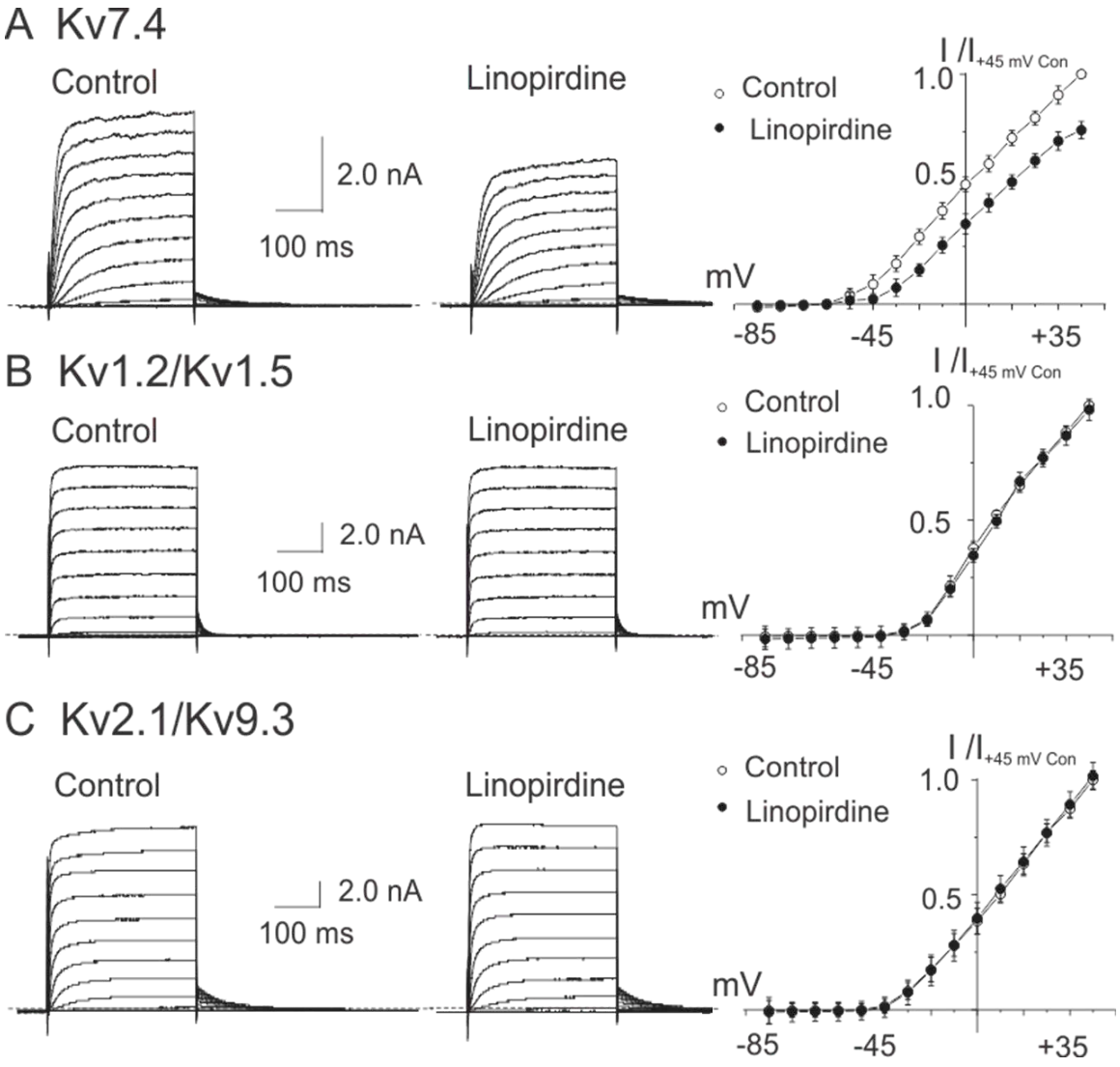

Figure 4.5: Suppression of recombinant homomultimeric K_v7.4 current, but not heteromultimeric K_v1.2/K_v1.5 and K_v2.1/K_v9.3 currents by linopirdine in HEK 293 cells.

(A) Representative families and mean ± SEM (n = 4) normalized (to peak current at +45 mV in control condition) I-V relations for whole-cell K_v7.4 current of HEK 293 cells in the absence (Control) and presence of 1 μM linopirdine. (B) Representative families and mean ± SEM (n = 3) normalized (to peak current at +45 mV in control condition) I-V

relations for whole-cell $K_v1.2/K_v1.5$ current of HEK 293 cells in the absence (Control) and presence of 1 μM linopirdine. (C) Representative families and mean ± SEM (n = 3) normalized (to peak current at +45 mV in control condition) I-V relations for whole-cell $K_v2.1/K_v9.3$ current of HEK 293 cells in the absence (Control) and presence of 1 μM linopirdine. Note the lack of suppression of $K_v1.2/K_v1.5$ and $K_v2.1/K_v9.3$ currents by linopirdine at 1 μM.

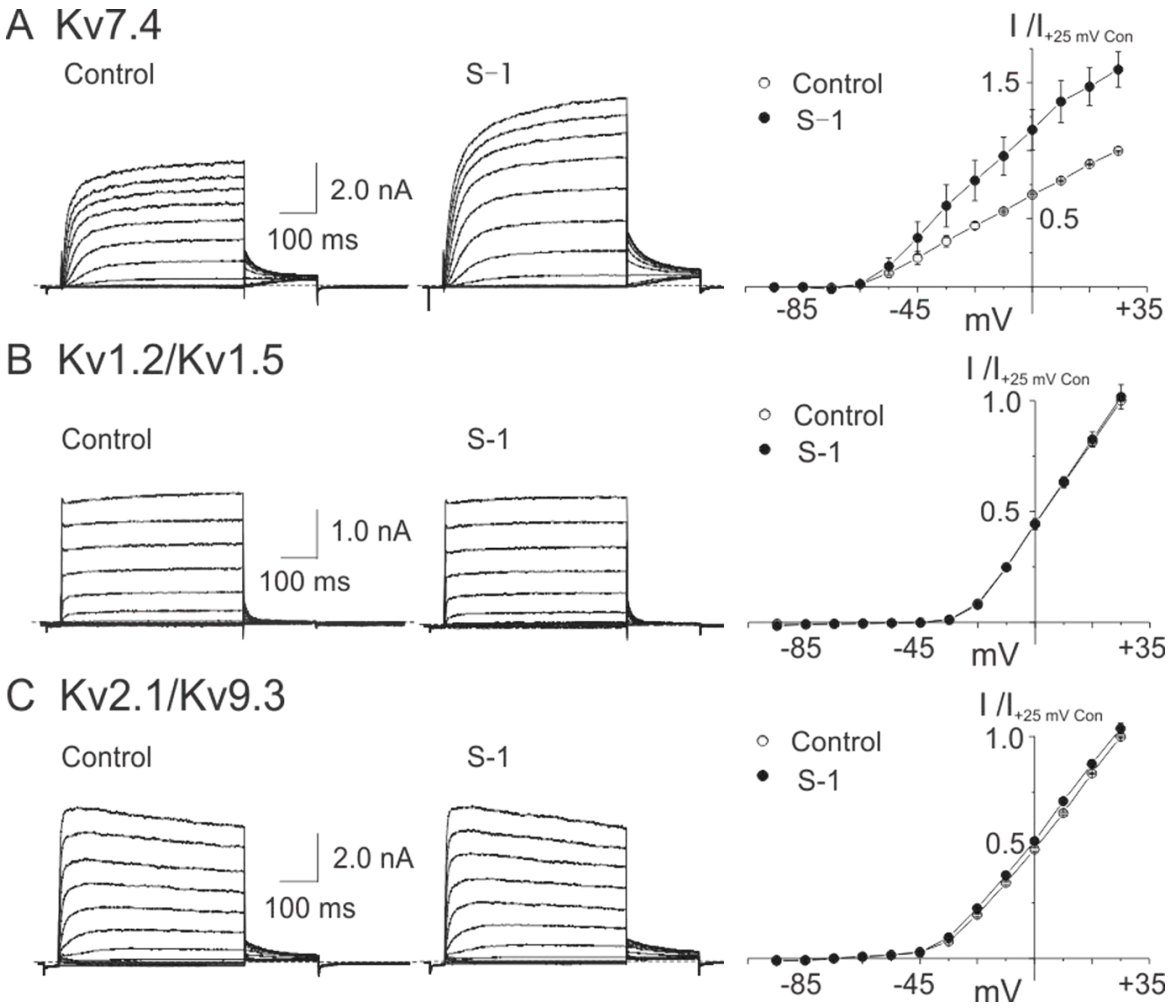

Figure 4.6: Stimulation of recombinant homomultimeric K_v7.4 current, but not heteromultimeric K_v1.2/K_v1.5 and K_v2.1/K_v9.3 currents by S-1 in HEK 293 cells.

(A) Representative families and mean ± SEM (n = 4) normalized (to peak current at +45 mV in control condition) I-V relations for whole-cell K_v7.4 currents of HEK 293 cells in the absence (Control) and presence of 3 μM S-1. (B) Representative families and mean ± SEM (n = 3) normalized (to peak current at +45 mV in control condition) I-V relations for whole-cell K_v1.2/K_v1.5 currents of HEK 293 cells in the absence (Control) and

presence of 3 μM S-1. (C) Representative families and mean ± SEM (n = 3) normalized (to peak current at +45 mV in control condition) I-V relations for whole-cell $K_v2.1/K_v9.3$ currents of HEK 293 cells in the absence (Control) and presence of 3 μM S-1. Note the lack of stimulation of $K_v1.2/K_v1.5$ and $K_v2.1/K_v9.3$ currents by S-1 at 3 μM.

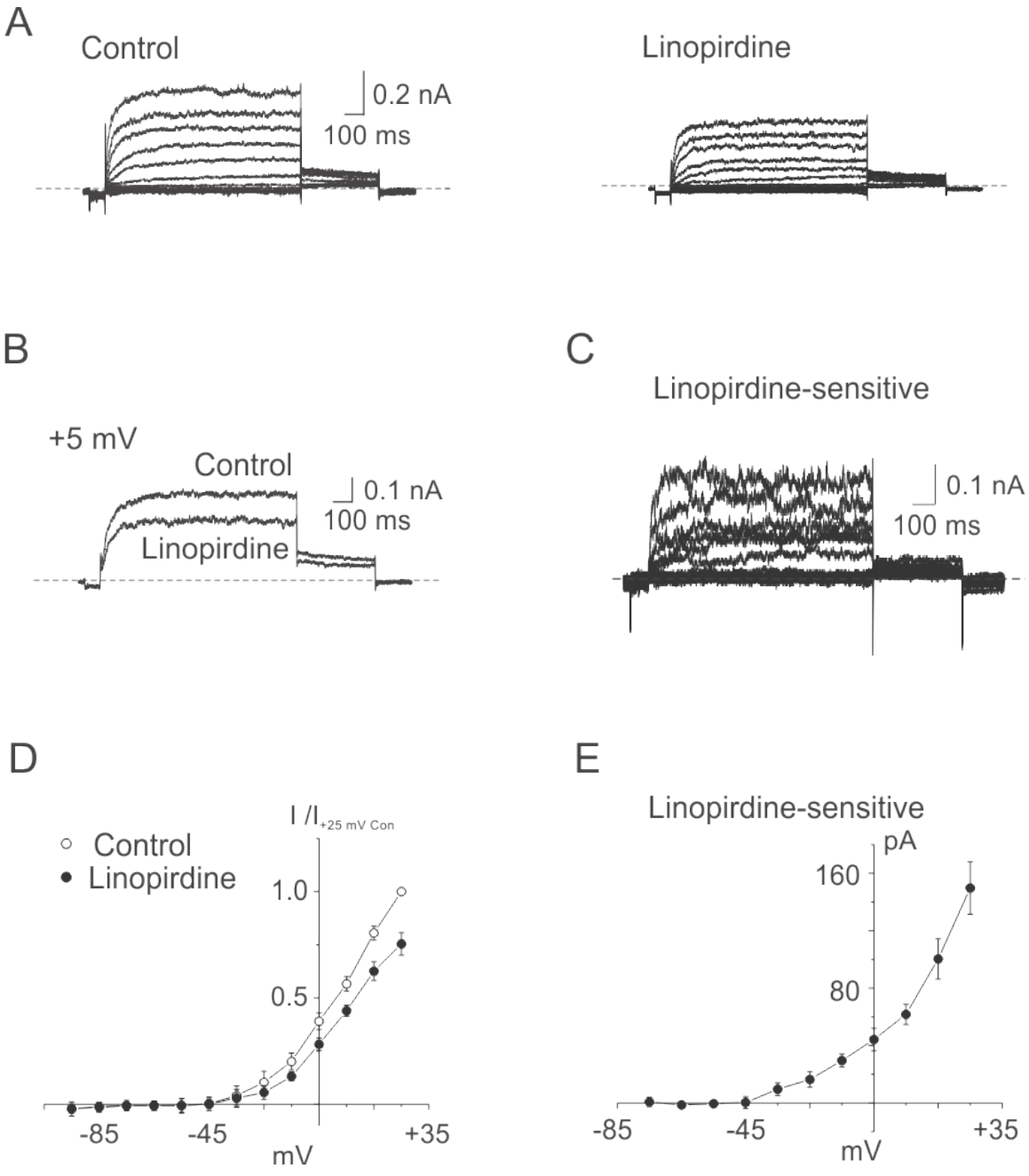
A
Control
0.2 nA
100 ms
Linopirdine
B
+5 mV
Control
0.1 nA
100 ms
Linopirdine
C
Linopirdine-sensitive
0.1 nA
100 ms
D
I /I+25 mV Con
Control
Linopirdine
1.0
0.5
-85
-45
+35
mV
E
Linopirdine-sensitive
pA
160
80
-85
-45
+35
mV

Figure 4.7: Suppression of native K_v currents by linopirdine in RCA myocytes.
(A) Representative families of whole-cell K_v currents of a RCA myocyte in the absence (Control) and presence of 1 μM linopirdine (note voltage clamp protocol included an 80 ms step to −95 mV prior to test steps to between −80 and +25 mV in 10 mV increments followed by repolarization to −45 mV). (B) Representative recordings of K_v currents at +5 mV in the absence and presence of linopirdine (1 μM). (C) Representative family of linopirdine-sensitive K_v currents obtained by digital subtraction of currents in linopirdine from those in control conditions in panel A. (D) Mean ± SEM (n = 3) normalized (to peak current at +25 mV in control condition) I-V relations for K_v currents in the absence (Control) and presence linopirdine. (E) Mean ± SEM (n = 3) I-V relation for linopirdine-sensitive K_v current determined from end-pulse difference current amplitude.

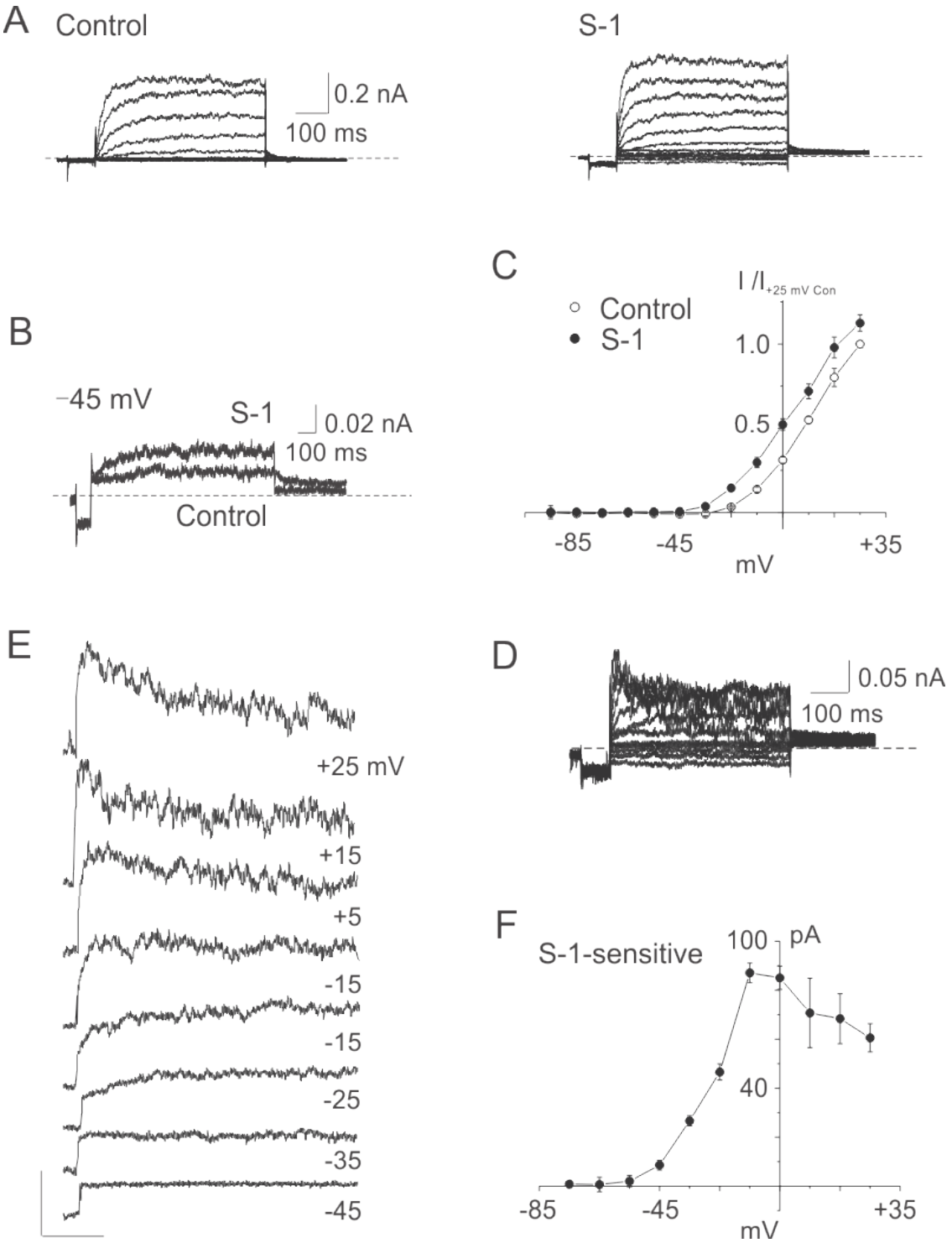
A
Control
S-1
0.2 nA
100 ms
B
−45 mV
S-1
0.02 nA
100 ms
Control
C
I /I+25 mV Con
Control
S-1
1.0
0.5
-85
-45
+35
mV
D
0.05 nA
100 ms
E
+25 mV
+15
+5
-15
-15
-25
-35
-45
F
S-1-sensitive
100
pA
40
-85
-45
+35
mV

Figure 4.8: Stimulation of native K_v currents by S-1 in RCA myocytes.

(A) Representative families of whole-cell K_v currents of a RCA myocyte in the absence (Control) and presence of 1 μM linopirdine (note voltage clamp protocol included an 80 ms step to −95 mV prior to test steps to between −80 and +25 mV in 10 mV increments followed by repolarization to −45 mV). (B) Representative expanded traces for currents ± S-1 (3 μM) at −45 mV from cell in panel A. (C) Mean ± SEM (n = 3) normalized (to peak current at +25 mV in control condition) I-V relations for K_v currents in the absence (Control) and presence of S-1 (3 μM). (D) Representative S-1-sensitive K_v current obtained by digital subtraction of control from S-1 current in panel A. (E) Expanded versions of each current recording for voltage steps to between −45 and +25 are shown for clarity. Note the increased apparent inactivation of the S-1-sensitive current at potentials positive to − 5 mV. (F) Mean ± SEM (n = 3) I-V relation of S-1-sensitive current determined from end pulse difference current amplitude. Note the decline in S-1-sensitive current positive to −15 mV (y-axis at −5 mV).

native K_v currents was time-dependent, activated positive to −45 mV and showed no indication of time-dependent inactivation (Figure 4.7C & E). In contrast, treatment with S-1 increased native K_v current amplitude at all potentials tested between -45 and +25 mV, as indicated in Figure 4.8A-C. Specifically, Figure 4.8B shows that S-1 increased native K_v current amplitude at −45 mV, which is within the range of membrane potential associated with the cerebral myogenic response (Knot & Nelson, 1995; 1998). The increase in amplitude of S-1-sensitive currents was voltage-dependent, reaching a peak at ~−15 mV and declining with steps to increasingly positive voltages (Figure 4.8D & E). The decline in current at positive voltages was associated with an apparent increase in time-dependent inactivation, likely resulting from open channel block. This is similar to the previously reported voltage-dependent, bimodal stimulation and block of murine portal vein K_v7 current by retigabine and flupirtine (Yeung *et al.*, 2008).

4.3.3 Effects of K_v7 channel blockers and activators on the cerebral myogenic response.

Figure 4.9 (left panels) shows representative recordings of RCA diameter for three sequential series of intraluminal pressure steps between 10 and 100 mmHg in: (1) control Krebs' solution, (2) linopirdine (1 μM) or S-1 (20 μM) and (3) 0 Ca^{2+} Krebs' solution. Figure 4.9 (right panels) shows mean ± SEM active constriction in control conditions and following the linopirdine and S-1 treatment, respectively. Linopirdine enhanced the level of active constriction of RCAs at all pressures between 20 and 100 mmHg, whereas S-1 suppressed active constriction at >20 mmHg. We also examined a second activator, retigabine (30 μM), and found that it inhibited the myogenic response at

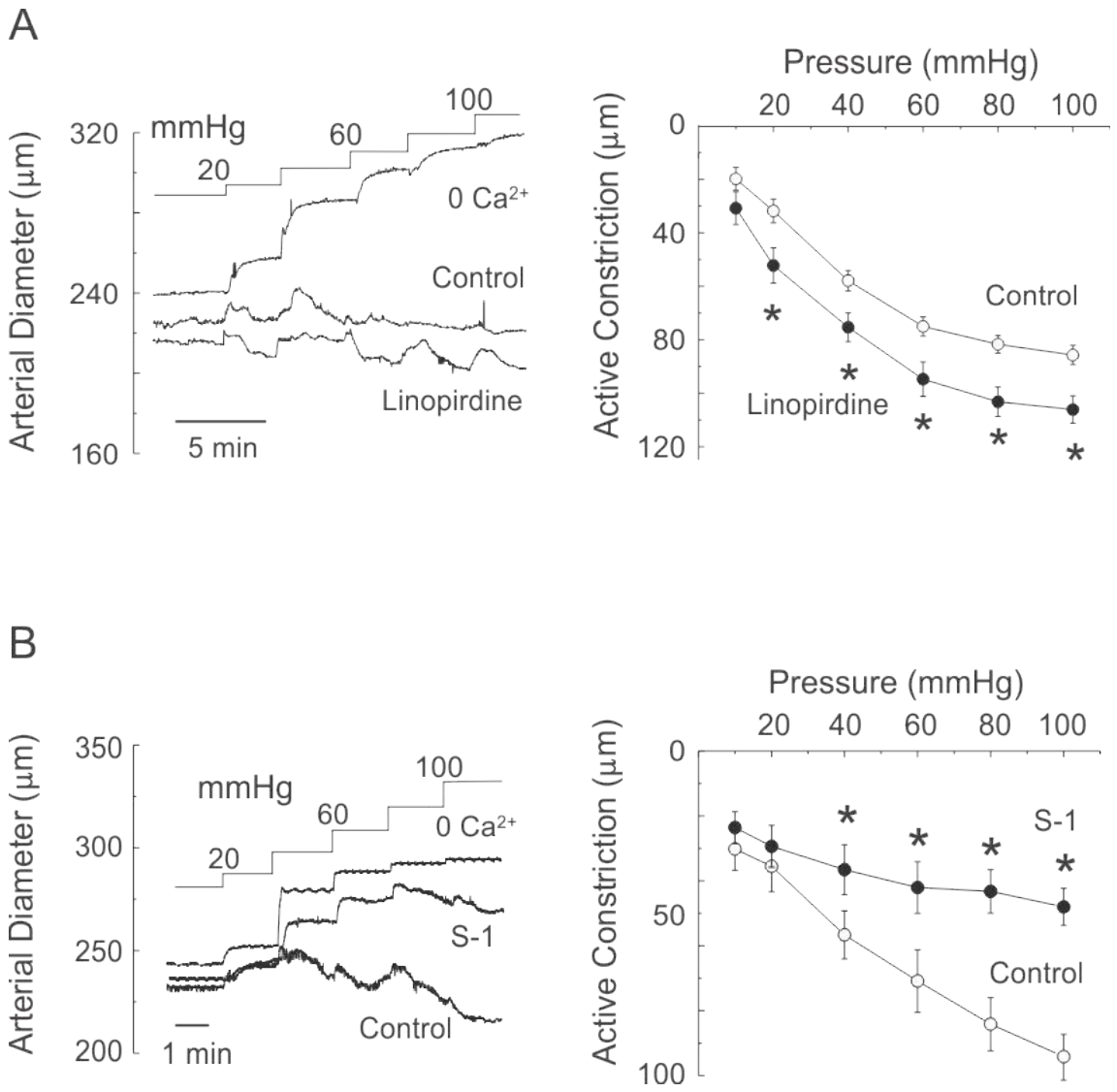

Figure 4.9: Effects of linopirdine and S-1 on the cerebral myogenic response.

(A) Representative recordings of RCA diameter during a series of pressure steps from 10 to between 20 and 100 mmHg in 20 mmHg increments in control Krebs' solution (Control), linopirdine (1 μM) and in 0 Ca^{2+} Krebs' solution (0 Ca^{2+}), and mean ± SEM (n = 5) active constriction in control and linopirdine (difference between diameter in 0 Ca^{2+} and in control or linopirdine). (B) Representative recordings of RCA diameter during a series of pressure steps from 10 to between 20 and 100 mmHg in 20 mmHg increments in

control Krebs' solution (Control), S-1 (20 μM) and in 0 Ca^{2+} Krebs' solution (0 Ca^{2+}), and mean ± SEM (n = 5) active constriction in control and S-1 (i.e. difference between diameter in 0 Ca^{2+} and in control or S-1). * Significantly different ($P < 0.05$) from the value in the control condition at each pressure.

>40 mmHg, although the effect was only ~50% of the magnitude of the dilation produced by 20 μM S-1 (Figure 4.10A).

Figure 4.10B shows representative recordings of diameter and mean ± SEM active constriction in the absence and presence of XE991. XE991 caused a pronounced vasoconstriction over the entire range of intraluminal pressure between 10 and 100 mmHg. This observation is consistent with the previous finding that XE991 is not a selective K_v7 channel blocker (Figure 4.4). The pronounced vessel constriction induced by XE 991 at <40 mmHg is probably due to XE991-indcued inhibition of K_v2-containing channels.

4.3.4 Effect of K_v7 activator, S-1, on enhanced vasoconstriction in pressurized RCAs

Figure 4.11A & D shows the ability of S-1 to reverse the enhanced vasoconstriction induced by activating VGCCs and inhibiting K_v2-containing channels, respectively, at an intraluminal pressure of 80 mmHg. Figure 4.11B & C and E & F shows representative recordings and mean ± SEM arterial diameter for RCAs that were subjected to four sequential series of pressure steps in: (1) control Krebs' solution, (2) L-type Ca^{2+} channel activator, 1,4-Dihydro-2,6-dimethyl-5-nitro-4-(2-[trifluoromethyl] phenyl)pyridine-3-carboxylic acid methyl ester (Bay K8644;10 μM) or ScTx1 (100 nM), (3) S-1 (3 μM), and (4) 0 Ca^{2+} Krebs' solution. Similarly, Figure 4.12A, D & G shows the ability of S-1 to reverse enhanced vasoconstriction induced by three different vasospasmogens, including endothelin-1 (10 nM), serotonin (3 μM) and the thromboxane-A2 mimetic, 9,11-Dideoxy-11α,9α-epoxymethanoprostaglandin $F_{2\alpha}$ (U46619; 1 μM), at an intraluminal pressure of 80 mmHg. Figure 4.12 B & C, E & F and H & I shows representative recordings and mean ± SEM arterial diameter for RCAs that

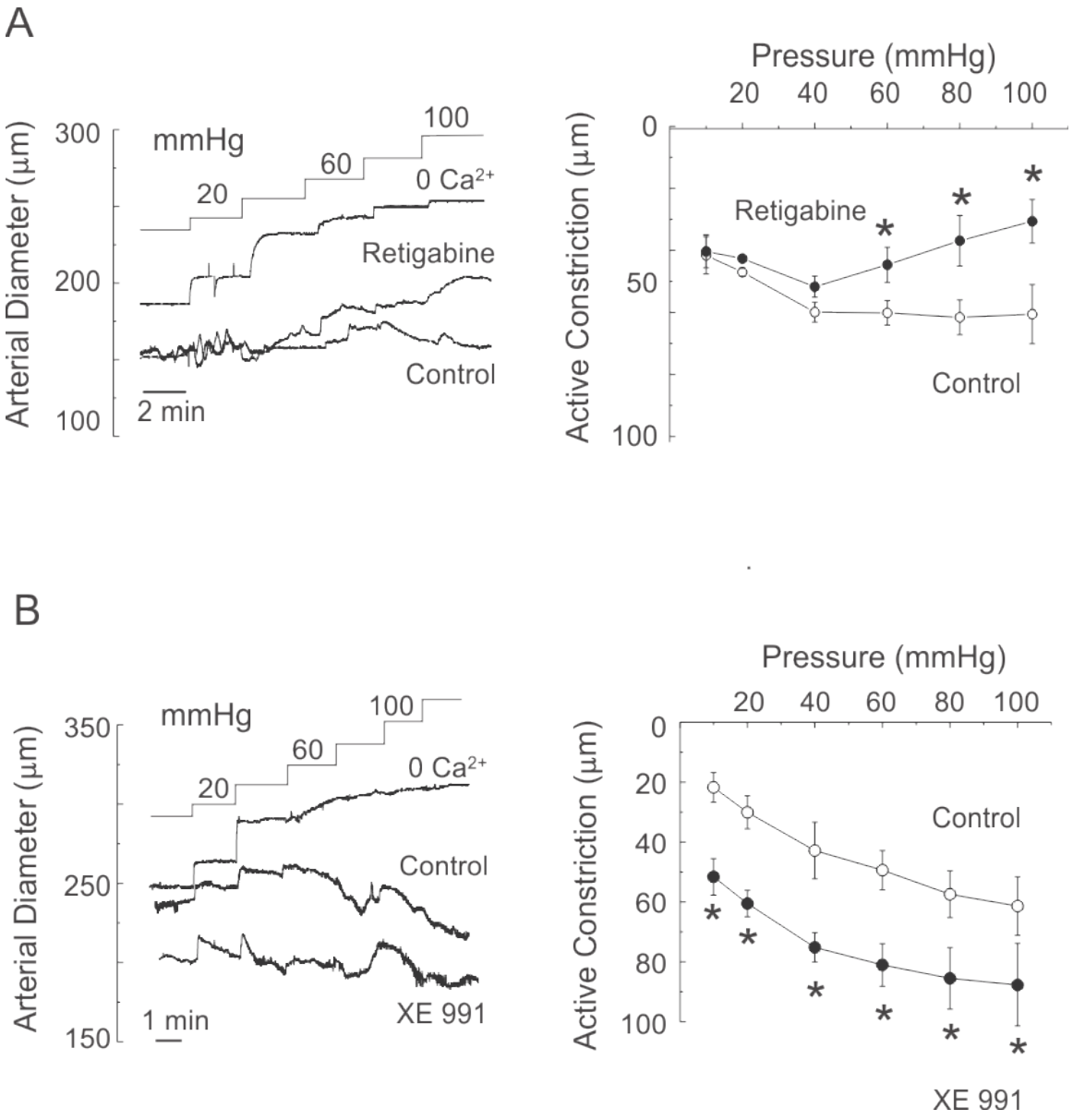

Figure 4.10: Effects of retigabine and XE 991 on the cerebral myogenic response.
(A) Representative recordings of RCA diameter during a series of pressure steps from 10 to between 20 and 100 mmHg in 20 mmHg increments in control Krebs' solution (Control), retigabine (30 µM) and in 0 Ca^{2+} Krebs' solution (0 Ca^{2+}) and mean ± SEM (n = 3) active constriction in control and retigabine (difference between diameter in 0 Ca^{2+} and control or retigabine). (B) Representative recordings of RCA diameter during a series

of pressure steps from 10 to between 20 and 100 mmHg in 20 mmHg increments in control Krebs' solution (Control), XE991 (10 μM) and in 0 Ca^{2+} Krebs' solution (0 Ca^{2+}), and mean ± SEM (n = 5) active constriction in control and XE991. * Significantly different ($P < 0.05$) from the value in the control solution at each pressure.

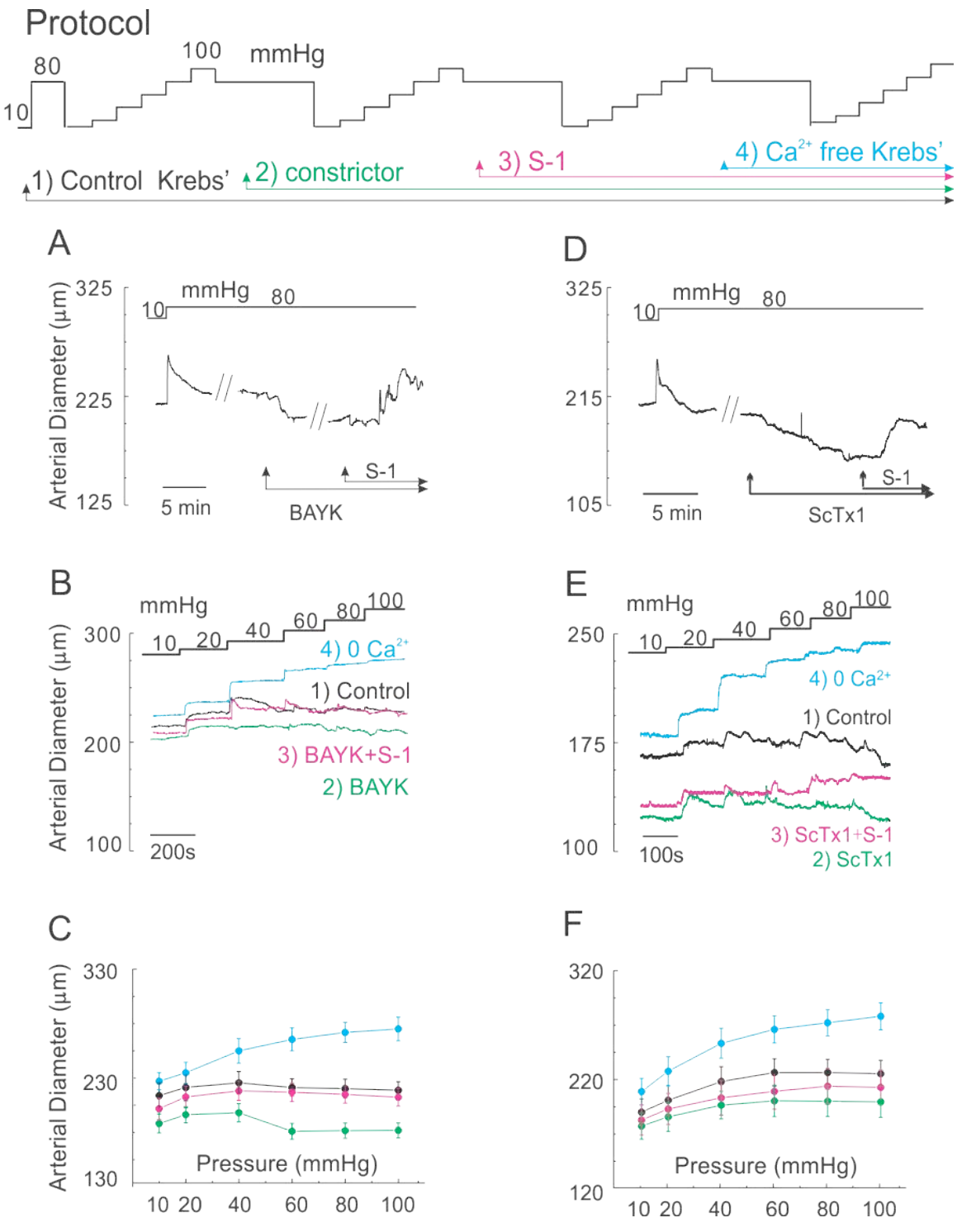
Protocol
80
100
mmHg
10
1) Control Krebs'
2) constrictor
3) S-1
4) Ca2+ free Krebs'
A
Arterial Diameter (µm)
325
225
125
mmHg
10
80
5 min
S-1
BAYK
D
325
215
105
mmHg
10
80
5 min
S-1
ScTx1
B
Arterial Diameter (µm)
300
200
100
mmHg
10
20
40
60
80
100
4) 0 Ca2+
1) Control
3) BAYK+S-1
2) BAYK
200s
E
250
175
100
mmHg
10
20
40
60
80
100
4) 0 Ca2+
1) Control
3) ScTx1+S-1
2) ScTx1
100s
C
Arterial Diameter (µm)
330
230
130
Pressure (mmHg)
10 20 40 60 80 100
F
320
220
120
Pressure (mmHg)
10 20 40 60 80 100

Figure 4.11: Effect of S-1 on enhanced vasoconstriction induced by activating VGCCs or inhibiting K_v2 channels.

(A & D) Representative arterial diameter recordings of S-1 (3 μM) that reversed enhanced vasoconstriction induced by activating VGCCs via Bay K8644 (BAYK; 2 μM) and inhibiting K_v2-containing channels via ScTx1 (100 nM), respectively, at an intraluminal pressure of 80 mmHg. (B & C and E & F) Representative recordings and mean ± SEM (n=3, each) arterial diameter for RCAs that were subjected to four sequential series of pressure steps in: (1) control Krebs' solution, (2) BAYK or ScTx1, (3) S-1 (3 μM) and (4) 0 Ca^{2+} Krebs' solution.

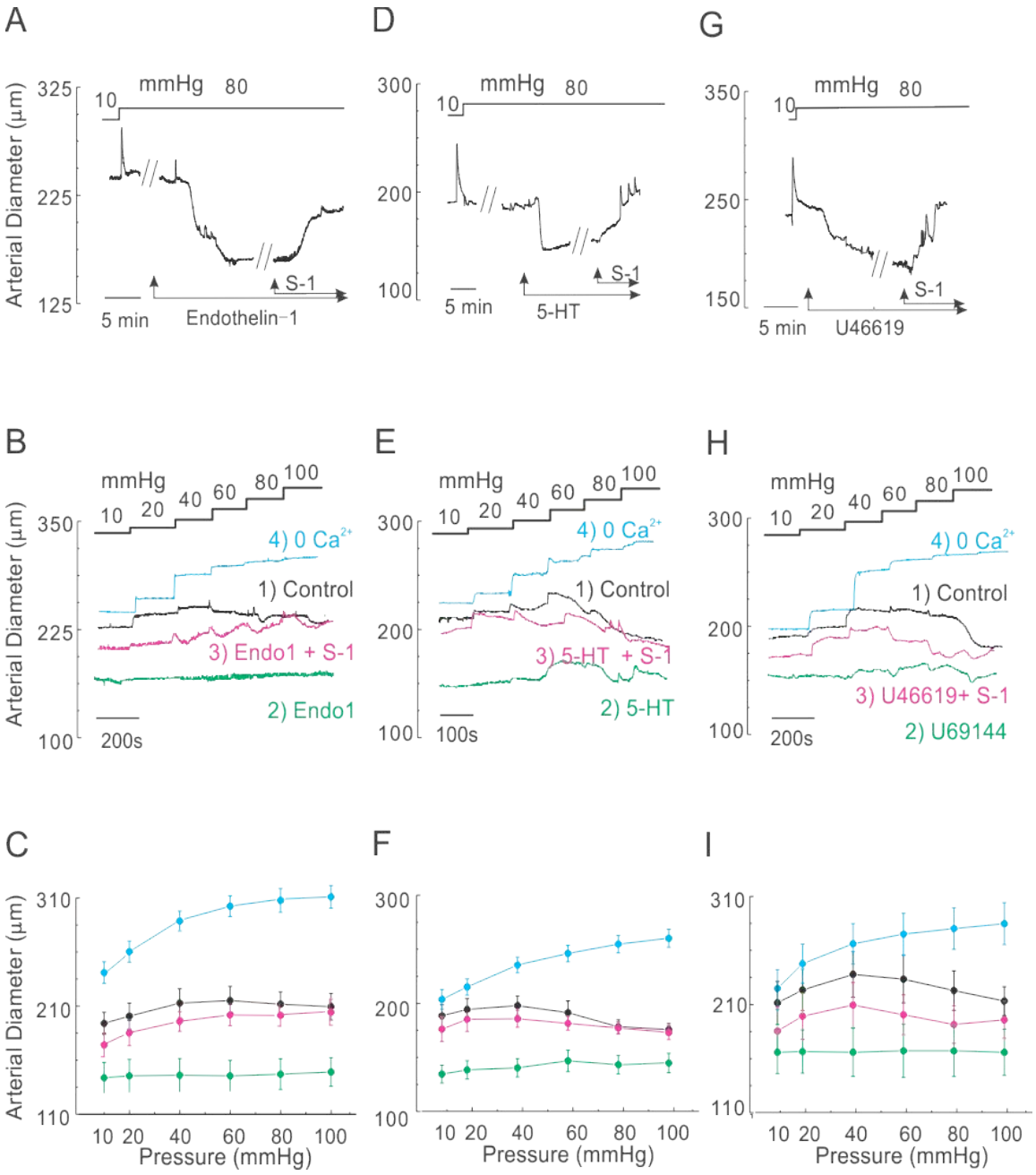

Figure 4.12: Effect of S-1 on enhanced vasoconstriction induced by different vasospasmogens.

(A, D and G) Representative arterial diameter recordings of S-1 (3 µM) that enhanced vasoconstriction induced by three vasospasmogens: endothelin-1 (10 nM), serotonin (5-HT; 3 µM) and thromboxane-A2 mimetic, U46619 (1 µM), respectively, at an

intraluminal pressure of 80 mmHg. (B & C, E & F and H & I) Representative recordings and mean ± SEM (n=3, each) arterial diameter for RCAs that were subjected to four sequential series of pressure steps in: (1) control Krebs' solution, (2) endothelin-1 (Endo1), 5-HT, or U46619, (3) S-1 (3 μM) and (4) 0 Ca^{2+} Krebs' solution.

were subjected to four sequential series of pressure steps in: (1) control Krebs' solution, (2) endothelin-1, serotonin, or U46619, (3) S-1 (3 μM), and (4) 0 Ca^{2+} Krebs' solution. These observations show that S-1 is able to reverse the vasoconstriction induced by vasoconstrictors. Moreover, it is significant to note that the treatment with S-1 in the presence of vasoconstrictors not only rescued the enhanced vasoconstriction, but also maintained the myogenic response of RCAs. Specifically, arterial diameter in the presence of vasoconstrictor and S-1 maintained the pressure-dependent increase in tone, and, therefore, myogenic regulation of arterial diameter.

4.4 Discussion

4.4.1 Summary of findings

This is the first study to identify the contribution of K_v7-containing channels to whole-cell K_v currents of RCA myocytes and myogenic regulation of cerebral arterial diameter. This view is supported by evidence of: (1) the expression of mRNAs encoding $K_v7.1$, $K_v7.4$ and $K_v7.5$ pore-forming subunits, (2) $K_v7.4$ and $K_v7.5$ membrane protein expression in freshly isolated RCA myocytes, (3) the presence of linopirdine- and S-1-sensitive components of whole-cell K_v current in RCA myocytes, and (4) the ability of pharmacological manipulation of K_v7 channels with linopirdine and S-1 to respectively enhance and depress the myogenic response of RCAs to changes in intravascular pressure. We also found that K_v7 activator, S-1, was able to rescue the enhanced myogenic constriction associated with serotonin, endothelin-1, thromboxane-A2 mimetic, activation of L-type Ca^{2+} channels or inhibition of K_v2-containing channels. These novel findings have important implications for physiological control of cerebral blood flow and

for the development of new pharmacological agents to treat clinical conditions of inappropriate control of cerebral arterial diameter.

4.4.2 XE991 is not a specific K_v7 channel blocker

XE991 has been widely used as a selective K_v7 channel blocker in determining the contribution of K_v7 channels to membrane current and/or the regulation of contractility in previous studies (Wang *et al.,* 2000; Dupuis *et al.,* 2002; Greenwood & Ohya, 2009). Although in some cases the effects of the drug were studied under conditions that minimize the contribution of other K_v currents (e.g. by pre-treating the cells with Kv1/Kv2 channel blockers or employing a holding potential of -4 mV; Mackie *et al.,* 2008), its potential non-selective effects were not considered in depth in the interpretation of the physiological responses of intact tissues.

Here, we found that XE991 at 10 μM: (1) almost completely blocked whole-cell K_v currents of RCA myocytes, which include a large contribution from K_v1 and K_v2 currents, and (2) caused marked vasoconstriction at 10 mmHg, a pressure outside of the range over which linopirdine and S-1 were observed to affect the myogenic response. The increase in vascular tone in the presence of XE991 at 10 mmHg was not mirrored by treatment with 1 μM linopirdine, but was observed after ScTx1 treatment (Figure 3.5), suggesting that the effect of XE991 may be the result of a non-selective block of K_v2-containing channels. In addition, we applied XE991 to HEK 293 cells expressing heterotetrameric K_v1.2/K_v1.5 or K_v2.1/9.3 channels that have been identified to contribute to K_v1 and K_v2 currents in RCA myocytes (Albarwani *et al.,* 2003; Chen *et al.,,* 2006; Zhong *et al.,* 2010b). We found that XE991 suppressed currents owing to K_v1.2/1.5 and K_v2.1/9.3 channels. Therefore, caution should be exercised in the

interpretation of experiments employing XE991, as it is very likely to have additional effects beyond specific blockade of K_v7 channels.

4.4.3 Molecular composition of K_v7-containing channels in RCA myocytes

A limitation of the present study is that we have not determined the molecular composition of the K_v7 channels or the potential association with KCNE gene products in RCA myocytes. KCNE genes encode a family of single transmembrane domain proteins, known as MinK-related peptides (MiRPs), which can function as ancillary or β subunits of K_v7 channels (Abbott & Goldstein, 2001). Variability in the biophysical properties of native M-currents of neurons are thought to result from several differences in molecular composition of the underlying K_v7 channels, including varied expression of K_v7 subunits, and interaction with KCNE subunits (McCrossan & Abbott, 2004; Greenwood & Ohya, 2009). Co-expression of KCNE1-5 with $K_v7.4$ in Xenopus oocytes affected current amplitude (with KCNE1-4 increasing, KCNE3 decreasing and KCNE5 having little effect) and caused a leftward shift in the voltage-dependence of activation (Strutz-Seebohm et al., 2006). The expression of $K_v7.1$, $K_v7.4$ and $K_v7.5$ along with KCNE1-4 transcripts suggests the possibility that both homomultimeric and heteromultimeric K_v7 channels may be present in the RCAs (Figure 4.2), as has been suggested for other vessels (Greenwood & Ohya, 2009). Unfortunately, based on the present observations, it is impossible to offer concrete conclusions regarding the subunit composition of the RCA K_v7-containing channels and whether KCNE gene products are present in the functional channel complex.

Nevertheless, the present data imply the presence of heteromultimeric K_v7-containing channels. This view is supported by the voltage-dependent stimulation of K_v

currents in the presence of S-1. S-1 was previously shown to preferentially activate $K_v7.2$-$K_v7.5$ channels, particularly $K_v7.4$ and $K_v7.5$, and to lack a stimulatory effect on $K_v7.1$ channels (Bentzen *et al.,* 2006). The lack of effect on $K_v7.1$ appears to be due to the absence of a transmembrane tryptophan residue that is required for the stimulatory actions of retigabine, flutirpine and S-1 (Schenzer *et al.,* 2005; Wuttke *et al.,* 2005). Given the lack of expression of $K_v7.2$ and $K_v7.3$ in RCA myocytes, the findings suggest that the effects of S-1 on K_v currents and the myogenic response were due to the modulation of $K_v7.4$- and/or $K_v7.5$-containing channels. In addition, it is important to note that the increase in K_v current amplitude of RCA myocytes reached peak at ~−15 mV and then progressively declined with increasing voltage in the presence of S-1. A similar voltage-dependent, bimodal increase and inhibition of native K_v7 currents was previously reported for retigabine and/or flupirtine in murine portal vein myocytes (Yeung *et al.,* 2008) and neurons (Rundfeldt, 1997; Tatulian *et al.,* 2001). Given the finding that the stimulation of homotetrameric $K_v7.4$ (and $K_v7.5$) channels by S-1 progressively increases with greater depolarization (Figure 4.6A and Bentzen *et al.,* 2006), it appears unlikely that the S-1-sensitive current of RCA myocytes is due to homotetrameric $K_v7.4$ and/or $K_v7.5$ channels. It will be of great interest to study whether heteromultimerization of $K_v7.4$ and $K_v7.5$, and/or association with KCNE gene product(s), yields channels that contribute to native K_v7-containing channels in VSM.

4.4.4 S-1 in the treatment of abnormal vasoconstriction

Pharmacological manipulation of K_v7 channel gating may represent a novel option for the treatment of clinical situations of abnormal control of cerebral arterial diameter associated with cerebral vasospasm following subarachnoid hemorrhage (SAH)

and other cardiovascular diseases. For example, a large number of patients experience intense cerebral vasospasm following SAH, but the mechanisms involved are not known with certainty, and there are few effective therapies for this condition (MacDonald *et al.,* 2007; Ferro *et al.,* 2008). Recent data imply that increased activities of spasmogens may be involved in the initiation and maintenance of the sustained vasoconstriction following SAH (Trandafir *et al.,* 2004; Nishizawa & Laher, 2005). Also, enhanced activities of VGCCs (Triggle, 2006; Wellman, 2006) and suppressed activities of K_v2-containing channels of VSMs may contribute to the vasospasm in the animal model of SAH (Jahromi *et al.,* 2008a,b). Here, we show that activation of K_v7-containing channels with S-1 rescued the enhanced myogenic constriction of RCAs evoked by serotonin, endothelin-1, thromboxane-A2 mimetic, activation of L-type Ca^{2+} channels or inhibition of $K_v2.1/9.3$ channels (Figures 4.11 & 4.12). Moreover, it is significant to note the ability of S-1 to attenuate enhanced vasoconstriction while preserving myogenic regulation and, therefore, the crucial physiological mechanism of cerebral blood flow autoregulation.

At present, there is only a very limited repertoire of pharmacologic agents that activate K^+ channels and dilate resistance arteries/arterioles; several compounds that stimulate BK_{Ca} (e.g. NS1619) and K_{ATP} channels (e.g. pinacidil, diazoxide, cromakalim) have been developed, but with the exception of K_v7 channel modulators, agents that stimulate K_v channel activity are lacking. Flupirtine has demonstrated effectiveness in pain management, and retigabine is being considered as a possible anti-epileptic agent, owing to their ability to activate $K_v7.2$-7.5 channels expressed in peripheral and central neurons (Main *et al.,* 2000, Porter *et al.,* 2007; Greenwood & Ohya, 2009). Whether Kv7 channel activators are also effective in the management of abnormal myogenic

depolarization and constriction, such as are associated with cerebral vasospasm following SAH, clearly warrants future examination.

4.4.5 The presence of multiple K_v channels in RCA myocytes

Precise control over the extent of myogenic depolarization is necessary to permit the low amplitude, steady-state changes in E_m and diameter that are essential for physiological regulation of blood pressure and blood flow (Nelson & Quayle, 1995; Nelson *et al.,* 1995; Davis & Hill, 1999). Numerous studies support that pressure-dependent stimulation of VSM K_{DR} currents permits negative-feedback control of myogenic depolarization. Previous studies provide pharmacological and molecular evidence that K_v1 channels are activated by myogenic depolarization to oppose the change in E_m, and prevent action potential initiation as well as oscillatory vasomotion (Albarwani *et al.,* 2003; Plane *et al.,* 2005; Chen *et al.,* 2006). These findings combined with the novel findings described in this chapter and Chapter 3 indicate that at least three different types of K_v channels expressed in cerebral myocytes contribute to control of the cerebral myogenic response.

The specific reasons why multiple types of K_v channels, as well as BK_{Ca} channels are required remain to be elucidated. However, it is reasonable to propose that multiple K^+ channels with different functional properties are required to integrate the complex array of intrinsic (E_m, cytosolic Ca^{2+} concentration, and intracellular modulators such as kinases) and extrinsic (e.g. endothelial, neuronal and metabolic) signals that determine the extent of myogenic depolarization and constriction under varied physiological conditions. For example, the different mechanisms of activation of K_v1 and BK_{Ca} are clearly able to provide for distinct modes of control of E_m via changes in E_m and $[Ca^{2+}]_i$,

respectively. Our findings also suggest that multiple K_v channel subtypes with differences in voltage dependence of activation may be required to permit graded, voltage-dependent control of E_m over the entire pressure range.

Note: The data presented in this chapter except for Figures 4.11 A-C and 4.12 were previously published in Zhong et al. (2010b) J Physiol 588: 3277-3293.

Chapter Five: Identification of a role for VASP in the regulation of cytoskeleton reorganization in the cerebral myogenic response and NO-mediated vasodilation

5.1 Introduction

5.1.1 Vasodilator-stimulated phosphoprotein (VASP)

VASP was first discovered and purified from human platelets in the 1980s (Halbrugge & Walter, 1989). Subsequently, VASP was cloned in 1995, and shown to encode a 380-residue polypeptide (Haffner *et al.*, 1995). Nowadays, emerging evidence has supported an important role for VASP in mediating cyclic nucleotide signaling pathways, as well as actin dynamics associated with various cellular events in a number of cell types.

5.1.1.1 Domain structure of VASP

VASP belongs to the Ena/VASP family, which consists of three mammalian members, including VASP, Mena (mammalian Enabled) and EVL (Ena-VASP-like) (Krause *et al.*, 2003). All members share a conserved domain structure: an N-terminal Ena/VASP homology 1 domain (EVH1), a central proline-rich domain (PRO) and a C-terminal Ena/VASP homology 2 domain (EVH2) (Bear & Gertler, 2009) (Figure 5.1).

The EVH1 domain consists of two β-sheets and a C-terminal α-helix. It mediates specific protein-protein interactions by directly binding to a motif that has the consensus sequence (D/E)-(F/W/Y/L)-PPPP-X-(D/E)-(D/E)-(D/E). This plays an important role in targeting VASP to specific cellular locations (Brindle *et al.*, 1996; Drees *et al.*, 2000). A central PRO domain contains proline-rich sequences that can bind to profilin. Profilin is a small actin-binding protein that contributes to F-actin assembly. It interacts with a large number of proteins containing proline-rich sequences (Jockusch *et al.*, 2007). The EVH2

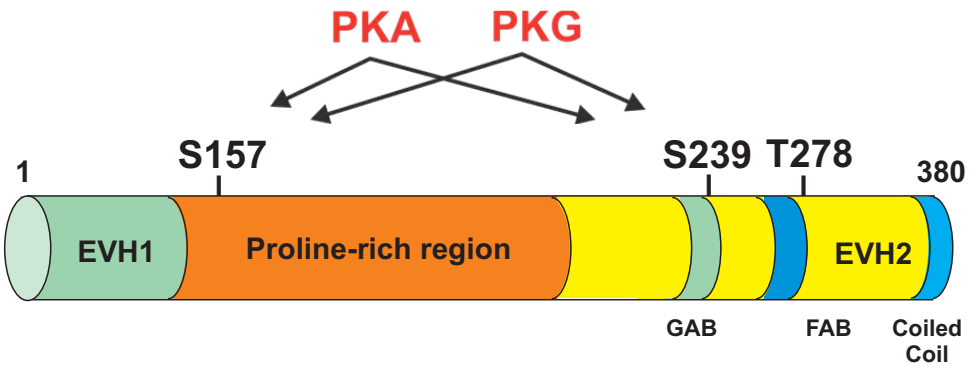

Figure 5.1: Domain organization and major phosphorylation sites of VASP.
VASP is composed of an N-terminal Ena/VASP homology 1 domain (EVH1), a central proline-rich domain (PRO) and a C-terminal Ena/VASP homology 2 domain (EVH2). The EVH1 domain mediates specific protein-protein interaction by directly binding to a motif that has the consensus sequence (D/E)-(F/W/Y/L)-PPPP-X-(D/E)-(D/E)-(D/E). The central PRO domain contains proline-rich sequences that bind to profilin. The EVH2 domain consists of a G-actin-binding region (GAB), an F-actin binding region (FAB) and a C-terminal coiled-coil region that may mediate VASP oligomerization. The function of VASP is tightly controlled by VASP phosphorylation. Three major phosphorylation sites were identified *in vivo*: Serine-239 (S239) and Serine-157 (S157) are phosphorylated by protein kinase A (PKA) and protein kinase G (PKG); Threonine-278 (T278) is phosphorylated by AMP-activated protein kinase. (Cartoon is modified from Bear & Gertler 2009; *J Cell Sci* 122:1947-1953.)

domain appears to be crucial in maintaining the normal function of VASP. It consists of three conserved regions of interest: a G-actin-binding region, an F-actin binding region and a C-terminal coiled-coil region. Direct interactions with G-actin and/or F-actin play an important role in VASP-mediated actin dynamics. The coiled-coil region involves VASP tetramerization *in vitro*, yet the physiological importance of VASP tetramerization *in vivo* remains unclear (Bachmann *et al.,* 1999; Zimmermann *et al.,* 2002; Kuhnel *et al.,* 2004).

5.1.1.2 VASP function

VASP localizes within the actin structures at the plasma membrane that are sites of actin dynamics, including for example, focal adhesions, actin stress fibres, leading edges of protrusion lamellipodia and the tips of filopodia (Reinhard *et al.,* 1992; Rottner *et al.,* 1999; Wei *et al.,* 2003; Lebrand *et al.,* 2004; Lindsay *et al.,* 2007; Bear & Gertler, 2009). Early evidence came from the study of *Listeria* motility. The movement of *Listeria* is facilitated through its bacterial surface protein, ActA. ActA can employ cytoskeleton elements from host cells and function as a nucleator for its own F-actin assembly. VASP was the first cytoskeletal protein found to be recruited to *Listeria* and promote actin polymerization (Theriot *et al.,* 1994; Chakraborty *et al.,* 1995; Niebuhr *et al.,* 1997). Depletion of VASP from cell extracts impaired *Listeria* movement, whereas add-back experiments rescued the movement (Kang *et al.,* 1997; Laurent *et al.,* 1999; Loisel *et al.,* 1999). Later on, VASP-mediated actin dynamics were documented for various cell types, including fibroblasts (Bear *et al.,* 2002), T-cells (Krause *et al.,* 2000; Castellano *et al.,* 2001), neurons and synapses (Lebrand *et al.,* 2004; Kwiatkowski *et al.,* 2007; Lin *et al.,* 2010), endothelial cells (Brindle *et al.,* 1996; Schmit *et al.,* 2012),

epithelial cells (Vasioukhin *et al.*, 2000; Lawrence *et al.*, 2002; Zimmermann *et al.*, 2002; Quinlan, 2004), cardiac myocytes (Heling *et al.*, 2000; Eigenthaler *et al.*, 2003; Sartoretto *et al.*, 2009) and vascular myocytes (Deruelle *et al.*, 2006; Thorsen *et al.*, 2010).

VASP is known to play an important role in actin dynamics associated with cell spreading, migration and adhesion (Krause *et al.*, 2003; Kwiatkowski *et al.*, 2003). It is proposed to act as an anti-capping protein in mediating actin dynamics (Bear *et al.*, 2002; Barzik *et al.*, 2005; Breitsprecher *et al.*, 2008; Pasic *et al.*, 2008). Capping proteins bind to barbed ends of actin filaments and interrupt filament elongation (DiNubile *et al.*, 1995; Wear *et al.*, 2003). VASP permits continued addition of actin monomers to the barbed ends and block of the effect of capping proteins. In addition, other VASP-associated events have been reported, including inhibition of branching (Skoble *et al.*, 2001; Samarin *et al.*, 2003), bundling (Bachmann *et al.*, 1999; Applewhite *et al.*, 2007), nucleation (Huttelmaier *et al.*, 1999; Skoble *et al.*, 2001) and profilin recruitment (Geese *et al.*, 2002; Chereau & Dominguez, 2006; Ferron *et al.*, 2007). They may facilitate VASP-mediated anti-capping or act in parallel as alternative events to promote actin dynamics.

Although considerable evidence indicates a role for VASP in actin dynamics, confounding issues remain. For example, with regards to the role of profilin in VASP-mediated actin elongation, some studies have suggested VASP can function by itself (Breitsprecher *et al.*, 2008), whereas others have suggested the opposite (Bear *et al.*, 2002; Barzik *et al.*, 2005). Therefore, a clear understanding of the molecular basis of VASP-mediated actin dynamics requires further investigation. The mechanism may vary among different cellular events and cell types. Also, it is important to note that the experimental

conditions (e.g. the concentration of salt solution) are likely to have a huge impact on the *in vitro* study of actin dynamics.

5.1.1.3 VASP phosphorylation

VASP has been extensively studied as a substrate for cyclic nucleotide-dependent kinases, PKA and PKG. Serine-157 (Ser157) and Serine-239 (Ser239) were identified as two major sites of PKA and PKG (Waldmann *et al.,* 1987; Butt *et al.,* 1994; Harbeck *et al.,* 2000). Early *in vitro* studies indicated that PKA signaling prefers to phosphorylate VASP at Ser157, whereas PKG signaling prefers to phosphorylate at Ser239 (Butt *et al.,* 1994). However, emerging *in vivo* studies performed using different cell types suggest that PKA and PKG signaling can lead to VASP phosphorylation at both Ser157 and Ser239 with no comparable differences (Smolenski *et al.,* 2000; Schafer *et al.,* 2003; Sartoretto *et al.,* 2009; Adderley *et al.,* 2012). More recent studies have also identified Threonine-278 (Thr278) as a novel VASP phosphorylation site, but this site is only phosphorylated by AMP-activated protein kinase (AMPK) *in vivo* (Blume *et al.,* 2007). It is interesting to note that phosphorylation of VASP at Ser157 rather than at the other two sites leads to an apparent shift in molecular mass from 46 to 50 kDa in standard SDS-PAGE (Halbrugge & Walter, 1989; Reinhard *et al.,* 1992; Smolenski *et al.,* 1998). The shift is probably due to a change in secondary structure that results from the addition of the phosphoryl group at Ser157.

The level of protein phosphorylation is not only determined by protein kinases but also by protein phosphatases. VASP dephosphorylation by the serine/threonine protein phosphatases PP1, PP2A, PP2B and PP2C has been reported *in vitro* (Abel *et al.,* 1995). Also, incubation of human platelets with okadaic acid, a potent inhibitor of PP1 and

PP2A, induced the accumulation of phosphorylated VASP (Abel *et al.,* 1995; Kwiatkowski *et al.,* 2003). These observations indicate that serine/threonine protein phosphatases may contribute to VASP dephosphorylation *in vivo*. However, the specific protein phosphatase(s) responsible for the regulation of VASP phosphorylation remains unknown.

5.1.1.4 VASP phosphorylation in control of VASP function

Phosphorylation of VASP has negative effects on VASP-mediated actin dynamics. Direct evidence on how phosphorylation alters its functions came from studies of VASP mutants. Phospho-mimetic and phospho-null VASP mutants were achieved by substituting one or more of the three major phosphorylation sites with acidic amino acids and alanine residues, respectively. VASP phospho-mimetic mutants were identified to impair the ability of VASP to promote actin polymerization and/or the ability of VASP to interact with G-actin, F-actin and to participate in dynamic cytoskeleton reassembly (Harbeck *et al.,* 2000; Smolenski *et al.,* 2000; Geese *et al.,* 2002; Grosse *et al.,* 2003; Zhuang *et al.,* 2004; Barzik *et al.,* 2005; Lindsay *et al.,* 2007; Benz *et al.,* 2009; Lee & Chung, 2009; Defawe *et al.,* 2010).

It has been shown that precise control of VASP phosphorylation plays an important role in mediating actin dynamics associated with various cellular events in a number of cell types. For example, in platelets, activation of PKA/PKG signaling promoted inhibition of platelet aggregation (Halbrugge *et al.,* 1990; Aszodi *et al.,* 1999; Bearer *et al.,* 2002; Khavandi *et al.,* 2009). Platelet aggregation is an actin-dynamic process that facilitates blood clotting. Analysis of VASP-knockout mice also suggests the requirement of VASP for cAMP/cGMP-mediated inhibition of platelet aggregation

(Aszodi *et al.,* 1999). In fibroblasts, cell adhesion was found to involve the regulation of VASP phosphorylation. Cellular detachment induced rapid VASP phosphorylation at Ser157 and Ser239, whereas reattachment resulted in dephosphorylation (Howe *et al.,* 2002). In microglia, PKA-mediated VASP phosphorylation was indicated to be important in chemotaxis controlled by focal adhesion formation, whereas VASP dephosphorylation was required for the growth of adhesion strength during membrane retraction (Lee & Chung, 2009). In endothelial cells, PKG-mediated VASP phosphorylation at Ser157 resulted in detachment of endogenous VASP from focal adhesions (Smolenski *et al.,* 2000). Similarly, AMPK-mediated VASP phosphorylation at Thr278 attenuated actin cytoskeleton formation and altered cell morphology (Blume *et al.,* 2007). In addition, phosphorylation of VASP and cytoskeleton reorganization were both altered when endothelial cells were exposed to laminar shear stress (Wei *et al.,* 2003; Wei *et al.,* 2004). In vascular myocytes, BAY 41-2272, a stimulator of soluble guanylyl cyclase (sGC), increased VASP phosphorylation and decreased vascular remodeling in the rat pulmonary vasculature during chronic hypoxia (Deruelle *et al.,* 2006; Thorsen *et al.,* 2010). BAY 41-2272 was also found to increase the intracellular levels of cAMP/ cGMP, VASP phosphorylation, and to attenuate proliferation of cultured VSMCs (Mendelev *et al.,* 2009).

In addition to serine/threonine phosphorylation, a recent study implied that VASP can be tyrosine-phosphorylated, as an Abi-1-bridged substrate of Ab1, and Tyr-39 was identified as a novel phosphorylation site responding to tyrosine phosphorylation (Maruoka *et al.,* 2012). Tyrosine phosphorylation suppressed the association of VASP with focal adhesions and altered leukaemic cell adhesion. A previous study reported that

the interaction of VASP with Ab1 tyrosine kinase was apparent in association with cell adhesion and was lost following cellular detachment (Howe *et al.,* 2002). Interestingly, activation of PKA abolished the interaction of VASP with Ab1, whereas inhibition of PKA prevented dissociation of VASP and Ab1 complex induced by cellular detachment.

5.1.2 NO-mediated vascular smooth muscle relaxation

NO is a major mediator of VSM relaxation. The mechanisms by which NO evokes VSM relaxation have been a subject of considerable interest (Hofmann *et al.,* 2000; Lincoln *et al.,* 2001; Morgado *et al.,* 2012). However, very few studies have analyzed the mechanism(s) of NO-mediated vasodilation of small resistance arteries in the presence of the myogenic response.

5.1.2.1 NO/sGC/cGMP signaling pathway

NO/sGC/cGMP is the best-characterized upstream signaling pathway associated with NO stimulation of VSMCs (Faraci & Sobey, 1999). NO is synthesized in vascular endothelium by endothelial nitric oxide synthase (eNOS). eNOS generates NO and L-citrulline from L-arginine and O_2 in response to receptor-dependent agonists, such as bradykinin, substance-P and acetylcholine (ACh), as well as physicochemical stimuli, such as flow-induced shear stress (Lincoln *et al.,* 2001; Fleming & Busse, 2003). NO is a small molecule, hydrophobic gas, that diffuses to the adjacent smooth muscle, and interacts with sGC. NO binding to sGC triggers enzyme activity and a hundred-fold increase in cyclic GMP (cGMP) formation (Potter *et al.,* 2006). PKG are serine/threonine kinases that are composed of an NH_2-terminal domain, a regulatory domain, and a catalytic domain. In the basal condition, catalytic activity is blocked by the regulatory

domain (Hofmann *et al.,* 2006). Interaction with cGMP releases this inhibition, and leads to PKG-mediated smooth muscle relaxation.

5.1.2.2 Mechanisms of NO-mediated vascular smooth muscle relaxation

Three signaling pathways have been proposed to contribute to NO/sGC/cGMP/PKG-mediated VSM relaxation. The first pathway is mediated by a reduction in $[Ca^{2+}]_{i,}$ leading to a decrease in MLCK activity (Hofmann *et al.,* 2000; Morgado *et al.,* 2012). Several events were documented to contribute to the change in $[Ca^{2+}]_i$, including: (1) decreased Ca^{2+} entry via VGCCs (Xiong *et al.,* 1994; Liu *et al.,* 1997), (2) decreased Ca^{2+} release from SR owing to IP_3 receptor-associated PKG-I substrate (IRAG)-dependent phosphorylation of IP_3 receptors (Koga *et al.,* 1994; Haug *et al.,* 1999), and (3) increased sequestration and removal of $[Ca^{2+}]_i$ via the stimulation of SR and plasma membrane Ca^{2+}-ATPase activities (Rashatwar *et al.,* 1987; Cornwell *et al.,* 1991; Kim & Perrino, 2007). In addition, NO signaling was found to activate BK_{Ca} (Zhou *et al.,* 1996; Fukao *et al.,* 1999; Zhang *et al.,* 2006), K_v (Zhao *et al.,* 1997; Sobey & Faraci, 1999) and K_{ATP} channels (Murphy & Brayden, 1995; Weidelt *et al.,* 1997), which causes E_m hyperpolarization resulting in a decrease in voltage-dependent Ca^{2+} entry via VGCCs leading to a reduction in $[Ca^{2+}]_i$.

The second pathway of NO-mediated VSM inhibition is mediated by a decrease in Ca^{2+} sensitization (Hofmann *et al.,* 2000; Morgado *et al.,* 2012). As described in Chapter 1.5.2, an important component of the Ca^{2+} sensitization mechanism involves the ROK-dependent inhibition of MLCP in response to contractile stimuli. Substantial evidence suggests that activation of PKG results in an increase in MLCP activity in VSM (Pfitzer, 2001). On one hand, PKG was identified to oppose ROK-dependent inhibition of

MCLP by phosphorylating distinct sites on MYPT1, which activated the catalytic activity of MLCP (Bolz *et al.,* 2003b; Nakamura *et al.,* 2007). On the other hand, PKG was shown to directly interfere with the RhoA-mediated stimulation of ROK through the phosphorylation of RhoA (Sauzeau *et al.,* 2000; Bolz *et al.,* 2003b). Also, some studies have indicated that a NO-mediated decrease in Ca^{2+} sensitization might involve the phosphorylation of telokin, an abundant protein found in some types of smooth muscle cells that is identical to the C-terminus of MLCK (Wu *et al.,* 1998; MacDonald, *et al.,* 2000).

As described in Chapter 1.5, the level of LC_{20} phosphorylation is tightly controlled by MLCK and MCLP activities. A NO-mediated decrease in MLCK activity, and/or increase in MLCP activity, would be expected to result in a reduction in LC_{20} phosphorylation, which impairs cross-bridge cycling and causes a decrease in force generation by VSMCs. However, some findings suggest that cyclic nucleotide-mediated smooth muscle relaxation is uncoupled from a change in $[Ca^{2+}]_i$ and/or LC_{20} phosphorylation. For example, isoprenaline- or forskolin-induced, PKA-mediated relaxation of bovine tracheal smooth muscle was not associated with a decrease in $[Ca^{2+}]_i$ and LC_{20} phosphorylation (Miller *et al.,* 1983; Takuwa *et al.,* 1988). In addition, both cAMP and cGMP were able to relax permeabilized rat mesenteric arteries when $[Ca^{2+}]_i$ was held constant (Nishimura & van Breemen, 1989). Furthermore, activation of PKA or PKG signaling in bovine carotid artery completely reversed serotonin-induced VSM contraction, yet neither had an effect on the level of LC_{20} phosphorylation (Woodrum *et al.,* 1999).

The third pathway of NO-mediated VSM relaxation is proposed to be mediated by cytoskeleton proteins. The 20-kDa heat shock-related protein, HSP20, and VASP have gained attention as potential mediators of this pathway (Lincoln *et al.,* 2001). An increase in the phosphorylation of HSP20 was shown to be associated with PKG/PKA-mediated VSM relaxation (Beall *et al.,* 1997; Woodrum *et al.,* 1999; Brophy *et al.,* 1999a, b), but the mechanism involved is unclear. Brophy *et al.* (1999a, b) suggested that it was via a thin-filament regulatory process, leading to an impairment of the cytoskeleton network. Also, Rembold *et al.* (2000) reported that cGMP-mediated phosphorylation of HSP20 resulted in relaxation in swine carotid arteries, which was not associated with a decrease in LC_{20} phosphorylation. VASP has been extensively studied as a substrate for PKG or PKA. Recent studies reported that an increase in phosphorylation of VASP at Ser157 and/or Ser239 was associated with NO-mediated relaxation in rat/rabbit aortas and swine carotid arteries (Oelze *et al.,* 2000; Schafer *et al.,* 2003; Ying *et al.,* 2012). However, there have been very few studies of the role of VASP phosphorylation in NO-mediated VSM vasodilation of cerebral arteries in the presence of the myogenic response.

5.1.2.3 NO-mediated vasodilation in the presence of the myogenic response

Despite the identification of multiple mechanisms of NO-mediated VSM relaxation, one should bear in mind that the relative importance of each mechanism appears to vary between different vessel types, as well as contractile stimuli (Hofmann *et al.,* 2000; Lincoln *et al.,* 2001; Morgado *et al.,* 2012). However, most studies regarding NO-mediated VSM relaxation are based on the use of cultured VSMCs, or vessels pre-contracted by agonists such as serotonin. Although the addition of agonists aims to provide vascular tone to facilitate detection of NO-mediated relaxation, it may also affect

the original signaling network underlying VSM contractility. That is to say, the signaling change associated with NO-mediated relaxation is likely to be interfered with by the signaling change associated with the agonist-induced pre-contraction.

Small resistance arteries are exposed to relatively high transmural pressures *in vivo*, and maintain a basal level of myogenic tone. Therefore, the employment of the pressurized resistance artery with spontaneous myogenic tone is of great significance in the study of molecular mechanisms underlying NO-mediated vasodilation. However, there are very few such studies in the literature, and none have tried to examine and compare multiple pathways under the same experimental conditions.

5.1.3 VASP in the regulation of VSM contractility

As described in 5.1.1, the role of VASP and VASP phosphorylation has received considerable attention in the context of cell spreading, migration and adhesion (Krause *et al.*, 2003; Kwiatkowski *et al.*, 2003). However, the role of VASP and VASP phosphorylation in control of VSM contractility is very poorly studied. Kim *et al.* (2010) indicated, for the first time, a role for VASP in promoting actin polymerization and smooth muscle contraction. Specifically, introduction of the EVH1 domain of VASP exerted a dominant negative effect on the normal function of VASP, leading to an inhibition of phenylephrine-induced actin polymerization in isolated myocytes. Furthermore, knockdown of VASP decreased phenylephrine-induced contraction in rat aorta rings.

Since VASP was shown to be associated with VSM contraction, VASP activity is tightly affected by NO signaling, VASP plays an important role in actin-dynamics, and cytoskeleton reorganization plays an important role in the myogenic response, it was of

great interest to study the role of VASP in NO-mediated vasodilation and the myogenic response.

5.2 Hypothesis and objectives of the study

Here, we tested the specific **hypothesis** that VASP contributes to the regulation of cytoskeleton reorganization in NO-mediated vasodilation and the pressure-dependent myogenic response of RCAs. The four primary objectives of this study were as follows:

(1) To identify whether NO-mediated vasodilation is associated with a decrease in LC_{20} phosphorylation in pressurized RCAs.

(2) To determine whether NO-mediated vasodilation involves cytoskeleton reorganization in pressurized RCAs.

(3) To assess whether NO-mediated vasodilation is associated with an increase in VASP phosphorylation in pressurized RCAs.

(4) To investigate whether the myogenic response is associated with a decrease in VASP phosphorylation in pressurized RCAs.

5.3 Results

5.3.1 Characteristics of DEANONOate and acetylcholine-induced vasodilation in pressurized RCAs.

DEANONOate (DEA) is widely used in the study of NO-mediated relaxation as an exogenous endothelium-independent NO donor, and ACh, as an endogenous endothelium-dependent stimulator. Here, we studied the effect of NO on myogenic regulation of arterial diameter by applying DEA and ACh to endothelium-denuded and endothelium-intact RCAs, respectively, in the presence of the myogenic response. As shown in Figure 5.2, treatment of RCAs with DEA (100 nM) or ACh (30 μM)

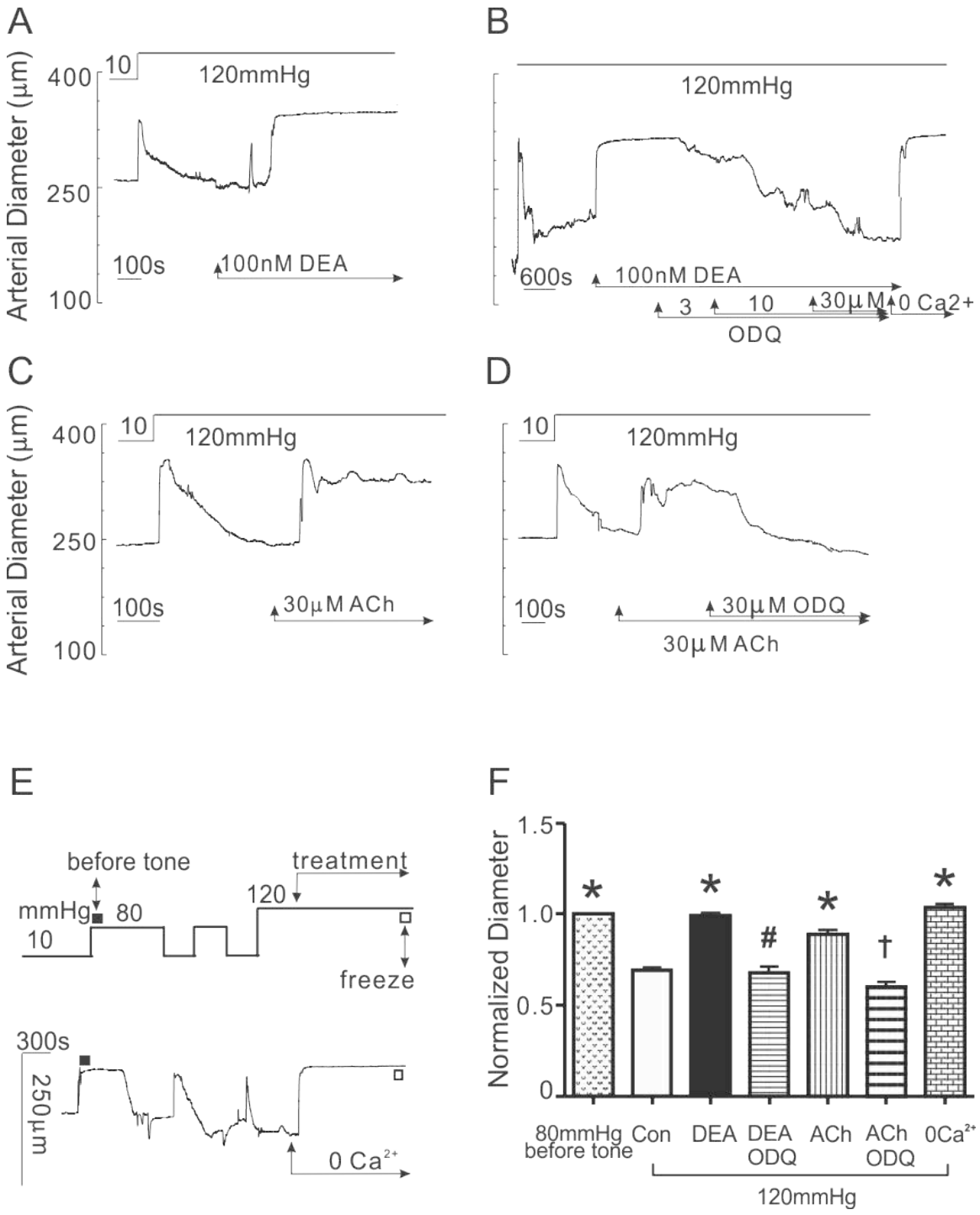
A
Arterial Diameter (μm)
400
250
100
10
120mmHg
100s
100nM DEA
B
120mmHg
600s
100nM DEA
3
10
30μM
0 Ca2+
ODQ
C
Arterial Diameter (μm)
400
250
100
10
120mmHg
100s
30μM ACh
D
10
120mmHg
100s
30μM ODQ
30μM ACh
E
before tone
treatment
mmHg
80
120
10
freeze
300s
250μm
0 Ca2+
F
Normalized Diameter
1.5
1.0
0.5
0
*
*
#
*
†
*
80mmHg before tone
Con
DEA
DEA ODQ
ACh
ACh ODQ
0Ca2+
120mmHg

Figure 5.2: NO-mediated vasodilation in pressurized RCAs.

(A-D) Representative diameter recordings of RCAs at 120 mmHg treated with DEANONOate (DEA, 100 nM), acetylcholine (ACh, 30 μM), DEA + 1H-[1,2, 4]oxadiazolo[4,3-a]quinoxalin-1-one (ODQ, 30 μM) and ACh + ODQ, respectively, (E) Experimental protocol and representative diameter recording of RCAs at 120 mmHg treated with 0 Ca^{2+} Krebs' solution prior to vessel collection for biochemical analysis. Closed and open squares indicate times for the measurement of diameter at 80 mmHg before the initial myogenic tone development and for vessel collection, respectively. (F) Mean ± SEM arterial diameter of RCAs at 120 mmHg in control (n=45), DEA (n=25), DEA + ODQ (n=5), ACh (n=20), ACh + ODQ (n=5) and 0 Ca^{2+} Krebs' solution (0 Ca^{2+}, n=9). Diameter under each condition is expressed as a % of the value of the same vessel at 80 mmHg before the initial tone development (the time for this diameter measurement is indicated by the closed square in panel E). * , # and ǂ indicate significantly different ($P < 0.05$) from value at 120 mmHg in control, DEA, and ACh, respectively.

substantially suppressed the myogenic constriction, and induced nearly maximal dilation at 120 mmHg. Figure 5.2F shows the normalized, mean diameter under each treatment. Each diameter was normalized to the diameter of the same vessel when first pressurized to 80 mmHg during the equilibrium period before the initial tone development (see Figure 5.2E; the time for this diameter measurement is indicated by the closed square). This diameter was found to be a reliable indicator of the fully dilated condition observed in vessels exposed to 0 Ca^{2+} Krebs' solution (Figure 5.2E & F). Figure 5.2B & D shows that the treatment with a sGC selective inhibitor, 1H-[1,2,4]oxadiazolo[4,3-a]quinoxalin-1-one (ODQ, 30 μM) reversed DEA/ACh-induced vasodilation. Also, we found that ACh did not induce vasodilation of endothelium-denuded RCAs, or of N (G)-nitro-L-arginine methyl ester (L-NAME, 10 μM) pre-treated RCAs, which selectively inhibits eNOS activity (n=3, each). These observations suggest that DEA/ACh induces significant vasodilation in pressurized RCAs owing to the activation of NO-sGC-cGMP signaling. Also, the data are consistent with a previous *in vivo* study showing that both NO donors and ACh caused vasodilation of rabbit cerebral arteries, and the dilation was sGC-dependent (Faraci & Sobey, 1999). Notably, some studies have reported that ACh did not induce significant vasodilation in pressurized RCAs (Lagaud *et al.*, 1999), which is contrary to our data. Here we found that some vessels (~30% in total) only exhibited transient vasodilation (<~0.5 min) in response to ACh stimulation, whereas most vessels were able to exhibit sustained vasodilation (>~5 min). We think that the reason for the lack of sustained ACh response in some vessels is probably because the endothelium of those vessels was partially damaged due to dissection and/or cannulation.

5.3.2 Tissue preparation for biochemical analysis of LC_{20}, MYPT1 and VASP phosphorylation as well as G-actin content

The effect of NO on the level of LC_{20}, MYPT1 and VASP phosphorylation was studied using vessel segments with a steady level of dilation or constriction (~5-10 min) following drug treatment(s) at 120 mmHg prior to TCA/DTT flash-freezing and subsequent western blot analysis (see the protocol in Figure 5.2E). For the control condition, vessel segments were collected when a steady level of myogenic constriction was achieved following a pressure step from 10 to 120 mmHg. In order to study the effect of NO on the extent of actin polymerization, vessel segments were transferred into F-actin stabilization buffer rather than TCA/DTT freezing solution, and then subjected to centrifugation to separate F- and G-actin prior to western blot analysis (see Chapter 2.9-10 for methods in detail).

The highly sensitive three-step western blotting technique was employed for quantitative analysis of LC_{20}, as well as MYPT1 and/or VASP phosphorylation in the same sample of extracted protein from 1-3 RCA segments (depending on the length of the segments). It was very important to ensure that the quality (i.e. the extent of myogenic constriction or NO-mediated vasodilation) of each vessel segment collected for biochemical analysis was comparable. Given that the magnitude of passive dilation in 0 Ca^{2+} Krebs' solution (and therefore, the level of active constriction) could not be evaluated in these experiments due to the need for vessel collection, diameter under each treatment prior to vessel collection was normalized to diameter of the same vessel at 80 mmHg before tone, as described in 5.3.1. Note the value of this diameter at 80 mmHg before tone was not different from the value of maximal diameter at 120 mmHg induced

by 0 Ca^{2+} Krebs' solution (Figure 5.2E & F). Therefore, the extent of constriction or dilation of each vessel segment in response to different treatments can be monitored by quantifying the normalized diameter.

5.3.3 MYPT1 phosphorylation at Thr855 in DEANONOate-induced vasodilation in pressurized RCAs

Since the regulation of VSM contraction through control of MYPT1 phosphorylation is proposed to be an important target of NO signaling (described in 5.1.2.2), and an increase in intraluminal pressure to 100 mmHg was shown to significantly enhance MYPT1 phosphorylation at Thr855 in association with the myogenic response of RCAs (Johnson *et al.*, 2009b), the effect of NO on MYPT1 phosphorylation at Thr855 in pressurized RCAs was determined through biochemical analysis. Figure 5.3A shows representative western blots of phosphorylated MYPT1 at Thr855 ($pMYPT1^{T855}$) and the corresponding actin content of each lane at 120 mmHg in control conditions, and in vessels treated with DEA (100 nM) or H1152 (0.3 μM). Figure 5.3B shows the normalized value of $pMYPT1^{T855}$ under each condition. H1152 induced a significant decrease in $pMYPT1^{T855}$ as previously reported (Johnson *et al.*, 2009b), however, DEA did not induce a significant decrease in $pMYPT1^{T855}$. As described in Chapter 1.5.2, H1152 is known to suppress VSM contraction through the inhibition of ROK-dependent Ca^{2+} sensitization. Since DEA induced a similar level of dilation as H1152 did (see Figure 5.11A for summarized data), the lack of a detectable change in $pMYPT1^{T855}$ in response to DEA treatment suggests that control of MYPT1 phosphorylation, and therefore, Ca^{2+} sensitization is not likely to play a significant role in NO-mediated dilation of pressurized RCAs.

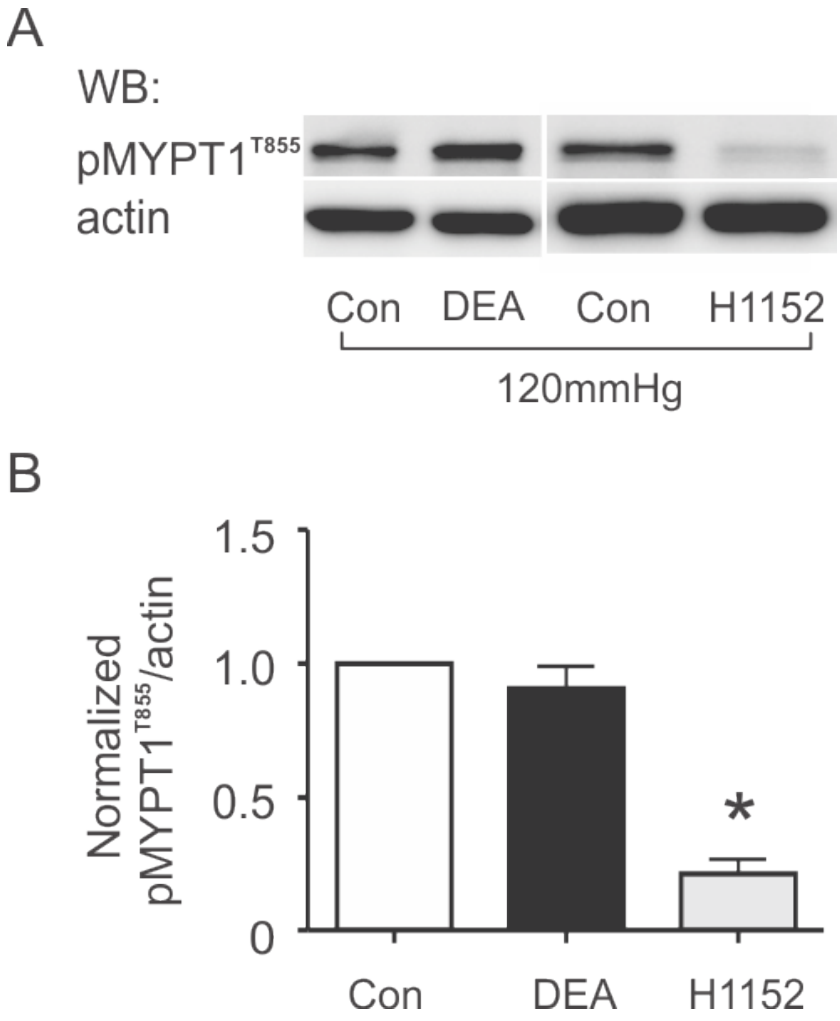

Figure 5.3: Effect of DEANONOate on MYPT1 phosphorylation at Thr855 in pressurized RCAs.

(A) Representative western blots of MYPT1 phosphorylation at Thr855 ($pMYPT1^{T855}$) and the corresponding actin content of each lane at 120 mmHg in control, DEANONOate (DEA, 100 nM) and H1152 (0.3 μM). (B) Mean ± SEM level of $pMYPT1^{T855}$ in control, DEA (n=9) or H1152 (n=3). The level is normalized to the corresponding actin content of each lane with the value in control for each blot set to a value of 1. *Significantly different ($P < 0.05$) from value in control at 120 mmHg.

5.3.4 Effect of 60 mM external K^+ on DEANONOate-induced vasodilation in pressurized RCAs

Since the regulation of VSM contraction through control of E_m and, therefore, $[Ca^{2+}]_i$ is proposed to be another important target of NO signaling (described in 5.1.2.2), the effect of E_m on NO-mediated vasodilation of pressurized RCAs was identified. As shown in Figure 5.4, pressurized RCAs with a stable myogenic constriction at 120 mmHg were treated with 60 mM external K^+-Krebs' solution followed by the cumulative addition of DEA (0.1-10 μM) prior to 0 Ca^{2+} Krebs' solution. Treatment with 60 mM external K^+-Krebs' solution caused a slight constriction, but it had no effect on DEA-induced vasodilation. Since treatment with a high external K^+ concentration is predicted to clamp E_m at a constant value of ~-20 mV and, therefore, evoke Ca^{2+} entry via VGCCs, the lack of effect on DEA-induced vasodilation suggests that NO-mediated vasodilation is not dependent on E_m hyperpolarization or a reduction in Ca^{2+} entry.

5.3.5 LC_{20} phosphorylation in DEANONOate/acetylcholine-induced vasodilation in pressurized RCAs

The level of LC_{20} phosphorylation is tightly controlled by the activity of MLCK and MLCP. The effect of NO on LC_{20} phosphorylation in pressurized RCAs was determined through biochemical analysis. Figure 5.5A shows a representative western blot of LC_{20} obtained using the pan LC_{20} antibody and a Phos-tag SDS-PAGE that permits the separation of phosphorylated LC_{20} protein from unphosphorylated protein. Only mono-phosphorylation of LC_{20} was apparent; this is consistent with previous reports regarding LC_{20} phosphorylation in pressurized RCAs (Johnson *et al.*, 2009b; El-Yazbi *et al.*, 2010). Figure 5.5B shows the mean level of phosphorylated LC_{20} as a percentage of total LC_{20} protein (pLC_{20}) for RCAs at 120 mmHg in control Krebs'

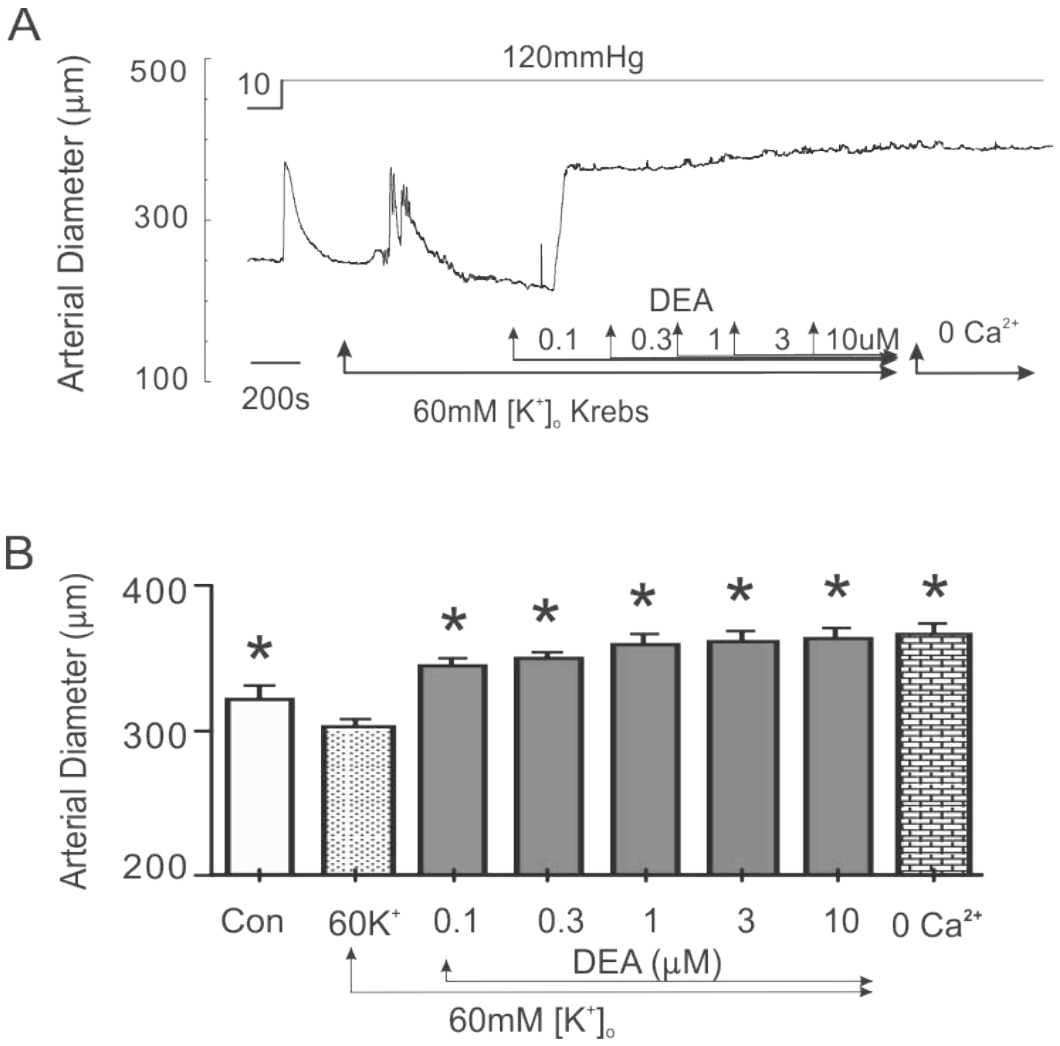

Figure 5.4: Effect of 60 mM external K^+ on DEANONOate-induced dilation of pressurized RCAs.

(A & B) Representative and mean ± SEM arterial diameter recording of pressurized RCAs at 120 mmHg treated with 60 mM external K^+-containing Krebs' solution followed by the addition of 0.1-10 µM DEANONOate (DEA) in a cumulative manner prior to 0 Ca^{2+} Krebs' solution (n=3). * Significantly different ($P < 0.05$) from value in 60 mM external K^+-containing Krebs' solution at 120 mmHg.

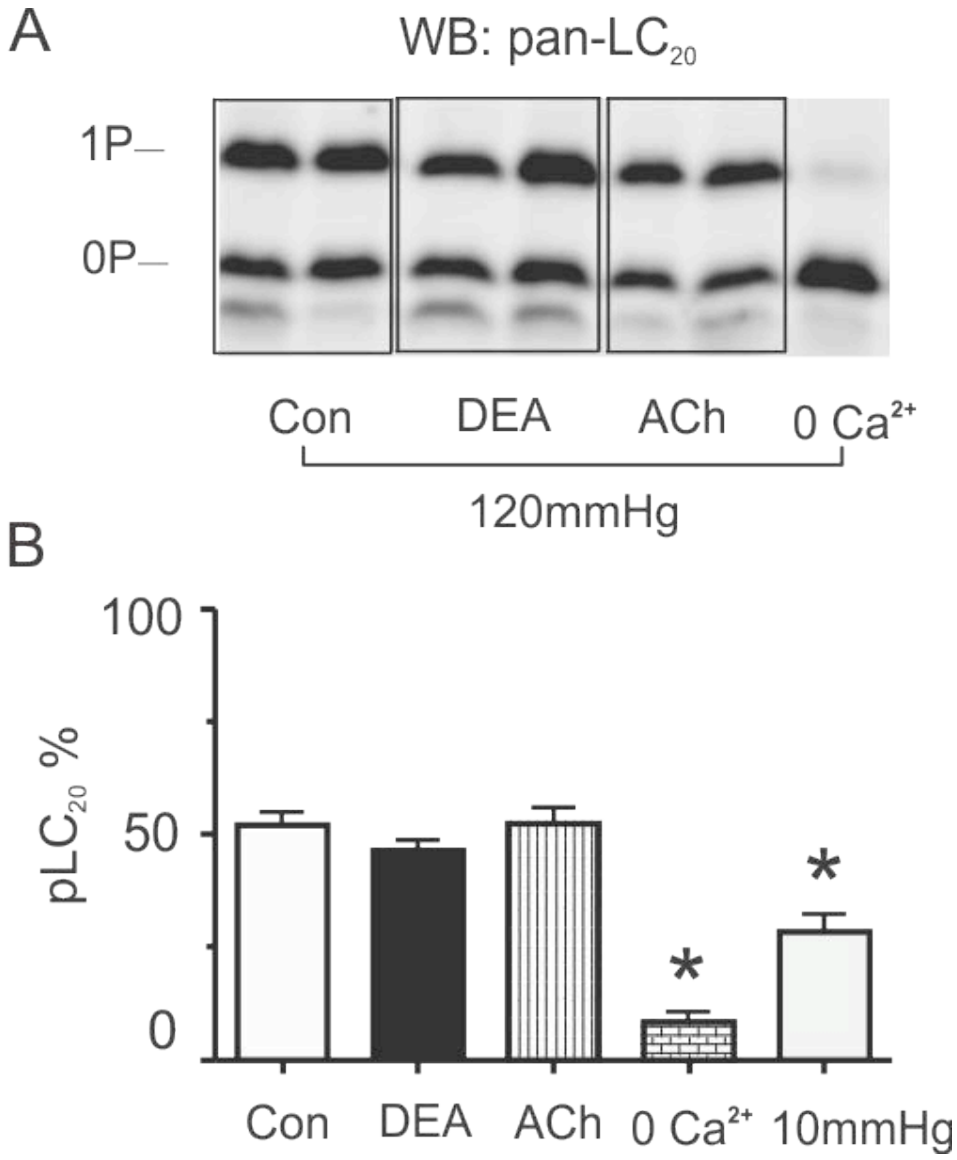

Figure 5.5: Effects of DEANONOate and acetylcholine on LC_{20} phosphorylation in pressurized RCAs.

(A & B) Representative western blot and mean ± SEM level of phosphorylated LC_{20} (pLC_{20}) as a % of total LC_{20} at 120 mmHg in control Krebs' solution (n=15), DEANONOate (DEA, 100 nM, n=25), acetylcholine (ACh, 30 μM, n=7), 0 Ca^{2+} Krebs' solution (n=5) or at 10 mmHg in control Krebs' solution (n=7). *Significantly different ($P < 0.05$) from value in control at 120 mmHg.

solution, treated with DEA (100 nM), ACh (30 μM) and 0 Ca^{2+} Krebs' solution, respectively, as well as at 10 mmHg in control Krebs' solution (vessel segments were collected after achieving a stable state (~5-10 min) following a pressure step from 80 to 10 mmHg). Consistent with previous reports (Johnson *et al.,* 2009b; El-Yazbi *et al.,* 2010), constriction associated with an increase in pressure from 10 to 120 mmHg was coincident with an increase in pLC_{20} from 28.6 ± 3.8% to 53% ± 3.7%. Also, 0 Ca^{2+} Krebs' solution induced a dramatic decrease in pLC_{20} (to 7.9 ± 2.7%) and an associated dilation to the passive diameter. Although the extent of DEA/ACh-induced vasodilation was similar to that of the passive diameter (Figure 5.2F), DEA/ACh-induced vasodilation was not accompanied by a significant decrease in pLC_{20} (47.6 ± 3.3% and 52% ± 3.4% in DEA and ACh, respectably), indicating that NO-mediated vasodilation in pressurized RCAs is not dependent on a detectable reduction in LC_{20} phosphorylation.

This observation of no alteration in phospho-LC_{20} content is consistent with the data of Figures 5.3 & 5.4 showing that NO-mediated dilation of pressurized RCAs was not dependent on a change in E_m or MYPT1 phosphorylation. Considering the huge dilatory effect of DEA and ACh on myogenic constriction (Figure 5.2), these findings suggest that LC_{20} phosphorylation-dependent mechanisms do not play a significant role in NO-mediated dilation of pressurized RCAs. This is an unexpected finding based on the current literature suggesting that mechanisms of NO-mediated VSM relaxation involve modulation of Ca^{2+} or K^+ channels, alterations in Ca^{2+} handling, or regulation of RhoA or MYPT1, all of which result in a decrease in LC_{20} phosphorylation (Hofmann *et al.,* 2000; Lincoln *et al.,* 2001; Morgado *et al.,* 2012).

5.3.6 Actin polymerization in DEANONOate/acetylcholine-induced dilation of pressurized RCAs

It is significant to note that DEA/ACh-induced dilation is similar to latrunculin B (LatB, 10 μM)-induced dilation of pressurized RCAs, which is characterized by a maximal dilation with a lack of detectable change in pLC_{20} (Figure 5.6). As described in Chapter 1.5.3, LatB is known to impair myogenic constriction through the inhibition of actin polymerization. Therefore, we determined whether the extent of actin polymerization was altered in NO-mediated vasodilation of pressurized RCAs.

The extent of actin polymerization was assessed by G-actin assay as described in Chapter 2.11. The content of G-actin was normalized to the corresponding SM22 content of each lane, and expressed as a fraction of the value detected at 120 mmHg in control Krebs' solution. SM22 is a 22 kDa smooth muscle protein that is exclusively retained in the supernatant along with G-actin during high-speed centrifugation (Luykenaar *et al.*, 2009; Walsh *et al.,* 2011). This is also evident in Figure 5.7A showing that SM22 was only present in the supernatant and not in the pellet as assayed by western blotting.

Figure 5.7B & C shows representative blots of G-actin and corresponding SM22 content of each lane, as well as the normalized level of G-actin content. Notably, DEA and ACh induced a significant increase in G-actin content of pressurized RCAs that was blocked by ODQ inhibition of sGC activity. Given that NO-mediated vasodilation was found to be accompanied by a minimal change in LC_{20} and MYPT1 phosphorylation, this novel observation that NO-mediated vasodilation was associated with a significant decrease in actin polymerization suggests that the cytoskeleton reorganization-dependent

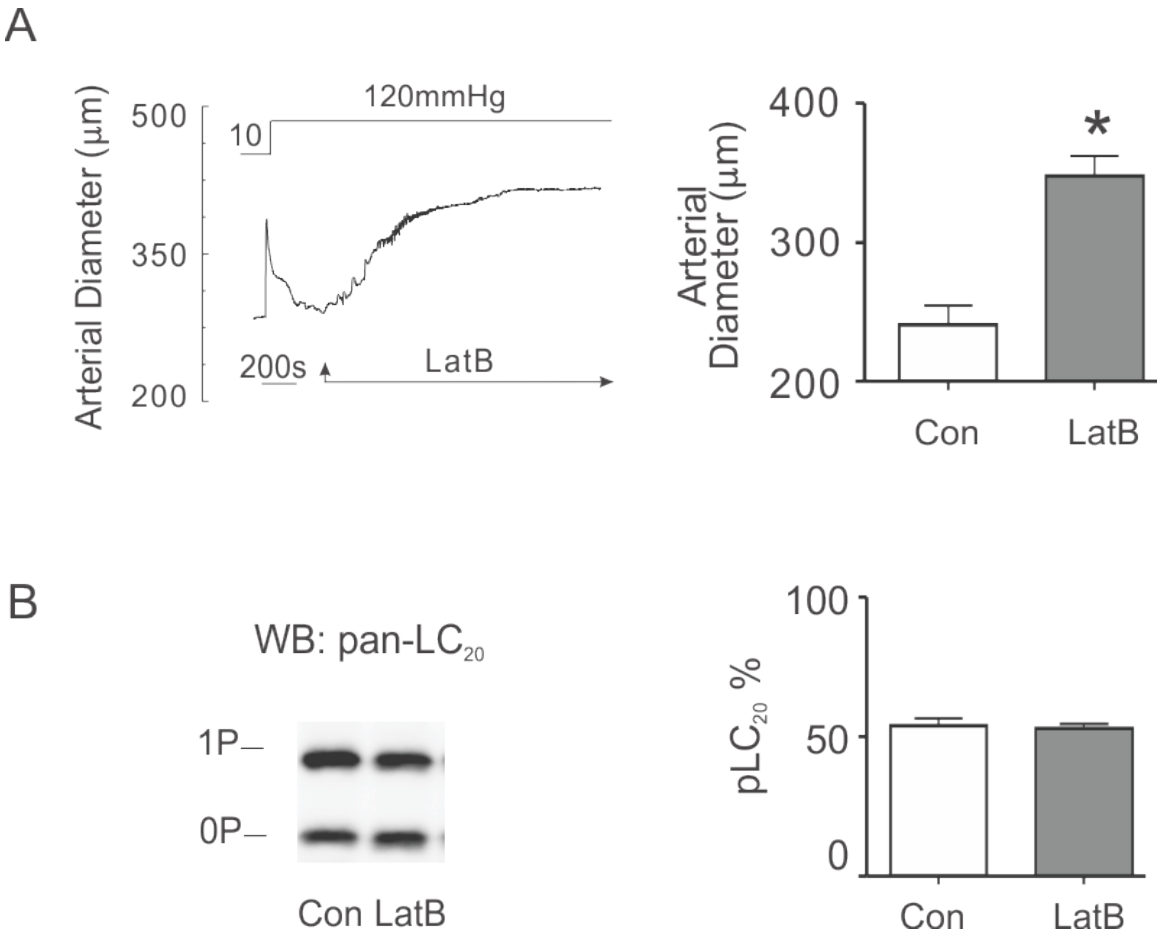

Figure 5.6: Effect of latrunculin B on LC_{20} phosphorylation in pressurized RCAs.
(A) Representative and mean ± SEM arterial diameter recording of RCAs at 120 mmHg in the absence (Con) and presence of latrunculin B (LatB, 10 µM) prior to vessel collection for biochemical analysis. (B) Representative western blot and mean ± SEM level of phosphorylated LC_{20} (pLC_{20}) as a % of total LC_{20} at 120 mmHg in the absence and presence of LatB (n=3). *Significantly different ($P < 0.05$) from value in control at 120 mmHg.

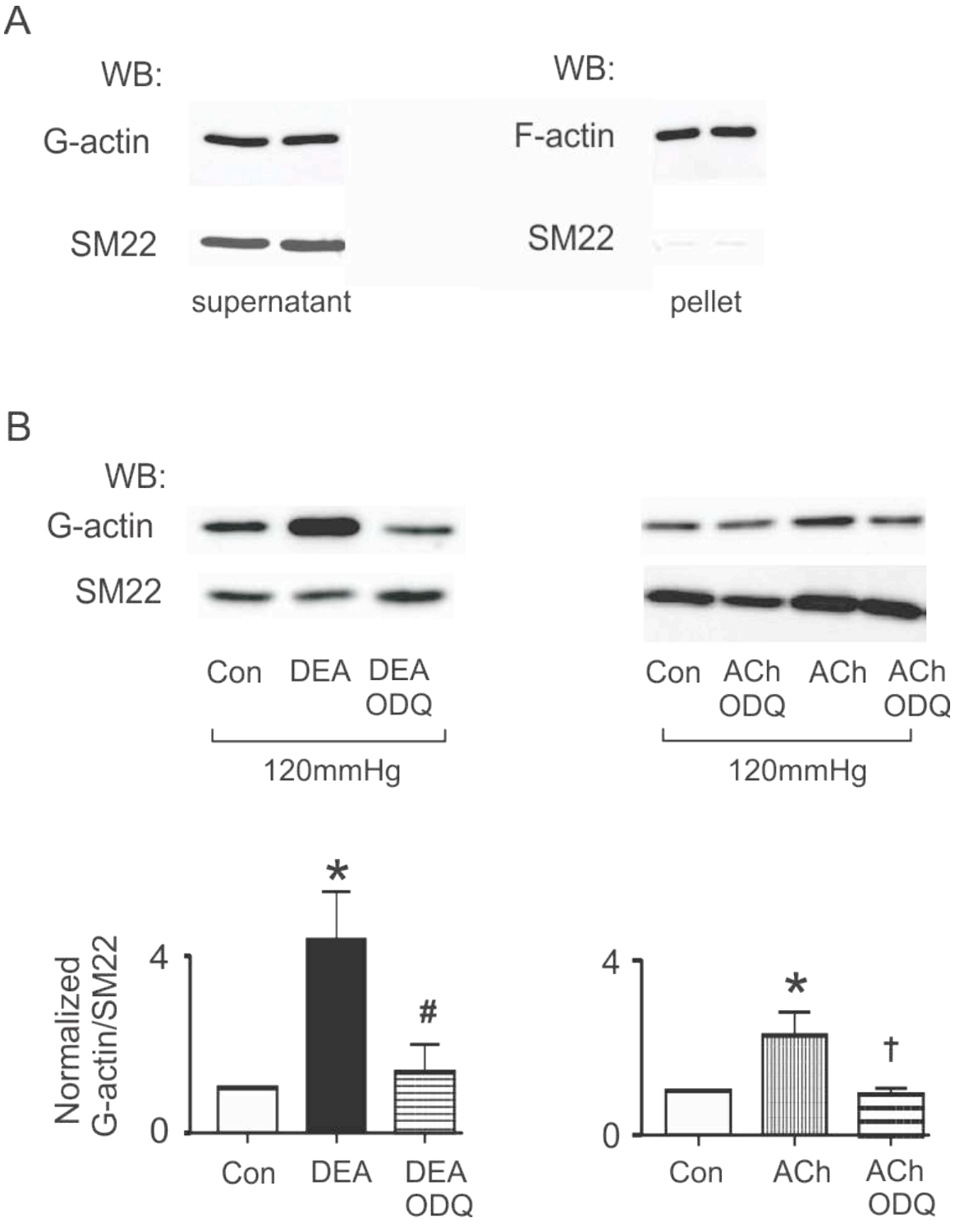
A
WB:
G-actin
SM22
supernatant
WB:
F-actin
SM22
pellet
B
WB:
G-actin
SM22
Con
DEA
DEA ODQ
120mmHg
Con
ACh ODQ
ACh
ACh ODQ
120mmHg
Normalized G-actin/SM22
4
0
*
#
Con
DEA
DEA ODQ
4
0
*
†
Con
ACh
ACh ODQ

Figure 5.7: Effects of DEANONOate and acetylcholine ± ODQ on G-actin content in pressurized RCAs.

(A) Representative blots of G-actin and SM22 using supernatants and corresponding pellets obtained from two vessel segments at 10 mmHg in control Krebs' solution following the separation by high-speed centrifugation. Note that SM22 was only present in the supernatant, but not in the pellet. (B) Representative western blots of G-actin and the corresponding SM22 of each lane at 120 mmHg in control, DEANONOate (DEA, 100 nM), DEA + 1H-[1,2,4]oxadiazolo[4,3-a]quinoxalin-1-one (ODQ, 30 μM), acetylcholine (ACh, 30 μM) andACh + ODQ. (C) Mean ± SEM level of G-actin content in DEA ± ODQ (n=6, each) or ACh ± ODQ (n=5, each). The level is normalized to the corresponding SM22 content of each lane with the value in control for each blot set to a value of 1. * , # and ǂ indicate significantly different ($P < 0.05$) from the value at 120 mmHg in control, DEA, and ACh, respectively.

mechanism may make a major contribution to NO-mediated dilation of pressurized RCAs.

5.3.7 VASP phosphorylation in DEANONOate/acetylcholine-induced dilation of pressurized RCAs

As described in 5.1, VASP is a well-known substrate of NO/sGC/cGMP/PKG signaling, and phosphorylation of VASP has an inhibitory effect on VASP-mediated actin dynamics. Therefore, we determined whether the regulation of VASP phosphorylation was involved in the inhibition of actin polymerization that was associated with NO-mediated dilation of pressurized RCAs.

The extent of VASP phosphorylation was determined through biochemical analysis. As shown in Figure 5.8A (left panel), a pan-VASP antibody recognized two bands, as previously reported (Halbrugge & Walter, 1989; Reinhard *et al.,* 1992; Smolenski *et al.,* 1998). The upper band represents VASP protein phosphorylated at Ser157, whereas the lower band represents VASP protein not phosphorylated at Ser157. Therefore, VASP phosphorylation at Ser157 can be expressed as the level of phosphorylated VASP at Ser157 (pVASP-Ser157) as a percentage of total VASP protein (Figure 5.8B). The representative blots and summarized data of Figure 5.8 clearly show that DEA/ACh-mediated dilation of pressurized RCAs is associated with an increase in VASP phosphorylation at Ser157 that is blocked by ODQ inhibition of sGC activity.

Sometimes, the same sample was loaded three times on the same gel and incubated with the pan-VASP antibody, VASP-Ser157 phospho-specific antibody or VASP-Ser239 phospho-specific antibody. As shown in Figure 5.8A (middle panel), the Ser157 phospho-specific antibody only recognized one band with a similar molecular

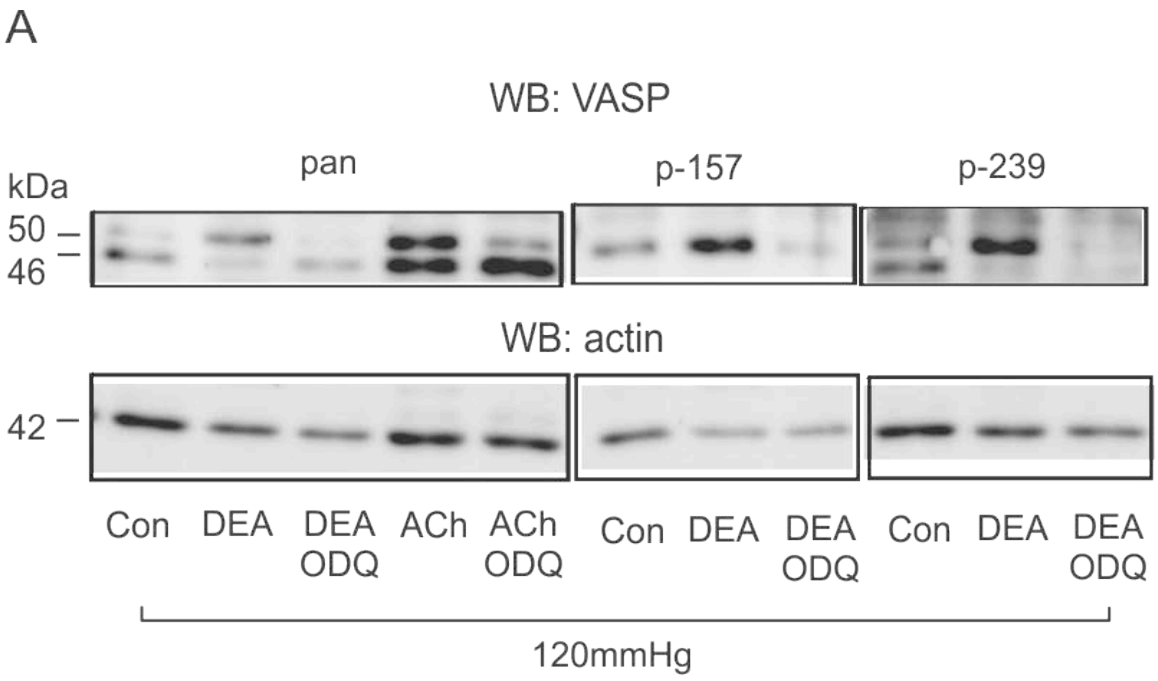
A
WB: VASP
pan
p-157
p-239
kDa
50
46
WB: actin
42
Con
DEA
DEA ODQ
ACh
ACh ODQ
Con
DEA
DEA ODQ
Con
DEA
DEA ODQ
120mmHg

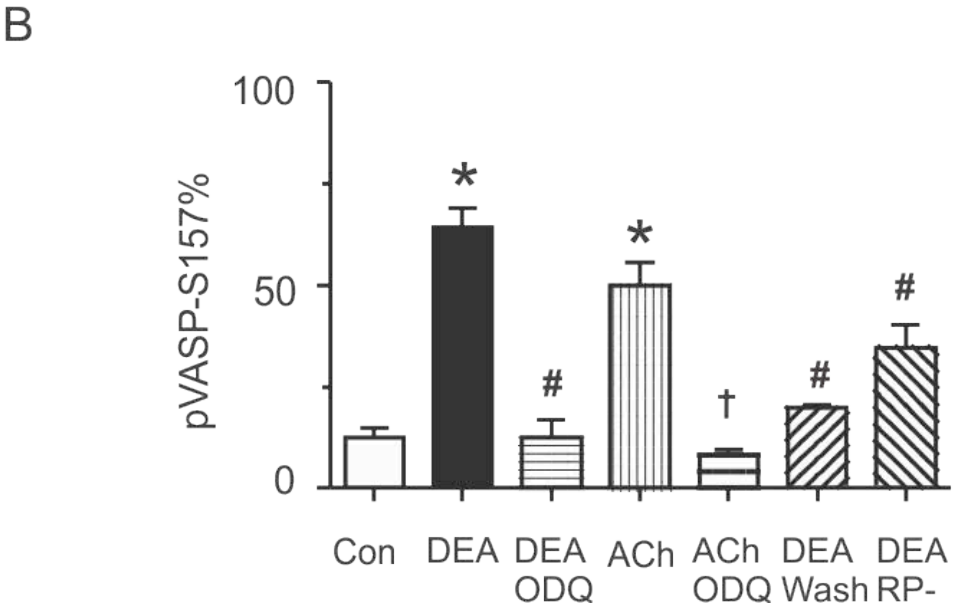
B
100
50
0
pVASP-S157%
*
*
#
†
#
#
Con
DEA
DEA ODQ
ACh
ACh ODQ
DEA Wash
DEA RP-

Figure 5.8: Effects of DEANONOate and acetylcholine ± ODQ on VASP phosphorylation at Ser157 in pressurized RCAs.

(A) Representative western blots of phosphorylated/unphosphorylated VASP protein at Ser157 using the pan-VASP antibody (pan), as well as phosphorylated VASP protein at Ser157 (p-157) and Ser239 (p-239), respectively, using phospho-specific antibodies, and corresponding actin level in each lane at 120 mmHg in control Krebs' solution, DEANONOate (DEA, 100-300 nM), DEA + 1H-[1,2,4] oxadiazolo[4,3-a]quinoxalin-1-one (ODQ, 30 µM), acetylcholine (ACh, 30 µM) or ACh + ODQ. Note the pan-VASP antibody detected two bands: the upper band represents VASP protein phosphorylated at Ser157, the lower band represents VASP protein not phosphorylated at Ser157. (B) Mean ± SEM level of phosphorylated VASP at Ser157 (pVASP-Ser157) as a % of total VASP at 120 mmHg in control (n=7), DEA (n=14), DEA +ODQ (n=5), ACh ± ODQ (n=4, each), DEA followed by washout with normal Krebs' solution (n=3), or DEA+RP-8-bromo-PET-cGMP (RP-cGMP, 30µM) (n=3). * , # and ǂ indicate significantly different ($P < 0.05$) from value at 120 mmHg in control, DEA, and ACh, respectively.

mass as the upper band that was recognized by a pan-VASP antibody (~50 kDa). The mean level of pVASP-Ser157 obtained using the Ser157 phospho-specific antibody was normalized to the corresponding actin content of each lane and expressed as a fraction of the value at 120 mmHg in control conditions. DEA induced an increase in pVASP-Ser157 from 1 to 5.5 ± 0.8 (n=3), whereas ODQ decreased the value to 0.52 ± 0.14 (n=3). The findings are consistent with the mean level of pVASP-Ser157 obtained using a pan-VASP antibody. DEA induced an increase in pVASP-Ser157 from 12.8% ± 3.3% to 70.5% ± 6.1% whereas the addition of ODQ decreased the value to 12.7% ± 4% (Figure 5.8B). As shown in Figure 5.8A (right panel), the VASP-Ser239 phospho-specific antibody recognized two bands. The upper band is due to dual phosphorylation at Ser239, as well as phosphorylation at Ser157 that is responsible for the apparent shift in molecular mass; i.e. the upper band is pVASP-Ser157. The mean level of phosphorylated VASP at Ser239 (pVASP-Ser239) obtained using the Ser239 phospho-specific antibody was normalized to actin content and expressed as a fraction of the control value at 120 mmHg. Similar to phosphorylation at Ser157, DEA induced an increase in pVASP-Ser239 from 1 to 4.6 ± 0.9 (n=3), whereas ODQ decreased the value to 0.36 ± 0.07 (n=3).

Figure 5.9 shows that DEA-induced dilation can be reversed by washout with normal Krebs' solution, or upon treatment with Rp-8-bromo-PET-cGMP (Rp-cGMP, 30 μM) that inhibits PKG. The recovery of myogenic constriction in these conditions was associated with a decrease in pVASP-Ser157. The findings of the washout experiments support the view that regulation of VASP phosphorylation is a dynamic process. The findings of Rp-cGMP experiments confirm the participation of PKG in NO-mediated VASP regulation and dilation of pressurized RCAs.

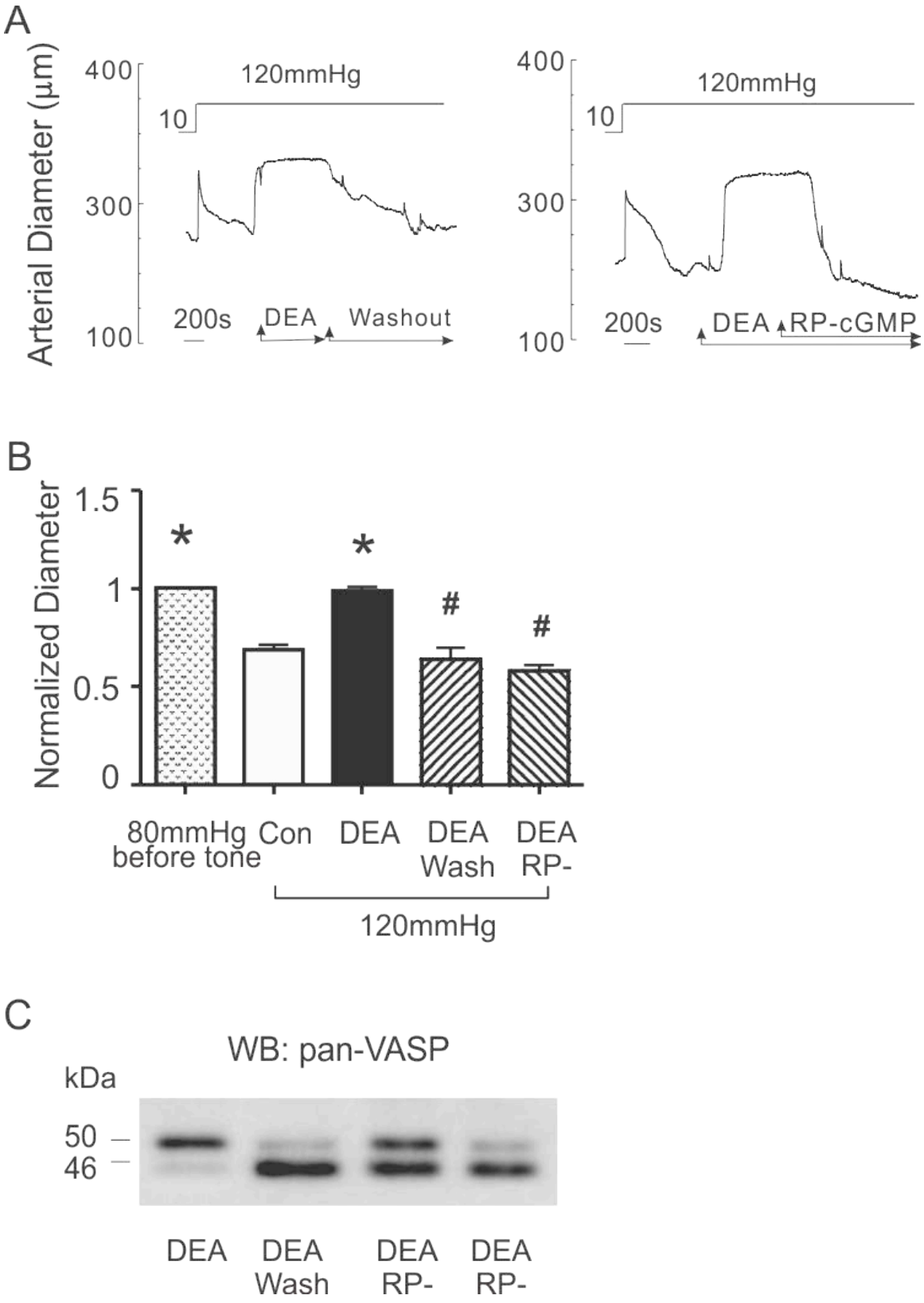
A
Arterial Diameter (μm)
400
300
100
120mmHg
10
200s
DEA
Washout
RP-cGMP
B
Normalized Diameter
1.5
1
0.5
0
*
#
80mmHg before tone
Con
DEA
DEA Wash
DEA RP-
120mmHg
C
WB: pan-VASP
kDa
50
46
DEA
DEA Wash
DEA RP-
DEA RP-

Figure 5.9: Effect of DEANONOate can be reversed by washout or PKG inhibition in pressurized RCAs.

(A, B) Representative and mean ± SEM diameter recordings of RCAs at 120 mmHg in control Krebs' solution or treated with DEANONOate (DEA, 100 nM) followed by washout with normal Krebs' solution or followed by RP-8-bromo-PET-cGMP (RP-cGMP, 30μM) inhibition of PKG (n=3, each). Diameter is expressed as a % of the value of the same vessel at 80 mmHg before the initial tone development. (C) Representative western blot of phosphorylated/unphosphorylated VASP protein at Ser157 using the pan-VASP antibody for RCAs at 120 mmHg, and treated with DEA followed by washout with normal Krebs' solution, or by RP-cGMP inhibition of PKG (n=3, each). Mean ± SEM level of phosphorylated VASP at Ser157 as a % of total VASP is shown in Figure 5.8B. *Significantly different ($P < 0.05$) from value in control at 120 mmHg.

Taken together, Figures 5.7-5.9 indicate that VASP phosphorylation may contribute to NO-mediated dilation of pressurized RCAs through the regulation of cytoskeleton reorganization.

5.3.8 VASP and LC_{20} phosphorylation in isoprenaline-induced dilation of pressurized RCAs

In addition to PKG, PKA is also able to induce VASP phosphorylation and vasodilation. Isoprenaline (ISO) is widely used as a β -adrenoreceptor agonist that activates PKA in VSM. Figure 5.10 A & B shows that ISO (10 μM) induced a maximal dilation of pressurized RCAs at 120 mmHg, and was reversed by the PKA inhibitor, Rp-cAMP (50 μM). The extent of VASP phosphorylation at Ser157 and LC_{20} phosphorylation in ISO-induced dilation of pressurized RCAs was determined though biochemical analysis. Figure 5.10 C & D shows that ISO-induced dilation of pressurized RCAs was associated with an increase in phosphorylated VASP at Ser157, yet with a lack of detectable change in phosphorylated LC_{20}. This finding is similar to NO-mediated vasodilation, suggesting that VASP phosphorylation in response to PKA activation may contribute to ISO-induced dilation of pressurized RCAs through the regulation of cytoskeleton reorganization.

5.3.9 VASP phosphorylation in the dilation of pressurized RCAs evoked by ROK/PKC inhibition, latrunculin B, 14 mM external K^+ or 0 Ca^{2+} Krebs' solution

The extent of VASP phosphorylation at Ser157 in response to a variety of vasodilators was examined. As shown in Figure 5.11, H1152 (0.3 μM) inhibition of ROK, GF 109203X (GF, 3 μM) inhibition of PKC, LatB (10 μM) attenuation of actin polymerization, 14 mM external K^+-induced E_m hyperpolarization, and 0 Ca^{2+} Krebs' solution all induced a maximal dilation of pressurized RCAs at 120 mmHg, yet they did

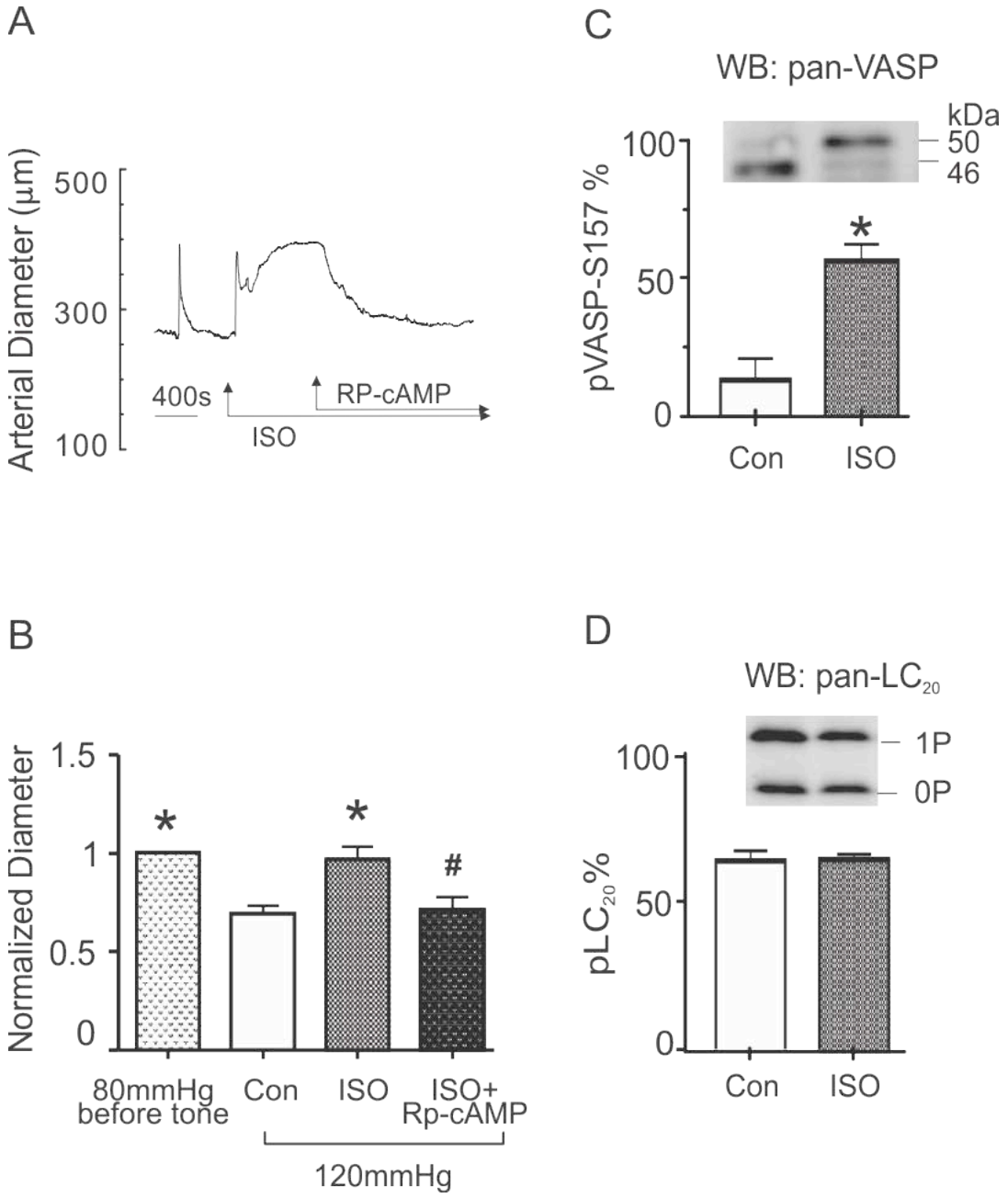

Figure 5.10: Effect of isoprenaline on VASP phosphorylation at Ser157 and LC_{20} phosphorylation in pressurized RCAs.

(A & B) Representative and mean ± SEM diameter recording of RCAs at 120 mmHg in control Krebs' solution, isoprenaline (ISO, 10 µM, n=11) and ISO + RP-cAMP (30 µM, n=5). Diameter is expressed as a % of the value of the same vessel at 80 mmHg before

initial tone development. (C) Representative western blot of phosphorylated/unphosphorylated VASP protein at Ser157 using the pan-VASP antibody, and mean ± SEM level of phosphorylated VASP at Ser157 (pVASP-Ser157) as a % of total VASP at 120 mmHg in control and ISO (n=5, each). (D) Representative western blot and mean ± SEM level of phosphorylated LC_{20} (pLC_{20}) as a % of total LC_{20} at 120 mmHg in control (n=4) and ISO (n=6). * Significantly different ($P < 0.05$) from value in control at 120 mmHg.

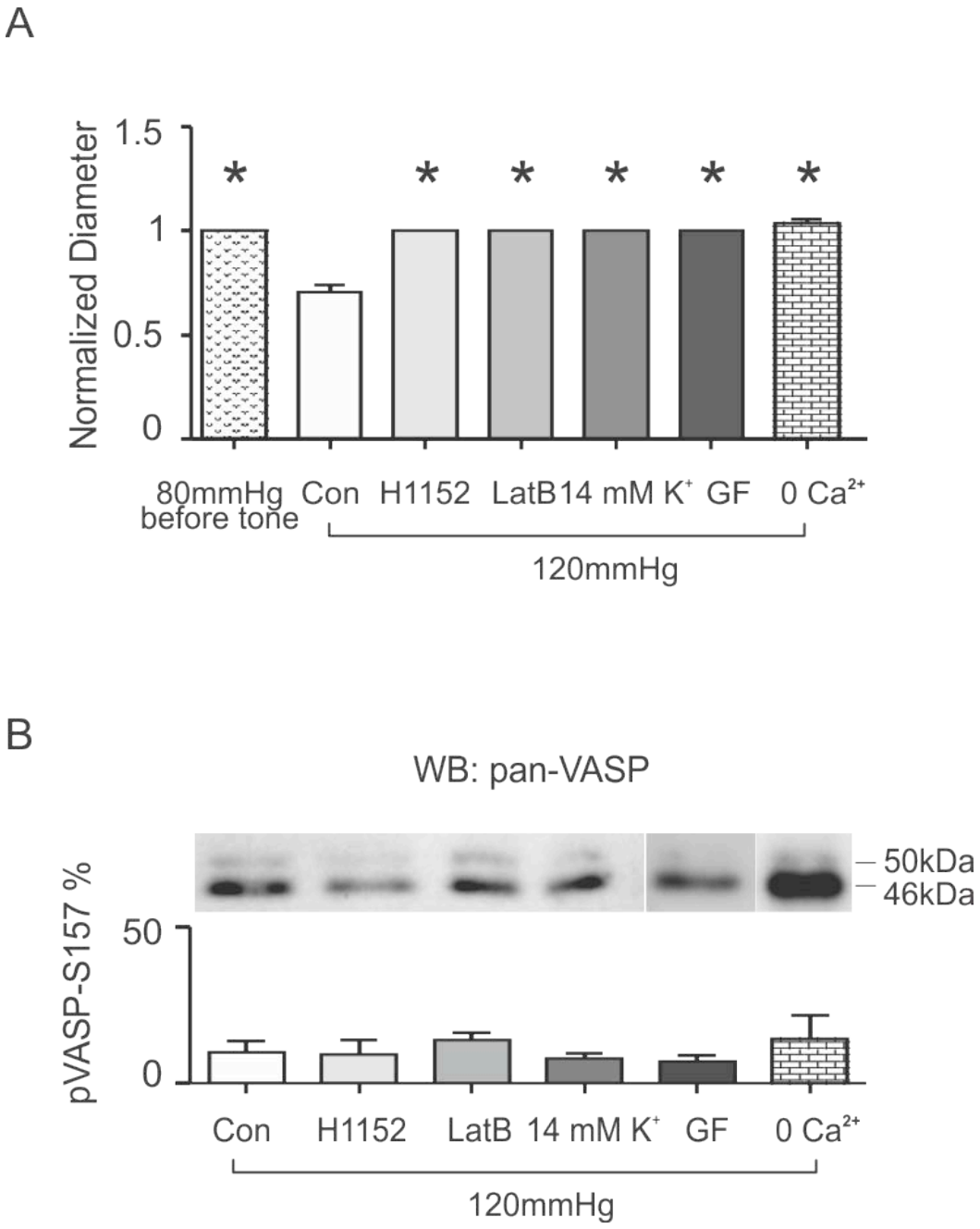

Figure 5.11: VASP phosphorylation at Ser157 in the dilation of pressurized RCAs evoked by ROK/PKC inhibition, latrunculin B, 14 mM external K^+, or 0 Ca^{2+} Krebs' solution.

(A) Mean ± SEM diameter recording of RCAs at 120 mmHg in control Krebs' solution or treated with H1152 (0.3 μM) inhibition of ROK, latrunculin B (LatB, 10 μM)

attenuation of actin polymerization, GF 109203X (GF, 3 μM) inhibition of PKC, 14 mM external K^+-containing Krebs' solution inducing E_m hyperpolarization or 0 Ca^{2+} Krebs' solution (n=3, each). Diameter is expressed as a % of the value of the same vessel at 80 mmHg before the initial tone development. (B) Representative western blot of phosphorylated/unphosphorylated VASP protein at Ser157 using the pan-VASP antibody, and mean ± SEM level of phosphorylated VASP at Ser157 (pVASP-Ser157) as a % of total VASP at 120 mmHg in control, H1152, LatB, GF, 14 mM external K^+ or Ca^{2+} -free treatment described in panel A. * Significantly different ($P < 0.05$) from value in control at 120 mmHg.

not alter the level of pVASP-Ser157. This suggests that VASP phosphorylation is a specific event that is only associated with dilation of pressurized RCAs induced by the activation of PKA/ PKG signaling.

5.3.10 VASP phosphorylation in the pressure-dependent myogenic response of RCAs

As described in Chapter 1.5.3, a cytoskeleton reorganization-dependent mechanism is believed to contribute to the pressure-dependent myogenic response. This view is supported by recent findings that pressure elevation evoked a concomitant decrease in G-actin content and an increase in active myogenic constriction (Moreno-Dominguez *et al.*, 2013; Cole lab, unpublished data). Considering the important role of VASP in actin dynamics, we therefore sought to determine whether the pressure-dependent alteration in actin polymerization in association with an increase in active myogenic constriction involved the regulation of VASP phosphorylation.

Figure 5.12A shows the experimental protocol and representative diameter recordings of RCAs pressurized to 10, 30, 50, 80 or 120 mmHg prior to vessel collection for biochemical analysis. Figure 5.12B shows mean arterial diameters of RCAs subjected to a series of step-wise increases in intraluminal pressure in control Krebs' solution and Ca^{2+}-free Krebs' solution. Note the concomitant increase in active myogenic constriction in response to an increase in intraluminal pressure. Figure 5.12C shows representative western blots and the mean level of normalized G-actin content at 10 and 120 mmHg, which is consistent with the previous findings of pressure-dependent alterations in actin polymerization (Moreno-Dominguez *et al.*, 2013; Cole lab, unpublished data). Figure 5.12D shows a representative western blot and the mean level of pVASP-Ser157 obtained using a pan-VASP antibody. Notably, a concomitant decrease

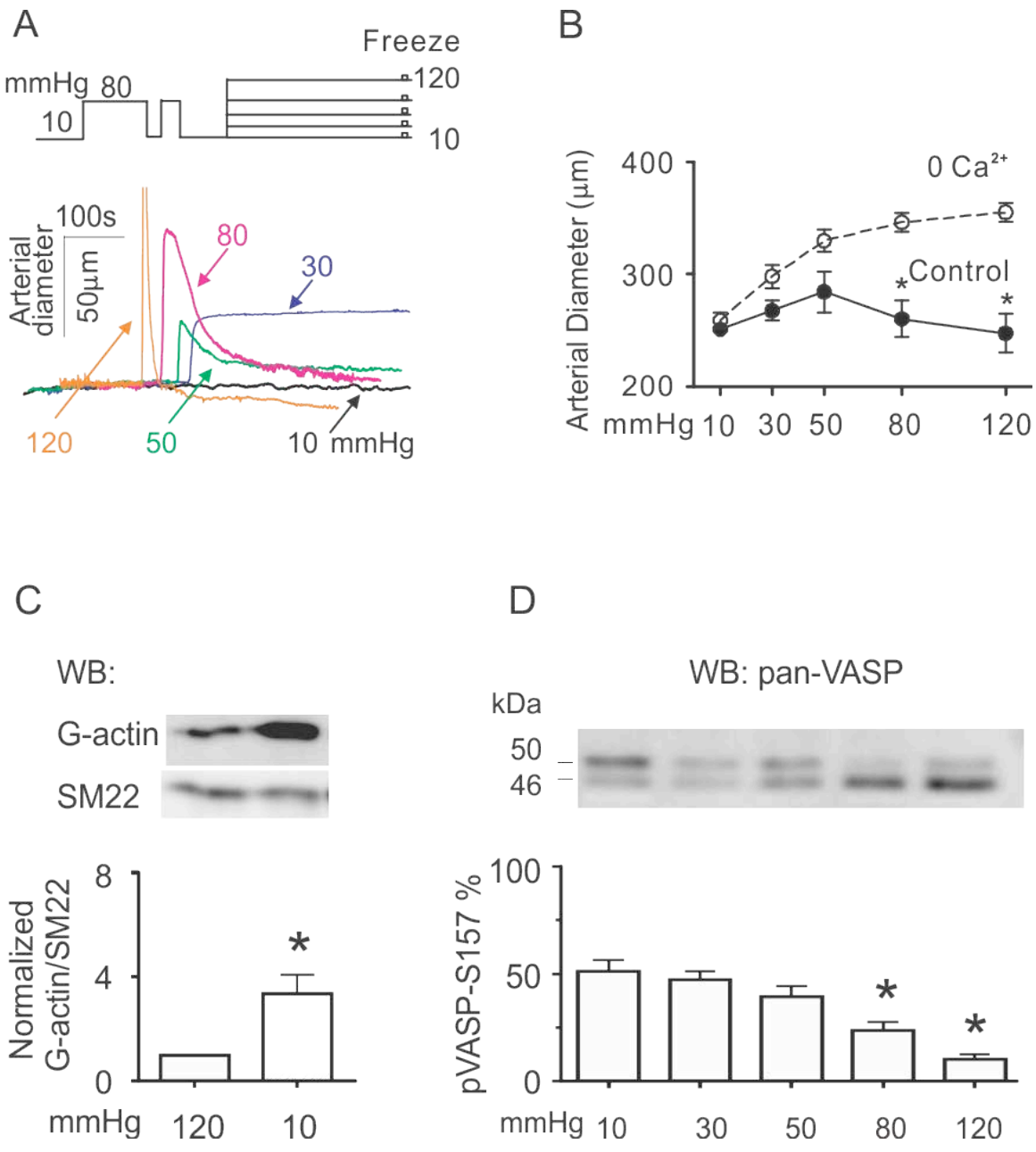

Figure 5.12: VASP phosphorylation at Ser157 in myogenic regulation of cerebral arterial diameter.

(A) Pressure protocol and representative diameter recordings of RCAs at an intraluminal pressure of 10, 30, 50, 80 or 120 mmHg prior to vessel collection for biochemical analysis. (B) Mean ± SEM arterial diameters of RCAs subjected to a series of step-wise

elevations in intraluminal pressure in control Krebs' solution and 0 Ca^{2+} Krebs' solution (n=4). *Significantly different ($P < 0.05$) from value in control Krebs' solution at each intraluminal pressure. (C) Representative western blots and mean ± SEM level of G-actin normalized to SM22 at 10 mmHg with the value at 120 mmHg in control Krebs' solution for each blot set to a value of 1 (n=4). *Significantly different ($P < 0.05$) from value at 120 mmHg. (D) Representative western blot of phosphorylated/unphosphorylated VASP protein at Ser157 using the pan-VASP antibody, and mean ± SEM level of phosphorylated VASP at Ser157 (pVASP-Ser157) as a % of total VASP at varied intraluminal pressures in control Krebs' solution (n=5-9). * and # indicate significantly different ($P < 0.05$) from value in control solution at 120 mmHg and 10 mmHg, respectively.

in VASP phosphorylation at Ser157 was associated with an increase in active myogenic constriction in response to the pressure elevation. We also determined VASP phosphorylation at Ser239 by biochemical analysis as described in 5.3.7, and found that the value of pVASP-Ser239 was decreased from 5.45 ± 1.1 at 10 mmHg to 1 at 120 mmHg (n=3). Taken together, these observations indicate that pressure elevation evokes a concomitant decrease in VASP phosphorylation and G-actin content associated with myogenic constriction.

Figure 5.13A & B shows that ODQ (30 μM) induced a significant vasoconstriction at 10 mmHg. Figure 5.13C & D show that ODQ-induced vasoconstriction at 10 mmHg was associated with a decrease in VASP phosphorylation at Ser157. Given that ODQ is a selective inhibitor of sGC, this effect of ODQ at 10 mmHg implies the presence of basal activity of sGC at low pressure, which may explain why VASP phosphorylation maintains a high level at low pressure (Figure 5.12D).

5.3.11 LC_{20} and VASP phosphorylation and G-actin content before and after the initial development of myogenic constriction of RCAs

When RCAs were mounted on the arterial pressure myograph, they always required a period of equilibration (~15-35 min) in the presence of intraluminal pressure prior to the development of myogenic constriction. Although this initial development of myogenic tone is not representative of a physiological response *in vivo*, it provides an experimental condition to compare the levels of activation of the various mechanisms mediated by LC_{20}, MYPT1, VASP phosphorylation and actin polymerization, before and after the development of myogenic tone.

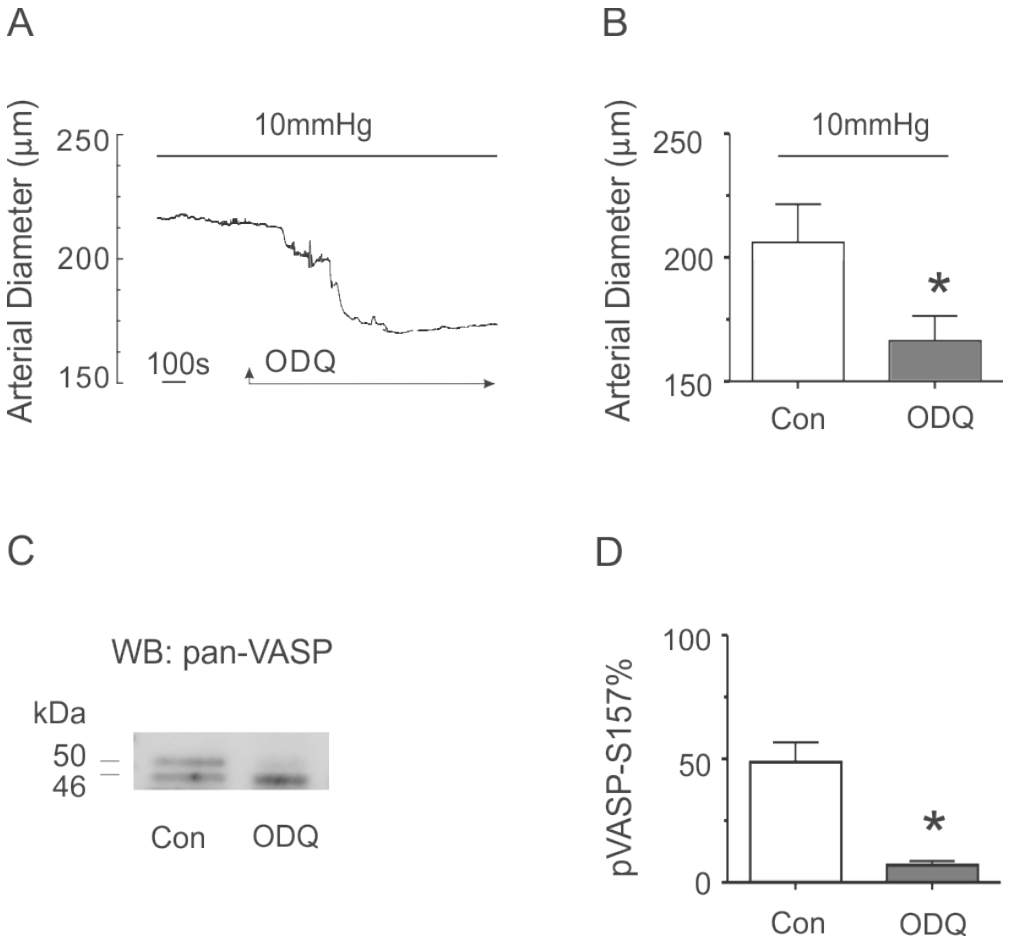

Figure 5.13: Inhibition of sGC at 10 mmHg results in vasoconstriction and a decrease in VASP phosphorylation at Ser157.

(A & B) representative and mean ± SEM arterial diameter recording of RCAs at 10 mmHg in the absence and presence of 1H-[1,2,4] oxadiazolo[4,3-a]quinoxalin-1-one (ODQ, 30 µM, n=5). (C & D) Representative western blot of phosphorylated/unphosphorylated VASP protein at Ser157 using the pan-VASP antibody, and mean ± SEM level of phosphorylated VASP at Ser157 (pVASP-Ser157) as a % of total VASP at 10 mmHg in the absence (Con) and presence of ODQ (n=3). *Significantly different ($P < 0.05$) from value at 10 mmHg in control Krebs' solution.

Figure 5.14A & B shows the experimental protocol, representative and mean values of diameter for RCAs pressurized to 120 mmHg before and after the initial myogenic tone development. Segments for the 'before tone group' were collected ~8 min after pressurization to 120 mmHg (note: these vessel did not exhibit myogenic tone), whereas segments for the 'after tone group' were collected at ~5-10 min after the development of stable myogenic constriction at 120 mmHg. Figure 5.14C & D shows a representative western blot of VASP proteins obtained using a pan-VASP antibody, as well as Ser157/Ser239 phospho-specific antibodies, and the mean level of pVASP-Ser157 as a % of total VASP. Figure 5.14E & F shows representative western blots and the mean level of G-actin normalized to SM22 as a fraction of the value of each blot at 120 mmHg before tone development. Figure 5.14G & H shows a representative western blot and the mean level of pLC_{20} as a % of total LC_{20}. The data suggests that the initial tone development of RCAs was associated with a significant decrease in VASP phosphorylation and G-actin content, but no detectable change in LC_{20} phosphorylation. Since the level of LC_{20} phosphorylation is ~22-30% at 10 mmHg (Figure 5.5D; Johnson *et al.,* 2009b; El-Yazbi *et al.,* 2010), it appears that an increase in LC_{20} phosphorylation occurred prior to initial myogenic tone development and, therefore, an increase in LC_{20} phosphorylation alone was not sufficient for constriction. Therefore, in this experimental condition, it is very likely that a decrease in VASP phosphorylation followed by an increase in actin polymerization was the indispensible step during the initial development of myogenic tone. The finding is consistent with Figure 5.12, providing further credence to the conclusion that VASP phosphorylation participates in the myogenic response of RCAs through the regulation of cytoskeleton reorganization.

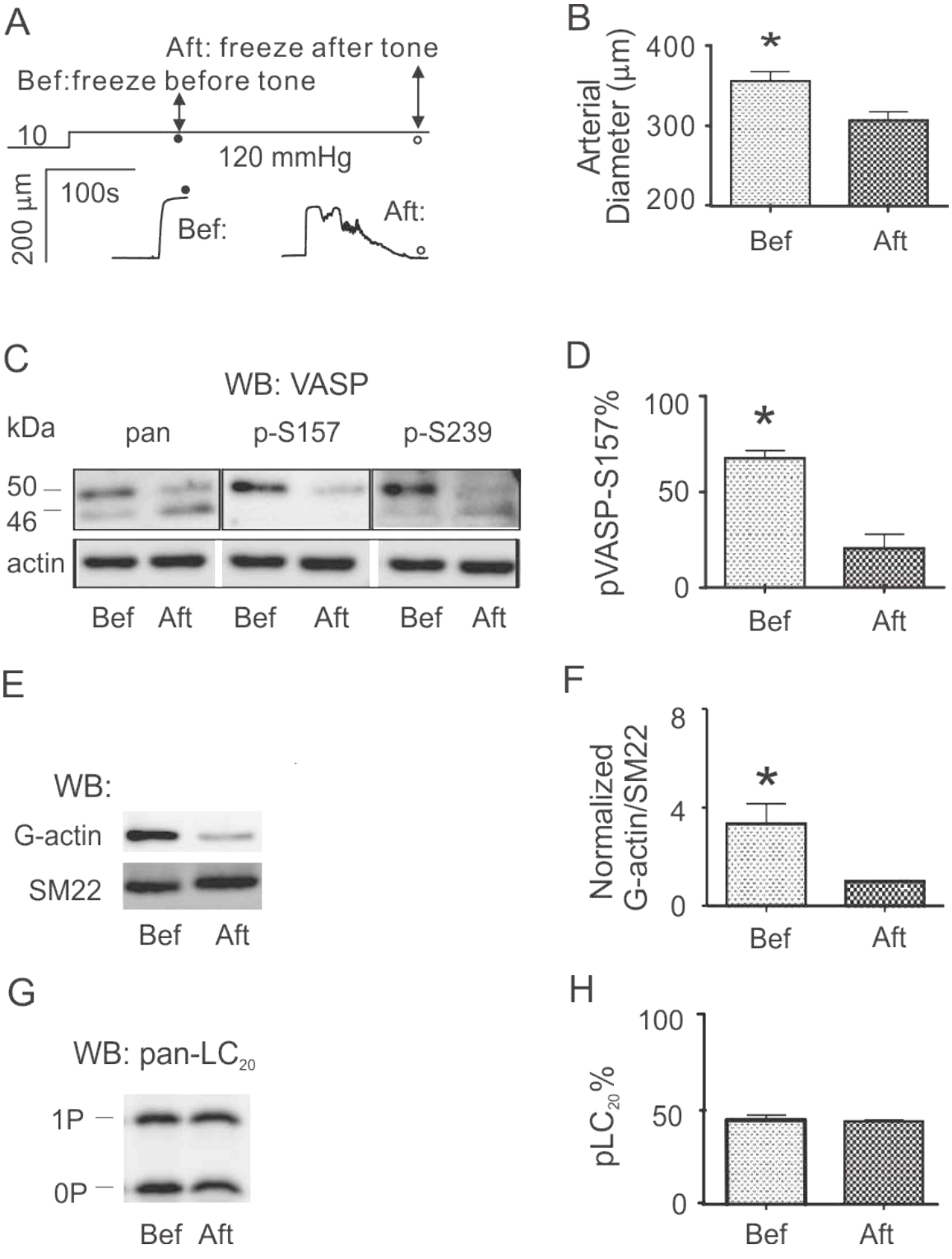
A
Aft: freeze after tone
Bef:freeze before tone
10
120 mmHg
100s
200 µm
Bef:
Aft:
B
Arterial Diameter (µm)
400
300
200
*
Bef
Aft
C
WB: VASP
kDa
pan
p-S157
p-S239
50
46
actin
Bef Aft Bef Aft Bef Aft
D
pVASP-S157%
100
50
0
*
Bef
Aft
E
WB:
G-actin
SM22
Bef Aft
F
Normalized G-actin/SM22
8
4
0
*
Bef
Aft
G
WB: pan-LC20
1P
0P
Bef Aft
H
pLC20 %
100
50
0
Bef
Aft

Figure 5.14: LC_{20} and VASP phosphorylation, as well as G-actin content before and after the initial development of myogenic tone.

(A & B) Experimental protocol, representative and mean ± SEM arterial diameter recording of RCAs subjected to a pressure step from 10 mmHg to 120 mmHg before (n=15) or after (n=11) the initial development of myogenic tone. (C) Representative western blots of phosphorylated/unphosphorylated VASP protein at Ser157 using the pan-VASP antibody (pan), as well as phosphorylated VASP protein at Ser157 (p-157) and Ser239 (p-239), respectively, using the phospho-specific antibodies, and corresponding actin level in each lane, at 120 mmHg before or after the initial development of myogenic tone. (D) Mean ± SEM level of phosphorylated VASP at Ser157 (pVASP-Ser157) as a % of total VASP, at 120 mmHg before (n=9) or after (n=5) the initial development of myogenic tone. (E & F) Representative western blots of G-actin and corresponding level of SM22, at 120 mmHg before or after the initial development of myogenic tone, and mean ± SEM level of G-actin content normalized to SM22 with the value at 120 mmHg after tone development for each blot set to a value of 1 (n=6). (G & H) Representative western blot and mean ± SEM level of phosphorylated LC_{20} (pLC_{20}) as a % of total $LC_{20,}$ at 120 mmHg before (n=9) or after (n=5) the initial development of myogenic tone.

5.4 Discussion

5.4.1 Summary of findings

This is the first study to identify the regulation of VASP phosphorylation in the context of mechanisms for myogenic and extrinsic control of cerebral arterial diameter. Here we show that NO-mediated vasodilation in pressurized RCAs was associated with a minimal decrease in LC_{20} and MYPT1 phosphorylation, but a significant increase in VASP phosphorylation and decrease in actin polymerization. An increase in VASP phosphorylation was also detected in the vasodilation caused by PKA activation, but not in the vasodilation caused by ROK or PKC inhibition, latrunculin B, 14 mM $[K^+]_o$ or 0 Ca^{2+} Krebs' solution. Pressure-dependent myogenic constriction of RCAs was associated with a concurrent decline in phosphorylation of VASP. In addition, the initial development of myogenic tone in RCAs during the equilibration period was associated with a significant decrease in VASP phosphorylation and G-actin content, but a change in LC_{20} phosphorylation was not detected in RCAs before compared to after the tone development. These novel findings imply that regulation of VASP phosphorylation may contribute to the control of cerebral arterial diameter through its effects on cytoskeleton reorganization.

5.4.2 Regulation of VASP phosphorylation in control of cerebral arterial diameter

The findings of this Chapter implicate a novel model for the role of VASP phosphorylation/dephosphorylation in control of cytoskeleton reorganization in NO-mediated vasodilation, as well as pressure-dependent myogenic constriction. As shown in Figure 5.15, NO production activates sGC/cGMP/PKG signaling that enhances VASP phosphorylation, leading to actin depolymerization and, therefore, dilation of

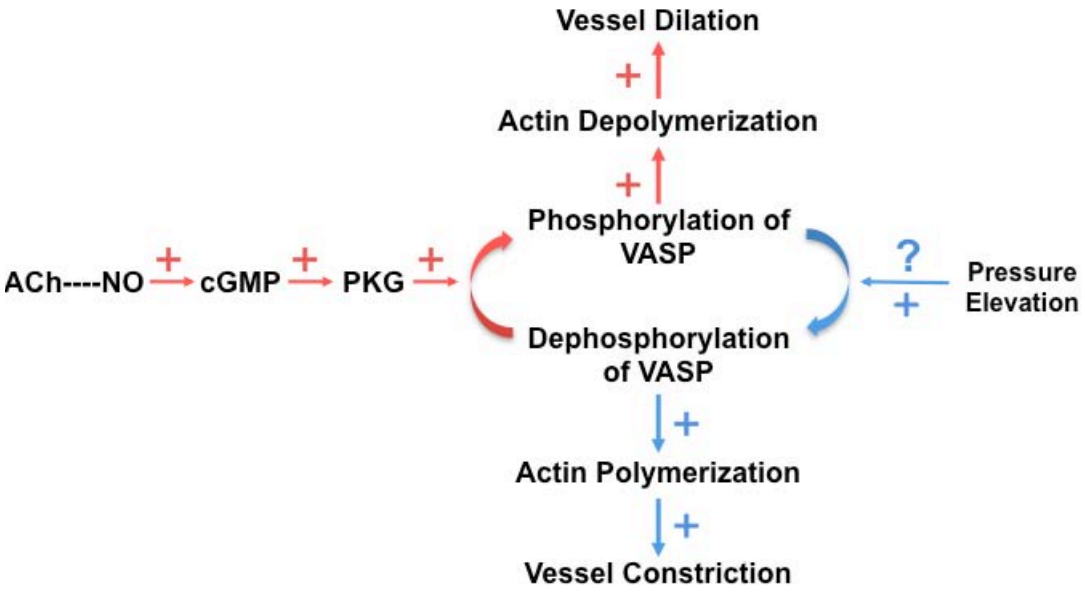

Figure 5.15: Flow chart showing the regulation of VASP phosphorylation in control of cerebral arterial diameter.

On one hand, NO production activates sGC/cGMP/PKG signaling that enhances VASP phosphorylation, leading to actin depolymerization and, therefore, dilation of pressurized cerebral arteries; on the other hand, pressure elevation induces VASP dephosphorylation through unknown mechanism(s), leading to actin polymerization and, therefore, myogenic constriction of cerebral arteries.

pressurized cerebral arteries. On the other hand, pressure elevation *per se* also induces VASP dephosphorylation through an as yet unknown mechanism(s), leading to actin polymerization and, therefore, myogenic constriction of cerebral arteries. The proposed model is based on the following reasoning.

First, we show that DEA/ACh induced significant vasodilation of pressurized, myogenic RCAs. We conclude that the DEA/ACh-induced dilation is due to activation of the NO/sGC/PKG signaling pathway, because ACh-induced dilation was suppressed by inhibition of NO production with L-NAME, and inhibition of sGC or PKG impaired the relaxation due to DEA and ACh treatment (Figures 5.2F & 5.9B). These findings are different from previous reports showing that the inhibition of sGC or PKG only partially inhibited NO donor-induced dilation of RCAs (Alonso-Galicia *et al.*, 1999; Sun *et al.*, 2000; Yu *et al.*, 2002). Notably, serotonin was employed in the previous study to pre-contract the vessels. Previous study showed that serotonin altered MYPT1 and LC_{20} phosphorylation of RCAs, but it could also affect cytoskeletal reorganization owing to the activation of ROK signaling. Therefore, the presence of serotonin may alter the extent of the NO-mediated cytoskeleton reorganization, and, therefore, the contribution of sGC/PKG signaling to NO-mediated dilation. We also propose that the activation of sGC/PKG signaling leads to VASP phosphorylation and actin depolymerization. This is supported by direct biochemical evidence for the alteration in VASP phosphorylation and G-actin content, respectively, in the treatments with DEA/ACh ± ODQ (Figures 5.8 & 5.7).

Second, we provide the first evidence suggesting that the regulation of VASP phosphorylation is associated with the pressure-dependent myogenic response. This is

supported by the observation that myogenic constriction associated with step-wise pressure elevation was accompanied by a pressure-dependent decrease in VASP phosphorylation and G-actin content (Figure 5.12). In addition, a decrease in VASP phosphorylation and G-actin content was found to be associated with the initial development of myogenic tone during the equilibration period, whereas LC_{20} phosphorylation was elevated prior to the initial tone development (Figure 5.14). The findings indicate that under these experimental conditions: (1) activation of LC_{20} phosphorylation-dependent mechanisms is not sufficient to evoke a myogenic response, and (2) the regulation of VASP phosphorylation and cytoskeleton reorganization appears to be indispensible for the development of myogenic tone.

Third, cytoskeleton reorganization is known to alter force transmission that is not associated with a change in LC_{20} phosphorylation or cross bridge cycling (Walsh & Cole, 2013). Emerging evidence has supported an important role of actin polymerization in the myogenic response of cerebral arteries (Cipolla *et al.,* 2002; Flavahan *et al.,* 2005; Moreno-Dominguez *et al.,* 2013). Here, we show that NO-mediated vasodilation of pressurized RCAs involves a significant change in G-actin content, but no or only minimal change in LC_{20} and MYPT1 phosphorylation. Therefore, we conclude that actin depolymerization plays a significant role in NO-mediated vasodilation of cerebral arteries.

Fourth, VASP, as a key cytoskeleton protein, plays an important role in actin dynamics (Reinhard *et al.,* 1992; Rottner *et al.,* 1999; Wei *et al.,* 2003; Lebrand *et al.,* 2004; Lindsay *et al.,* 2007; Bear & Gertler, 2009). VASP activity is tightly regulated by phosphorylation/dephosphorylation reactions (Krause *et al.,* 2003; Kwiatkowski *et al.,* 2003). Numerous studies suggest that phosphorylation of VASP has negative effects on

VASP-mediated actin polymerization and/or cytoskeleton reassembly (Harbeck *et al.,* 2000; Smolenski *et al.,* 2000; Geese *et al.,* 2002; Grosse *et al.,* 2003; Zhuang *et al.,* 2004; Barzik *et al.,* 2005; Lindsay *et al.,* 2007; Benz *et al.,* 2009; Lee & Chung, 2009; Defawe *et al.,* 2010). Based on these findings, it is concluded that the regulation of VASP phosphorylation plays an important role in mediating dynamic cytoskeleton reorganization that contributes to the control of cerebral arterial diameter. Specifically, decreased VASP phosphorylation leads to increased actin polymerization in pressure-dependent myogenic constriction, whereas increased VASP phosphorylation leads to actin depolymerization in NO-mediated dilation.

5.4.3 Lack of cause-and-effect evidence for the role of VASP in control of cerebral arterial diameter

In this study, we show that a decrease and increase in VASP phosphorylation is tightly associated with pressure-dependent myogenic constriction and NO-mediated vasodilation, respectively. However, the data obtained to date do not provide cause-and-effect evidence for the contribution of VASP phosphorylation to the control of cerebral arterial diameter. We are very interested to know, for example, whether promotion and suppression of VASP phosphorylation would cause an inhibition and enhancement of the myogenic response of RCAs, respectively. Several approaches could be taken in the future to address this important issue. On one hand, it would be interesting to determine the effect of VASP inhibition on the myogenic response. Because of the lack of a membrane permeable inhibitor of VASP, a siRNA approach could be employed to knockdown the expression of VASP protein. Alternatively, given that the EVH1 domain of VASP protein is required for normal function of VASP, an exogenous EVH1 protein

could be introduced into VSMCs to act as a decoy that would interrupt normal activities of VASP. The EVH1 protein could be fused to an HIV-1 TAT sequence to allow entry into intact VSMCs (Kim *et al.,* 2010a). On the other hand, VASP phosphorylation could be manipulated by expressing VASP phospho-mutants that imitate the phosphorylated or unphosphorylated states of the protein in VSMCs. We expect that the expression of phosphomimetic mutants of VASP at Ser157 and Ser239 (via exchange of the serine with acidic amino acids to maintain a constitutively phosphorylated state) would attenuate the myogenic response, whereas the expression of non-phosphorylation mutants of VASP at Ser157 and Ser239 (via exchange of the serine with alanine residue to maintain a non-phosphorylated state) will enhance the myogenic response.

It is important to note that both siRNA and phospho-mutant approaches require short-term vessel culture for ~1-3 days. We know that an inappropriate culture procedure results in abnormal myogenic behaviour of vessels owing to a change in the properties of VSMCs due to removal from their normal environment. A change in myogenic behaviour during culture may obscure the effects on VSM contractility of the different treatments. Therefore, appropriate control experiments (e.g. employing scrambled oligonucleotides, empty vector) must be conducted at the same time to make sure that the myogenic behaviour of the vessels is not altered by the culture environment.

5.4.4 LC_{20} phosphorylation in NO-mediated vasodilation in pressurized RCAs

The traditional view of NO-mediated VSM relaxation is that it is mainly achieved by alterations in E_m, $[Ca^{2+}]_{i,}$ and/or the level of Ca^{2+} sensitization, leading to a decrease in LC_{20} phosphorylation, and cross-bridge cycling (Hofmann *et al.,* 2000; Lincoln *et al.,* 2001; Morgado *et al.,* 2012). This view is supported by an extensive body of literature

gained through the studies of cultured cells or large conduit vessels, such as aorta. However, it is worthwhile noting that the physiological role and behavior of large conduit vessels is significantly different from that of small resistance vessels. For example, in the brain, NO-mediated modulation of arterial diameter is most apparent in small resistance arteries, and NO stimulation is sufficient to induce a significant vasodilation of pressurized vessels that develop spontaneous myogenic tone. In contrast, the dilatory effect of NO on conduit arteries is only obtained when the vessels are pre-constricted by agonists, which may alter the relative contribution of MLCK, MLCP and actin polymerization mechanisms to the contractile event. Therefore, the understanding of the molecular mechanisms underlying myogenic regulation of arterial diameter in response to NO stimulation demands that attention be focused on small resistance arteries. However, such studies were not previously performed. Because of the small size of resistance arteries and the time-consuming nature of vessel collection from pressure myograph experiments, direct biochemical analysis has proven to be methodologically challenging. Fortunately, we have developed unique techniques that are capable of quantifying phosphoprotein levels from a single, pressurized segment of small resistance arteries.

Here, we provide the first biochemical evidence suggesting that LC_{20} phosphorylation-dependent mechanisms may not play a major role in NO-mediated vasodilation of pressurized RCAs. Specifically, we show that DEA/ACh-induced vasodilation in pressurized RCAs was not associated with a significant decrease in LC_{20} phosphorylation (Figure 5.5). In addition, we show that DEA-mediated vasodilation was not dependent on E_m hyperpolarization (Figure 5.4), or a significant decrease in MYPT1 phosphorylation at Thr855 (Figure 5.3). Although we did not examine the change in

$[Ca^{2+}]_i$ responding to DEA/ACh treatment, previous studies reported a lack of effect of DEA or 8-Br-cGMP on $[Ca^{2+}]_i$ in VSM cells isolated from RCAs (Yu *et al.,* 2002). It is possible that NO evokes a small, but significant change in LC_{20} and MYPT1 phosphorylation, below the range of detection in our experimental conditions. Nevertheless, the fact that significant changes in LC_{20} phosphorylation were detected in all instances of pressure elevation or agonist stimulation, but not in NO-mediated vasodilation of pressurized RCAs, suggests that NO-mediated vasodilation cannot be simply explained by a small decline in LC_{20} phosphorylation. Notably, a number of previous studies have also reported a lack of detectable change in LC_{20} phosphorylation in association with smooth muscle relaxation; e.g. in tracheal muscles contracted with carbachol and relaxed with okadaic acid (Tansey *et al.,* 1990); in swine uterine muscle contracted with carbachol/histamine and relaxed with PKA agonist or NO donors (Barany & Barany, 1993); in swine carotid arterial smooth muscle contracted with histamine and relaxed with NO donors (McDaniel *et al.,* 1992); and several other instances of PKA/PKG-mediated vessel dilations as described in 5.1.2.2.

5.4.5 NO-mediated cytoskeleton reorganization

We identify, for the first time, a novel mechanism of NO-mediated cytoskeleton reorganization in VSM. In our experimental conditions, NO stimulation was achieved by the treatment of pressurized RCAs with a NO donor, DEA, or by the endothelium-dependent NO stimulator, ACh. One should bear in mind that NO production evoked by DEA/ACh may be beyond its physiological level in our experiments, especially considering the large, almost maximal dilation induced by DEA/ACh treatment (Figure 5.2). In this case, it may mimic pathological conditions of abnormal NO production, for

example, in sepsis. Sepsis is a worldwide health concern with the presence of both infection and a systemic inflammatory response that is characterized by an excessive production of NO (Moss & Martin, 2004; Fortin *et al.,* 2010). Many studies report that sepsis is associated with abnormal vasodilation, as well as impaired agonist-induced vasoconstriction, but the molecular basis underlying this abnormal relaxation is poorly understood (Lubbe *et al.,* 1992; Baker & Sutton, 1993; Hollenberg *et al.,* 1993; Gocan *et al.,* 2000). The novel mechanism of NO-mediated cytoskeleton reorganization identified here may provide important insights for understanding the molecular basis of impaired vascular responsiveness in sepsis and other diseases when NO production is extremely high.

On the other hand, blood flow is known to induce shear stress leading to the endothelium-dependent release of NO (Juncos *et al.,* 1995; Sun *et al.,* 1995). Cerebral arteries *in vivo* exhibit a perpetual myogenic constriction due to the presence of transmural pressure at ~60-140 mmHg, and are continuously exposed to NO-mediated modulation owing to blood flow-induced shear stress (Pohl & de Wit, 1999). Whether flow-mediated dilation of pressurized, myogenically active cerebral arteries is mediated by the novel mechanism of cytoskeleton reorganization is an intriguing question. Answering this question will promote the understanding of flow-mediated dilation, and enhance our knowledge of the integration of intrinsic myogenic regulation and extrinsic NO-mediated modulation in cerebral arteries.

5.4.6 VASP phosphorylation at different sites

VASP is a well-known substrate for PKA and PKG, with two major residues, Ser157 and Ser239, the major sites of phosphorylation. It has been well defined in

numerous cell types including SMCs that VASP phosphorylation at Ser157 and Ser239 has an inhibitory effect on cytoskeleton reorganization, yet whether these sites play the exact same role remains unclear. Some studies have reported that VASP phosphorylation at both Ser157 and Ser239 impaired VASP-mediated actin polymerization, whereas others suggested that phosphorylation at Ser157 had a minor effect on attenuating actin polymerization compared to phosphorylation at Ser239, but Ser157 phosphorylation was found to affect VASP recruitment to the plasma membrane (Harbeck *et al.,* 2000; Smolenski *et al.,* 2000; Geese *et al.,* 2002; Grosse *et al.,* 2003; Zhuang *et al.,* 2004; Barzik *et al.,* 2005; Lindsay *et al.,* 2007; Benz *et al.,* 2009; Lee & Chung, 2009; Defawe *et al.,* 2010). Notably, recruitment of VASP to the plasma membrane was also proposed to be important in mediating cytoskeleton reorganization (Kim *et al.,* 2010a).

In further studies, it will be interesting to compare VASP phosphorylation at the two sites in pressurized RCAs. Phosphorylation of VASP at Ser157 results in a motility shift from 46 kDa to 50 kDa on a standard SDS-PAGE gel, which is helpful in recognizing the phosphorylation at Ser157, but not at Ser239. The employment of Phos-tag gel electrophoresis may be able to further separate the phosphorylated VASP at distinct sites, which permits the quantification of the amount of phosphorylation at each site responding to various stimuli. A direct comparison of the contribution of VASP phosphorylation at each site to, for example, actin polymerization, VASP assembly and control of arterial diameter can be achieved by expressing in the vessel VASP phospho-specific mutants targeting each site.

In addition to Ser157 and Ser239, VASP is a substrate for AMPK, which phosphorylates residue Thr278, and VASP phosphorylation at Thr278 was also shown to

result in impaired actin polymerization (Blume *et al.,* 2007; Benz *et al.,* 2010). Since Thr278 is not responding to PKA or PKG *in vivo*, VASP phosphorylation at Thr278 is not likely to participate in NO-mediated vasodilation in pressurized RCAs. Yet whether the regulation of VASP phosphorylation at Thr278 is associated with the myogenic response remains to be determined.

5.4.7 How does a change in pressure alter VASP phosphorylation?

We provide a novel observation that the extent of VASP phosphorylation was altered in response to a change in intraluminal pressure. How a change in intraluminal pressure alters VASP phosphorylation remains unknown. We show that the inhibition of sGC by ODQ at 10 mmHg induced a significant vasoconstriction, as well as a decrease in VASP phosphorylation at Ser157 (Figure 5.13), suggesting that the high amount of phosphorylated VASP at low pressure may be due to a high level of basal sGC activity. Therefore, it may be possible that pressure-dependent regulation of VASP phosphorylation is due to different levels of sGC activities at varied pressures. However, the possibility that sGC activity is pressure-dependent requires further evidence (i.e. the direct measurement of sGC activity in RCAs at varied pressures).

Alternatively, considering that serine/threonine protein phosphatases PP1 and PP2A have been shown to affect VASP phosphorylation *in vivo* (as described in 5.1.3), it is possible that the pressure-dependent regulation of VASP phosphorylation is achieved via some specific PP1/PP2A phosphatase(s). Specifically, pressure elevation may stimulate unique signaling molecules leading to the activation of specific phosphatase(s) that cause VASP dephosphorylation, whereas pressure reduction may impair unique

signaling molecules leading to the inactivation of phosphatase(s), leading to VASP phosphorylation.

Nevertheless, pressure-dependent regulation of VASP phosphorylation is not likely to be regulated by $[Ca^{2+}]_i$ or Ca^{2+}, ROK/PKC signaling. This is supported by the observations that 0 Ca^{2+} solution treatment or inhibition of ROK/ PKC signaling did not alter VASP phosphorylation at Ser157 in pressurized RCAs (Figure 5.11).

5.4.8 Other signaling pathways contributing to cytoskeleton reorganization in myogenic regulation

Emerging evidence has supported the contribution of cytoskeleton reorganization-dependent mechanisms to myogenic regulation of arterial diameter. However, the specific signaling pathways contributing to cytoskeleton reorganization remain unclear. This study suggests for the first time that the regulation of VASP phosphorylation may represent an important signaling pathway in control of cytoskeleton reorganization associated with the myogenic response. Notably, recent findings demonstrated that inhibition of ROK or PKC via H1152 or GF109203X blocked the decreased G-actin content as well as myogenic constriction in response to pressure elevation (Cole lab, unpublished data), suggesting the contribution of activation of ROK/PKC signaling to cytoskeleton reorganization in the cerebral myogenic response. Considering that myogenic regulation of arterial diameter is such a complicated and important, physiological event, it is not surprising that multiple signaling pathways are involved in the control of cytoskeleton reorganization in association with myogenic regulation. Further studies are required to elucidate these signaling pathways mediated by ROK, PKC or VASP.

Chapter Six: General discussion

6.1 Summary of the findings

The myogenic response has been studied extensively since it was discovered by Sir William Bayliss more than a hundred years ago (Bayliss, 1902). Although the general concepts of myogenic regulation of arterial diameter have been well defined, many aspects are still poorly understood. The work presented in this thesis aimed to clarify several issues in two major areas of study concerning the molecular mechanisms that underlie myogenic control of cerebral arterial diameter. First, heteromultimeric Kv2.1/9.3 channels and Kv7-containing channels were identified as important components of native K_{DR} currents that contribute to myogenic control of E_m and diameter in RCAs. On one hand, ScTx1-sensitive channels were shown to affect arterial diameter over a wider range of intraluminal pressure than that previously reported for Kv1 or BK_{Ca} channels (Brayden & Nelson, 1992; Nelson et al. 1995; Knot & Nelson, 1995; Chen et al. 2006; Yang et al. 2009). Based on the expression of Kv2.1 and Kv9.3 transcripts, the co-localization of K_v2.1 and 9.3 proteins and comparison of the functional properties of recombinant K_v2.1/9.3 current and native ScTx1-sensitive current of RCA myocytes, the native ScTx1-sensitive channels were concluded to be heteromultimeric K_v2.1/K_v9.3 channels. On the other hand, evidence was provided indicating the presence of K_v7 currents in RCA myocytes, as well as their contribution to myogenic control of cerebral arterial diameter. Moreover, we have shown the unique ability of the Kv7 activator, S-1, to reverse vasoconstriction while preserving the myogenic response. This latter finding provides ample justification for consideration of Kv7 activators as a novel therapeutic

strategy to ameliorate arterial dysfunction in the form of vasospasm that is associated with cardiovascular diseases.

Second, evidence was provided that implicates a role for VASP phosphorylation in regulation of the actin cytoskeleton in myogenic and endothelial NO-mediated control of cerebral arterial diameter. This portion of the thesis research relied on a highly sensitive, western blot approach to perform quantitative measurements of LC_{20}, MYPT1 and VASP phosphorylation, as well as G-actin content in pressurized, myogenically active cerebral arteries. VASP phosphorylation and dephosphorylation and actin depolymerization and polymerization, were respectively shown to contribute to NO-mediated vasodilation and pressure-dependent myogenic constriction. These findings suggest the presence of a novel signaling pathway that contributes to cytoskeleton reorganization in the context of cerebral arterial constriction and dilatation.

6.2 Molecular mechanisms underlying myogenic regulation of cerebral arterial diameter

Myogenic regulation of arterial diameter plays a fundamental role in the maintenance of appropriate blood flow to the brain. Emerging evidence has demonstrated that myogenic regulation of cerebral arterial diameter involves at least three distinct molecular mechanisms, including: (1) a Ca^{2+}-dependent mechanism that is mediated by E_m, $[Ca^{2+}]_i$ and MLCK activity, (2) a Ca^{2+} sensitization-dependent mechanism that is mediated by ROK signaling and MLCP inhibition, and (3) a cytoskeleton reorganization-dependent mechanism that is mediated by actin polymerization/depolymerization. Although PKC-dependent suppression of thin filament regulation was shown to modulate force generation by smooth muscle cells (Kim *et al.*, 2008a), a change in caldesmon or

calponin phosphorylation in response to pressure elevation was not detected in RCAs, suggesting a minimum contribution of this mechanism to the myogenic response (Cole lab, unpublished observation). Considering that the extent of myogenic constriction and dilatation is determined by a complex array of intrinsic and extrinsic factors, it is perhaps not surprising that multiple signaling pathways and effector proteins are now recognized to participate in the regulation of these principal mechanisms in different physiological and pathological conditions. Thus, defining how the molecular mechanisms of the myogenic response are precisely controlled and integrated so that diameter and flow are exactly matched to demand is one of the most intriguing and complicated questions to answer in the study of VSM contractility.

6.2.1 Three-phase model of in vitro myogenic behaviour

Osol *et al.* (2002) proposed that myogenic control of arterial diameter consists of three different phases, as summarized by Figure 6.1. Phase I occurs over the pressure range of $\leq$ 60 mmHg and involves myogenic tone development. It is accompanied by a marked depolarization of E_m and a substantial increase in $[Ca^{2+}]_i$ in VSMCs of RCAs. Phase II occurs between 60 and 140 mmHg and is referred to as the phase of myogenic reactivity. It is characterized by minimal further changes in E_m and $[Ca^{2+}]_i$ despite the maintenance of diameter at a constant or further constricted level in the presence of elevated pressure. Notably, previous studies have reported that myogenic reactivity was retained in vessels exposed to a high concentration external K^+ solution that clamped E_m at a constant value and precluded any change in voltage-dependent Ca^{2+} entry (Lagaud et al., 2002). These observations suggest that myogenic reactivity may not depend on an

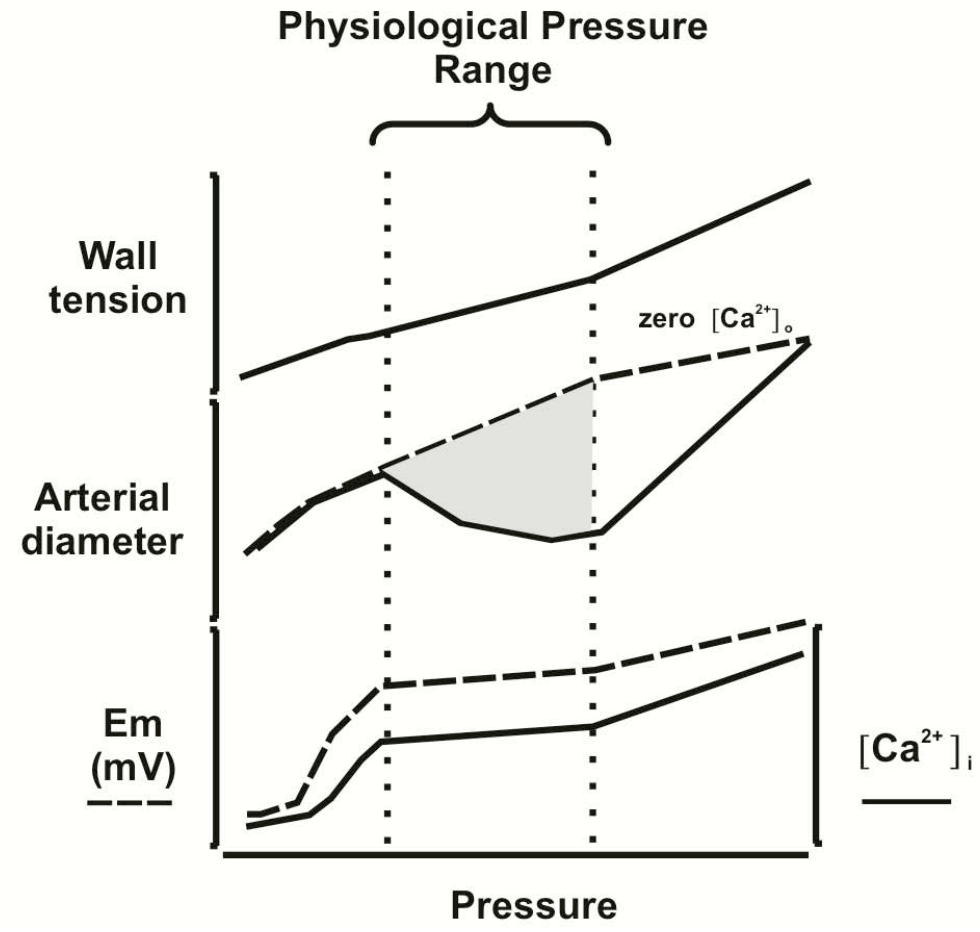

Figure 6.1 Diagramatic representation of three-phase model of *in vitro* myogenic behaviour.

Schematic diagram summarizing changes in wall tension, arterial diameter and arterial wall $[Ca^{2+}]_i$ in resistance arteries responding to stepwise increases in intraluminal pressure. The *in vitro* myogenic behaviour is characterized by three phases, including the development of myogenic tone (MT), myogenic reactivity (MR) and forced dilation (FD). (Figure is modified from Osol *et al.*, 2002; Am J Physiol Heart Circ Physiol 283, H2260-2267.)

increase in $[Ca^{2+}]_i$-CaM-MLCK activity. Phase III of the myogenic response occurs at ≥ 140 mmHg and is marked by forced dilatation, as tone development by VSMCs is not sufficient to overcome the distending influence of intraluminal pressure.

The findings above would seem to imply that the three principal mechanisms of myogenic contraction (i.e. MLCK activation, MLCP inhibition and actin polymerization) contribute to different phases of the myogenic response. However, it is important to note that it is only the relative contribution in relation to pressure that varies, as each mechanism is indispensible for myogenic control of arterial diameter regardless of the level of intraluminal pressure. This is indicated by the fact that inhibition of any one of the mechanisms (e.g. via E_m hyperpolarization, inhibition of Ca^{2+} entry, ROK signaling or inhibition of actin polymerization) will result in an impaired myogenic response between 0 and 200 mmHg (Knot & Nelson, 1995; Quayle *et al.,* 1997; Johnson *et al.,* 2009b; Moreno-Dominguez *et al.,* 2012). However, one should also notice that the inhibition of a single mechanism in these conditions might affect the other mechanism(s) as well. For example, blocking VGCCs leads to a decrease in $[Ca^{2+}]_i$-CaM-MLCK activity, yet it may also result in a feedback increase in MLCP activity. Inhibition of ROK signaling via H1152 not only affects ROK-mediated Ca^{2+} sensitization, but also influences ROK-mediated actin polymerization associated with the myogenic constriction.

The biochemical analyses conducted here and in previous studies detected changes in LC_{20}, MYPT1 and VASP phosphorylation, as well as G-actin content at all pressures studied between 10 and 120 mmHg (Johnson *et al.,* 2009b; Moreno-Dominguez *et al.,* 2012;), suggesting that specific mechanisms are not restricted to a limited range of pressure, rather it is the relative contribution of each mechanism that varies according to

the level of intraluminal pressure. In normal physiological conditions, cerebral arteries are permanently exposed to a transmural pressure of between 60 and 140 mmHg, and, therefore, the mechanisms for control of diameter in Phase II myogenic reactivity predominate. Specifically, pathways leading to Ca^{2+} sensitization and cytoskeleton reorganization, rather than E_m and $[Ca^{2+}]_i$, may play a more significant role in minute-to-minute regulation of diameter in cerebral arteries exposed to a normal level of intraluminal pressure *in vivo*. The Ca^{2+} sensitization mechanism also appears to be activated over the range from 0 to 60 mmHg, as ROK-inhibitor (H1152)-sensitive MYPT1 and LC_{20} phosphorylation was detected in this range of pressure (Johnson et al., 2009b), but the predominant determinant of force generation is the change in E_m, $[Ca^{2+}]_i$ and MLCK activity. Above ~80 mmHg, actin polymerization may play the predominant role until the G-actin supply is exhausted, as suggested by Cipolla *et al.* (1998). This is supported by the current and previous measurements of LC_{20} phosphorylation and G-actin in RCAs, that show a lack of further change in phospho-LC_{20}, but a decrease in G-actin content in vessels pressurized to >~80 mmHg. However, the contribution of actin polymerization to myogenic constriction is not limited to >80 mmHg, as a significantly lower level of G-actin was detected at 80 compared to 10 mmHg in skeletal muscle arterioles and RCAs (Moreno-Dominguez et al., 2013; Cole lab, unpublished observations).

6.2.2 Extrinsic modulation of VSM tone

Although the myogenic response is inherent to VSMCs, it is subjected to modulation by a variety of extrinsic factors released from adjacent or distant cell types (Davis & Hill, 1999). The precise signaling pathways by which these extrinsic factors

influence the myogenic response is not clearly understand, but it appears to be achieved by affecting Ca^{2+}-CaM-MLCK activation, Ca^{2+} sensitization and cytoskeleton reorganization. It is worthwhile noting that extrinsic modulation of VSM tone may affect more than one mechanism. For example, serotonin released from nerve fibres is known to increase VSM tone. Previous findings suggest that serotonin resulted in enhanced myogenic constriction through E_m depolarization in cat cerebral arteries (Harder, 1988), and through a decrease in MLCP activity in rat cerebral arteries (El-Yazbi *et al.*, 2010). In addition, β-adrenoceptor agonists are known to activate Gs/AC/PKA signaling leading to VSM relaxation. Isoprenaline-induced dilation of rat renal arteries was suggested to involve an enhancement of VSM K_v7 current leading to E_m hyperpolarization (Chadha *et al.*, 2012), forskolin-induced relaxation of rat caudal arterial smooth muscle was suggested to involve an increase in MLCP activity (Grassie *et al.*, 2012), and isoprenaline-induced dilatation of pressurized RCAs was found to involve a decrease in VASP phosphorylation, suggesting a role of the cytoskeleton reorganization-dependent mechanism (Figure 5.10). Furthermore, with regards to NO-mediated VSM relaxation, some studies suggested a role of E_m hyperpolarization, some studies suggested a role for decreased Ca^{2+} sensitization (Hofmann *et al.*, 2000; Lincoln *et al.*, 2001; Morgado *et al.*, 2012), and the findings presented in Chapter 5 indicate a role for VASP phosphorylation and cytoskeleton reorganization in NO-mediated vasodilation of pressurized RCAs. Whether the presence of more than one mechanism in extrinsic modulation of VSM tone is due to the differences in species, vessel types and/or experimental conditions remains to be clarified. Nevertheless, it seems very likely that multiple molecular mechanisms are involved in the integration of the intrinsic myogenic response and extrinsic modulation of

VSM tone so that appropriate control of blood flow can be achieved regardless of the level of intraluminal pressure or varied presence of vasomotor agonists.

6.3 Significance of findings

Abnormal myogenic behaviour is a hallmark feature of a number of cardiovascular diseases, including hypertension, cerebral vasospasm, hemorrhagic stroke, chronic heart failure, endotoxic shock, cerebral hyperaemia, cerebral microhemorrhage, diabetes and Alzheimer's disease (Niwa *et al.,* 2002; Gschwend *et al.,* 2003; Izzard *et al.,* 2003; Sonoyama *et al.,* 2007; Ren *et al.,* 2010; Ryan *et al.,* 2011; Giles *et al.,* 2012). A clear understanding of molecular mechanisms responsible for myogenic control of arterial diameter is essential for the identification of pathological mechanisms leading to abnormal myogenic regulation and the development of therapeutic strategies to treat arterial dysfunction. The findings of the present study contribute several new pieces that fill holes in the myogenic response puzzle and the data may provide some clues as to possible sites of dysfunction in the myogenic response that contribute to abnormal arterial regulation in disease.

The findings presented in Chapter 3 identified the distinct functional contribution of heteromultimeric $K_v2.1/9.3$ channels to control of cerebral arterial diameter over a wider range of intraluminal pressure than that reported for Kv1 and BK_{Ca} channels (Brayden & Nelson, 1992; Nelson et al. 1995; Knot & Nelson, 1995; Chen et al. 2006; Yang et al. 2009). Substantial evidence suggests that a lack of K_v2 current in VSM contributes to the altered E_m and, therefore, Ca^{2+}-CaM-MLCK activity, resulting in abnormal myogenic regulation in disease (Thorneloe *et al.,* 2001; Thorneloe & Nelson, 2005). Many studies showed that altered expression of K_v2 subunits in VSMCs resulted

in inappropriate K_v2 current in disease (Yuan *et al.*, 1998; Wang *et al.*, 2005; Amberg & Santana, 2006; Jahromi *et al.*, 2008a,b). However, some studies also reported altered expression of the silent subunit as a reason for the change in K_v2 current. For example, in mesenteric arteries, *de novo* expression of $K_v6.3$ subunits was suggested to be the cause of diminished K_v2 current and abnormal VSM contractility in spontaneously hypertensive mice (Moreno-Dominguez *et al.*, 2009). Our novel findings on the presence of heteromultimeric $K_v2.1/K_v9.3$ channels in RCA myocytes suggest that altered expression or regulation of $K_v9.3$ subunits may significantly affect native K_v2 currents, and therefore, myogenic control of the E_m depolarization in cerebral arteries. Understanding the contribution of $K_v9.3$ subunits to impaired K_v2 current associated with many diseases may represent an area of intriguing future research.

The findings presented in Chapter 4 provided the first evidence for the contribution of $K_v7.4$-containing channels to K_v currents of RCA myocytes and to control of cerebral arterial diameter. The identification of $K_v7.4$-containing channels represents a novel area in the study of abnormal VSM tone. In fact, recent evidence has implicated a contribution of altered expression of K_v7 subunits to abnormal VSM contractility in several vessel types. For example, down regulation of K_v7 currents in mesenteric arteries owning to reduced expression of $K_v7.4$ subunits was observed in hypertensive rats and mice (Jepps *et al.*, 2011). Reduced expression of $K_v7.4$ subunits was also proposed to underlie impaired β-adrenoceptor-mediated relaxation of rat renal arteries in hypertension (Chadha *et al.*, 2012). Moreover, our novel findings on a Kv7 activator, S-1, in adjusting abnormal constriction imply that inappropriate control of cerebral arterial diameter may

be corrected by manipulating K_v7 channel activities while preserving the crucial physiological mechanism of cerebral blood flow autoregulation.

The findings presented in Chapter 5 evaluate, for the first time, a potential role of VASP regulation in control of cytoskeleton reorganization associated with cerebral myogenic regulation. We show that there is a pressure-dependent decrease in VASP phosphorylation associated with normal cerebral myogenic regulation. We have now gone on to study the pressure-dependent change in VASP phosphorylation associated with the impaired cerebral myogenic response of Goto-Kakizaki (GK) rats, a genetic model of type 2 diabetes (Cole lab, unpublished observation). We have shown that VASP phosphorylation at Ser157 is lost concomitant with vasoconstriction and abrogation of the cerebral myogenic response in GK rats. This observation raises the possibility that altered regulation of VASP phosphorylation represents an important pathological mechanism, leading to abnormal cytoskeleton reorganization and myogenic dysfunction. This example also highlights the importance of continued examination of the molecular mechanisms responsible for the myogenic response. Without the novel observation that VASP phosphorylation declines with pressurization (Figure 5.12D), there would be no reason to evaluate its status in the context of the dysfunctional response of type 2 diabetic rats.

The findings presented in Chapter 5 also provide novel evidence for the contribution of VASP phosphorylation and cytoskeleton reorganization to NO-mediated vasodilation in pressurized cerebral arteries. This is significant because an excessive production of NO has been associated with the loss of VSM contractility in several disease conditions, such as sepsis (Moss & Martin, 2004; Fortin *et al.,* 2010). NO-

mediated VASP phosphorylation leading to reduced actin polymerization may represent an important mechanism contributing to the impaired VSM contractility in sepsis and other disease conditions marked by elevated levels of NO production. A clear understanding of the regulation of VASP phosphorylation in control of cerebral arterial diameter may provide insights into the development of therapeutic strategies to correct abnormal vasodilation in these diseases.

6.4 Conclusions

Myogenic control of cerebral arterial diameter plays a central role in the maintenance of normal vascular resistance and blood flow in the brain. Myogenic control of cerebral artery diameter is achieved by inherent pressure-dependent mechanisms of Ca^{2+}-CaM-MLCK activation, ROK-mediated Ca^{2+} sensitization and cytoskeleton reorganization. The findings presented in this thesis identify novel elements in these molecular mechanisms, including: (1) $K_v9.3$ subunits that co-assemble with $K_v2.1$ subunits to form ScTx1-sensitive channels that regulate E_m, (2) $K_v7.4$-containing channels that also regulate E_m, and (3) a cytoskeleton protein, VASP, that is involved in a dynamic process of actin polymerization in response to pressure elevation. Both $K_v2.1/9.3$ channels and $K_v7.4$-containing channels of cerebral myocytes were shown to contribute to native K_v currents in myogenic control of cerebral arterial diameter. The regulation of VASP phosphorylation in the process of cytoskeleton reorganization was shown to participate in the pressure-dependent myogenic response and NO-mediated vasodilation of cerebral arteries. In summary, the thesis work provides a novel understanding of molecular mechanisms underlying myogenic control of cerebral arterial diameter. How these mechanisms are precisely integrated, and whether alterations in

these mechanisms contribute to abnormal myogenic regulation in disease represent intriguing areas for future research.

Chapter Seven: Future directions

7.1 Most intriguing areas of future study

The work presented in this thesis involved the study of a broad range of processes that participate in myogenic control of cerebral arterial diameter. Several important areas of research have been discussed in each Chapter. The following text will emphasize some future directions that are particularly intriguing and deserve immediate attention.

7.1.1 K_v9.3 subunits in abnormal K_v2 current

When silent subunits combine with K_v2 subunits to form heteromultimeric channels, the biophysical properties of the channel complex are significantly changed. Therefore, the alteration in function and expression of silent subunits has the potential to cause abnormal K_v2 current, which affects whole-cell K_{DR} currents that participate in controlling the level of E_m and arterial diameter. Abnormal regulation of cerebral arterial diameter in several diseases, such as hypertension and subarachnoid hemorrhagic stroke, was shown to be associated with a reduction in K_v2 current of cerebral myocytes (Amberg & Santana, 2006; Wellman, 2006; Jahromi *et al.*, 2008a,b). Since K_v2 current of cerebral myocytes is attributed to heteromultimeric $K_v2.1/9.3$ channels, and Kv9.3 subunits substantially enhance the activity of Kv2.1/9.3 of cerebral myocytes at resting E_m (as described in Chapter 3), it will be of great interest to determine whether abnormal expression of $K_v9.3$ causes the change in K_v2 current in these diseases. Traditional molecular and biochemical approaches can be employed to determine the expression of $K_v9.3$ gene and protein of cerebral myocytes in health and disease. Moreover, the PLA

technique can be employed to visualize the *in situ* co-localization of $K_v9.3$ protein and $K_v2.1$ protein in the plasma membrane of cerebral myocytes in health and disease.

In addition, hypoxia can have profound influences on the circulation. Acute exposure to hypoxia is known to cause cerebral vasodilation of blood vessels so as to maintain normal blood flow and oxygen delvery to the brain. Several signaling pathways (e.g. the activation of K_{ATP} or BK_{Ca} channels, the release of endothelial derived substances) have been shown to participate in the compensatory vasodilatation observed during hypoxia, yet the precise mechanisms are not known with certainty (Taguchi *et al.*, 1994; Casey *et al.*, 2010; Casey *et al.*, 2012). Notably, Patel *et al.* (1997) reported that the activity of $K_v2.1/9.3$ channels in pulmonary artery myocytes was tightly controlled by internal ATP, and reversibly inhibited by hypoxia. It will be of interest to determine whether $K_v2.1/9.3$ channels of cerebral myocytes are oxygen-sensitive, and whether the activity of the channels is altered in response to hypoxia. Also, it is important to identify if altered activity of Kv2.1/9.3 channels, and/or expression of Kv2.1/9.3, contributes to the impaired hypoxic cerebral vasodilation associated with several hypoxic diseases, including metabolic syndrome (Harrell *et al.*, 2013).

7.1.2 S-1 in the treatment of abnormal vasoconstriction

As discussed in Chapter 4, pharmacological manipulation of K_v7 channel gating may represent an option for the treatment of clinical situations of abnormal control of cerebral arterial diameter. The ability of the K_v7 channel activator, S-1, to attenuate enhanced vasoconstriction while preserving the crucial physiological mechanism of cerebral blood flow autoregulation is unique. Future work should involve the use of S-1 to treat abnormal cerebral vasoconstriction and blood flow in diseased animals *in vivo*

(e.g. animal models of hypertension or subarachnoid hemorrhagic stroke). The findings may provide information for the development of a novel strategy for combating abnormal vasoconstriction, especially in the setting of subarachnoid hemorrhage that is resistant to standard vasodilators including dihydropyridine L-type Ca^{2+} channel blockers.

In addition, a number of studies suggest a contribution of K_v7-containing channels to whole-cell K_v currents in several other resistance arteries, such as femoral, small mesenteric and renal arteries (Yeung *et al.*, 2007). It will be of interest to determine whether S-1 has a similar ability to reverse enhanced vasoconstriction while preserving the myogenic response in these arteries. However, this idea is not without a caveat. Recent studies reported that a decrease in $K_v7.4$ expression was associated with the reduced whole-cell K_{DR} current of mesenteric and renal arterial myocytes from hypertensive rats and mice, and the effect of S-1 was markedly reduced (Jepps *et al.*, 2011; Chadha *et al.*, 2012). Therefore, caution is required in the interpretation of experiments using S-1 if it is found to have a smaller effect on diameter in disease, because this response may reflect the lack of Kv7-containing channels in the disease condition.

7.1.3 Cytoskeleton reorganization and VASP phosphorylation in NO-mediated vasodilation

The work presented in Chapter 5 provided the first evidence for a novel signaling pathway for regulation of cytoskeleton reorganization involving control of VASP phosphorylation. As discussed in Chapter 5.4.5, DEA/ACh-treated vessels with impaired VSM contractility may mimic the vessels in sepsis and other diseases in which NO production is dramatically elevated (Lubbe *et al.*, 1992; Baker & Sutton, 1993;

Hollenberg *et al.,* 1993; Gocan *et al.,* 2000). It will be of great interest to evaluate the regulation of cytoskeleton reorganization and VASP phosphorylation in pressurized cerebral arteries of animals with sepsis. The extent of actin polymerization can be determined using the G-actin assay as applied in Chapter 5.3.6. Since the assay requires normalizing the level of G-actin to SM22, it will be important to confirm that SM22 expression is not altered in vessels of diseased and control animals. Alternatively, the extent of actin polymerization could be determined by measuring the ratio of F-actin to G-actin, not excluding the difficulties associated with detection of only F-actin in the pellet following high-speed centrifugation. The level of VASP phosphorylation at Ser157 (phosphorylated VASP at Ser157 as a percentage of total VASP protein) can be determined via the use of a pan-VASP antibody and ratiometric measurement of percent VASP phosphorylation. An important point for the future is to address the relationship between the level of VASP phosphorylation at S157, S239 and other sites on the protein in determining the effect of extrinsic regulators, and vasoconstrictors that activate PKC in particular, on the myogenic response and VASP activity.

It is also of great interest to determine the regulation of cytoskeleton reorganization and VASP phosphorylation in the context of flow-mediated dilatation of pressurized RCAs. The data will provide essential information in determining whether the regulation of VASP phosphorylation plays a physiological role in control of cerebral arterial diameter. The problem here is to develop an approach that avoids contamination of the VSMC signal from that due to endothelial cells. This is because flow-mediated dilation requires an intact endothelium, endothelial cells express VASP, and they are very likely to display an identical regulation of VASP phosphorylation and cytoskeleton

reorganization in response to flow-mediated shear stress as demonstrated here for VSMCs in the myogenic response.

With regards to the regulation of cytoskeleton reorganization in the context of flow-mediated dilatation of pressurized RCAs, Morgan's group indicated that at least three types of actin isoforms are present in VSMCs (including α-, β- and γ- actin), and that β- and γ- actin are probably the more dynamic population of actin responsible for actin dynamics (Kim *et al.*, 2008b; Kim *et al.*, 2010b; Yamin & Morgan, 2012). Given that β-actin was not found to be expressed by primary endothelial cells (Galustain *et al.*, 1995), we can determine whether flow-mediated shear stress leads to a change in the β-actin component of the G-actin pool that is specifically present in VSMCs. Alternatively, the extent of actin polymerization may be observed in a cell specific manner using fluorescent confocal microscopy, and the β- and γ-actin specific antibodies.

7.1.4 Examination of signaling pathways involved in the myogenic response

Direct measurement of a change in E_m, $[Ca^{2+}]_i$, LC_{20}, MYPT1 phosphorylation and G/F-actin, respectively, supports the view that multiple signaling pathways are involved in the myogenic response. Yet how they are precisely integrated to match the current model of myogenic behaviour remains unclear. In our experimental conditions, LC_{20}, MYPT1 phosphorylation and G/F-actin content were sampled at 5-10 minutes after a step elevation in intraluminal pressure at a time when a stable level of arterial diameter was achieved (Johnson *et al.*, 2009b; Moreno-Dominguez *et al.*, 2012). Future work should involve the identification of the temporal changes in E_m, $[Ca^{2+}]_i$, LC_{20}, MYPT1 phosphorylation and G-actin content associated with the myogenic response. The findings will expand our knowledge concerning when each pathway is activated, and

whether the activation persists after prolonged exposure to elevated intraluminal pressure. The findings may provide evidence of differences in the temporal contribution of the three mechanisms and associated upstream signalling pathway to the myogenic response, as was previously shown for MLCK *versus* MLCP in the initial compared to sustained agonist-evoked contraction (El-Yazbi *et al.,* 2010). Since a large number of myograph experiments will be required for these measurements, it will be important to make sure that the myogenic behaviour in terms of the rate and extent of tone development of each vessel segment analyzed is as similar as possible to limit variations owing to the unpaired experimental design of this analysis.

In addition, it is important to remember that the experimental conditions of pressure myograph experiments *in vitro* do not exactly mimic the physiological conditions *in vivo*. Under normal physiological conditions, cerebral arteries are constantly subjected to shear stress due to blood flow, which activates endothelium-dependent arterial regulation, and the normal physiological pressure range lies between ~60 and ~120 mmHg, with pulsatile pressures that are superimposed on graded changes in transmural pressure with each cardiac cycle (Cipolla, 2009). Although an increase in intraluminal pressure (mean pressure elevation) leads to the myogenic response of resistance arteries *in vitro*, the extent of the myogenic response *in vivo* may be more dependent on the systolic pressure rather than the mean pressure (Davis & Hill, 1999; Bidani *et al.,* 2009). For example, studies using the *in vitro* perfused hydronephrotic rat kidney preparation have shown that increased systolic pressure resulted in constriction of the afferent arteriole despite unaltered mean pressure (Loutzenhiser *et al.,* 2002). Also, reductions in the diastolic and mean pressures had no effect on the level of myogenic

tone evoked by elevated systolic pressure. Moreover, the frequency of the pressure oscillation owing to heart rate frequency may also affect the myogenic mechanism in control of blood flow (Loutzenhiser *et al.,* 2006). Therefore, pulsatile pressure and flow *versus* constant pressure and flow or no flow in control of arterial diameter should be considered in the study of molecular mechanisms of arterial regulation with the help of improved techniques.

7.2 Summary of additional areas of future research

Several additional areas are also very intriguing for future research. One relates to the study of $K_v9.3$ expression and its contribution to K_v2 current in different resistance vascular beds with varied degrees of the myogenic response (e.g. small mesenteric arteries, skeletal muscle arterioles), as well as in non-resistance vessels that lack a myogenic response (e.g. large mesenteric arteries or aorta). The findings will expand our knowledge of the role of $K_v9.3$ in control of K_v2 current, and may provide a rational explanation for abnormal K_v2 current associated with several diseases.

Although evidence was provided for the contribution of K_v7-containing channels to whole-cell K_v currents of cerebral myocytes, the molecular composition of the K_v7-containing channels remains unclear. As discussed in Chapter 4.4.3, indirect evidence suggests that heteromultimeric $K_v7.4/7.5$ channels may contribute to S-1 sensitive current of RCA myocytes. Further studies including comparison of biophysical properties of recombinant $K_v7.4/7.5$ current and S-1 sensitive current, detection of $K_v7.4$, Kv7.5 protein co-assembly, and determination of the contribution of associated KCNE subunits are required to test the view that the channels are heteromultimeric in nature.

The regulation of VASP phosphorylation in cytoskeleton reorganization was identified as a novel signaling pathway in the pressure-dependent cerebral myogenic response, as well as NO-mediated vasodilation. The precise control of VASP regulation and cytoskeleton reorganization may be a result of integration of the intrinsic myogenic response and extrinsic NO-mediated modulation in cerebral arteries. It will be of great interest to identify whether the novel signaling pathway is also present in other vascular beds, particularly in small resistance arteries with a myogenic response *versus* large conduit vessels which lack a myogenic response. Since NO-mediated VSM relaxation of large conduit vessels was shown to be mediated by MCLK- and MCLP-dependent mechanisms (Hofmann *et al.,* 2000; Lincoln *et al.,* 2001; Morgado *et al.,* 2012), VASP phosphorylation and cytoskeleton reorganization may not play a significant role in large conduit vessels. This may also be consistent with a lack of regulation of VASP phosphorylation and cytoskeleton reorganization in response to pressure stimulation in these vessels.

Moreover, in addition to the important role in regulating VSM contractility played by NO/cGMP/PKG signaling, several lines of evidence indicate a contribution to the regulation of VSMCs phenotype as well (Lincoln *et al.,* 2001; Lincoln *et al.,* 2006). VSMCs display altered phenotype plasticity, switching from a contractile phenotype to a synthetic or secretory phenotype in response to, for example, vessel growth stimuli, vascular injury, and *in vitro* culturing of VSMCs (Owens *et al.,* 1995). Many studies have demonstrated a role for NO or NO/cGMP/PKG signaling in the inhibition of VSMC proliferation or migration *in vitro* and *in vivo* (Garg & Hassid 1989; McNamara *et al.,* 1993; Cayatte *et al.,* 1994; Wang & Li, 2009). Cerebral arteries *in vivo* exhibit a

perpetual myogenic constriction due to the presence of transmural pressure at ~60-140 mmHg, and are continuously exposed to NO-mediated modulation owing to blood flow-induced shear stress (Pohl & de Wit, 1999). It is possible that this constitutive NO signaling due to shear stress is involved in preventing cytoskeleton reorganization-dependent events associated with proliferation or migration, and maintaining the differentiated state of the VSMCs of cerebral arteries. Although the mechanism(s) by which NO signaling regulates smooth muscle contractile phenotype remains unclear, identifying whether basal NO signaling is required for the maintenance of contractile VSMCs in cerebral arteries *in vivo*, and whether this event involves the regulation of VASP phosphorylation and cytoskeleton reorganization would expand our knowledge of the importance of NO signaling in VSM function, and possibly provide a rational explanation as to why NO-mediated vasodilation of cerebral arteries appears to depend exclusively on the cytoskeleton reorganization-dependent mechanism.

Emerging evidence supports an important role for cytoskeleton reorganization in the myogenic response (Walsh & Cole, 2013). However, the signaling pathways and effector proteins that contribute to actin polymerization/depolymerization remain to be determined. The work presented in Chapter 5 suggested a role of the regulation of VASP phosphorylation in this event. Recent studies in our lab have also provided biochemical evidence for a role of ROK/PKC signaling in this event. How a change in pressure leads to a change in VASP phosphorylation, how ROK and PKC contribute to the myogenic response by altering cytoskeleton reorganization in terms of the downstream effectors, the mechanisms by which VASP, ROK or PKC signaling pathways interact to control cytoskeleton reorganization are all intriguing questions. Answering these questions will

be essential for understanding the cytoskeleton reorganization-dependent mechanism for control of cerebral arterial diameter.

References

Abbott GW & Goldstein SA. (2001). Potassium channel subunits encoded by the KCNE gene family: physiology and pathophysiology of the MinK-related peptides (MiRPs). *Mol Interv* **1,** 95-107.

Abd El-Rahman RR, Harraz OF, Brett SE, Anfinogenova Y, Mufti RE, Goldman D & Welsh DG. (2013). Identification of L- and T-type Ca2+ channels in rat cerebral arteries: role in myogenic tone development. *Am J Physiol Heart Circ Physiol* **304,** H58-71.

Abel K, Mieskes G & Walter U. (1995). Dephosphorylation of the focal adhesion protein VASP in vitro and in intact human platelets. *FEBS Lett* **370,** 184-188.

Adderley SP, Joshi CN, Martin DN & Tulis DA. (2012). Phosphodiesterases Regulate BAY 41-2272-Induced VASP Phosphorylation in Vascular Smooth Muscle Cells. *Front Pharmacol* **3,** 10.

Aiello EA, Clement-Chomienne O, Sontag DP, Walsh MP & Cole WC. (1996). Protein kinase C inhibits delayed rectifier K+ current in rabbit vascular smooth muscle cells. *Am J Physiol Heart Circ Physiol* **271,** H109-H119.

Aiello EA, Malcolm AT, Walsh MP & Cole WC. (1998). Beta-adrenoceptor activation and PKA regulate delayed rectifier K+ channels of vascular smooth muscle cells. *Am J Physiol* **275,** H448-459.

Aiello EA, Walsh MP & Cole WC. (1995). Phosphorylation by protein kinase A enhances delayed rectifier K+ current in rabbit vascular smooth muscle cells. *Am J Physiol* **268,** H926-934.

Albarwani S, Nemetz LT, Madden JA, Tobin AA, England SK, Pratt PF & Rusch NJ. (2003). Voltage-gated K+ channels in rat small cerebral arteries: molecular identity of the functional channels. *J Physiol* **551,** 751-763.

Alonso-Galicia M, Hudetz AG, Shen H, Harder DR & Roman RJ. (1999). Contribution of 20-HETE to vasodilator actions of nitric oxide in the cerebral microcirculation. *Stroke* **30,** 2727-2734; discussion 2734.

ALPERS BJ, BERRY RG & PADDISON RM. (1959). Anatomical studies of the circle of Willis in normal brain. *AMA Arch Neurol Psychiatry* **81,** 409.

Amberg GC, Baker SA, Koh SD, Hatton WJ, Murray KJ, Horowitz B & Sanders KM. (2002). Characterization of the A-type potassium current in murine gastric antrum. *J Physiol* **544,** 417-428.

Amberg GC, Rossow CF, Navedo MF & Santana LF. (2004). NFATc3 regulates Kv2.1 expression in arterial smooth muscle. *J Biol Chem* **279,** 47326-47334.

Amberg GC & Santana LF. (2006). Kv2 channels oppose myogenic constriction of rat cerebral arteries. *Am J Physiol Cell Physiol* **291,** C348-356.

Andresen J, Shafi NI & Bryan RM, Jr. (2006). Endothelial influences on cerebrovascular tone. *J Appl Physiol* **100,** 318-327.

Anschutz S & Schubert R. (2005). Modulation of the myogenic response by neurogenic influences in rat small arteries. *Br J Pharmacol* **146,** 226-233.

Applewhite DA, Barzik M, Kojima S, Svitkina TM, Gertler FB & Borisy GG. (2007). Ena/VASP proteins have an anti-capping independent function in filopodia formation. *Mol Biol Cell* **18,** 2579-2591.

Archer SL, Wu XC, Thebaud B, Nsair A, Bonnet S, Tyrrell B, McMurtry MS, Hashimoto K, Harry G & Michelakis ED. (2004). Preferential expression and function of voltage-gated, O2-sensitive K+ channels in resistance pulmonary arteries explains regional heterogeneity in hypoxic pulmonary vasoconstriction: ionic diversity in smooth muscle cells. *Circ Res* **95,** 308-318.

Aszodi A, Pfeifer A, Ahmad M, Glauner M, Zhou XH, Ny L, Andersson KE, Kehrel B, Offermanns S & Fassler R. (1999). The vasodilator-stimulated phosphoprotein (VASP) is involved in cGMP- and cAMP-mediated inhibition of agonist-induced platelet aggregation, but is dispensable for smooth muscle function. *EMBO J* **18,** 37-48.

Bachmann C, Fischer L, Walter U & Reinhard M. (1999). The EVH2 domain of the vasodilator-stimulated phosphoprotein mediates tetramerization, F-actin binding, and actin bundle formation. *J Biol Chem* **274,** 23549-23557.

Baker CH & Sutton ET. (1993). Arteriolar endothelium-dependent vasodilation occurs during endotoxin shock. *AM J Physiol Heart Circ Physiol* **264,** H1118-H1123.

Barany M & Barany K. (1993). Dissociation of relaxation and myosin light chain dephosphorylation in porcine uterine muscle. *Arch Biochem Biophys* **305,** 202-204.

Barany M, Barron JT, Gu L & Barany K. (2001). Exchange of the actin-bound nucleotide in intact arterial smooth muscle. *J Biol Chem* **276,** 48398-48403.

Barzik M, Kotova TI, Higgs HN, Hazelwood L, Hanein D, Gertler FB & Schafer DA. (2005). Ena/VASP proteins enhance actin polymerization in the presence of barbed end capping proteins. *J Biol Chem* **280,** 28653-28662.

Bayliss WM. (1902). On the local reactions of the arterial wall to changes of internal pressure. *J Physiol* **28,** 220-231.

Beall AC, Kato K, Goldenring JR, Rasmussen H & Brophy CM. (1997). Cyclic nucleotide-dependent vasorelaxation is associated with the phosphorylation of a small heat shock-related protein. *J Biol Chem* **272,** 11283-11287.

Bear JE & Gertler FB. (2009). Ena/VASP: towards resolving a pointed controversy at the barbed end. *J Cell Sci* **122,** 1947-1953.

Bear JE, Svitkina TM, Krause M, Schafer DA, Loureiro JJ, Strasser GA, Maly IV, Chaga OY, Cooper JA, Borisy GG & Gertler FB. (2002). Antagonism between Ena/VASP proteins and actin filament capping regulates fibroblast motility. *Cell* **109,** 509-521.

Bearer EL, Prakash JM & Li Z. (2002). Actin dynamics in platelets. *Int Rev Cytol* **217,** 137-182.

Beech DJ & Barnes S. (1989). Characterization of a voltage-gated K+ channel that accelerates the rod response to dim light. *Neuron* **3,** 573-581.

Beech DJ & Bolton TB. (1989a). Two components of potassium current activated by depolarization of single smooth muscle cells from the rabbit portal vein. *J Physiol* **418,** 293-309.

Beech DJ & Bolton TB. (1989b). A voltage-dependent outward current with fast kinetics in single smooth muscle cells isolated from rabbit portal vein. *J Physiol* **412,** 397-414.

Belevych AE, Beck R, Tammaro P, Poston L & Smirnov SV. (2002). Developmental changes in the functional characteristics and expression of voltage-gated K+ channel currents in rat aortic myocytes. *Cardiovasc Res* **54,** 152-161.

Bentzen BH, Schmitt N, Calloe K, Dalby Brown W, Grunnet M & Olesen SP. (2006). The acrylamide (S)-1 differentially affects Kv7 (KCNQ) potassium channels. *Neuropharmacology* **51,** 1068-1077.

Benz PM, Blume C, Seifert S, Wilhelm S, Waschke J, Schuh K, Gertler F, Munzel T & Renne T. (2009). Differential VASP phosphorylation controls remodeling of the actin cytoskeleton. *J Cell Sci* **122,** 3954-3965.

Berczi V, Greene AS, Dornyei G, Csengody J, Hodi G, Kadar A & Monos E. (1992). Venous myogenic tone: studies in human and canine vessels. *Am J Physiol* **263,** H315-320.

Bezanilla F. (2000). The voltage sensor in voltage-dependent ion channels. *Physiol Rev* **80,** 555-592.

Bidani AK, Griffin KA, Williamson G, Wang X & Loutzenhiser R. (2009). Protective importance of the myogenic response in the renal circulation. *Hypertension* **54,** 393-398.

Bixby KA, Nanao MH, Shen NV, Kreusch A, Bellamy H, Pfaffinger PJ & Choe S. (1999). Zn2+-binding and molecular determinants of tetramerization in voltage-gated K+ channels. *Nat Struct Biol* **6,** 38-43.

Blume C, Benz PM, Walter U, Ha J, Kemp BE & Renne T. (2007). AMP-activated protein kinase impairs endothelial actin cytoskeleton assembly by phosphorylating vasodilator-stimulated phosphoprotein. *J Biol Chem* **282,** 4601-4612.

Bocksteins E, Labro AJ, Mayeur E, Bruyns T, Timmermans JP, Adriaensen D & Snyders DJ. (2009). Conserved negative charges in the N-terminal tetramerization domain mediate efficient assembly of Kv2.1 and Kv2.1/Kv6.4 channels. *J Biol Chem* **284,** 31625-31634.

Bocksteins E & Snyders DJ. (2012). Electrically silent Kv subunits: their molecular and functional characteristics. *Physiology (Bethesda)* **27,** 73-84.

Bolz SS, Vogel L, Sollinger D, Derwand R, Boer C, Pitson SM, Spiegel S & Pohl U. (2003a). Sphingosine kinase modulates microvascular tone and myogenic responses through activation of RhoA/Rho kinase. *Circulation* **108,** 342-347.

Bolz SS, Vogel L, Sollinger D, Derwand R, de Wit C, Loirand G & Pohl U. (2003b). Nitric oxide-induced decrease in calcium sensitivity of resistance arteries is attributable to activation of the myosin light chain phosphatase and antagonized by the RhoA/Rho kinase pathway. *Circulation* **107,** 3081-3087.

Brayden JE. (2002). Functional roles of KATP channels in vascular smooth muscle. *Clin Exp Pharmacol Physiol* **29,** 312-316.

Brayden JE, Earley S, Nelson MT & Reading S. (2008). Transient receptor potential (TRP) channels, vascular tone and autoregulation of cerebral blood flow. *Clin Exp Pharmacol Physiol* **35,** 1116-1120.

Brayden JE & Nelson MT. (1992). Regulation of arterial tone by activation of calcium-dependent potassium channels. *Science* **256,** 532-535.

Breitsprecher D, Kiesewetter AK, Linkner J, Urbanke C, Resch GP, Small JV & Faix J. (2008). Clustering of VASP actively drives processive, WH2 domain-mediated actin filament elongation. *EMBO J* **27,** 2943-2954.

Brekke JF, Gokina NI & Osol G. (2002). Vascular smooth muscle cell stress as a determinant of cerebral artery myogenic tone. *Am J Physiol Heart Circ Physiol* **283,** H2210-2216.

Brenner R, Perez GJ, Bonev AD, Eckman DM, Kosek JC, Wiler SW, Patterson AJ, Nelson MT & Aldrich RW. (2000). Vasoregulation by the beta1 subunit of the calcium-activated potassium channel. *Nature* **407,** 870-876.

Brindle NP, Holt MR, Davies JE, Price CJ & Critchley DR. (1996). The focal-adhesion vasodilator-stimulated phosphoprotein (VASP) binds to the proline-rich domain in vinculin. *Biochem J* **318 (Pt 3),** 753-757.

Brophy CM, Dickinson M & Woodrum D. (1999a). Phosphorylation of the small heat shock-related protein, HSP20, in vascular smooth muscles is associated with changes in the macromolecular associations of HSP20. *J Biol Chem* **274,** 6324-6329.

Brophy CM, Lamb S & Graham A. (1999b). The small heat shock-related protein-20 is an actin-associated protein. *J Vasc Surg* **29,** 326-333.

Brueggemann LI, Mackie AR, Mani BK, Cribbs LL & Byron KL. (2009). Differential effects of selective cyclooxygenase-2 inhibitors on vascular smooth muscle ion channels may account for differences in cardiovascular risk profiles. *Mol Pharmacol* **76,** 1053-1061.

Brueggemann LI, Moran CJ, Barakat JA, Yeh JZ, Cribbs LL & Byron KL. (2007). Vasopressin stimulates action potential firing by protein kinase C-dependent inhibition of KCNQ5 in A7r5 rat aortic smooth muscle cells. *Am J Physiol Heart Circ Physiol* **292,** H1352-1363.

Burton AC. (1951). On the physical equilibrium of small blood vessels. *Am J Physiol--Legacy Content* **164,** 319-329.

Butt E, Abel K, Krieger M, Palm D, Hoppe V, Hoppe J & Walter U. (1994). cAMP- and cGMP-dependent protein kinase phosphorylation sites of the focal adhesion vasodilator-stimulated phosphoprotein (VASP) in vitro and in intact human platelets. *J Biol Chem* **269,** 14509-14517.

Casey DP & Joyner MJ. (2012). Compensatory vasodilatation during hypoxic exercise: mechanisms responsible for matching oxygen supply to demand. *J Physiol* **590,** 6321-6326.

Casey DP, Madery BD, Curry TB, Eisenach JH, Wilkins BW & Joyner MJ. (2010). Nitric oxide contributes to the augmented vasodilatation during hypoxic exercise. *J Physiol* **588,** 373-385.

Castellano F, Le Clainche C, Patin D, Carlier MF & Chavrier P. (2001). A WASp-VASP complex regulates actin polymerization at the plasma membrane. *EMBO J* **20,** 5603-5614.

Cayatte AJ, Palacino JJ, Horten K & Cohen RA. (1994). Chronic inhibition of nitric oxide production accelerates neointima formation and impairs endothelial function in hypercholesterolemic rabbits. *Arterioscler Thromb* **14,** 753-759.

Chadha PS, Zunke F, Zhu HL, Davis AJ, Jepps TA, Olesen SP, Cole WC, Moffatt JD & Greenwood IA. (2012). Reduced KCNQ4-encoded voltage-dependent potassium channel activity underlies impaired beta-adrenoceptor-mediated relaxation of renal arteries in hypertension. *Hypertension* **59,** 877-884.

Chakraborty T, Ebel F, Domann E, Niebuhr K, Gerstel B, Pistor S, Temm-Grove CJ, Jockusch BM, Reinhard M, Walter U & et al. (1995). A focal adhesion factor directly linking intracellularly motile Listeria monocytogenes and Listeria ivanovii to the actin-based cytoskeleton of mammalian cells. *EMBO J* **14,** 1314-1321.

Chen M, Kellett WF & Petkov GV. (2010). Voltage-gated K(+) channels sensitive to stromatoxin-1 regulate myogenic and neurogenic contractions of rat urinary bladder smooth muscle. *Am J Physiol Regul Integr Comp Physiol* **299,** R177-184.

Chen TT, Luykenaar KD, Walsh EJ, Walsh MP & Cole WC. (2006). Key role of Kv1 channels in vasoregulation. *Circ Res* **99,** 53-60.

Chereau D & Dominguez R. (2006). Understanding the role of the G-actin-binding domain of Ena/VASP in actin assembly. *J Struct Biol* **155,** 195-201.

Cipolla MJ. (2009). The cerebral circulation. *Integrated Systems Physiology: From Molecule to Function* **1,** 1-59.

Cipolla MJ, Gokina NI & Osol G. (2002). Pressure-induced actin polymerization in vascular smooth muscle as a mechanism underlying myogenic behavior. *FASEB J* **16,** 72-76.

Cipolla MJ, Lessov N, Hammer ES & Curry AB. (2001). Threshold duration of ischemia for myogenic tone in middle cerebral arteries: effect on vascular smooth muscle actin. *Stroke* **32,** 1658-1664.

Cipolla MJ & Osol G. (1998). Vascular smooth muscle actin cytoskeleton in cerebral artery forced dilatation. *Stroke* **29,** 1223-1228.

Clement-Chomienne O, Walsh MP & Cole WC. (1996). Angiotensin II activation of protein kinase C decreases delayed rectifier K+ current in rabbit vascular myocytes. *J Physiol* **495,** 689-700.

Cole WC, Chen TT & Clement-Chomienne O. (2005). Myogenic regulation of arterial diameter: role of potassium channels with a focus on delayed rectifier potassium current. *Can J Physiol Pharmacol* **83,** 755-765.

Cole WC & Welsh DG. (2011). Role of myosin light chain kinase and myosin light chain phosphatase in the resistance arterial myogenic response to intravascular pressure. *Arch Biochem Biophys* **510,** 160-173.

Coppock EA & Tamkun MM. (2001). Differential expression of K(V) channel alpha- and beta-subunits in the bovine pulmonary arterial circulation. *Am J Physiol Lung Cell Mol Physiol* **281,** L1350-1360.

Cornwell TL, Pryzwansky KB, Wyatt TA & Lincoln TM. (1991). Regulation of sarcoplasmic reticulum protein phosphorylation by localized cyclic GMP-dependent protein kinase in vascular smooth muscle cells. *Mol Pharmacol* **40,** 923-931.

Coulson RJ, Chesler NC, Vitullo L & Cipolla MJ. (2002). Effects of ischemia and myogenic activity on active and passive mechanical properties of rat cerebral arteries. *Am J Physiol Heart Circ Physiol* **283,** H2268-2275.

Cox DH & Aldrich RW. (2000). Role of the beta1 subunit in large-conductance Ca(2+)-activated K(+) channel gating energetics. Mechanisms of enhanced Ca(2+) sensitivity. *J Gen Physiol* **116,** 411-432.

Cox RH, Fromme SJ, Folander KL & Swanson RJ. (2008). Voltage gated K+ channel expression in arteries of Wistar-Kyoto and spontaneously hypertensive rats. *Am J Hypertens* **21,** 213-218.

Davies AR & Kozlowski RZ. (2001). Kv channel subunit expression in rat pulmonary arteries. *Lung* **179,** 147-161.

Davis MJ & Hill MA. (1999). Signaling mechanisms underlying the vascular myogenic response. *Physiol Rev* **79,** 387-423.

Deruelle P, Balasubramaniam V, Kunig AM, Seedorf GJ, Markham NE & Abman SH. (2006). BAY 41-2272, a direct activator of soluble guanylate cyclase, reduces

right ventricular hypertrophy and prevents pulmonary vascular remodeling during chronic hypoxia in neonatal rats. *Biol Neonate* **90,** 135-144.

DiNubile MJ, Cassimeris L, Joyce M & Zigmond SH. (1995). Actin filament barbed-end capping activity in neutrophil lysates: the role of capping protein-beta 2. *Mol Biol Cell* **6,** 1659-1671.

Doughty JM & Langton PD. (2001). Measurement of chloride flux associated with the myogenic response in rat cerebral arteries. *J Physiol* **534,** 753-761.

Dowell ML, Lakser OJ, Gerthoffer WT, Fredberg JJ, Stelmack GL, Halayko AJ, Solway J & Mitchell RW. (2005). Latrunculin B increases force fluctuation-induced relengthening of ACh-contracted, isotonically shortened canine tracheal smooth muscle. *J Appl Physiol* **98,** 489-497.

Drees B, Friederich E, Fradelizi J, Louvard D, Beckerle MC & Golsteyn RM. (2000). Characterization of the interaction between zyxin and members of the Ena/vasodilator-stimulated phosphoprotein family of proteins. *J Biol Chem* **275,** 22503-22511.

Drewe JA, Verma S, Frech G & Joho RH. (1992). Distinct spatial and temporal expression patterns of K+ channel mRNAs from different subfamilies. *J Neurosci* **12,** 538-548.

Dupuis DS, Schroder RL, Jespersen T, Christensen JK, Christophersen P, Jensen BS & Olesen SP. (2002). Activation of KCNQ5 channels stably expressed in HEK293 cells by BMS-204352. *Eur J Pharmacol* **437,** 129-137.

Edwards G, Dora KA, Gardener MJ, Garland CJ & Weston AH. (1998). K+ is an endothelium-derived hyperpolarizing factor in rat arteries. *Nature* **396,** 269-272.

Eigenthaler M, Engelhardt S, Schinke B, Kobsar A, Schmitteckert E, Gambaryan S, Engelhardt CM, Krenn V, Eliava M, Jarchau T, Lohse MJ, Walter U & Hein L. (2003). Disruption of cardiac Ena-VASP protein localization in intercalated disks causes dilated cardiomyopathy. *Am J Physiol Heart Circ Physiol* **285,** H2471-2481.

El-Yazbi AF, Johnson RP, Walsh EJ, Takeya K, Walsh MP & Cole WC. (2010). Pressure-dependent contribution of Rho kinase-mediated calcium sensitization in serotonin-evoked vasoconstriction of rat cerebral arteries. *J Physiol* **588,** 1747-1762.

Escoubas P, Diochot S, Celerier ML, Nakajima T & Lazdunski M. (2002). Novel tarantula toxins for subtypes of voltage-dependent potassium channels in the Kv2 and Kv4 subfamilies. *Mol Pharmacol* **62,** 48-57.

Eto M. (2009). Regulation of cellular protein phosphatase-1 (PP1) by phosphorylation of the CPI-17 family, C-kinase-activated PP1 inhibitors. *J Biol Chem* **284,** 35273-35277.

Eto M, Ohmori T, Suzuki M, Furuya K & Morita F. (1995). A novel protein phosphatase-1 inhibitory protein potentiated by protein kinase C. Isolation from porcine aorta media and characterization. *J Biochem* **118,** 1104-1107.

Euser AG & Cipolla MJ. (2007). Cerebral blood flow autoregulation and edema formation during pregnancy in anesthetized rats. *Hypertension* **49,** 334-340.

Faraci FM & Heistad DD. (1990). Regulation of large cerebral arteries and cerebral microvascular pressure. *Circ Res* **66,** 8-17.

Faraci FM & Sobey CG. (1999). Role of soluble guanylate cyclase in dilator responses of the cerebral microcirculation. *Brain Res* **821,** 368-373.

Feliciano A, do Rosario HS, Goulao I, Borges MG, Silva M, Rego P, Silverio S & Pedro V. (1993). [Vasoactive endothelial factors]. *Rev Port Cardiol* **12,** 557-560, 510-551.

Feng J, Ito M, Ichikawa K, Isaka N, Nishikawa M, Hartshorne DJ & Nakano T. (1999). Inhibitory phosphorylation site for Rho-associated kinase on smooth muscle myosin phosphatase. *J Biol Chem* **274,** 37385-37390.

Ferro JM, Canhao P & Peralta R. (2008). Update on subarachnoid haemorrhage. *J Neurol* **255,** 465-479.

Ferron F, Rebowski G, Lee SH & Dominguez R. (2007). Structural basis for the recruitment of profilin-actin complexes during filament elongation by Ena/VASP. *EMBO J* **26,** 4597-4606.

Flavahan NA, Bailey SR, Flavahan WA, Mitra S & Flavahan S. (2005). Imaging remodeling of the actin cytoskeleton in vascular smooth muscle cells after mechanosensitive arteriolar constriction. *Am J Physiol Heart Circ Physiol* **288,** H660-669.

Fleming I & Busse R. (2003). Molecular mechanisms involved in the regulation of the endothelial nitric oxide synthase. *Am J Physiol Regul Integr Comp Physiol* **284,** R1-12.

Folkow B. (1949). Intravascular pressure as a factor regulating the tone of the small vessels. *Acta Physiol Scand* **17,** 289-310.

Folkow B. (1952). A study of the factors influencing the tone of denervated blood vessels perfused at various pressures. *Acta Physiol Scand* **27,** 99-117.

Fortin CF, McDonald PP, Fulop T & Lesur O. (2010). Sepsis, leukocytes, and nitric oxide (NO): an intricate affair. *Shock* **33,** 344-352.

Fredriksson S, Gullberg M, Jarvius J, Olsson C, Pietras K, Gustafsdottir SM, Ostman A & Landegren U. (2002). Protein detection using proximity-dependent DNA ligation assays. *Nat Biotechnol* **20,** 473-477.

Fukao M, Mason HS, Britton FC, Kenyon JL, Horowitz B & Keef KD. (1999). Cyclic GMP-dependent protein kinase activates cloned BKCa channels expressed in mammalian cells by direct phosphorylation at serine 1072. *J Biol Chem* **274,** 10927-10935.

Furman C, Sieminski AL, Kwiatkowski AV, Rubinson DA, Vasile E, Bronson RT, Fassler R & Gertler FB. (2007). Ena/VASP is required for endothelial barrier function in vivo. *J Cell Biol* **179,** 761-775.

Galustian C, Dye J, Leach L, Clark P & Firth JA. (1995). Actin cytoskeletal isoforms in human endothelial cells in vitro: alteration with cell passage. *In Vitro Cell Dev Biol Anim* **31,** 796-802.

Gardener MJ, Johnson IT, Burnham MP, Edwards G, Heagerty AM & Weston AH. (2004). Functional evidence of a role for two-pore domain potassium channels in rat mesenteric and pulmonary arteries. *Br J Pharmacol* **142,** 192-202.

Garg UC & Hassid A. (1989). Nitric oxide-generating vasodilators and 8-bromo-cyclic guanosine monophosphate inhibit mitogenesis and proliferation of cultured rat vascular smooth muscle cells. *J Clin Invest* **83,** 1774-1777.

Ge S, Song L & Pachter JS. (2005). Where is the blood-brain barrier ... really? *J Neurosci Res* **79,** 421-427.

Geese M, Loureiro JJ, Bear JE, Wehland J, Gertler FB & Sechi AS. (2002). Contribution of Ena/VASP proteins to intracellular motility of listeria requires phosphorylation and proline-rich core but not F-actin binding or multimerization. *Mol Biol Cell* **13,** 2383-2396.

Geese M, Schluter K, Rothkegel M, Jockusch BM, Wehland J & Sechi AS. (2000). Accumulation of profilin II at the surface of Listeria is concomitant with the onset of motility and correlates with bacterial speed. *J Cell Sci* **113 (Pt 8),** 1415-1426.

Gerthoffer WT. (2005). Actin cytoskeletal dynamics in smooth muscle contraction. *Can J Physiol Pharmacol* **83,** 851-856.

Giles TD, Sander GE, Nossaman BD & Kadowitz PJ. (2012). Impaired vasodilation in the pathogenesis of hypertension: focus on nitric oxide, endothelial-derived hyperpolarizing factors, and prostaglandins. *J Clin Hypertens (Greenwich)* **14,** 198-205.

Gocan NC, Scott JA & Tyml K. (2000). Nitric oxide produced via neuronal NOS may impair vasodilatation in septic rat skeletal muscle. *Am J Physiol Heart Circ Physiol* **278,** H1480-H1489.

Gokina NI & Osol G. (2002). Actin cytoskeletal modulation of pressure-induced depolarization and Ca(2+) influx in cerebral arteries. *Am J Physiol Heart Circ Physiol* **282,** H1410-1420.

Gokina NI, Park KM, McElroy-Yaggy K & Osol G. (2005). Effects of Rho kinase inhibition on cerebral artery myogenic tone and reactivity. *J Appl Physiol* **98,** 1940-1948.

Golding EM, Marrelli SP, You J & Bryan RM, Jr. (2002). Endothelium-derived hyperpolarizing factor in the brain: a new regulator of cerebral blood flow? *Stroke* **33,** 661-663.

Grassie ME, Sutherland C, Ulke-Lemee A, Chappellaz M, Kiss E, Walsh MP & MacDonald JA. (2012). Cross-talk between Rho-associated kinase and cyclic nucleotide-dependent kinase signaling pathways in the regulation of smooth muscle myosin light chain phosphatase. *J Biol Chem* **287,** 36356-36369.

Greenwood IA & Ohya S. (2009). New tricks for old dogs: KCNQ expression and role in smooth muscle. *Br J Pharmacol* **156,** 1196-1203.

Grosse R, Copeland JW, Newsome TP, Way M & Treisman R. (2003). A role for VASP in RhoA-Diaphanous signalling to actin dynamics and SRF activity. *EMBO J* **22,** 3050-3061.

Gschwend S, Henning RH, Pinto YM, de Zeeuw D, van Gilst WH & Buikema H. (2003). Myogenic constriction is increased in mesenteric resistance arteries from rats with chronic heart failure: instantaneous counteraction by acute AT1 receptor blockade. *Br J Pharmacol* **139,** 1317-1325.

Guia A, Wan X, Courtemanche M & Leblanc N. (1999). Local Ca2+ entry through L-type Ca2+ channels activates Ca2+-dependent K+ channels in rabbit coronary myocytes. *Circ Res* **84,** 1032-1042.

Gulbis JM, Zhou M, Mann S & MacKinnon R. (2000). Structure of the cytoplasmic beta subunit-T1 assembly of voltage-dependent K+ channels. *Science* **289,** 123-127.

Gunst SJ & Zhang W. (2008). Actin cytoskeletal dynamics in smooth muscle: a new paradigm for the regulation of smooth muscle contraction. *Am J Physiol Cell Physiol* **295,** C576-587.

Gurney AM, Osipenko ON, MacMillan D & Kempsill FE. (2002). Potassium channels underlying the resting potential of pulmonary artery smooth muscle cells. *Clin Exp Pharmacol Physiol* **29,** 330-333.

Gurney AM, Osipenko ON, MacMillan D, McFarlane KM, Tate RJ & Kempsill FE. (2003). Two-pore domain K channel, TASK-1, in pulmonary artery smooth muscle cells. *Circ Res* **93,** 957-964.

Gutman GA, Chandy KG, Adelman JP, Aiyar J, Bayliss DA, Clapham DE, Covarriubias M, Desir GV, Furuichi K, Ganetzky B, Garcia ML, Grissmer S, Jan LY, Karschin A, Kim D, Kuperschmidt S, Kurachi Y, Lazdunski M, Lesage F, Lester HA, McKinnon D, Nichols CG, O'Kelly I, Robbins J, Robertson GA, Rudy B, Sanguinetti M, Seino S, Stuehmer W, Tamkun MM, Vandenberg CA, Wei A, Wulff H & Wymore RS. (2003). International Union of Pharmacology. XLI. Compendium of voltage-gated ion channels: potassium channels. *Pharmacol Rev* **55,** 583-586.

Haffner C, Jarchau T, Reinhard M, Hoppe J, Lohmann SM & Walter U. (1995). Molecular cloning, structural analysis and functional expression of the proline-rich focal adhesion and microfilament-associated protein VASP. *EMBO J* **14,** 19-27.

Halbrugge M, Friedrich C, Eigenthaler M, Schanzenbacher P & Walter U. (1990). Stoichiometric and reversible phosphorylation of a 46-kDa protein in human platelets in response to cGMP- and cAMP-elevating vasodilators. *J Biol Chem* **265,** 3088-3093.

Halbrugge M & Walter U. (1989). Purification of a vasodilator-regulated phosphoprotein from human platelets. *Eur J Biochem* **185,** 41-50.

Harbeck B, Huttelmaier S, Schluter K, Jockusch BM & Illenberger S. (2000). Phosphorylation of the vasodilator-stimulated phosphoprotein regulates its interaction with actin. *J Biol Chem* **275,** 30817-30825.

Harder DR. (1988). Increased sensitivity of cat cerebral arteries to serotonin upon elevation of transmural pressure. *Pflugers Arch* **411,** 698-700.

Harder DR & Waters A. (1983). Electromechanical coupling in feline basilar artery in response to serotonin. *Eur J Pharmacol* **93,** 95-100.

Harper SL, Bohlen HG & Rubin MJ. (1984). Arterial and microvascular contributions to cerebral cortical autoregulation in rats. *Am J Physiol* **246,** H17-24.

Harrell JW, Morgan BJ & Schrage WG. (2013). Impaired hypoxic cerebral vasodilation in younger adults with metabolic syndrome. *Diab Vasc Dis Res* **10,** 135-142.

Haug LS, Jensen V, Hvalby O, Walaas SI & Ostvold AC. (1999). Phosphorylation of the inositol 1,4,5-trisphosphate receptor by cyclic nucleotide-dependent kinases in vitro and in rat cerebellar slices in situ. *J Biol Chem* **274,** 7467-7473.

Hauser W, Knobeloch KP, Eigenthaler M, Gambaryan S, Krenn V, Geiger J, Glazova M, Rohde E, Horak I, Walter U & Zimmer M. (1999). Megakaryocyte hyperplasia and enhanced agonist-induced platelet activation in vasodilator-stimulated phosphoprotein knockout mice. *Proc Natl Acad Sci U S A* **96,** 8120-8125.

Heagerty AM, Heerkens EH & Izzard AS. (2010). Small artery structure and function in hypertension. *J Cell Mol Med* **14,** 1037-1043.

Heginbotham L, Lu Z, Abramson T & MacKinnon R. (1994). Mutations in the K+ channel signature sequence. *Biophys J* **66,** 1061-1067.

Heling A, Zimmermann R, Kostin S, Maeno Y, Hein S, Devaux B, Bauer E, Klovekorn WP, Schlepper M, Schaper W & Schaper J. (2000). Increased expression of cytoskeletal, linkage, and extracellular proteins in failing human myocardium. *Circ Res* **86,** 846-853.

Herrera AM, Martinez EC & Seow CY. (2004). Electron microscopic study of actin polymerization in airway smooth muscle. *Am J Physiol Lung Cell Mol Physiol* **286,** L1161-1168.

Hill M & Davis M. (2012). Local Control of Microvascular Perfusion. In *Colloquium Series on Integrated Systems Physiology: From Molecule to Function*, pp. 1-148. Morgan & Claypool Life Sciences.

Hill MA, Zou H, Potocnik SJ, Meininger GA & Davis MJ. (2001). Invited review: arteriolar smooth muscle mechanotransduction: Ca(2+) signaling pathways underlying myogenic reactivity. *J Appl Physiol* **91,** 973-983.

Hilton S & Spyer K. (1980). Central nervous regulation of vascular resistance. *Annu Rev Physiol* **42,** 399-411.

Hirano K. (2007). Current topics in the regulatory mechanism underlying the Ca2+ sensitization of the contractile apparatus in vascular smooth muscle. *J Pharmacol Sci* **104,** 109-115.

Hofmann F, Ammendola A & Schlossmann J. (2000). Rising behind NO: cGMP-dependent protein kinases. *J Cell Sci* **113,** 1671-1676.

Hollenberg SM, Cunnion RE & Zimmerberg J. (1993). Nitric oxide synthase inhibition reverses arteriolar hyporesponsiveness to catecholamines in septic rats. *Am J Physiol Heart Circ Physiol* **264,** H660-H663.

Holt MR, Critchley DR & Brindle NP. (1998). The focal adhesion phosphoprotein, VASP. *Int J Biochem Cell Biol* **30,** 307-311.

Howe AK, Hogan BP & Juliano RL. (2002). Regulation of vasodilator-stimulated phosphoprotein phosphorylation and interaction with Abl by protein kinase A and cell adhesion. *J Biol Chem* **277,** 38121-38126.

Hugnot JP, Salinas M, Lesage F, Guillemare E, de Weille J, Heurteaux C, Mattei MG & Lazdunski M. (1996). Kv8.1, a new neuronal potassium channel subunit with specific inhibitory properties towards Shab and Shaw channels. *EMBO J* **15,** 3322-3331.

Huttelmaier S, Harbeck B, Steffens O, Messerschmidt T, Illenberger S & Jockusch BM. (1999). Characterization of the actin binding properties of the vasodilator-stimulated phosphoprotein VASP. *FEBS Lett* **451,** 68-74.

Ihara E & MacDonald JA. (2007). The regulation of smooth muscle contractility by zipper-interacting protein kinase. *Can J Physiol Pharmacol* **85,** 79-87.

Imaizumi Y. (1993). [Mechanisms involved in diversity of membrane excitability in smooth muscle cells]. *Nihon Yakurigaku Zasshi* **101,** 219-231.

Izzard AS, Graham D, Burnham MP, Heerkens EH, Dominiczak AF & Heagerty AM. (2003). Myogenic and structural properties of cerebral arteries from the stroke-prone spontaneously hypertensive rat. *Am J Physiol Heart Circ Physiol* **285,** H1489-1494.

Jackson WF. (2005). Potassium channels in the peripheral microcirculation. *Microcirculation* **12,** 113-127.

Jaggar JH. (2001). Intravascular pressure regulates local and global Ca(2+) signaling in cerebral artery smooth muscle cells. *Am J Physiol Cell Physiol* **281,** C439-448.

Jahromi BS, Aihara Y, Ai J, Zhang ZD, Nikitina E & Macdonald RL. (2008a). Voltage-gated K+ channel dysfunction in myocytes from a dog model of subarachnoid hemorrhage. *J Cereb Blood Flow Metab* **28,** 797-811.

Jahromi BS, Aihara Y, Ai J, Zhang ZD, Weyer G, Nikitina E, Yassari R, Houamed KM & Macdonald RL. (2008b). Temporal profile of potassium channel dysfunction in cerebrovascular smooth muscle after experimental subarachnoid haemorrhage. *Neurosci Lett* **440,** 81-86.

Jarajapu YP & Knot HJ. (2005). Relative contribution of Rho kinase and protein kinase C to myogenic tone in rat cerebral arteries in hypertension. *Am J Physiol Heart Circ Physiol* **289,** H1917-1922.

Jentsch TJ. (2000). Neuronal KCNQ potassium channels: physiology and role in disease. *Nat Rev Neurosci* **1,** 21-30.

Jepps TA, Chadha PS, Davis AJ, Harhun MI, Cockerill GW, Olesen SP, Hansen RS & Greenwood IA. (2011). Downregulation of Kv7.4 channel activity in primary and secondary hypertension. *Circulation* **124,** 602-611.

Jockusch BM, Murk K & Rothkegel M. (2007). The profile of profilins. *Rev Physiol Biochem Pharmacol* **159,** 131-149.

Johnson PC. (1986). Autoregulation of blood flow. *Circ Res* **59,** 483-495.

Johnson RP, El-Yazbi AF, Hughes MF, Schriemer DC, Walsh EJ, Walsh MP & Cole WC. (2009a). Identification and functional characterization of protein kinase A-catalyzed phosphorylation of potassium channel Kv1.2 at serine 449. *J Biol Chem* **284,** 16562-16574.

Johnson RP, El-Yazbi AF, Takeya K, Walsh EJ, Walsh MP & Cole WC. (2009b). Ca2+ sensitization via phosphorylation of myosin phosphatase targeting subunit at threonine-855 by Rho kinase contributes to the arterial myogenic response. *J Physiol* **587,** 2537-2553.

Joshi S, Balan P & Gurney AM. (2006). Pulmonary vasoconstrictor action of KCNQ potassium channel blockers. *Respir Res* **7,** 31.

Joshi S, Sedivy V, Hodyc D, Herget J & Gurney AM. (2009). KCNQ modulators reveal a key role for KCNQ potassium channels in regulating the tone of rat pulmonary artery smooth muscle. *J Pharmacol Exp Ther* **329,** 368-376.

Juncos LA, Garvin J, Carretero OA & Ito S. (1995). Flow modulates myogenic responses in isolated microperfused rabbit afferent arterioles via endothelium-derived nitric oxide. *J Clin Invest* **95,** 2741.

Kang F, Laine RO, Bubb MR, Southwick FS & Purich DL. (1997). Profilin interacts with the Gly-Pro-Pro-Pro-Pro-Pro sequences of vasodilator-stimulated phosphoprotein

(VASP): implications for actin-based Listeria motility. *Biochemistry* **36,** 8384-8392.

Kerschensteiner D, Monje F & Stocker M. (2003). Structural determinants of the regulation of the voltage-gated potassium channel Kv2.1 by the modulatory alpha-subunit Kv9.3. *J Biol Chem* **278,** 18154-18161.

Kerschensteiner D, Soto F & Stocker M. (2005). Fluorescence measurements reveal stoichiometry of K+ channels formed by modulatory and delayed rectifier alpha-subunits. *Proc Natl Acad Sci U S A* **102,** 6160-6165.

Kerschensteiner D & Stocker M. (1999). Heteromeric assembly of Kv2.1 with Kv9.3: effect on the state dependence of inactivation. *Biophys J* **77,** 248-257.

Khavandi K, Greenstein AS, Sonoyama K, Withers S, Price A, Malik RA & Heagerty AM. (2009). Myogenic tone and small artery remodelling: insight into diabetic nephropathy. *Nephrol Dial Transplant* **24,** 361-369.

Kim HR, Appel S, Vetterkind S, Gangopadhyay SS & Morgan KG. (2008a). Smooth muscle signalling pathways in health and disease. *J Cell Mol Med* **12,** 2165-2180.

Kim HR, Gallant C, Leavis PC, Gunst SJ & Morgan KG. (2008b). Cytoskeletal remodeling in differentiated vascular smooth muscle is actin isoform dependent and stimulus dependent. *Am J Physiol Cell Physiol* **295,** C768-778.

Kim HR, Graceffa P, Ferron F, Gallant C, Boczkowska M, Dominguez R & Morgan KG. (2010a). Actin polymerization in differentiated vascular smooth muscle cells requires vasodilator-stimulated phosphoprotein. *Am J Physiol Cell Physiol* **298,** C559-571.

Kim HR, Leavis PC, Graceffa P, Gallant C & Morgan KG. (2010b). A new method for direct detection of the sites of actin polymerization in intact cells and its application to differentiated vascular smooth muscle. *Am J Physiol Cell Physiol* **299,** C988-993.

Kim M & Perrino BA. (2007). CaM kinase II activation and phospholamban phosphorylation by SNP in murine gastric antrum smooth muscles. *Am J Physiol Gastrointest Liver Physiol* **292,** G1045-1054.

Knot HJ & Nelson MT. (1995). Regulation of membrane potential and diameter by voltage-dependent K+ channels in rabbit myogenic cerebral arteries. *Am J Physiol* **269,** H348-355.

Knot HJ & Nelson MT. (1998). Regulation of arterial diameter and wall [Ca2+] in cerebral arteries of rat by membrane potential and intravascular pressure. *J Physiol* **508 (Pt 1),** 199-209.

Ko EA, Han J, Jung ID & Park WS. (2008). Physiological roles of K+ channels in vascular smooth muscle cells. *J Smooth Muscle Res* **44,** 65-81.

Koga T, Yoshida Y, Cai JQ, Islam MO & Imai S. (1994). Purification and characterization of 240-kDa cGMP-dependent protein kinase substrate of vascular smooth muscle. Close resemblance to inositol 1,4,5-trisphosphate receptor. *J Biol Chem* **269,** 11640-11647.

Kotecha N & Hill MA. (2005). Myogenic contraction in rat skeletal muscle arterioles: smooth muscle membrane potential and Ca(2+) signaling. *Am J Physiol Heart Circ Physiol* **289,** H1326-1334.

Krause M, Dent EW, Bear JE, Loureiro JJ & Gertler FB. (2003). Ena/VASP proteins: regulators of the actin cytoskeleton and cell migration. *Annu Rev Cell Dev Biol* **19,** 541-564.

Krause M, Sechi AS, Konradt M, Monner D, Gertler FB & Wehland J. (2000). Fyn-binding protein (Fyb)/SLP-76-associated protein (SLAP), Ena/vasodilator-stimulated phosphoprotein (VASP) proteins and the Arp2/3 complex link T cell receptor (TCR) signaling to the actin cytoskeleton. *J Cell Biol* **149,** 181-194.

Kreusch A, Pfaffinger PJ, Stevens CF & Choe S. (1998). Crystal structure of the tetramerization domain of the Shaker potassium channel. *Nature* **392,** 945-948.

Kubo Y, Adelman JP, Clapham DE, Jan LY, Karschin A, Kurachi Y, Lazdunski M, Nichols CG, Seino S & Vandenberg CA. (2005). International Union of Pharmacology. LIV. Nomenclature and molecular relationships of inwardly rectifying potassium channels. *Pharmacol Rev* **57,** 509-526.

Kuhnel K, Jarchau T, Wolf E, Schlichting I, Walter U, Wittinghofer A & Strelkov SV. (2004). The VASP tetramerization domain is a right-handed coiled coil based on a 15-residue repeat. *Proc Natl Acad Sci U S A* **101,** 17027-17032.

Kuo IY, Ellis A, Seymour VA, Sandow SL & Hill CE. (2010). Dihydropyridine-insensitive calcium currents contribute to function of small cerebral arteries. *J Cereb Blood Flow Metab* **30,** 1226-1239.

Kwiatkowski AV, Gertler FB & Loureiro JJ. (2003). Function and regulation of Ena/VASP proteins. *Trends Cell Biol* **13,** 386-392.

Kwiatkowski AV, Rubinson DA, Dent EW, Edward van Veen J, Leslie JD, Zhang J, Mebane LM, Philippar U, Pinheiro EM, Burds AA, Bronson RT, Mori S, Fassler R & Gertler FB. (2007). Ena/VASP Is Required for neuritogenesis in the developing cortex. *Neuron* **56,** 441-455.

Lagaud G, Gaudreault N, Moore ED, Van Breemen C & Laher I. (2002). Pressure-dependent myogenic constriction of cerebral arteries occurs independently of voltage-dependent activation. *Am J Physiol Heart Circ Physiol* **283,** H2187-2195.

Lagaud GJ, Skarsgard PL, Laher I & van Breemen C. (1999). Heterogeneity of endothelium-dependent vasodilation in pressurized cerebral and small mesenteric resistance arteries of the rat. *J Pharmacol Exp Ther* **290,** 832-839.

Laurent V, Loisel TP, Harbeck B, Wehman A, Grobe L, Jockusch BM, Wehland J, Gertler FB & Carlier MF. (1999). Role of proteins of the Ena/VASP family in actin-based motility of Listeria monocytogenes. *J Cell Biol* **144,** 1245-1258.

Lawrence DW, Comerford KM & Colgan SP. (2002). Role of VASP in reestablishment of epithelial tight junction assembly after Ca2+ switch. *Am J Physiol Cell Physiol* **282,** C1235-1245.

Lebrand C, Dent EW, Strasser GA, Lanier LM, Krause M, Svitkina TM, Borisy GG & Gertler FB. (2004). Critical role of Ena/VASP proteins for filopodia formation in neurons and in function downstream of netrin-1. *Neuron* **42,** 37-49.

Lee S & Chung CY. (2009). Role of VASP phosphorylation for the regulation of microglia chemotaxis via the regulation of focal adhesion formation/maturation. *Mol Cell Neurosci* **42,** 382-390.

Lin WH, Nebhan CA, Anderson BR & Webb DJ. (2010). Vasodilator-stimulated phosphoprotein (VASP) induces actin assembly in dendritic spines to promote their development and potentiate synaptic strength. *J Biol Chem* **285,** 36010-36020.

Lincoln TM, Dey N & Sellak H. (2001). Invited review: cGMP-dependent protein kinase signaling mechanisms in smooth muscle: from the regulation of tone to gene expression. *J Appl Physiol* **91,** 1421-1430.

Lincoln TM, Wu X, Sellak H, Dey N & Choi CS. (2006). Regulation of vascular smooth muscle cell phenotype by cyclic GMP and cyclic GMP-dependent protein kinase. *Front Biosci* **11,** 356-367.

Lindsay SL, Ramsey S, Aitchison M, Renne T & Evans TJ. (2007). Modulation of lamellipodial structure and dynamics by NO-dependent phosphorylation of VASP Ser239. *J Cell Sci* **120,** 3011-3021.

Liu H, Xiong Z & Sperelakis N. (1997). Cyclic nucleotides regulate the activity of L-type calcium channels in smooth muscle cells from rat portal vein. *J Mol Cell Cardiol* **29,** 1411-1421.

Livak KJ & Schmittgen TD. (2001). Analysis of relative gene expression data using real-time quantitative PCR and the 2(-Delta Delta C(T)) Method. *Methods* **25,** 402-408.

Loisel TP, Boujemaa R, Pantaloni D & Carlier MF. (1999). Reconstitution of actin-based motility of Listeria and Shigella using pure proteins. *Nature* **401,** 613-616.

Lombard JH, Eskinder H, Kauser K, Osborn JL & Harder DR. (1990). Enhanced norepinephrine sensitivity in renal arteries at elevated transmural pressure. *Am J Physiol* **259,** H29-33.

Long SB, Campbell EB & Mackinnon R. (2005). Crystal structure of a mammalian voltage-dependent Shaker family K+ channel. *Science* **309,** 897-903.

Longman SD & Hamilton TC. (1992). Potassium channel activator drugs: mechanism of action, pharmacological properties, and therapeutic potential. *Med Res Rev* **12,** 73-148.

Loutzenhiser R, Bidani A & Chilton L. (2002). Renal myogenic response: kinetic attributes and physiological role. *Circ Res* **90,** 1316-1324.

Loutzenhiser R, Griffin K, Williamson G & Bidani A. (2006). Renal autoregulation: new perspectives regarding the protective and regulatory roles of the underlying mechanisms. *Am J Physiol Regul Integr Comp Physiol* **290,** R1153-1167.

Lubbe A, Garrison R, Cryer H, Alsip N & Harris P. (1992). EDRF as a possible mediator of sepsis-induced arteriolar dilation in skeletal muscle. *Am J Physiol Heart Circ Physiol* **262,** H880-H887.

Luykenaar KD, El-Rahman RA, Walsh MP & Welsh DG. (2009). Rho-kinase-mediated suppression of KDR current in cerebral arteries requires an intact actin cytoskeleton. *Am J Physiol Heart Circ Physiol* **296,** H917-926.

MacDonald JA, Walker LA, Nakamoto RK, Gorenne I, Somlyo AV, Somlyo AP & Haystead TA. (2000). Phosphorylation of telokin by cyclic nucleotide kinases and the identification of in vivo phosphorylation sites in smooth muscle. *FEBS Lett* **479,** 83-88.

Macdonald RL, Pluta RM & Zhang JH. (2007). Cerebral vasospasm after subarachnoid hemorrhage: the emerging revolution. *Nat Clin Pract Neurol* **3,** 256-263.

Mackie AR, Brueggemann LI, Henderson KK, Shiels AJ, Cribbs LL, Scrogin KE & Byron KL. (2008). Vascular KCNQ potassium channels as novel targets for the control of mesenteric artery constriction by vasopressin, based on studies in single cells, pressurized arteries, and in vivo measurements of mesenteric vascular resistance. *J Pharmacol Exp Ther* **325,** 475-483.

Main MJ, Cryan JE, Dupere JR, Cox B, Clare JJ & Burbidge SA. (2000). Modulation of KCNQ2/3 potassium channels by the novel anticonvulsant retigabine. *Mol Pharmacol* **58,** 253-262.

Mani BK, Brueggemann LI, Cribbs LL & Byron KL. (2011). Activation of vascular KCNQ (Kv7) potassium channels reverses spasmogen-induced constrictor responses in rat basilar artery. *Br J Pharmacol* **164,** 237-249.

Martens JR, Sakamoto N, Sullivan SA, Grobaski TD & Tamkun MM. (2001). Isoform-specific localization of voltage-gated K+ channels to distinct lipid raft populations. Targeting of Kv1.5 to caveolae. *J Biol Chem* **276,** 8409-8414.

Martinez-Lemus LA, Crow T, Davis MJ & Meininger GA. (2005). alphavbeta3- and alpha5beta1-integrin blockade inhibits myogenic constriction of skeletal muscle resistance arterioles. *Am J Physiol Heart Circ Physiol* **289,** H322-329.

Maruoka M, Sato M, Yuan Y, Ichiba M, Fujii R, Ogawa T, Ishida-Kitagawa N, Takeya T & Watanabe N. (2012). Abi-1-bridged tyrosine phosphorylation of VASP by Abelson kinase impairs association of VASP to focal adhesions and regulates leukaemic cell adhesion. *Biochem J* **441,** 889-899.

Mauss S, Koch G, Kreye VA & Aktories K. (1989). Inhibition of the contraction of the isolated longitudinal muscle of the guinea-pig ileum by botulinum C2 toxin: evidence for a role of G/F-actin transition in smooth muscle contraction. *Naunyn Schmiedebergs Arch Pharmacol* **340,** 345-351.

McCrossan ZA & Abbott GW. (2004). The MinK-related peptides. *Neuropharmacology* **47,** 787-821.

McDaniel NL, Chen XL, Singer HA, Murphy RA & Rembold CM. (1992). Nitrovasodilators relax arterial smooth muscle by decreasing [Ca2+] i and uncoupling stress from myosin phosphorylation. *Am J Physiol Cell Physiol* **263,** C461-C467.

McNamara DB, Bedi B, Aurora H, Tena L, Ignarro LJ, Kadowitz PJ & Akers DL. (1993). L-arginine inhibits balloon catheter-induced intimal hyperplasia. *Biochem Biophys Res Commun* **193,** 291-296.

Mederos y Schnitzler M, Storch U, Meibers S, Nurwakagari P, Breit A, Essin K, Gollasch M & Gudermann T. (2008). Gq-coupled receptors as mechanosensors mediating myogenic vasoconstriction. *EMBO J* **27,** 3092-3103.

Mehta D & Gunst SJ. (1999). Actin polymerization stimulated by contractile activation regulates force development in canine tracheal smooth muscle. *J Physiol* **519 Pt 3,** 829-840.

Meininger GA & Faber JE. (1991). Adrenergic facilitation of myogenic response in skeletal muscle arterioles. *Am J Physiol* **260,** H1424-1432.

Mendelev NN, Williams VS & Tulis DA. (2009). Antigrowth properties of BAY 41-2272 in vascular smooth muscle cells. *J Cardiovasc Pharmacol* **53,** 121-131.

Miller JR, Silver PJ & Stull JT. (1983). The role of myosin light chain kinase phosphorylation in beta-adrenergic relaxation of tracheal smooth muscle. *Mol Pharmacol* **24,** 235-242.

Mironneau J & Gargouil YM. (1979). Action of indapamide on excitation-contraction coupling in vascular smooth muscle. *Eur J Pharmacol* **57,** 57-67.

Moreno-Dominguez A, Cidad P, Miguel-Velado E, Lopez-Lopez JR & Perez-Garcia MT. (2009). De novo expression of Kv6.3 contributes to changes in vascular smooth muscle cell excitability in a hypertensive mice strain. *J Physiol* **587,** 625-640.

Moreno-Dominguez A, Colinas O, El-Yazbi A, Walsh E, Hill MA, Walsh MP & Cole WC. (2013). Calcium Sensitization Due to Myosin Light Chain Phosphatase Inhibition and Cytoskeletal Reorganization in The Myogenic Response of Skeletal Muscle Resistance Arteries. *J Physiol*.

Morgado M, Cairrao E, Santos-Silva AJ & Verde I. (2012). Cyclic nucleotide-dependent relaxation pathways in vascular smooth muscle. *Cell Mol Life Sci* **69,** 247-266.

Moss M & Martin GS. (2004). A global perspective on the epidemiology of sepsis. *Intensive Care Med* **30,** 527-529.

Mufti RE, Brett SE, Tran CH, Abd El-Rahman R, Anfinogenova Y, El-Yazbi A, Cole WC, Jones PP, Chen SR & Welsh DG. (2010). Intravascular pressure augments cerebral arterial constriction by inducing voltage-insensitive Ca2+ waves. *J Physiol* **588,** 3983-4005.

Mulvany MJ & Aalkjaer C. (1990). Structure and function of small arteries. *Physiol Rev* **70,** 921-961.

Muranyi A, Derkach D, Erdodi F, Kiss A, Ito M & Hartshorne DJ. (2005). Phosphorylation of Thr695 and Thr850 on the myosin phosphatase target subunit: inhibitory effects and occurrence in A7r5 cells. *FEBS Lett* **579,** 6611-6615.

Murphy ME & Brayden JE. (1995). Apamin-sensitive K+ channels mediate an endothelium-dependent hyperpolarization in rabbit mesenteric arteries. *J Physiol* **489 (Pt 3),** 723-734.

Nakajo K, Ulbrich MH, Kubo Y & Isacoff EY. (2010). Stoichiometry of the KCNQ1 - KCNE1 ion channel complex. *Proc Natl Acad Sci U S A* **107,** 18862-18867.

Nakamura K, Koga Y, Sakai H, Homma K & Ikebe M. (2007). cGMP-dependent relaxation of smooth muscle is coupled with the change in the phosphorylation of myosin phosphatase. *Circ Res* **101,** 712-722.

Nelson MT, Cheng H, Rubart M, Santana LF, Bonev AD, Knot HJ & Lederer WJ. (1995). Relaxation of arterial smooth muscle by calcium sparks. *Science* **270,** 633-637.

Nelson MT & Quayle JM. (1995). Physiological roles and properties of potassium channels in arterial smooth muscle. *Am J Physiol* **268,** C799-822.

Niebuhr K, Ebel F, Frank R, Reinhard M, Domann E, Carl UD, Walter U, Gertler FB, Wehland J & Chakraborty T. (1997). A novel proline-rich motif present in ActA of Listeria monocytogenes and cytoskeletal proteins is the ligand for the EVH1 domain, a protein module present in the Ena/VASP family. *EMBO J* **16,** 5433-5444.

Nishimura J & van Breemen C. (1989). Direct regulation of smooth muscle contractile elements by second messengers. *Biochem Biophys Res Commun* **163,** 929-935.

Nishizawa S & Laher I. (2005). Signaling mechanisms in cerebral vasospasm. *Trends Cardiovasc Med* **15,** 24-34.

Niwa K, Kazama K, Younkin L, Younkin SG, Carlson GA & Iadecola C. (2002). Cerebrovascular autoregulation is profoundly impaired in mice overexpressing amyloid precursor protein. *Am J Physiol Heart Circ Physiol* **283,** H315-H323.

Niwa N & Nerbonne JM. (2010). Molecular determinants of cardiac transient outward potassium current (I(to)) expression and regulation. *J Mol Cell Cardiol* **48,** 12-25.

Obara K & Yabu H. (1994). Effect of cytochalasin B on intestinal smooth muscle cells. *Eur J Pharmacol* **255,** 139-147.

Oelze M, Mollnau H, Hoffmann N, Warnholtz A, Bodenschatz M, Smolenski A, Walter U, Skatchkov M, Meinertz T & Munzel T. (2000). Vasodilator-stimulated phosphoprotein serine 239 phosphorylation as a sensitive monitor of defective nitric oxide/cGMP signaling and endothelial dysfunction. *Circ Res* **87,** 999-1005.

Ohashi J, Sawada A, Nakajima S, Noda K, Takaki A & Shimokawa H. (2012). Mechanisms for enhanced endothelium-derived hyperpolarizing factor-mediated responses in microvessels in mice. *Circ J* **76,** 1768-1779.

Ohya S, Sergeant GP, Greenwood IA & Horowitz B. (2003). Molecular variants of KCNQ channels expressed in murine portal vein myocytes: a role in delayed rectifier current. *Circ Res* **92,** 1016-1023.

Okabe K, Terada K, Kitamura K & Kuriyama H. (1987). Selective and long-lasting inhibitory actions of the dihydropyridine derivative, CV-4093, on calcium currents in smooth muscle cells of the rabbit pulmonary artery. *J Pharmacol Exp Ther* **243,** 703-710.

Olschewski A, Li Y, Tang B, Hanze J, Eul B, Bohle RM, Wilhelm J, Morty RE, Brau ME, Weir EK, Kwapiszewska G, Klepetko W, Seeger W & Olschewski H. (2006). Impact of TASK-1 in human pulmonary artery smooth muscle cells. *Circ Res* **98,** 1072-1080.

Olsen TS, Larsen B, Skriver EB, Herning M, Enevoldsen E & Lassen NA. (1981). Focal cerebral hyperemia in acute stroke. Incidence, pathophysiology and clinical significance. *Stroke* **12,** 598-607.

Opazo Saez A, Zhang W, Wu Y, Turner CE, Tang DD & Gunst SJ. (2004). Tension development during contractile stimulation of smooth muscle requires recruitment of paxillin and vinculin to the membrane. *Am J Physiol Cell Physiol* **286,** C433-447.

Osol G, Brekke JF, McElroy-Yaggy K & Gokina NI. (2002). Myogenic tone, reactivity, and forced dilatation: a three-phase model of in vitro arterial myogenic behavior. *Am J Physiol Heart Circ Physiol* **283,** H2260-2267.

Ottschytsch N, Raes A, Van Hoorick D & Snyders DJ. (2002). Obligatory heterotetramerization of three previously uncharacterized Kv channel alpha-subunits identified in the human genome. *Proc Natl Acad Sci U S A* **99,** 7986-7991.

Owens GK. (1995). Regulation of differentiation of vascular smooth muscle cells. *Physiol Rev* **75,** 487-517.

Padget DH. (1944). The circle of Willis. Its embryology and anatomy. *Intracranial Arterial Aneurysms New York, Hafner,* 67-90.

Pang H, Guo Z, Su W, Xie Z, Eto M & Gong MC. (2005). RhoA-Rho kinase pathway mediates thrombin- and U-46619-induced phosphorylation of a myosin phosphatase inhibitor, CPI-17, in vascular smooth muscle cells. *Am J Physiol Cell Physiol* **289,** C352-360.

Pasic L, Kotova T & Schafer DA. (2008). Ena/VASP proteins capture actin filament barbed ends. *J Biol Chem* **283,** 9814-9819.

Patel AJ, Lazdunski M & Honore E. (1997). Kv2.1/Kv9.3, a novel ATP-dependent delayed-rectifier K+ channel in oxygen-sensitive pulmonary artery myocytes. *EMBO J* **16,** 6615-6625.

Pfitzer G. (2001). Invited review: regulation of myosin phosphorylation in smooth muscle. *J Appl Physiol* **91,** 497-503.

Plane F, Johnson R, Kerr P, Wiehler W, Thorneloe K, Ishii K, Chen T & Cole W. (2005). Heteromultimeric Kv1 channels contribute to myogenic control of arterial diameter. *Circ Res* **96,** 216-224.

Platoshyn O, Yu Y, Golovina VA, McDaniel SS, Krick S, Li L, Wang JY, Rubin LJ & Yuan JX. (2001). Chronic hypoxia decreases K(V) channel expression and function in pulmonary artery myocytes. *Am J Physiol Lung Cell Mol Physiol* **280,** L801-812.

Pohl U & de Wit C. (1999). A unique role of NO in the control of blood flow. *Physiology* **14,** 74-80.

Porter RJ, Nohria V & Rundfeldt C. (2007). Retigabine. *Neurotherapeutics* **4,** 149-154.

Potocnik SJ & Hill MA. (2001). Pharmacological evidence for capacitative Ca(2+) entry in cannulated and pressurized skeletal muscle arterioles. *Br J Pharmacol* **134,** 247-256.

Quayle JM, Nelson MT & Standen NB. (1997). ATP-sensitive and inwardly rectifying potassium channels in smooth muscle. *Physiol Rev* **77,** 1165-1232.

Quinlan MP. (2004). Vinculin, VASP, and profilin are coordinately regulated during actin remodeling in epithelial cells, which requires de novo protein synthesis and protein kinase signal transduction pathways. *J Cell Physiol* **200,** 277-290.

Raina H, Ella SR & Hill MA. (2008). Decreased activity of the smooth muscle Na+/Ca2+ exchanger impairs arteriolar myogenic reactivity. *J Physiol* **586,** 1669-1681.

Rashatwar SS, Cornwell TL & Lincoln TM. (1987). Effects of 8-bromo-cGMP on Ca2+ levels in vascular smooth muscle cells: possible regulation of Ca2+-ATPase by cGMP-dependent protein kinase. *Proc Natl Acad Sci U S A* **84,** 5685-5689.

Reinhard M, Halbrugge M, Scheer U, Wiegand C, Jockusch BM & Walter U. (1992). The 46/50 kDa phosphoprotein VASP purified from human platelets is a novel protein associated with actin filaments and focal contacts. *EMBO J* **11,** 2063-2070.

Rembold CM, Foster DB, Strauss JD, Wingard CJ & Eyk JE. (2000). cGMP-mediated phosphorylation of heat shock protein 20 may cause smooth muscle relaxation without myosin light chain dephosphorylation in swine carotid artery. *J Physiol* **524 Pt 3,** 865-878.

Ren Y, D'Ambrosio MA, Liu R, Pagano PJ, Garvin JL & Carretero OA. (2010). Enhanced myogenic response in the afferent arteriole of spontaneously hypertensive rats. *Am J Physiol Heart Circ Physiol* **298,** H1769-1775.

Robbins J. (2001). KCNQ potassium channels: physiology, pathophysiology, and pharmacology. *Pharmacol Ther* **90,** 1-19.

Rottner K, Behrendt B, Small JV & Wehland J. (1999). VASP dynamics during lamellipodia protrusion. *Nat Cell Biol* **1,** 321-322.

Rundfeldt C. (1997). The new anticonvulsant retigabine (D-23129) acts as an opener of K+ channels in neuronal cells. *Eur J Pharmacol* **336,** 243-249.

Ryan MJ, Gilbert EL, Glover PH, George EM, Masterson CW, McLemore GR, Jr., LaMarca B, Granger JP & Drummond HA. (2011). Placental ischemia impairs middle cerebral artery myogenic responses in the pregnant rat. *Hypertension* **58,** 1126-1131.

Saito SY, Hori M, Ozaki H & Karaki H. (1996). Cytochalasin D inhibits smooth muscle contraction by directly inhibiting contractile apparatus. *J Smooth Muscle Res* **32,** 51-60.

Sakai H, Hirano T, Takeyama H, Chiba Y & Misawa M. (2005). Acetylcholine-induced phosphorylation of CPI-17 in rat bronchial smooth muscle: the roles of Rho-kinase and protein kinase C. *Can J Physiol Pharmacol* **83,** 375-381.

Salinas M, de Weille J, Guillemare E, Lazdunski M & Hugnot JP. (1997a). Modes of regulation of shab K+ channel activity by the Kv8.1 subunit. *J Biol Chem* **272,** 8774-8780.

Salinas M, Duprat F, Heurteaux C, Hugnot JP & Lazdunski M. (1997b). New modulatory alpha subunits for mammalian Shab K+ channels. *J Biol Chem* **272,** 24371-24379.

Salinthone S, Tyagi M & Gerthoffer WT. (2008). Small heat shock proteins in smooth muscle. *Pharmacol Ther* **119,** 44-54.

Samarin S, Romero S, Kocks C, Didry D, Pantaloni D & Carlier MF. (2003). How VASP enhances actin-based motility. *J Cell Biol* **163,** 131-142.

Sano Y, Mochizuki S, Miyake A, Kitada C, Inamura K, Yokoi H, Nozawa K, Matsushime H & Furuichi K. (2002). Molecular cloning and characterization of Kv6.3, a novel modulatory subunit for voltage-gated K(+) channel Kv2.1. *FEBS Lett* **512,** 230-234.

Sartoretto JL, Jin BY, Bauer M, Gertler FB, Liao R & Michel T. (2009). Regulation of VASP phosphorylation in cardiac myocytes: differential regulation by cyclic nucleotides and modulation of protein expression in diabetic and hypertrophic heart. *Am J Physiol Heart Circ Physiol* **297,** H1697-1710.

Sausbier M, Schubert R, Voigt V, Hirneiss C, Pfeifer A, Korth M, Kleppisch T, Ruth P & Hofmann F. (2000). Mechanisms of NO/cGMP-dependent vasorelaxation. *Circ Res* **87,** 825-830.

Sauzeau V, Le Jeune H, Cario-Toumaniantz C, Smolenski A, Lohmann SM, Bertoglio J, Chardin P, Pacaud P & Loirand G. (2000). Cyclic GMP-dependent protein kinase signaling pathway inhibits RhoA-induced Ca2+ sensitization of contraction in vascular smooth muscle. *J Biol Chem* **275,** 21722-21729.

Schafer A, Burkhardt M, Vollkommer T, Bauersachs J, Munzel T, Walter U & Smolenski A. (2003). Endothelium-dependent and -independent relaxation and VASP serines 157/239 phosphorylation by cyclic nucleotide-elevating vasodilators in rat aorta. *Biochem Pharmacol* **65,** 397-405.

Schmit MA, Mirakaj V, Stangassinger M, Konig K, Kohler D & Rosenberger P. (2012). Vasodilator phosphostimulated protein (VASP) protects endothelial barrier function during hypoxia. *Inflammation* **35,** 566-573.

Schubert R, Lidington D & Bolz SS. (2008). The emerging role of Ca2+ sensitivity regulation in promoting myogenic vasoconstriction. *Cardiovasc Res* **77,** 8-18.

Schubert R & Mulvany MJ. (1999). The myogenic response: established facts and attractive hypotheses. *Clin Sci (Lond)* **96,** 313-326.

Schwake M, Athanasiadu D, Beimgraben C, Blanz J, Beck C, Jentsch TJ, Saftig P & Friedrich T. (2006). Structural determinants of M-type KCNQ (Kv7) K+ channel assembly. *J Neurosci* **26,** 3757-3766.

Sharif-Naeini R, Dedman A, Folgering JH, Duprat F, Patel A, Nilius B & Honore E. (2008). TRP channels and mechanosensory transduction: insights into the arterial myogenic response. *Pflugers Arch* **456,** 529-540.

Shen NV & Pfaffinger PJ. (1995). Molecular recognition and assembly sequences involved in the subfamily-specific assembly of voltage-gated K+ channel subunit proteins. *Neuron* **14,** 625-633.

Shimamura K & Sunano S. (1990). Effects of Bay K 8644 on the spontaneous electrical and mechanical activities of the rat portal vein. *Naunyn Schmiedebergs Arch Pharmacol* **342,** 554-558.

Shimokawa H. (2010). Hydrogen peroxide as an endothelium-derived hyperpolarizing factor. *Pflugers Arch* **459,** 915-922.

Shiraishi T, Sakaki S & Uehara Y. (1986). Architecture of the media of the arterial vessels in the dog brain: a scanning electron-microscopic study. *Cell Tissue Res* **243,** 329-335.

Skoble J, Auerbuch V, Goley ED, Welch MD & Portnoy DA. (2001). Pivotal role of VASP in Arp2/3 complex-mediated actin nucleation, actin branch-formation, and Listeria monocytogenes motility. *J Cell Biol* **155,** 89-100.

Smirnov SV, Beck R, Tammaro P, Ishii T & Aaronson PI. (2002). Electrophysiologically distinct smooth muscle cell subtypes in rat conduit and resistance pulmonary arteries. *J Physiol* **538,** 867-878.

Smolenski A, Burkhardt AM, Eigenthaler M, Butt E, Gambaryan S, Lohmann SM & Walter U. (1998). Functional analysis of cGMP-dependent protein kinases I and II as mediators of NO/cGMP effects. *Naunyn Schmiedebergs Arch Pharmacol* **358,** 134-139.

Smolenski A, Poller W, Walter U & Lohmann SM. (2000). Regulation of human endothelial cell focal adhesion sites and migration by cGMP-dependent protein kinase I. *J Biol Chem* **275,** 25723-25732.

Sobey CG & Faraci FM. (1999). Inhibitory effect of 4-aminopyridine on responses of the basilar artery to nitric oxide. *Br J Pharmacol* **126,** 1437-1443.

Soderberg O, Gullberg M, Jarvius M, Ridderstrale K, Leuchowius KJ, Jarvius J, Wester K, Hydbring P, Bahram F, Larsson LG & Landegren U. (2006). Direct

observation of individual endogenous protein complexes in situ by proximity ligation. *Nat Methods* **3,** 995-1000.

Somlyo AP & Somlyo AV. (2000). Signal transduction by G-proteins, rho-kinase and protein phosphatase to smooth muscle and non-muscle myosin II. *J Physiol* **522 Pt 2,** 177-185.

Somlyo AP & Somlyo AV. (2003). Ca2+ sensitivity of smooth muscle and nonmuscle myosin II: modulated by G proteins, kinases, and myosin phosphatase. *Physiol Rev* **83,** 1325-1358.

Somlyo AP & Somlyo AV. (2004). Signal transduction through the RhoA/Rho-kinase pathway in smooth muscle. *J Muscle Res Cell Motil* **25,** 613-615.

Sonoyama K, Greenstein A, Price A, Khavandi K & Heagerty T. (2007). Vascular remodeling: implications for small artery function and target organ damage. *Ther Adv Cardiovasc Dis* **1,** 129-137.

Standen NB & Quayle JM. (1998). K+ channel modulation in arterial smooth muscle. *Acta Physiol Scand* **164,** 549-557.

Stocker M, Hellwig M & Kerschensteiner D. (1999). Subunit assembly and domain analysis of electrically silent K+ channel alpha-subunits of the rat Kv9 subfamily. *J Neurochem* **72,** 1725-1734.

Stocker M & Kerschensteiner D. (1998). Cloning and tissue distribution of two new potassium channel alpha-subunits from rat brain. *Biochem Biophys Res Commun* **248,** 927-934.

Strutz-Seebohm N, Seebohm G, Fedorenko O, Baltaev R, Engel J, Knirsch M & Lang F. (2006). Functional coassembly of KCNQ4 with KCNE-beta- subunits in Xenopus oocytes. *Cell Physiol Biochem* **18,** 57-66.

Sumpio BE. (1993). *Hemodynamic forces and vascular cell biology*. RG Landes.

Sun CW, Falck JR, Okamoto H, Harder DR & Roman RJ. (2000). Role of cGMP versus 20-HETE in the vasodilator response to nitric oxide in rat cerebral arteries. *Am J Physiol Heart Circ Physiol* **279,** H339-350.

Sun D, Huang A, Koller A & Kaley G. (1995). Flow-dependent dilation and myogenic constriction interact to establish the resistance of skeletal muscle arterioles. *Microcirculation* **2,** 289-295.

Sward K, Mita M, Wilson DP, Deng JT, Susnjar M & Walsh MP. (2003). The role of RhoA and Rho-associated kinase in vascular smooth muscle contraction. *Curr Hypertens Rep* **5,** 66-72.

Swartz KJ. (2007). Tarantula toxins interacting with voltage sensors in potassium channels. *Toxicon* **49,** 213-230.

Taguchi H, Heistad DD, Kitazono T & Faraci FM. (1994). ATP-sensitive K+ channels mediate dilatation of cerebral arterioles during hypoxia. *Circ Res* **74,** 1005-1008.

Takeya K, Loutzenhiser K, Shiraishi M, Loutzenhiser R & Walsh MP. (2008). A highly sensitive technique to measure myosin regulatory light chain phosphorylation: the first quantification in renal arterioles. *Am J Physiol Renal Physiol* **294,** F1487-1492.

Takuwa Y, Takuwa N & Rasmussen H. (1988). The effects of isoproterenol on intracellular calcium concentration. *J Biol Chem* **263,** 762-768.

Tang DD & Gunst SJ. (2004). The small GTPase Cdc42 regulates actin polymerization and tension development during contractile stimulation of smooth muscle. *J Biol Chem* **279,** 51722-51728.

Tansey MG, Hori M, Karaki H, Kamm KE & Stull JT. (1990). Okadaic acid uncouples myosin light chain phosphorylation and tension in smooth muscle. *FEBS Lett* **270,** 219-221.

Tatulian L, Delmas P, Abogadie FC & Brown DA. (2001). Activation of expressed KCNQ potassium currents and native neuronal M-type potassium currents by the anti-convulsant drug retigabine. *J Neurosci* **21,** 5535-5545.

Theriot JA, Rosenblatt J, Portnoy DA, Goldschmidt-Clermont PJ & Mitchison TJ. (1994). Involvement of profilin in the actin-based motility of L. monocytogenes in cells and in cell-free extracts. *Cell* **76,** 505-517.

Thornbury KD, Ward SM & Sanders KM. (1992). Participation of fast-activating, voltage-dependent K currents in electrical slow waves of colonic circular muscle. *Am J Physiol* **263,** C226-236.

Thorne GD, Conforti L & Paul RJ. (2002). Hypoxic vasorelaxation inhibition by organ culture correlates with loss of Kv channels but not Ca(2+) channels. *Am J Physiol Heart Circ Physiol* **283,** H247-253.

Thorneloe KS, Chen TT, Kerr PM, Grier EF, Horowitz B, Cole WC & Walsh MP. (2001). Molecular composition of 4-aminopyridine-sensitive voltage-gated K(+) channels of vascular smooth muscle. *Circ Res* **89,** 1030-1037.

Thorneloe KS & Nelson MT. (2003). Properties and molecular basis of the mouse urinary bladder voltage-gated K+ current. *J Physiol* **549,** 65-74.

Thorneloe KS & Nelson MT. (2005). Ion channels in smooth muscle: regulators of intracellular calcium and contractility. *Can J Physiol Pharmacol* **83,** 215-242.

Thorsen LB, Eskildsen-Helmond Y, Zibrandtsen H, Stasch JP, Simonsen U & Laursen BE. (2010). BAY 41-2272 inhibits the development of chronic hypoxic pulmonary hypertension in rats. *Eur J Pharmacol* **647,** 147-154.

Trauner D. (2005). A glimpse at the grail. *Nat Chem Biol* **1,** 189-191.

Triggle DJ. (2006). L-type calcium channels. *Curr Pharm Des* **12,** 443-457.

VanBavel E, Sorop O, Andreasen D, Pfaffendorf M & Jensen BL. (2002). Role of T-type calcium channels in myogenic tone of skeletal muscle resistance arteries. *Am J Physiol Heart Circ Physiol* **283,** H2239-2243.

VanBavel E, van der Meulen ET & Spaan JA. (2001). Role of Rho-associated protein kinase in tone and calcium sensitivity of cannulated rat mesenteric small arteries. *Exp Physiol* **86,** 585-592.

Vasioukhin V, Bauer C, Yin M & Fuchs E. (2000). Directed actin polymerization is the driving force for epithelial cell-cell adhesion. *Cell* **100,** 209-219.

Walders-Harbeck B, Khaitlina SY, Hinssen H, Jockusch BM & Illenberger S. (2002). The vasodilator-stimulated phosphoprotein promotes actin polymerisation through direct binding to monomeric actin. *FEBS Lett* **529,** 275-280.

Waldmann R, Nieberding M & Walter U. (1987). Vasodilator-stimulated protein phosphorylation in platelets is mediated by cAMP- and cGMP-dependent protein kinases. *Eur J Biochem* **167,** 441-448.

Walsh MP. (2011). Vascular smooth muscle myosin light chain diphosphorylation: mechanism, function, and pathological implications. *IUBMB Life* **63,** 987-1000.

Walsh MP & Cole WC. (2013). The role of actin filament dynamics in the myogenic response of cerebral resistance arteries. *J Cereb Blood Flow Metab* **33,** 1-12.

Walsh MP, Thornbury K, Cole WC, Sergeant G, Hollywood M & McHale N. (2011). Rho-associated kinase plays a role in rabbit urethral smooth muscle contraction, but not via enhanced myosin light chain phosphorylation. *Am J Physiol Renal Physiol* **300,** F73-85.

Wang HS, Brown BS, McKinnon D & Cohen IS. (2000). Molecular basis for differential sensitivity of KCNQ and I(Ks) channels to the cognitive enhancer XE991. *Mol Pharmacol* **57,** 1218-1223.

Wang J, Weigand L, Wang W, Sylvester JT & Shimoda LA. (2005). Chronic hypoxia inhibits Kv channel gene expression in rat distal pulmonary artery. *Am J Physiol Lung Cell Mol Physiol* **288,** L1049-1058.

Wang S & Li Y. (2009). Expression of constitutively active cGMP-dependent protein kinase inhibits glucose-induced vascular smooth muscle cell proliferation. *Am J Physiol Heart Circ Physiol* **297,** H2075-2083.

Wang T, Kendig DM, Smolock EM & Moreland RS. (2009). Carbachol-induced rabbit bladder smooth muscle contraction: roles of protein kinase C and Rho kinase. *Am J Physiol Renal Physiol* **297,** F1534-1542.

Wang T, Kendig DM, Trappanese DM, Smolock EM & Moreland RS. (2012). Phorbol 12,13-dibutyrate-induced, protein kinase C-mediated contraction of rabbit bladder smooth muscle. *Front Pharmacol* **2,** 83.

Wareing M, Bai X, Seghier F, Turner CM, Greenwood SL, Baker PN, Taggart MJ & Fyfe GK. (2006). Expression and function of potassium channels in the human placental vasculature. *Am J Physiol Regul Integr Comp Physiol* **291,** R437-446.

Watanabe J, Karibe A, Horiguchi S, Keitoku M, Satoh S, Takishima T & Shirato K. (1993). Modification of myogenic intrinsic tone and [Ca2+]i of rat isolated arterioles by ryanodine and cyclopiazonic acid. *Circ Res* **73,** 465-472.

Wear MA, Yamashita A, Kim K, Maeda Y & Cooper JA. (2003). How capping protein binds the barbed end of the actin filament. *Curr Biol* **13,** 1531-1537.

Wei AD, Gutman GA, Aldrich R, Chandy KG, Grissmer S & Wulff H. (2005). International Union of Pharmacology. LII. Nomenclature and molecular relationships of calcium-activated potassium channels. *Pharmacol Rev* **57,** 463-472.

Wei L, Muller S, Ouyang J, Stoltz JF & Wang X. (2003). Changes of vasodilator-stimulated phosphoprotein (VASP) and its phosphorylation in endothelial cells exposed to laminar flow. *Clin Hemorheol Microcirc* **28,** 113-120.

Wei L, Ouyang JP, Li K, Muller S, Stoltz JF & Wang X. (2004). [Changes of VASP in shear stress induced cytoskeleton reorganization in endothelial cells]. *Zhongguo Ying Yong Sheng Li Xue Za Zhi* **20,** 313-317.

Weidelt T, Boldt W & Markwardt F. (1997). Acetylcholine-induced K+ currents in smooth muscle cells of intact rat small arteries. *J Physiol* **500 (Pt 3),** 617-630.

Wellman GC. (2006). Ion channels and calcium signaling in cerebral arteries following subarachnoid hemorrhage. *Neurol Res* **28,** 690-702.

Wilson DP, Sutherland C, Borman MA, Deng JT, MacDonald JA & Walsh MP. (2005). Integrin-linked kinase is responsible for Ca2+-independent myosin diphosphorylation and contraction of vascular smooth muscle. *Biochem J* **392,** 641-648.

Woodrum DA, Brophy CM, Wingard CJ, Beall A & Rasmussen H. (1999). Phosphorylation events associated with cyclic nucleotide-dependent inhibition of smooth muscle contraction. *Am J Physiol* **277,** H931-939.

Wright G & Hurn E. (1994). Cytochalasin inhibition of slow tension increase in rat aortic rings. *Am J Physiol* **267,** H1437-1446.

Wu X, Haystead TA, Nakamoto RK, Somlyo AV & Somlyo AP. (1998). Acceleration of myosin light chain dephosphorylation and relaxation of smooth muscle by telokin. Synergism with cyclic nucleotide-activated kinase. *J Biol Chem* **273,** 11362-11369.

Xia F, Gao X, Kwan E, Lam PP, Chan L, Sy K, Sheu L, Wheeler MB, Gaisano HY & Tsushima RG. (2004). Disruption of pancreatic beta-cell lipid rafts modifies Kv2.1 channel gating and insulin exocytosis. *J Biol Chem* **279,** 24685-24691.

Xiong Z, Sperelakis N & Fenoglio-Preiser C. (1994). Regulation of L-type calcium channels by cyclic nucleotides and phosphorylation in smooth muscle cells from rabbit portal vein. *J Vasc Res* **31,** 271-279.

Xu C, Lu Y, Tang G & Wang R. (1999). Expression of voltage-dependent K(+) channel genes in mesenteric artery smooth muscle cells. *Am J Physiol* **277,** G1055-1063.

Yamin R & Morgan KG. (2012). Deciphering actin cytoskeletal function in the contractile vascular smooth muscle cell. *J Physiol* **590,** 4145-4154.

Yan L, Figueroa DJ, Austin CP, Liu Y, Bugianesi RM, Slaughter RS, Kaczorowski GJ & Kohler MG. (2004). Expression of voltage-gated potassium channels in human and rhesus pancreatic islets. *Diabetes* **53,** 597-607.

Yang Y, Murphy TV, Ella SR, Grayson TH, Haddock R, Hwang YT, Braun AP, Peichun G, Korthuis RJ, Davis MJ & Hill MA. (2009). Heterogeneity in function of small artery smooth muscle BKCa: involvement of the beta1-subunit. *J Physiol* **587,** 3025-3044.

Yeon DS, Kim JS, Ahn DS, Kwon SC, Kang BS, Morgan KG & Lee YH. (2002). Role of protein kinase C- or RhoA-induced Ca(2+) sensitization in stretch-induced myogenic tone. *Cardiovasc Res* **53,** 431-438.

Yeung S, Schwake M, Pucovsky V & Greenwood I. (2008). Bimodal effects of the Kv7 channel activator retigabine on vascular K+ currents. *Br J Pharmacol* **155,** 62-72.

Yeung SY & Greenwood IA. (2005). Electrophysiological and functional effects of the KCNQ channel blocker XE991 on murine portal vein smooth muscle cells. *Br J Pharmacol* **146,** 585-595.

Yeung SY, Ohya S, Sergeant GP, Pucovsky V & Greenwood IA. (2006). Pharmacological and molecular evidence for the involvement of Kv4.3 in ultra-fast activating K+ currents in murine portal vein myocytes. *Br J Pharmacol* **149,** 676-686.

Yeung SY, Pucovsky V, Moffatt JD, Saldanha L, Schwake M, Ohya S & Greenwood IA. (2007). Molecular expression and pharmacological identification of a role for K(v)7 channels in murine vascular reactivity. *Br J Pharmacol* **151,** 758-770.

Ying L, Xu X, Liu J, Dou D, Yu X, Ye L, He Q & Gao Y. (2012). Heterogeneity in relaxation of different sized porcine coronary arteries to nitrovasodilators: role of PKG and MYPT1. *Pflugers Arch* **463,** 257-268.

Yu M, Sun CW, Maier KG, Harder DR & Roman RJ. (2002). Mechanism of cGMP contribution to the vasodilator response to NO in rat middle cerebral arteries. *Am J Physiol Heart Circ Physiol* **282,** H1724-1731.

Yuan JX, Aldinger AM, Juhaszova M, Wang J, Conte JV, Jr., Gaine SP, Orens JB & Rubin LJ. (1998). Dysfunctional voltage-gated K+ channels in pulmonary artery smooth muscle cells of patients with primary pulmonary hypertension. *Circulation* **98,** 1400-1406.

Zaczek R, Chorvat RJ, Saye JA, Pierdomenico ME, Maciag CM, Logue AR, Fisher BN, Rominger DH & Earl RA. (1998). Two new potent neurotransmitter release enhancers, 10,10-bis(4-pyridinylmethyl)-9(10H)-anthracenone and 10,10-bis(2-fluoro-4-pyridinylmethyl)-9(10H)-anthracenone: comparison to linopirdine. *J Pharmacol Exp Ther* **285,** 724-730.

Zawieja DC. (1996). Lymphatic microcirculation. *Microcirculation* **3,** 241-243.

Zhang W & Gunst SJ. (2008). Interactions of airway smooth muscle cells with their tissue matrix: implications for contraction. *Proc Am Thorac Soc* **5,** 32-39.

Zhang W, Wu Y, Du L, Tang DD & Gunst SJ. (2005). Activation of the Arp2/3 complex by N-WASp is required for actin polymerization and contraction in smooth muscle. *Am J Physiol Cell Physiol* **288,** C1145-1160.

Zhang Y, Tazzeo T, Chu V & Janssen LJ. (2006). Membrane potassium currents in human radial artery and their regulation by nitric oxide donor. *Cardiovasc Res* **71,** 383-392.

Zhao W & Wang R. (2002). H(2)S-induced vasorelaxation and underlying cellular and molecular mechanisms. *Am J Physiol Heart Circ Physiol* **283,** H474-480.

Zhao YJ, Wang J, Rubin LJ & Yuan XJ. (1997). Inhibition of K(V) and K(Ca) channels antagonizes NO-induced relaxation in pulmonary artery. *Am J Physiol* **272,** H904-912.

Zhong XZ, Abd-Elrahman KS, Liao CH, El-Yazbi AF, Walsh EJ, Walsh MP & Cole WC. (2010a). Stromatoxin-sensitive, heteromultimeric Kv2.1/Kv9.3 channels contribute to myogenic control of cerebral arterial diameter. *J Physiol* **588,** 4519-4537.

Zhong XZ, Harhun MI, Olesen SP, Ohya S, Moffatt JD, Cole WC & Greenwood IA. (2010b). Participation of KCNQ (Kv7) potassium channels in myogenic control of cerebral arterial diameter. *J Physiol* **588,** 3277-3293.

Zhou XB, Ruth P, Schlossmann J, Hofmann F & Korth M. (1996). Protein phosphatase 2A is essential for the activation of Ca2+-activated K+ currents by cGMP-dependent protein kinase in tracheal smooth muscle and Chinese hamster ovary cells. *J Biol Chem* **271,** 19760-19767.

Zhu XR, Netzer R, Bohlke K, Liu Q & Pongs O. (1999). Structural and functional characterization of Kv6.2 a new gamma-subunit of voltage-gated potassium channel. *Receptors Channels* **6,** 337-350.

Zimmermann J, Labudde D, Jarchau T, Walter U, Oschkinat H & Ball LJ. (2002). Relaxation, equilibrium oligomerization, and molecular symmetry of the VASP (336-380) EVH2 tetramer. *Biochemistry* **41,** 11143-11151.

Zou H, Ratz PH & Hill MA. (1995). Role of myosin phosphorylation and [Ca2+] i in myogenic reactivity and arteriolar tone. *American Journal of Physiology-Heart and Circulatory Physiology* **269,** H1590-H1596.

Zou H, Ratz PH & Hill MA. (2000). Temporal aspects of Ca(2+) and myosin phosphorylation during myogenic and norepinephrine-induced arteriolar constriction. *J Vasc Res* **37,** 556-567.